

La borsa di dottorato è stata cofinanziata con risorse del
Programma Operativo Nazionale Ricerca e Innovazione 2014-2020 (CCI 2014IT16M2OP005)
Fondo Sociale Europeo, Azione I.1 "Dottorati Innovativi con caratterizzazione Industriale"



UNIONE EUROPEA
Fondo Sociale Europeo



UNIVERSITA' DELLA CALABRIA

Dipartimento di Ingegneria dell'Ambiente

Dottorato di Ricerca in Scienze e Ingegneria dell'Ambiente, delle Costruzioni e dell'Energia

Con il contributo di *Ministero dell'Università e della Ricerca*


CICLO XXXIII

TITOLO TESI

***Valorisation of plastic Wastes from Electrical and Electronic Equipment (WEEE)
containing PVC by MFI-zeolites mediated catalytic pyrolysis.***

Settore Scientifico Disciplinare: ING-IND/27


Coordinatore: Ch.mo Prof. Salvatore CRITELLI

Firma  Critelli Salvatore
29.09.2021 11:44:18 GMT+00:00

Supervisore: Ch.mo Prof. Girolamo GIORDANO

Firma  Firma oscurata in base alle linee
guida del Garante della privacy

Co-Supervisore: Ch.mo Prof. David P. SERRANO

Firma  Firma oscurata in base alle linee
guida del Garante della privacy

Dottoranda: Dott.sa Alessia MARINO

Firma  Firma oscurata in base alle linee
guida del Garante della privacy

PREFACE

This doctoral work has been performed at the Laboratory of Industrial Chemistry and Catalysis of *Università della Calabria* (UNICAL), from March 2018 until now, under the supervision of Professor Girolamo Giordano.

The project has been developed in close collaboration with the Thermochemical Processes Unit of *Instituto IMDEA Energía* (Mòstoles, Madrid, Spain) and *Universidad Rey Juan Carlos* (Mòstoles, Madrid, Spain), where I spent 15 months under the guidance of Professor David P. Serrano, Professor Patricia Pizarro, and Dr. Javier Feroso.

Part of this doctoral project has been carried out in close collaboration with the company R.ED.EL. srl (Reggio Calabria, Italy), where I spent 6 months supervised by Dr. Umberto Barreca (Chief Executive Officer).

This work was co-financed by the Italian *Ministero dell'Università e della Ricerca* (MUR) as part of *Programma Operativo Nazionale Ricerca e Innovazione 2014-2020 (CCI 2014IT16M2OP005) Fondo Sociale Europeo, Azione I.1 "Dottorati Innovativi con caratterizzazione Industriale"*, and carried out within the Doctorate in Sciences and Engineering of Environment, Construction and Energy (SIACE).

At the end of this work, I gratefully acknowledge all my supervisors for the boundless lessons in both scientific and personal fields, all my fellow travellers, who have contributed to develop my work and my life by practically helping me and by gifting me love, laughter and support, and to all my family, who is always on my side. Without each of you, this would not have been possible.

THANK YOU.

Alessia



ABSTRACT

The issue concerning the plastic Wastes from Electrical and Electronic Equipment (WEEE) recycling and management is still a global challenge, due to the high heterogeneity of the matrixes to be treated, as well as to the lack of suitable technologies. According to the last data, nowadays only the 28 % of WEEE plastic is properly collected and recycled in Europe. Therefore, safe and efficient recycling processes of waste plastics still need to be developed and/or improved, with the aim to produce high-quality secondary raw materials and finished products, by simultaneously preventing the emission of hazardous substances and greenhouse gases. Among the current recycling technologies, chemical recycling by pyrolysis represents the most promising one, since it provides the opportunity to produce valuable raw chemicals and fuels from waste plastics, which can be further enhanced by tailoring the process parameters and by employing appropriate catalysts.

This doctoral thesis fits into this context, aiming to reduce the existing research gap by studying the thermo-catalytic fast-pyrolysis of the real PVC-containing WEEE plastic mixture provided by the company R.ED.EL. srl. In this work, both polymer and chemical compositions of the real WEEE plastic were firstly investigated. The physicochemical characterization revealed the presence of polyethylene, polyvinyl chloride, metals and oxygen, as a consequence of photooxidation and contamination of products during their lifetime. PVC amounts to 3.44 ± 0.85 wt.%, that corresponds to a total chlorine concentration greater than 19000 ppm. A such high halogen concentration compromises the use of pyrolysis oils as fuels, since the following combustion may lead to the formation of partially oxidized polyhalogenated dioxins, classified as toxic and carcinogenic agents. In addition, hydrochloric acid and volatile halogenated compounds can be released, which are dangerous for human health and corrosive to the industrial plants. Therefore, thermal dechlorination treatments at different temperatures were studied in this work, which allowed to remove up 87 % of the initial chlorine (in form of HCl safely collected) from the raw WEEE plastic mixture to be used as feedstock in pyrolysis tests, with the concurrent reduction of the oxygen content. The thermo-catalytic fast-pyrolysis experiments were carried out in a downdraft fixed-bed stainless steel reactor, with the thermal and catalytic zones of the reaction system independently heated. The main process parameters were deeply studied, such as temperature of thermal and catalytic zones, catalyst-to-feedstock ratio, type of feedstock (raw and dechlorinated WEEE plastic), aiming to drive the pyrolysis products

distribution towards high-quality oils formation. To that end, ZSM-5 zeolites with different acidity and accessibility were synthesized, characterized and tested as catalysts in the WEEE plastic fast-pyrolysis reactions. Liquid, gaseous and solids pyrolysis products were analyzed in detail, with a special focus on chlorine quantification and distribution. In comparison with thermal pyrolysis, which mainly produces waxes, the products distribution changed considerably by contacting the pyrolysis vapours with ZSM-5 zeolites, leading to a strong enhancement in the yield of lighter hydrocarbons, i.e. oil and gases. The largest oil yields, showing high monoaromatics concentrations (mainly BTX, which are valuable chemicals), were obtained by using MFI_100 and desilicated ZSM-5 samples, in the range of 60 - 70 wt.%, due to the combination between the Brønsted acidity and improved accessibility of the catalysts active sites. Regarding chlorine distribution, most of the residual halogen still present in the dechlorinated WEEE plastic (≈ 2600 ppm) was accumulated in the char fraction (≈ 90 wt.%), and this has been attributed to the inorganic components present in the waste mixture which may capture Cl by forming the corresponding metallic chlorides. The following fractions in terms of chlorine concentration were coke, wax and oil, suggesting the halogen is mainly released in form of bulky chlorinated compounds during the pyrolysis process, that thus tend to be accumulated in the heavier fractions.

It is noteworthy that the specific properties of the desilicated ZSM-5 zeolite, i.e., the enhanced external surface and bimodal pore size distribution combined with a relatively high Brønsted acidity, led to the lowest chlorine concentration in oil, with a value of about 88 ppm, which is within recommended limits to be processed in refineries facilities.

TABLE OF CONTENTS

List of abbreviations	IX
1. Introduction	1
1.1 Background: zero-waste circular economy of R.ED.EL. srl.....	1
1.2 Waste from Electrical and Electronic Equipment.....	2
1.3 WEEE-derived plastics recycling	3
1.4 Thesis objectives and novelty	5
2. Pyrolysis of plastic materials.....	7
2.1 Thermal decomposition of plastics	7
2.1.1 Feedstock composition	8
2.1.2 Operating parameters.....	11
2.2 Catalytic pyrolysis of plastics	17
2.2.1 Zeolites in catalytic pyrolysis of plastics: structure and mechanism.....	18
2.2.2 Literature overview on zeolites as catalyst in plastics pyrolysis	24
2.3 Plastics de-halogenation treatments	30
2.3.1 De-chlorination treatments	31
2.3.2 De-bromination treatments	33
2.3.3 Ex situ de-halogenation treatments of pyrolysis oil	34
3. Materials and methods.....	37
3.1 Catalysts preparation.....	37
3.1.1 Nanocrystalline ZSM-5 zeolite.....	37
3.1.2 Synthesis of ZSM-5 zeolites.....	37
3.1.3 Preparation of hierarchical ZSM-5 zeolite	38
3.2 Characterization techniques	40
3.2.1 X-Ray Powder Diffraction (XRD).....	40
3.2.2 Ultimate and proximate analyses.....	40

TABLE OF CONTENTS

3.2.3	Fourier-Transform Infrared Spectroscopy (FT-IR) in Attenuated Total Reflectance (ATR) mode.....	41
3.2.4	Oxidative combustion followed by Ion Chromatography (AOD/IC)	41
3.2.5	Inductively Coupled Plasma Optical Emission Spectrometry (ICP-OES)..	41
3.2.6	Nitrogen physisorption at 77 K	42
3.2.7	Temperature Programmed Desorption (NH ₃ -TPD).....	42
3.2.8	Fourier-Transform Infrared Spectroscopy (FT-IR) with CD ₃ CN adsorption	43
3.2.9	Magic Angle Spinning solid state Nuclear Magnetic Resonance (²⁷ Al MAS ssNMR).....	43
3.2.10	Scanning Electron Microscopy (SEM).....	43
3.3	Reaction system	44
3.3.1	Experimental setup	44
3.3.2	Analytical methods for products characterization	47
4.	Results and discussion.....	49
4.1	Physicochemical properties of WEEE plastic	49
4.1.1	Proximate and ultimate analysis	49
4.1.2	XRD and FT-IR analyses	52
4.1.3	Conclusions	54
4.2	Physicochemical properties of investigated catalysts	55
4.2.1	Commercial nanocrystalline ZSM-5 zeolite.....	55
4.2.2	Synthesized ZSM-5 zeolites	59
4.2.3	Hierarchical h-ZSM-5 zeolite.....	68
4.2.4	Conclusions	74
4.3	Dehydrochlorination of WEEE Plastic	76
4.3.1	Reaction yields	76

TABLE OF CONTENTS

4.3.2	Products characterization.....	77
4.3.3	Conclusions.....	83
4.4	Thermal pyrolysis of raw WEEE plastic.....	84
4.4.1	Reaction yields.....	84
4.4.2	Products characterization.....	86
4.4.3	Conclusions.....	91
4.5	Catalytic pyrolysis of raw WEEE plastic at different catalytic temperatures.....	93
4.5.1	Reaction yields.....	94
4.5.2	Products characterization.....	95
4.5.3	Conclusions.....	100
4.6	Catalytic pyrolysis of raw WEEE plastic with different catalyst to feedstock ratios.....	102
4.6.1	Reaction yields.....	102
4.6.2	Products characterization.....	103
4.6.3	Conclusions.....	107
4.7	Catalytic pyrolysis of raw and dechlorinated WEEE plastic.....	109
4.7.1	Reaction yields.....	110
4.7.2	Products characterization.....	111
4.7.3	Conclusions.....	116
4.8	Catalytic pyrolysis of dechlorinated WEEE plastic in presence of synthesized ZSM-5 zeolites.....	117
4.8.1	Reaction yields.....	118
4.8.2	Products characterization.....	120
4.8.3	Conclusions.....	126
4.9	Catalytic pyrolysis over hierarchical ZSM-5 zeolite.....	128
4.9.1	Reaction yields.....	128

TABLE OF CONTENTS

4.9.2 Products characterization	130
4.9.3 Conclusions	135
5. Conclusions and future trends.....	137
List of Figures	147
List of Tables.....	153
References	155

LIST OF ABBREVIATIONS

ABS	Acrylonitrile Butadiene Styrene
BE	Brominated Epoxy resin
BFR	Brominated Flame Retardant
BTX	Benzene, Toluene, Xylene
CSBR	Conical Spouted Bed Reactor
FBR	Fluidized Bed Reactor
GC	Gas Chromatography
HBCD	Hexabromocyclododecane
HDPE	High Density Polyethylene
LDPE	Low Density polyethylene
LPG	Liquefied Petroleum Gas
Micro-GC	Micro-Gas Chromatography
MPW	Municipal Plastic Waste
MS	Mass Spectrometry
MSW	Municipal Solid Waste
PA	Polyamide
PBB	Polybromobiphenyls
PBDE	Polybrominated Diphenyl Ethers
PBT	Polybutylene Terephthalate
PC	Polycarbonate
PE	Polyethylene
PET	Polyethylene Terephthalate
PMMA	Poly(Methyl Methacrylate)
PO	Polyolefins
PP	Polypropylene
PS	Polystyrene
PUR	Polyurethane
PVC	Polyvinyl Chloride
SA	Silica Alumina
SEM	Scanning Electron Microscope

TABLE OF CONTENTS

TBBPA	Tetrabromobisphenol A
TGA	Thermogravimetric Analysis
WEEE	Waste from Electrical and Electronic Equipment
ZSM	Zeolite Socony Mobil

1. INTRODUCTION

1.1 Background: zero-waste circular economy of R.ED.EL. srl

The concept of circular economy is based on a zero-waste society, where everything is produced and consumed can return to the society itself or to the environment in a safe and low-impact way.

The *zero-waste circular economy* model includes the “3Rs” program, i.e., Reduce, Reuse, and Recycle, and overcomes it by including a more comprehensive virtuous synergetic transformation of resources production and consumption, with the aim to reach zero emissions and zero wastes.

The company R.ED.EL. srl has been inserted in this context for several years now. The company, located in Reggio Calabria (Italy), was founded in 1981 and its core business is focused on construction and maintenance of low and medium voltage electrical installations. Downstream of obsolete plants replacement, the company accumulates about 25 ton/year of pre- and post-consumer scrap electric wires, which are listed in Waste from Electrical and Electronic Equipment (WEEE) class [1].

The low and medium voltage wires consist of multi-layer systems, in which different plastic sheaths alternate with semiconductors and metallic conductors (Figure 1.1), and as a consequence, they represent a complex matrix to be recycled.

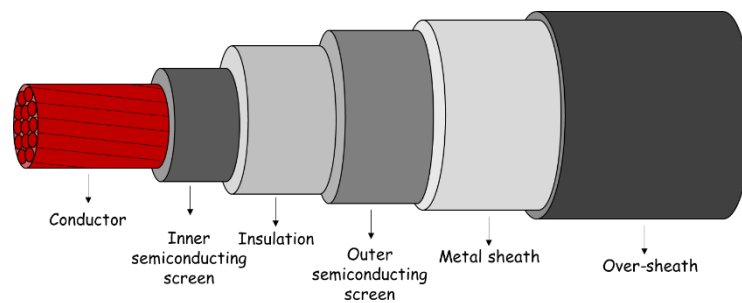


Figure 1.1 - Schematic representation of electric medium voltage cable.

To this purpose, R.ED.EL. srl has set up a recycle process which includes the size reduction of the waste cables to 5 – 10 cm in length and the mechanical separation of the plastic portion, accounting on average for the 50 %, from the metallic component, that mainly consists of copper and aluminum (Figure 1.2).

1. INTRODUCTION

The obtained metallic fraction is thus directly recovered and marketed, so that the plastic portion represents the only waste to be disposed of.

The whole recycling process requires a processing time of 15 h/ton of wastes, with a power consumption of 480 kWh/ton. However, the electricity needed by the recycle chain is provided by photovoltaic modules, of which R.ED.EL. srl has been equipped with the aim to also reach the energy self-sufficiency.

Therefore, to close the virtuous cycle and achieve a zero-waste process, the valorization of the plastic fraction, which represents the only residual waste, has become necessary, and this need arises as starting point of this thesis work.

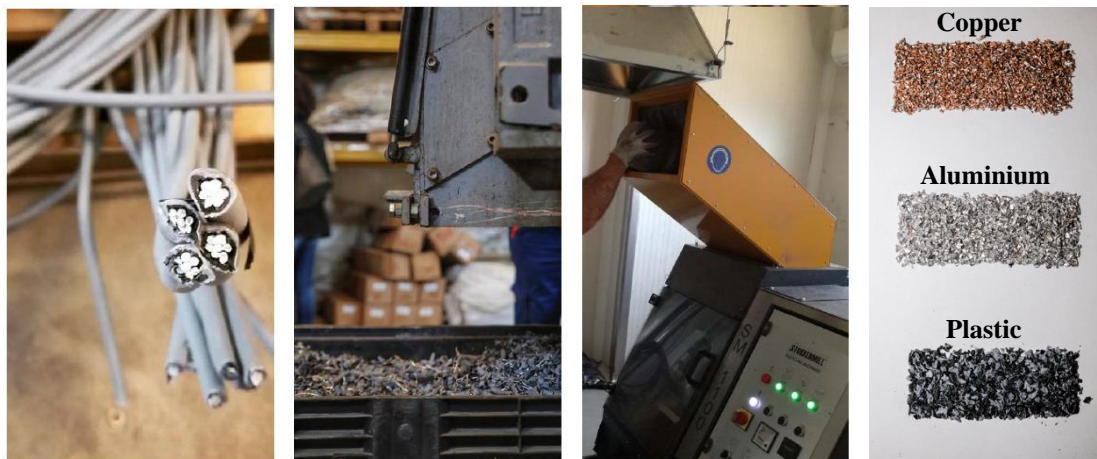


Figure 1.2 - Pictures of the recycle chain set up by R.ED.EL. srl.

1.2 Waste from Electrical and Electronic Equipment

On the basis of the current legislation [1], the WEEE class includes a great variety of electronic end-of-life products, such as electrical equipment, batteries, large and small appliances, as well as the components that make them up.

It has been estimated that WEEE represent the 2 % of the total solid waste streams, amounting to 53.6 million tons in 2019 [2], corresponding to 7.3 kg/year per each person on the planet, and that these numbers are expected to double by 2050 if no action will be taken [3]. Besides, just a worldwide average of 20 % of the total WEEE is properly recovered and

1. INTRODUCTION

processed up to now, which reaches the 35 % in Europe, being the remaining part still landfilled [4].

Such low rate of WEEE recycling stands in the high complexity of the matrixes, since a single WEEE product can be constituted by hundreds of different materials (plastics, metals, ceramics, hazardous substances, etc.), which make challenging the treatment [5].

Therefore, the first issue concerns the goods disassembly, necessary to separate their components as a function of the type of materials that compose them, in order to facilitate the selective recovery and treatment. Research on disassembly is still an active area, despite different technologies are already available on a commercial scale. Among the others, one of the most employed method involves a multi-step process, in which a first sizing by rotary cylindrical trommels or vibratory screens is followed by a magnetic separation for the ferrous metals removal from the mixtures. Subsequently, a separation on the basis of the densities of materials is carried out by means of jigs, shaking tables, corona electrostatic separation, etc. However, a complete separation of the different constituents is still difficult to achieve, since some metallic and non-metallic particles may have comparable consistency in such complex mixtures, and, as a consequence, different fractions that contaminate each other are produced downstream the separation processes [6].

It must be taken into account that, even without considering the contamination by other materials, the plastic fraction represents itself a complex matrix, being composed of different types of polymers, which may also have been undergone modification during the goods use (by oxidation and ageing), resulting in unpredictable changes in their physicochemical properties which make separation and recycling even more challenging [7].

Therefore, the improvement of WEEE separation and recycling processes still account for a global challenge, and the valorization of the WEEE-derived plastic fraction represents an even more intricate issue to be faced.

1.3 WEEE-derived plastics recycling

It has been estimated that the plastic fraction accounts for more than 30 % of the total WEEE [8]. In Europe, the amount of collected WEEE plastics is about 0.7 Mt/y, of which just a small portion ($\approx 28\%$) is properly recycled [9]. The main issues concern both the limited

1. INTRODUCTION

treatment capacity, being equal to 0.2 Mt/y in Europe, and especially the lack of appropriate technologies.

As mentioned above, this last problem arises mainly from the complexity of the matrixes to be treated, since different polymers, additives, hazardous substances and residues from separation pretreatments are simultaneously present, so that appropriate, safe and efficient recycling processes are required.

In general, different plastics recycling methods are already available, classified as “primary”, “secondary”, “tertiary”, and “energy recovery” [10].

Primary and secondary recycling processes, also identified as mechanical recycling, are related to the reprocessing of the WEEE-derived plastics into new products with similar or lower performance than the original ones. Both technologies involve grinding followed by washing and extrusion, giving rise to products to be used for the same purpose of the initial goods (primary recycling) or for different uses (secondary recycling).

The main drawbacks of these recycling methods are associated to both feedstock types and output products. In fact, just near-pristine plastics can be subjected to mechanical recycling, mainly pre-consumer wastes or post-consumer materials deriving from reliable sources. On the other hand, the repeated thermal treatments cause polymers degradation, resulting in a decline of the physicochemical properties, and then limiting the number of reprocessing cycles [5]. Therefore, the products obtained by mechanical recycling generally have a lower overall value compared to the starting material, so that the process is often called “downgrading” or “downcycling” [10].

Tertiary recycling, also identified as chemical recycling, refers to the processes which chemically convert the waste plastic into monomers or other valuable chemicals, such as building-blocks or fuels. An example of this class of technologies is pyrolysis, in which the polymers are thermally decomposed in absence of oxygen (see next chapter).

If compared with mechanical processes, chemical recycling can be applied to more complex matrixes, such as polymers mixtures. However, the presence of contaminants to be managed, as well as the significant energy inputs required, make it not easily implementable yet on industrial scale.

Finally, energy recovery consists of a waste-to-energy process, which involves the production of power and heat by plastics burning. However, this method is considered as the last valid option, since not only the energy generated by plastics burning is lower than the

1. INTRODUCTION

energy conserved by recycling [11], but also the presence of contaminants, such as BFRs, chlorine, and metals, can lead to the formation of green-house gases and toxins [5].

Therefore, it clearly appears that the existing recycling methodologies are closely related to the matrix composition, so that a complete physicochemical characterization of WEEE-derived plastic mixtures is essential prior to any treatment. In fact, due to the constant evolution of new electronic apparatus entering the market, it is not easy to define a priori the average composition of WEEE plastics, and this constitutes an additional problem in the improvement and scale-up of the recycling processes.

According to the latest estimate, in terms of types of polymers PP and PS account for about the 43 % of the total WEEE plastics, mainly complemented by PE, ABS, PA, PC, PBT, PMMA, PUR, and PVC [12]. With regard to the other components, chlorine and bromine amount on the average to the 2 and 1.5 %, respectively, while different metals (Sb, As, Cd, Co, Cr, Cu, Hg, Mn, Ni, Pb, Sn, and Zn) can be found in concentrations ranging from 1 to 1000 ppm [5].

In this context, pyrolysis represents the most suitable technology to enhance the highly heterogeneous WEEE-derived plastics mixtures, as high value-added products can be obtained not only by properly tailoring the process parameters, but also by selecting appropriate catalysts and/or sorbents for the contaminants management.

1.4 Thesis objectives and novelty

The primary purpose of this doctoral thesis is the valorisation of the WEEE-derived plastic fraction, which represents the only residue in the recycling process carried out by R.ED.EL. srl, in the view of driving the company to a zero-waste circular economy.

To this aim, the chemical (tertiary) recycling by fast-pyrolysis has been selected, since it represents a promising method to chemically convert the contaminated real waste plastic into valuable raw chemicals and fuels.

Despite the plastic pyrolysis process has already been widely investigated, most of the works in literature are focused on the understanding of reactions mechanisms and products distribution by using pure polymers mixtures as feedstock (see next chapter). The concerns

1. INTRODUCTION

regarding the presence of contaminants, as well as the intrinsic variability of real wastes, have been thus poorly addressed.

Furthermore, little attention has been paid on the distribution of halogen compounds, typically present as additives (BFRs) or as intrinsic composition of the polymer (PVC), during the pyrolysis process of real contaminated plastics wastes.

In this context, this work aims to reduce the research gap still existing in literature by investigating the thermo-catalytic fast-pyrolysis of a real PVC-containing plastic waste mixture (WEEE), with special focus on the chlorine distribution among the different products and, in particular on its concentration in the oil fractions.

To this purpose, this study was divided into different stages, that can be summarized as follows:

- Physicochemical characterization of the real waste plastic, in terms of polymers composition, chlorine quantification, presence of contaminants, and thermal behaviour.
- Synthesis and characterization of ZSM-5 zeolite catalysts, to be tested in the following catalytic pyrolysis of WEEE plastic, with different structural and acidic properties (Si/Al, pores size).
- Study of thermal dehydrochlorination treatment of the WEEE plastic as a function of the temperature, in the view of reducing the halogen content in the feedstock to be pyrolyzed, and thus in the following pyrolysis products.
- Investigation of the thermal fast-pyrolysis reactions (in absence of catalyst) of the real WEEE plastic as feedstock for the determination of the operating conditions.
- Study of the effects of reactions parameters (catalytic temperature, catalyst-to-feedstock ratio) and feedstock properties (raw and dechlorinated plastic) on the products and chlorine distribution in thermo-catalytic fast-pyrolysis experiments.
- Study of the impact of acidic and textural properties of synthesized ZSM-5 zeolites in pyrolysis vapours upgrading during the thermo-catalytic fast-pyrolysis of dechlorinated WEEE plastic, in the view of reaching high yields and low-chlorine content oils.

Therefore, the novelty of this doctoral thesis mainly lies in the improvement of the catalytic pyrolysis process so that it can be used for real waste plastics treatment, thus contributing to the development of efficient recycling strategies for the production of valuable chemicals and fuels from waste products.

2. PYROLYSIS OF PLASTIC MATERIALS

2.1 Thermal decomposition of plastics

Pyrolysis is a thermal decomposition process in which feedstock materials undergo thermal-induced cracking reactions, in an oxygen free environment.

On the basis of the reaction conditions and material properties, the heating of the feedstock can cause physical (e.g., melting) or chemical transformations. These last consist of the breaking of chemical bonds, that can occur homolytically, producing two radicals, or heterolytically, leading to charged ions formation. The progressive bonds breaking produces compounds in a wide molecular weight range, which can then undergo secondary reactions, such as further decomposition and/or recombination. Downstream the reactions, the formed products are split into a solid fraction and a vapour stream, which leaves the bulk material usually conveyed by an inert gas flow. Depending on their nature and molecular weight, some compounds can be condensed in liquid phase, while the others are permanent gases. Therefore, the final reaction products consist of three main fractions, i.e., liquid, gas, and the carbonaceous solid residue identified as char.

In general, the plastic-derived oil may consist of a light liquid fraction and/or a high viscosity wax. This last is predominantly composed of alkanes and alkenes with a high boiling point ($> C_{20}$) and it is typically an intermediate product which requires further cracking processes to be converted into liquid fuels [13].

The light liquid pyrolysis oil can be a promising precursor for fuel applications, since its composition can be tailored by adjusting the pyrolysis parameters, as discussed in the next sections. It usually consists of hundreds of aliphatic and aromatic hydrocarbons in a wide molecular weight range, which can be used, once properly treated, as source of gasoline ($C_4 - C_{12}$) and diesel ($C_{12} - C_{20}$), as well as of raw chemicals [14]. Moreover, the plastic pyrolysis-derived oil can be also subjected to further reforming, to be converted into valuable gaseous products, e.g. ethylene and propylene.

The plastic pyrolysis-derived gas fraction is generally made up of light paraffins and olefins in $C_1 - C_4$ carbon number range (methane, ethane, ethylene, propane, propene, butane, and butene), also including carbon mono-oxide and dioxide in presence of oxygenated feedstock (e.g. PET). The gaseous products can be used as an energy source, even in the pyrolysis

2. PYROLYSIS OF PLASTIC MATERIALS

process itself to make it self-sufficient, or as raw chemicals after appropriate separation processing. [15].

Finally, a solid carbonaceous residue (char) is generally produced from the pyrolysis of plastic materials, which is usually considered as a by-product but it has recently found applications e.g. as adsorbent material (activated carbon), and additive in epoxy resins and in concretes [16].

The products composition and distribution are strictly related to the feedstock properties, as well as the process parameters, i.e., temperature, heating rate, type of reactor, the presence of catalyst, among others. The main factors affecting the pyrolysis reaction and their impact on the products yield will be outlined in the next sections.

2.1.1 Feedstock composition

Different works are reported in literature studying the pyrolysis of single and mixtures of pure polymers. It has been showed that the thermal cracking of polyvinyl polymers, such as PE, PS, and PP involves a chain radical mechanism, which leads to a random cleavage of the C-C backbone bonds, without involving the side functional groups. The reaction pathway consists of three reaction mechanism steps, i.e., initiation, propagation, and termination.

The first step (initiation) is mainly related to C-C random scission, which leads to the formation of two end-chain radicals. The intermediate radicals can undergo different intramolecular or intermolecular reactions, such as disproportionation, H-transfer and abstraction, β -scission, and isomerization, resulting in a wide range of unstable compounds.

The termination reactions occur when the unstable radicals react to form stable molecules.

Quite different thermal cracking mechanisms have been observed for polymers incorporating heteroatoms. Among the most commercially employed plastics, PET and PVC have been widely studied as feedstock in thermal pyrolysis reactions.

The thermal decomposition of PET starts from random scission of ester bonds via β -hydrogen transfer, leading to the formation of carboxylic acid and olefinic-end groups. The primary products further decompose by ester scission, decarboxylation and decarbonylation reactions, mainly resulting in CO₂, acetaldehyde, benzoic acid, vinyl benzoate, and divinyl terephthalate [17].

2. PYROLYSIS OF PLASTIC MATERIALS

Different thermal decomposition pathways have been proposed for Polyvinylchloride [18], all consisting of multi-steps mechanisms. In general, based on the binding energies, the PVC cracking firstly involves the breaking of C-Cl and C-H bonds, which already occurs during the melting stage (in 200 – 300 °C temperature range). This leads to hydrochloric acid release from side-groups-elimination and unsaturated chains formation. Subsequently, (2) random chain scission and recombination, (3) cyclization/aromatization, and (4) degradation from coke formation take place, according to Gui et al [19]. However, Marongiu et al. demonstrated the complexity in defining a certain reaction pathway, since more than 250 reactions involving several intermediate radicals simultaneously occur after the dehydrochlorination step, due to the chains rearrangement through cyclization and cross-linking reactions [20].

The differences in the polymers structure result therefore in different reactions pathways, which in turn drive the products distribution and composition. Polyolefinic polymers (PE and PP) thermal cracking results in olefins and paraffins mixture, covering a wide range of carbon number (C1 – C>40). However, each fraction consists mainly of the respective alkane, 1-alkene, and diene, since the branching formation during the pyrolysis is precluded [21]. The thermal degradation of PS mostly leads to high yields of styrene monomer, ranging from about 50 to 80 %, complemented by other aromatics, such as styrene oligomers, benzene, and ethylbenzene [22,32]. Moreover, relatively high methane concentration and low char formation have been observed under different operating conditions [23,24].

Thermal pyrolysis of PET gives rise mostly to gaseous products and this is attributed to the volatility of its original constituting monomers resulting from condensation polymerization of ethylene glycol and terephthalic acid. The formed gases are rich in ethane, as well as in CO and CO₂, due to the presence of oxygen in the polymer structure. The oil fraction accounts for 30 – 40 wt.%, half of which is made up of benzoic acid [18,19,25].

As mentioned above, PVC represents one of the most challenging polymers to pyrolyze, being high yields of HCl (> 50 wt.%) released during the process (see section 2.3). On the other side, the thermal pyrolysis of PVC leads to the formation of high-aromatics content oils (mainly BTX), as well as low char quantity, which varies according to the operating conditions [14,20].

An important issue is related to the decomposition behaviours of the polymers when blended, as they effectively are in the real wastes. It has been showed that, in general, the pyrolysis

2. PYROLYSIS OF PLASTIC MATERIALS

of polymers mixtures leads to the formation of lower oil yields (≈ 50 wt.%), compared to the single polymers degradation [26,27,30], and that this effect is even more pronounced in presence of PS, which shifts the products distribution toward the gaseous fraction [28].

On the other hand, Miskolczi *et al.* have conducted pyrolysis experiments by mixing different concentrations of PVC (from 0 to 3 %) to HDPE, PP, and PS, in a horizontal tubular reactor at 530 °C, with a holding time of 25 mins. Reported results show that with the PVC content rise, both total conversion and aromatics concentration in oil were augmented, together with the hydrochloric acid content in the gaseous phase [29].

More recently, Li *et al.* investigated the interaction effects of the plastics components during the pyrolysis in a TG analyser equipped with FT-IR (semi-batch mode), from 30 to 800 °C, at 10 °C/min [30]. By pyrolyzing PS, PE, and PVC in various combinations and proportions, the authors demonstrated that the different reactions pathways occur, compared to the single polymers decompositions, according to the type of plastics which constitute the mixture. More specifically, the decomposition of PE proved to be delayed by the presence of PS. On the contrary, the PS cracking was enhanced, due to the reactions between PE-hydrogen and PS-derived radicals. The simultaneous presence of PVC and PE led to an increment of both chlorinated hydrocarbons and HCl released, related to the interaction between the chlorine (from PVC) and H (from PE) radicals. Also PVC and PS polymers influenced each other, resulting in a mutual decomposition improvement. In this case, the reaction pathway involves two stages, i.e., i) the HCl release from PVC and the concurrent depolymerization of PS into its monomer, and ii) the cracking of the resulting conjugated alkenes. Furthermore, the hydrochloric acid release was inhibited by the presence of polystyrene, due to the transfer of chlorine radicals from PVC to PS-derived non-stable compounds.

Finally, just the PS decomposition was enhanced, if compared to the pure polymer pyrolysis, when a mixture of PE, PS, and PVC was pyrolyzed, whilst PE and PVC cracking proved to be delayed. However, taking into account the complexity of the inter-polymer reactions, as well as the great variety of radicals developed, a comprehensive understanding of the reactions pathways is still difficult to achieve [28].

2. PYROLYSIS OF PLASTIC MATERIALS

2.1.2 Operating parameters

The pyrolysis process parameters play a key role in optimizing both products yields and composition, since they impact on the formation of gas, oil and char fractions. Different works are present in literature investigating the influence of each single parameter on the whole pyrolysis process, even if the complete assessment is difficult due to the mutual dependence among the variables. For instance, the pyrolysis temperature is related to the heating rate, and both parameters are linked to the type of reactor used [31].

However, the cracking temperature represents one of the most important variables among the others, since it dominates the polymers cracking reactions providing the energy required to break the chains bonds.

Pyrolysis temperature

As mentioned above, polypropylene, polystyrene, and polyethylene show different thermal degradation behaviours, despite being all constituted only by carbon and hydrogen atoms. The breaking of PS chain bonds already starts at 350 °C, mainly resulting in a dark heavy viscous fraction [32]. By pyrolyzing the pure polymer in a batch pressurised autoclave reactor with a heating rate of 10 °C/min, the maximum oil yield can be obtained at 425 °C, whilst temperature higher than 450 °C shifts the products distribution towards gas and coke formation [33].

Instead, even higher temperature is required to maximize the oil production from the thermal pyrolysis of PP (447 °C), as shown by Marcilla *et al.*, which pyrolyzed the pure polymer in a thermobalance at 5 °C/min [34]. Moreover, it has been demonstrated that the thermal degradation of PP occurs faster compared to linear polymers, such as HDPE, since the presence of side-groups tertiary carbons favours the formation of the more stable tertiary cations and radicals [35].

As mentioned to earlier, the degree of branching of the polymer chain, as well as the side-groups properties, affect its thermal degradation behaviour. This applies to high- and low-density polyethylene (HDPE and LDPE), which differ in the branching intensity, showing linear and branched structures, respectively. The HDPE thermal cracking starts at around 390 °C [36], while LDPE requires a slightly higher temperature, i.e., 410 °C [32].

2. PYROLYSIS OF PLASTIC MATERIALS

Furthermore, significant differences have been observed in terms of the cracking temperature that promotes the oil production, since 467 °C was identified as the best temperature for HDPE, whilst 425 °C, 480 °C, and 550 °C were detected for LDPE, depending on both the branching degree of the feedstock and the other process parameters [32,34,37,38].

The thermal degradation temperature of PET extends from 350 to 520 °C, whilst that of PVC covers an even wider range, i.e., 260 – 520 °C [39]. However, it must be recalled that the thermal decomposition of polyvinylchloride occurs in two steps, which include the HCl removal in 260 – 385 °C temperature range. Therefore, the polymer chain cracking takes place in the same temperature range as the other polyolefins polymers, i.e., 385 – 520 °C.

It is possible to conclude that, since the temperature drives the pyrolysis products distribution by controlling the cracking reactions, it should be properly selected on the basis of the required target products. In fact, for all the described polymers, the oil yield proved to be maximized in 300 – 500 °C temperature range, whilst higher temperatures (> 550 °C) should be chosen in the view of shifting the equilibrium toward gas and char production [31].

Type of reactor

The type of reactor is another fundamental parameter to consider since the heat transfer, the pyrolysis vapours residence time, and the feasibility of the whole pyrolysis process directly depend on it. A wide variety of reactors have been developed and tested in the plastics pyrolysis processes, and the characteristics, benefits and challenges of the main types are described below.

Batch and semi-batch reactors have similar and simple configuration, consisting of a reactor body in which the feedstock is located and heated up. However, a batch reactor is completely closed, without any inflow or out-flow of reactants and products, whilst in a semi-batch system the pyrolysis products in vapour phase are conveyed outside the reactor while the pyrolysis reaction is carried out [40]. The main advantages of these systems lie in the easy operating conditions control and high conversions. On the other hand, the scale up is problematic since the products composition and distribution are difficult to be controlled, being strictly related to both the type of batch and the secondary reactions of the pyrolysis products, especially in the closed system because of the long vapours residence time.

2. PYROLYSIS OF PLASTIC MATERIALS

Moreover, the carbonaceous solid residue (char fraction) is accumulated inside the reactor at the end of the reaction, so that the separation of the products proves to be complex, and even more in presence of a catalyst, which is directly mixed with the feedstock [31].

Fixed-bed systems usually involve a stainless-steel reactor in which the feedstock is located and externally heated by an electrical furnace. The formed vapours are continuously discharged from the reactor by an inert gas flow while the reaction is occurring, whilst the char fraction remains inside and is collected at the end of the pyrolysis process. This is one of the most used reactors for lab-scale pyrolysis of plastics since it proves to be low-cost and of simple design. However, a uniform heating is hard to achieve when large amounts of feedstock are employed, and this represents the main drawback for the implementation of this system on industrial scale [40].

Fluidized-bed reactor is usually used for fast-pyrolysis experiments, favouring low residence times. The fluidizing gas passes through the feedstock, which is located on a distributor plate, carrying the particles in a fluid state. In such a system, the main advantage lies in the enhanced heat and mass transfer, as well as the improved accessibility of the catalyst, when it is used, reducing the variability of the process. On the other side, the char separation from the bed (and the catalyst, if present) and the need to use small particles still remain the main limits for the scale-up of this system [40,41].

Spouted bed reactor (CSBR) consists of a conical system in which the feedstock is continuously fed over the annular zone of the bed by an inlet tube. The inertizing gas is piped from the bottom part, so as to lead the particles to a vigorous cyclic movement. The improved heat and mass transfer makes this system suitable for flash pyrolysis of mixed materials (e.g., MSW), as well as for handling particles with a wide size distribution. Moreover, CSBR operates continuously, favouring the use on larger scale. Nevertheless, also in this case the separation of the pyrolysis products from the bed can be difficult, as the char remains within the reactor, and the problem becomes even more pronounced when a catalyst is employed [40].

Rotary kiln reactor is made up of a horizontal heated system in which the feedstock can be charged continuously or in batch mode. The rotation improves both heat transfer and solid mixing, if compared with the fixed-bed reactors, and the simple configuration makes it suitable for the industrial scale-up. However, it requires long residence times, so that it can be mostly employed in slow-pyrolysis processes [40].

2. PYROLYSIS OF PLASTIC MATERIALS

It must be considered that the type of reactor, together with the other process parameters, strongly affects the products composition and distribution. Just to give an example, Sakata *et al.* carried out HDPE thermal pyrolysis experiment in a glass reactor in batch mode, by heating the sample at 3 °C/min up to 430 °C. In these reaction conditions, the oil fraction accounted for 69.3 wt.%, whilst the 9.6 and 21.1 wt.% were collected as gas and char, respectively [42]. A similar test was conducted by Seo *et al.*, which pyrolyzed HDPE in batch mode by adding an internal stirrer system working at 200 rpm. The improvement in mass and heat transfer promoted by the stirring moved the product distribution toward oil formation, accounting for the 84 wt.%, despite the other variables being comparable (heating rate = 5 °C/min, pyrolysis temperature = 450 °C) [43]. When a CSBR in continuous mode was employed for the thermal pyrolysis of pure HDPE, the 80 wt.% accounted for solid heavy wax at 450 °C, and just a residual 20 wt.% of lighter compounds was obtained due to the much lower residence time of the vapours in the reactor [13]. Flash-pyrolysis experiments in a fluidized bed reactor were carried out by Del Remedio Hernández *et al.* At 500 °C and with a very short vapours residence time (1.3 – 1.7 s), HDPE decomposed giving rise to the 40.9 wt.% of oil, complemented by 7.4, 15.2, and 36.5 wt.% of wax, gas and char, respectively [44]. More recently, a new fixed-bed reactor has been developed and tested by Al-Salem in the thermal pyrolysis of the same pure polymer. By heating the sample at 5 °C/min up to 500 °C, a total of 60 % of liquid fraction (consisting of wax and oil) was detected, whilst the remaining part was equally divided into gas and char [45].

Pyrolysis vapours residence time

Another important parameter is the residence time of the pyrolysis vapours, on the basis of which (as well as of the other previously described parameters, i.e., temperature and type of reactor) the pyrolysis processes are classified into slow, fast and flash pyrolysis (Table 1) [59].

2. PYROLYSIS OF PLASTIC MATERIALS

Table 1 - Type of pyrolysis processes and target products.

Process	Heating rate	Residence time	Temperature	Target products
Slow pyrolysis	10 – 100 °C/min	10 – 60 min	450 – 600 °C	Gas, char, oil
Fast pyrolysis	Up to 1000 °C/min	0.5 – 5 s	550 – 650 °C	Oil, gas, char
Flash pyrolysis	Up to 10000 °C/min	< 1 s	450 – 900 °C	Oil, gas, char

Different definitions have been reported for the residence time: in general, it is described as the time the feedstock particles spend inside the reactor [46]. However, in fast or continuous pyrolysis processes it refers to the contact time of the feedstock inside the reactor, whilst in slow and batch pyrolysis it is related to the total time between the start of the heating and the products removal.

In addition to those already described, also this variable strongly affects the pyrolysis products distribution, since the occurrence of secondary reactions depends on it. In fact, long residence times favour the further cracking of the primary pyrolysis vapours, resulting in the formation of more thermally stable compounds (lighter hydrocarbons and non-condensable gases) [31,35,47]. The carbonization is also promoted in these reaction conditions, which moves the products distribution toward char formation [59].

Moreover, it has been showed that the influence of the vapours residence time on the products distribution is related to the pyrolysis temperature. In this concern, Mastral *et al.* studied the effects of the residence time at different pyrolysis temperatures by pyrolyzing pure HDPE in a fluidized bed reactor, demonstrating that the lower the temperature, the stronger the influence of the residence time on the gas formation [48]. This finding was also confirmed by Onwudili *et al.*, which pyrolyzed LDPE in a closed batch reactor, detecting an increment of about 20 wt.% of the gaseous fraction by increasing the residence time from 0 to 120 min [32].

However, while a closed pyrolysis system (batch reactor) allows a simple measurement of the vapours residence time (from the start of the heating to the products collection), semi-closed and continuous processes need an indirect assessment by adjusting other parameters i.e., the feeding rate, the inert gas flow, and the products discharge rate [59].

2. PYROLYSIS OF PLASTIC MATERIALS

Therefore, despite the great variety of works existing in literature and investigating the effects of the operating parameters on the pyrolysis products composition and distribution, the complexity related to the mutual dependence among the variables makes this research field still challenging.

2. PYROLYSIS OF PLASTIC MATERIALS

2.2 Catalytic pyrolysis of plastics

As previously described, the thermal pyrolysis of pure and mixed plastics requires medium-high temperatures and long residence times, and it results in long and mainly straight hydrocarbons covering a wide range of carbon numbers, from C1 to C80, especially in the case of PE polymers decomposition.

In this concern, the use of catalysts allows improving the pyrolysis products quality, by simultaneously increasing the conversion rate at lower temperature and time, compared to the thermal pyrolysis process, and then reducing the overall energy costs. One of the main purposes of using a catalyst is to shorten the carbon chain length of the pyrolysis products, considering that petroleum fuels, such as LPG, petrol, kerosene, and diesel, are made up of hydrocarbons in the carbon number range C1 - C24. Moreover, catalysts can be specifically applied to promote secondary reactions, such as isomerization, cyclization, and aromatization, increasing therefore the yields of more valuable hydrocarbons [49].

Homogeneous and heterogeneous catalysts have been studied for the catalytic cracking of plastics. In homogeneous catalysis, Lewis acids, such as $AlCl_3$, have been tested in PO polymers decomposition [50]. However, heterogeneous catalysts are preferred due to the easier separation and recovery from the reacting medium.

A solid catalyst can be either directly contacted with the plastic feedstock (*in-situ* conditions) or with the primary pyrolysis vapours (*ex-situ* conditions) [51,52,53,54,55]. If compared with the *in-situ* catalytic mode, the vapours phase contact mode (*ex-situ*) requires higher pyrolysis temperature and times [56, 57]. However, it allows an easier separation of the catalyst from the solid pyrolysis products and prevents its deactivation related to the physical blockage from the melted plastic, as well as from the impurities deposition [55,58].

Different solid catalysts have been tested in both *in-situ* and *ex-situ* catalytic pyrolysis of plastic materials, such as zeolites, mesoporous aluminosilicates, metal oxides and metals over different supports [59].

Among the catalysts investigated up to now, zeolites exhibit excellent performance in polyolefins pyrolysis due to their acidity and pore architecture [60,61], and this type of catalysts will be discussed in more details as follows.

2. PYROLYSIS OF PLASTIC MATERIALS

2.2.1 Zeolites in catalytic pyrolysis of plastics: structure and mechanism

Zeolites structure and properties

Zeolites are a wide range of natural and artificial crystalline aluminosilicates formed by well-defined three-dimensional frameworks of silicon and aluminium atoms, which are tetrahedrally coordinated through shared oxygen atoms. The three-dimensional arrangement of SiO_4 and AlO_4 tetrahedra (TO_4) generates nanometric-sized structure voids and cages, and the channels size is defined on the basis of the number of T-atoms forming their entrance (Figure 2.1). According to this definition, zeolites are classified in small, medium, and large pores zeolites, consisting of up to 8, 10, and 12 member-ring channel openings, respectively [62].

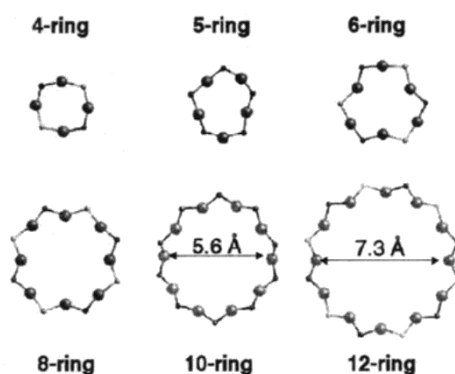


Figure 2.1 - Size of rings in the zeolitic frameworks (adapted from [63]).

On the basis of the three-dimensional structure, 176 zeolite framework types have been confirmed, classified with a three-letter code (Figure 2.2) [64].

2. PYROLYSIS OF PLASTIC MATERIALS













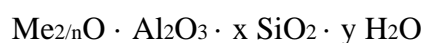
<p>5T</p>  <p>LOV, NAB, OBW, OSO, RSN, VSV, WEI</p>	<p>6T</p>  <p>EDI, NAT, THO</p>	<p>6T</p>  <p>LOV, NAB, OBW, -RON, RSN, VNI, VSV, WEI</p>	<p>7T</p>  <p>AFN, CGF, MEI, USI</p>
<p>8T</p>  <p>ACO, AFY, AST, ASV, BEC, -CLO, DFO, ISV, ITH, ITW, IWR, IWV, IWW, LTA, UFI, UOZ, UTL</p>	<p>8T</p>  <p>*BEA, BEC, DAC, EON, EPI, IMF, ISV, IWW, MEL, MFI, MOR, MSE, RWR, TUN</p>	<p>8T</p>  <p>AFR, DFO, OWE, SAO, SBE, SBS, SBT, SFO, STI, ZON</p>	<p>10T</p>  <p>*BEA, CON, IFR, MSE, STT</p>
<p>10T</p>  <p>BOG, BRE, CON, HEU, IWR, IWW, RRO, STI, TER</p>	<p>10T</p>  <p>JBW, MTT, MTW, SFE, SFN, SSY, TON</p>	<p>11T</p>  <p>CFI, IMF, MFS, MTT, SFE, SSY, SZR, TON, TUN</p>	<p>12T</p>  <p>AEL, AET, AFI, AFO, ATV, DON, SFH, VFI</p>

Figure 2.2 - Zeolite framework types and number of T-atoms in the unit (adapted from [60]).

In general, the zeolites chemical composition is defined as follow:



Where Me is any alkali or alkaline earth atom, n is the valence charge of Me atom, x is the number of Si tetrahedron varying from 2 to ∞ , and y is the number of water molecules [65]. The IA or IIA group metal (Me), such as sodium, potassium magnesium and calcium [62], represents an exchangeable cation which allows to balance the negative charge characteristic for certain zeolite frameworks and related to the presence of trivalent atoms (typically Al) in the tetrahedral units (Figure 2.3).

2. PYROLYSIS OF PLASTIC MATERIALS

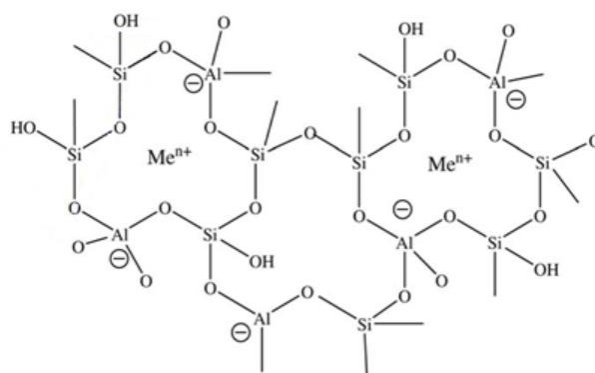


Figure 2.3 - Two-dimensional representation of the zeolite framework (adapted from [60]).

Zeolites can be also classified according to the Si/Al ratio as “low silica zeolites”, “intermediate silica zeolites” and “high silica zeolites”, as listed in Table 2 [66,67].

Table 2 - Classification of zeolites on Si/Al ratio basis [64].

Zeolite grade	Si/Al molar ratio	Some common zeolites and their framework codes
Low silica	≤ 2	Analcime (ANA), Cancrinite (CAN), Natrolite (NAT), Phillipsite (PHI), Sodalite (SOD)
Intermediate silica	2 – 5	Chabazite (CHA), Faujasite (FAU), Mordenite (MOR)
High silica	> 5	ZSM-5 (MFI), Zeolite- β (BEA)

The aluminium content strongly affects the zeolites catalytic performances, since the structural and the acidic properties depend on it. In fact, as mentioned above, it generates a formal charge of -1 by tetrahedrally coordinating in the framework unit. The negative charge can be balanced by a metal cation or by a hydrogen ion H^+ , giving rise to a weak Lewis acid site (L-AS) or a strong Brønsted acid site (B-AS), respectively (Figure 2.4) [62,68].

2. PYROLYSIS OF PLASTIC MATERIALS

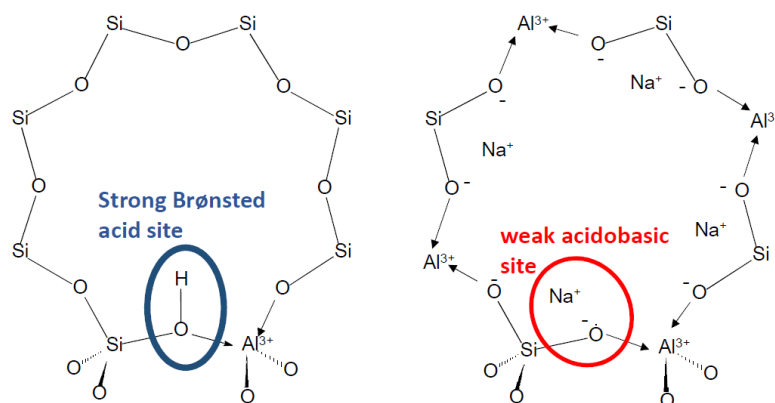


Figure 2.4 - Representation of strong B-AS and weak L-AS in the zeolite framework (adapted from [69]).

Therefore, the amount of B-AS can be modulated by varying the Al content, and then by reducing the Si/Al molar ratio. Moreover, the H^+ strength in Si-OH-Al bridge is dependent on the Si-O-T angle, which affects the distribution of the partial negative charge, and can be controlled by substituting Al atom with other trivalent cations, such as Ga, Fe, B, resulting in Brønsted acid sites with a strength decreasing in the order $SiOHB < SiOHFe < SiOHGa < SiOHAl$ [70].

Also the nature of L-AS in the zeolites is related to both aluminium content and environment. In fact, extra-framework Al^{VI} (EFAL) species in octahedral coordination are usually referred as Lewis acid sites, since they exhibit a positive vacancy able to accept an electron pair [71,72]. EFAL, as well as other aluminium species acting as L-AS (AlO^+ , $Al(OH)_2^+$, $AlO(OH)$, and $Al(OH)_3$), are commonly generated during the calcination process at temperature above 500 °C [62,72]. However, the location and nature of these sites are still a matter of debate, since various studies reported the presence of L-AS in zeolites even in absence of EFAL species, being attributed to tri-coordinated Al, partially located within the zeolite framework [73,74].

Therefore, a proper setting of both acid sites concentration and typology represents a key factor for using zeolites as catalysis in plastics pyrolysis processes, and this matter will be further discussed below.

Besides the acidity, zeolites are widely used as catalysts due to their molecular shape-selectivity properties, which are directly related to their microporous structure. In fact, this

2. PYROLYSIS OF PLASTIC MATERIALS

last drives the transformation of reactants in products by sterically confining them, so that the occurrence and rate of conversion are strictly dependent on how the molecules spatially fit the active sites of the catalyst. Zeolites act then as sieves on a molecular scale, giving access to, and letting out from the crystal, just molecules of appropriate size, which have been adsorbed and reacted on the internal catalytic sites [62,63,65].

It must be considered that due to the comparable size between molecules and zeolites channels, the diffusing molecules continuously suffer from the interaction with the solid walls [75]. In this concern, the crystal size plays a key role, since too large crystals slow down the mass transfer leading to a too fast catalyst deactivation for pore filling, whilst too small crystals may result in uncomplete catalyst activity due to the too fast species diffusion [76]. Therefore, besides the tuning of acidity and channels size, the crystals size can be modulated in the view of reducing diffusional limitations. To the same purpose, hierarchical structures have been recently developed, consisting of interconnected micro- and mesopores, which allow to keep the shape-selectivity and to improve the diffusivity, respectively [77,78].

Plastic cracking mechanism of zeolites

The reactivity of zeolites towards hydrocarbons is due to the presence of both Brønsted and Lewis acid sites in the framework. According to their nature, B-AS protonate the polymer chain, resulting in pentacoordinated carbonium ions, whilst L-AS promote hydride abstraction, generating carbenium ions [59]. Therefore, the catalytic cracking takes place following carbocationic reaction pathways, in contrast with the thermal cracking, which proceeds toward radical mechanisms (see section 2.1) [79,80].

In general, the first step of the catalytic decomposition thus involves the formation of a carbocation, which is even more favoured in presence of branchings and double bonds, that constitute more reactive points of the carbon chain. The formed carbocation can then undergo disproportionation and/or β -scission reactions, this last giving rise to a shorter carbenium ion and a shorter olefin. On the basis of the acid strength of the catalyst, the polymer breaking can be either random or end-chain, in presence of weak-medium or strong acidity, respectively. Afterwards, the primary cracking products can undergo secondary reactions, such as isomerization, oligomerization, cyclization, and aromatization, resulting

2. PYROLYSIS OF PLASTIC MATERIALS

in a wide range of hydrocarbons. The mechanism of catalytic cracking of polyolefins over acid solid catalysts and the overview of the resulting products are shown in Figure 2.5.

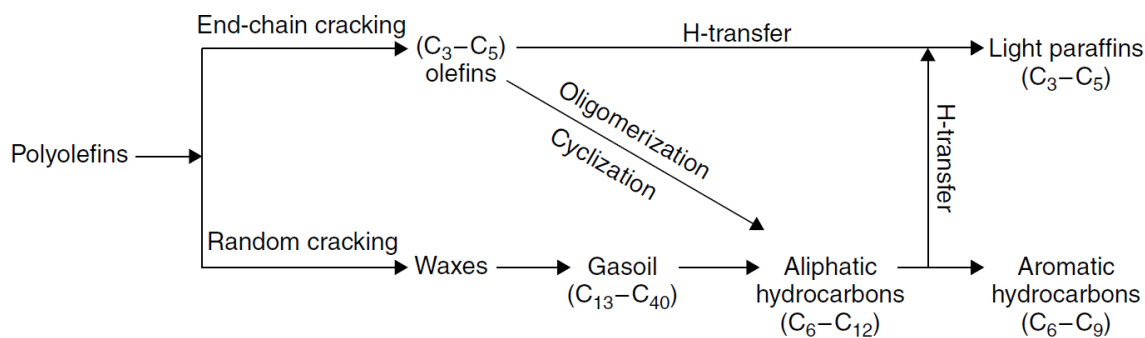


Figure 2.5 - Products and reaction pathways of catalytic cracking of polyolefins over acid solid catalysts [181].

In terms of products distribution, the random cracking over weak acid sites mainly leads to the formation of waxes and middle distillates, such as gasoil and gasoline, comprising a huge variety of isomers which are difficult to be separated. Therefore, this fraction can mostly be used as fuel or, alternatively, subjected to a further upgrading.

On the other hand, the strong acid sites-mediated end-chain cracking results in lighter hydrocarbons in C3 – C5 carbon numbers, which are easier to be separated since the number of possible isomers are lower in this molecular weight range. This is a valuable fraction covering a wider range of applications, since light paraffins and olefins can be used as fuel and raw chemicals.

Depending on the type of catalyst, the reaction operating conditions (temperature, vapours residence time, type of reactor) and the formed intermediates, secondary reactions can further occur, leading to the formation of linear, branched or cyclic aliphatics and/or aromatics hydrocarbons [59].

Finally, besides being responsible for cracking reactions, the zeolite acid sites also determine the coke formation [81,82,83]. The coke deposition reduces the overall catalyst activity, as well as it affects the products distribution, by reducing aromatics and paraffins yields due to the decline of hydrogen transfer reactions over the deactivated acid sites [84,85].

2. PYROLYSIS OF PLASTIC MATERIALS

Both Lewis and Brønsted acid sites suffer deactivation by coke deposition, although the last in a larger extent [82]. In addition, weak acid sites deactivate much more slowly than the stronger ones [84].

Two types of coke have been identified as a result of the HDPE pyrolysis in presence of ZSM-5 zeolites [84], labelled as coke I and coke II. Coke I formation preferentially occurs over the catalyst external surface and it mainly consists of aliphatic compounds. In contrast, coke II is mostly made up of aromatics, deposited inside the zeolite micropores. Accordingly, the maximum combustion rates in TG experiments proved to be in the ranges 440 – 460 °C and 520 – 540 °C for coke types I and II, respectively.

While the coke formation is mainly related to the acid sites catalytic activity, the degree of deposition is predominantly dependent on the zeolites pores size, since the smaller the pores, the greater the constraints which inhibit the growth of coke precursors. Thus, ZSM-5 zeolite undergoes lower deactivation, if compared for instance to Y and Beta zeolites, in agreement with the respective pores size (ZSM-5: $D \approx 0.55$ nm; Beta: $D \approx 0.65$ nm; Y: $D \approx 0.74$ nm) [81,86].

Therefore, in the view of driving the products distribution towards specific valuable hydrocarbons families, it is necessary to select an appropriate catalyst to be employed in the catalytic pyrolysis of plastic materials. However, apart from promoting specific reaction pathways, a proper catalyst should be also able to overcome steric hindrances, allowing the bulky molecules to access to the acidic active sites [87], by simultaneously limiting the deactivation by coke deposition. Several efforts have been made to this end, by designing catalysts with enhanced external surface and bimodal pore size distributions (micropores and mesopores), as in the case of nanocrystalline and hierarchical zeolites.

2.2.2 Literature overview on zeolites as catalyst in plastics pyrolysis

Different zeolites have been tested as catalysts in the catalytic pyrolysis of pure and mixed plastics. As described above, an overall increase of light gaseous hydrocarbons is generated as a function of the increasing acid strength of the zeolitic catalyst, due to the improvement in the cracking reactions effectiveness. However, since the secondary reactions are also promoted by this type of catalysts, the quality of produced oils proves to be enhanced, both

2. PYROLYSIS OF PLASTIC MATERIALS

in terms of selectivity and narrower carbon numbers distribution, compared to the thermal pyrolysis products.

In this regard, Artetxe *et al.* pyrolyzed pure HPDE in presence of HZSM-5 with Si/Al ratios ranging from 30 to 280. With the total acidity rise, the gaseous olefins yield was increased by 22 wt.%, at the expenses of the C12 – C20 fraction. On the other hand, the oil obtained with the highest acidic catalyst proved to be richer in light alkanes and aromatics, especially benzene [88]. By pyrolyzing PE over HZSM-5 and in similar operating conditions (batch reactor), both Panda *et al.* and Van Grieken *et al.* have confirmed that cracking and aromatization reactions pathways are promoted, also proving that isomerization reactions play a key role, since shorter branched hydrocarbons were formed rather than longer linear paraffins and olefins observed in thermal pyrolysis-derived oils [89,90]. Similar results were also observed in the catalytic pyrolysis of pure PP in presence of HZSM-5, which led to a high gaseous fraction yield and an oil with a high content of aromatics and branched aliphatics, indicating the strong cracking activity of the catalyst, as well as its efficiency in promoting secondary reactions [43,91]. Aguado *et al.* investigated the catalytic conversion of LDPE between 425 and 475 °C in a two-steps reaction process (semi-batch and fixed bed reactor), in which the primary thermal pyrolysis vapours were carried through the n-HZSM-5 catalyst bed by the inert gas flow. In this configuration, just the 22 % of oil was recovered at the highest temperature, being instead favoured the light hydrocarbons formation. Moreover, the authors demonstrated the close relationship between the process temperature and the catalyst activity in terms of conversion [55]. The influence of the pyrolysis temperature on the products distribution in presence of HZSM-5 catalyst was also showed by Seo *et al.* and Hernandez *et al.*, by pyrolyzing HDPE at 450 and 500 °C, respectively. The oil yield decreased from 35 % to 4 % with the temperature rise, in favour of gaseous fraction formation, which was augmented by 21 wt.%, despite being the other pyrolysis process parameters comparable [43,92].

Besides HZSM-5, other zeolites have been tested as catalysts in the plastics pyrolysis processes. The efficiency of HUSY and HMOR catalysts was investigated by Garfoth *et al.*, and compared with that of HZSM-5 zeolite, in HDPE pyrolysis using a fluidised-bed reactor operating in the 290 – 430 °C range. In terms of conversion, the tested catalysts followed the order HZSM-5 > HUSY > HMOR, resulting in solid residues equal to 4.5, 7.1, and 8.9 wt.%, respectively. Furthermore, HZSM-5 showed the highest selectivity toward C3 – C5 olefins

2. PYROLYSIS OF PLASTIC MATERIALS

(over 80 wt.%), whilst HMOR and HUSY produced more paraffinic compounds centred at C4 (19 and 14 wt.%, respectively). Finally, both HMOR and HUSY deactivated for coke deposition faster than HZSM-5, and all observed differences have been attributed to the differences in the investigated zeolites structure [93].

A comparison between the HZSM-5 and HUSY catalytic efficiency was also carried out by Marcilla *et al.* by separately pyrolyzing pure HDPE and LDPE at 550 °C in a batch reactor. HUSY zeolite resulted in higher oil yields, accounting for 41 and 62 wt.% with HDPE and LDPE, respectively, compared to 17 and 18 wt.% detected in presence of HZSM-5, this last leading to the 73 and 71 wt.% of gaseous products [37].

Similar trend of products selectivity was reported by Lin and Yen who tested the same catalysts (HZSM-5 and HUSY zeolites) in PP catalytic pyrolysis in a fluidized bed reactor, under different operating conditions. At 360 °C and with a feedstock-to-catalyst ratio of 40 wt.%, HZSM-5 produced just the 2.3 wt.% of liquid oil, complemented by around 95 and 4 wt.% of gases and char, respectively. On the other side, in presence of HUSY and in the same reaction conditions, the oil yield increased up to 4 wt.%, at the expenses of gases, reaching the 6 and 5 wt.% lowering the temperature to 290 °C or the feedstock-to-catalyst ratio to 100 wt.%, respectively, and then demonstrating that not only the temperature, but also the relative amount of catalyst affects the polymer decomposition [94].

Serrano *et al.* conducted catalytic pyrolysis experiments of a polymers mixture (LDPE = 46.5 %, HDPE = 25 %, PP = 28.5 %) in a semi-batch reactor at 400 °C, comparing the activity of various catalysts which differ in structure and acidity. The acid strength of the investigated catalysts increases in the order HZSM-5 > n-HZSM-5 > HBeta > HMCM-41 > HY \approx amorphous silica-alumina (SA). However, as showed in Figure 2.6, the observed conversion was not proportional to the acidity, being instead directly related to the catalysts structure. In fact, the high activity of HBeta has been attributed to the large micropores size accompanied by a medium acidity, whilst that of HMCM-41 has been ascribed to the large surface area, as well as the mesoporous structure [95].

2. PYROLYSIS OF PLASTIC MATERIALS

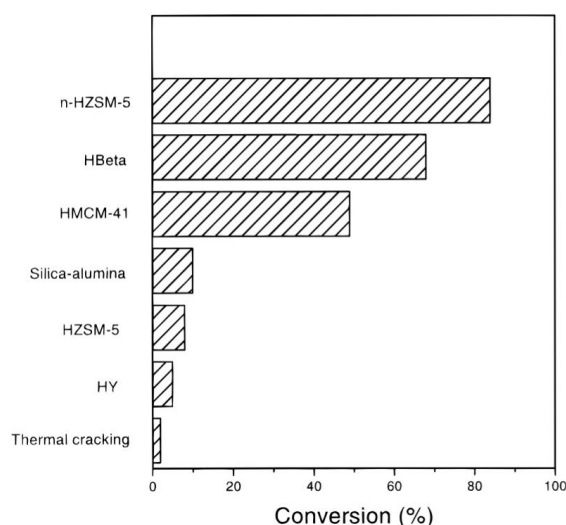


Figure 2.6 - Conversions in thermal and catalytic cracking of the polyolefin mixture (feedstock/catalyst = 50, temperature = 400 °C, holding time = 30 min) [95].

It must be noted that nanocrystalline n-HZSM-5 showed a much higher activity if compared with the micrometer-size HZSM-5. The higher conversion observed in presence of n-HZSM-5 has been ascribed to the smaller crystals size (equal to 0.075 and 3 μm , for and HZSM-5 and n-HZSM-5, respectively), which leads to a higher external surface area, as previously described, increasing the amount of active acid sites accessible to the bulky molecules [95]. The catalytic activity of n-HZSM-5 with crystals size within the range 25 – 60 nm was further studied in the catalytic pyrolysis of pure LDPE, HDPE, and PP, in a semi-batch reactor, under different operating conditions. Reported results show the higher activity of this catalyst already at low temperature (360 °C) and using a low feedstock-to-catalyst ratio (100), compared to standard H-ZSM-5 (HDPE conversions: 93 % with n-ZSM-5 and 44 % with H-ZSM-5). Moreover, gaseous hydrocarbons represented the main fraction in all the experiments, while the selectivity toward compounds families proved to be dependent on the process parameters, i.e., pyrolysis temperature and residence time [96].

Besides pure polymers and model mixtures, ZSM-5 zeolites have been also tested in the catalytic pyrolysis of real plastic wastes. As described in section 1.3, with this kind of feedstocks additional variables need to be considered, related to the heterogeneity of the wastes and the presence of contaminants.

Lin and Yang carried out catalytic pyrolysis experiments of post-consumer plastic wastes (PE \approx 62 %, PP \approx 30 %, PS \approx 7 %, PVC \approx 1 %) by testing various catalysts in a fluidized

2. PYROLYSIS OF PLASTIC MATERIALS

bed reactor, in 290 – 430 °C temperature range. H-ZSM-5 showed the highest selectivity toward C3 – C5 compounds, as well as the lowest deactivation, also depending on the process parameters. Moreover, PVC-derived hydrochloric acid was collected, whose yield was comparable in all tests, whilst chlorine- and sulphur-containing compounds were not detectable [97].

Waste polyethylene from packaging industry was pyrolyzed in a tubular reactor at 545 °C in presence of H-ZSM-5 (feedstock/catalyst = 50). Reported results show that the olefins concentration was more than doubled, compared to the thermal test, and that the contaminants originally present in the raw material (calcium = 2220 ppm and titanium = 20 ppm) were accumulated on the catalyst surface, causing a catalytic activity loss of 86 % after one pyrolysis run, related to both coke deposition and metal poisoning [98].

Larger scale experiments were performed by Miskolczi *et al.* who pyrolyzed HDPE and PP from agriculture and packaging sectors at 520 °C in a continuous reactor with a feed rate of 9 kg/h. The presence of 5% of H-ZSM-5 shifted the products distribution toward lighter hydrocarbons formation, especially in C5 – C15 carbon number range, with a significant content of unsaturated compounds in both liquid and gas fractions, confirming the catalyst-mediated end-chain cracking reactions mechanism. Furthermore, the catalyst allowed to drastically reduce the impurities contaminating the raw waste plastics (N, S, P, and Ca) since just 12 ppm of sulphur and no other contaminants were detected in PP-derived oil [99].

In another work, Miskolczi *et al.* carried out catalytic pyrolysis tests of municipal plastic waste (MPW) in absence and presence of different catalysts to study both products and contaminants distribution among the products. The experiments were performed in a batch reactor between 500 and 600 °C, and the employed raw feedstock was found to be rich in metals and halogens (Table 3) [100].

2. PYROLYSIS OF PLASTIC MATERIALS

Table 3 - Typical contaminants in raw MPW and in pyrolysis products at 500 °C [100].

Contaminants	S (ppm)	Cl (ppm)	Zn (ppm)	Ca (ppm)	Br (ppm)	Sb (ppm)
Raw MPW	135	2689	1310	1504	2316	749
Oil						
No catalyst	51	618	124	297	253	105
Zeolite-Y	34	457	146	282	194	99
Zeolite-β	37	399	128	273	201	114
HZSM-5	42	487	132	304	266	104
Gas						
No catalyst	< 10	926	-	-	520	-
Zeolite-Y	< 10	1355	-	-	594	-
Zeolite-β	< 10	1291	-	-	601	-
HZSM-5	< 10	1210	-	-	555	-
Solid (%) ^a						
No catalyst ^b	62	43	90	80	67	86
Catalysts ^c	72	36	90	81	65	86

^a Average % calculated by difference.

^b Concentration in char fraction.

^c Concentration in char + coke fractions.

Reported results show that the investigated catalysts allowed to reduce chlorine and bromine contents in oil, increasing their concentrations in gas phase, and this has been attributed to the dehalogenation of PVC and BFRs to form hydrohalic gaseous acids (see next section). However, from the calculated average residues in the solid phases, it can be observed that the investigated catalysts had just a slight effect on S and Ca trapping, being the other impurities mainly accumulated in the char fraction.

So far, few studies are still present in literature focusing on the pyrolysis of real waste plastics that take account of both products composition and the contaminants distribution among the products themselves, as well as how the presence of a catalyst can affect them.

The main limitations lie in the complexity of the matrixes to be treated, as well as in large number of variables governing the pyrolysis processes.

In this context, especially the management of halogens in waste plastics is still an open issue, since the quality of the pyrolysis products is strongly influenced by their presence, as detailed below.

2. PYROLYSIS OF PLASTIC MATERIALS

2.3 Plastics de-halogenation treatments

As previously mentioned, the presence of halogens represents one of the main issues to be faced in polymers thermal recovery, which affects both process management and pyrolysis products to be used in the recovery chain.

With particular regard to pyrolysis oil, a maximum halogens concentration of 100 ppm is required to be used as fuel, according to Stockholm Convention (2015) [101], and this limit is further lowered down to 0.5 ppm by some EU Member States. That is because, as effect of combustion, the pyrolysis oil organohalides can be partially oxidized to the toxic and carcinogenic polyhalogenated dioxins. Additionally, hydro-halogen acids (dangerous for human health and corrosive to the plants) can be released, as well as volatile halogenated compounds, classified as greenhouse gases.

From these needs, different dehalogenation processes have been developed supporting pyrolysis technology: dechlorination by thermal pre-treating (stepwise pyrolysis), in situ dehalogenation sorbent/catalyst-mediated, and ex situ upgrading of pyrolysis oil [102]. A scheme of the dehalogenation processes is reported in Figure 2.7.

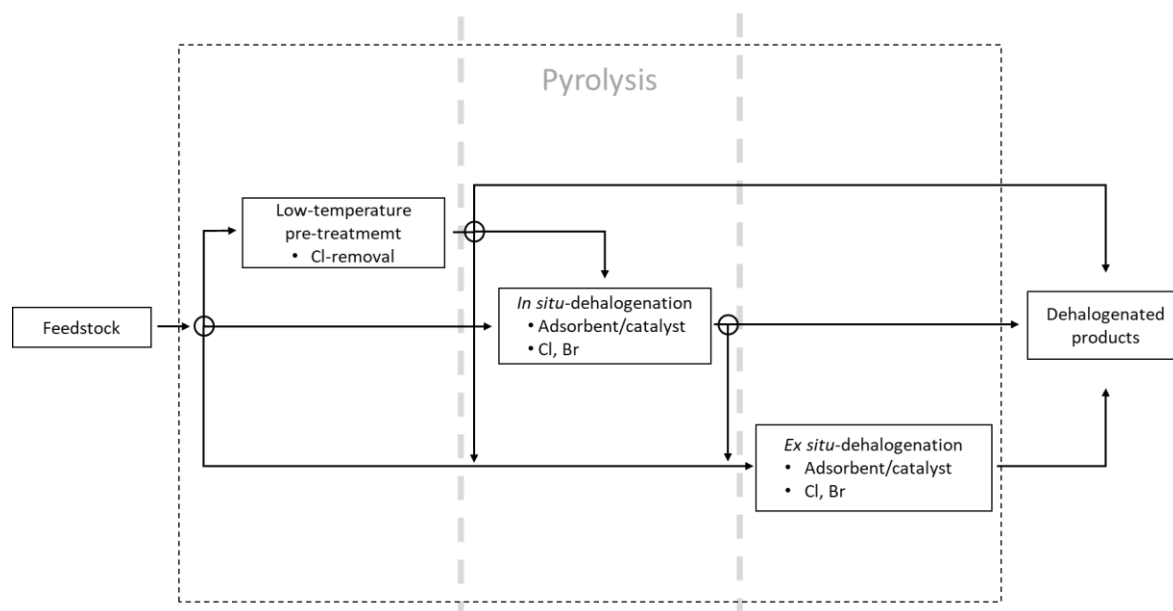


Figure 2.7 - Scheme of plastic waste dehalogenation processes.

2. PYROLYSIS OF PLASTIC MATERIALS

2.3.1 De-chlorination treatments

Among halogenated polymers, polyvinylchloride (PVC) is the most diffused and its high chlorine content (≈ 58 wt.%) represents the main problem for a sustainable pyrolysis of waste plastic. As discussed in section 2.1.1, on the binding energies basis, the breaking order of the polymer bonds is C-Cl, C-H and C-C. Therefore, the early stages of thermal cracking are characterized by hydrochloric acid release from side-groups-elimination, resulting in an unsaturated carbon chain [103,104].

On this basis, a preliminary low-temperature dehydrochlorination step, generally performed in 200-400 °C range and inert atmosphere, is a good option to reduce the halogen content. This technological solution of a stepwise pyrolysis consists of thermochemical two-stages process, wherein the dehalogenation is followed by conventional pyrolysis [105]. The dehydrochlorination efficiency is related to the feedstock composition and reactor type, as well as the reaction parameters, e.g., temperature and holding time.

Bockhorn et al. [106] investigated stepwise pyrolysis of a pure polymers mixture (PA, PS, PE, and PVC) up to 800 °C. Reported results indicated that for a heating rate of 2 °C/min, hydrochloric acid release starts at 220 °C, with a maximum evolution rate at 280 °C, reaching the highest chlorine removal of 83 % at 400 °C. Since it was established that the dehydrochlorination efficiency was independent of the heating rate [107], the influence of holding time and temperature was studied by López *et al.* [108]. It has been showed that the 99.2 % of the initial chlorine can be removed by treating a PVC-containing polymer mixture at 300 °C for 30 mins, in a semi-batch reactor. Furthermore, the authors demonstrated that distribution and composition of the subsequent pyrolysis products are affected by the dehydrochlorination step, as the stronger the treatment, the higher the gas yield and the heavier the hydrocarbons in the oil, indicating a polymers rearrangement during the pre-treatment. This evidence was also confirmed by Yuan *et al.* performing dehydrochlorination pre-treatment of pure PVC in a lab-scale gas-liquid fluidized bed reactor [109]. HCl release started during the melting stage and 300 °C was confirmed as the most efficient temperature. A further rise in temperature was accompanied by the polymer chain decomposition, resulting in an increment of light hydrocarbons emitted. In these conditions, up to 99.5 % of the initial chlorine was eliminated, with a severe reduction of the time required, limited to 96 seconds.

2. PYROLYSIS OF PLASTIC MATERIALS

Experiments at bigger scale were carried out by Lei et al. [110], using a vented screw conveyor to continuously dechlorinate and feed 1kg/h of PVC-containing waste plastic into a stirred batch reactor, before the pyrolysis step. Investigating the residence time and the rotational speed at 300 °C, the authors concluded that long residence time and low screw speed favourably impact on the halogen removal efficiency (greater than 98%). Furthermore, all thermal and catalytic pyrolysis experiments resulted in low-chlorine oil and char with residual halogen mainly accumulated in the gaseous fraction.

In order to achieve a single-step process, dechlorination by thermal co-pyrolysis with adsorbents has been developed. The sorbent materials can trap the emitted HCl by physicochemical adsorption, retaining it in the solid fraction. For the same purpose, some catalysts and catalyst/sorbent composites have been tested, with the dual function of upgrading the pyrolysis products and inhibiting the hydrochloric acid release. A great variety of materials have been designed and tested, including zeolites, calcium- and aluminium-based sorbents, Al-Zn composites, heavy metals, and metal oxides [100–105].

Calcium-based sorbents were extensively studied for their ability to fix chlorine as CaCl₂. It has been demonstrated that in presence of CaO, the temperature of 500 °C represents the limiting operating parameter, given that a higher temperature leads to the volatilization of metallic chlorides rather than the progress in chemical fixation [111]. The calcium chloride formation is also affected by both the chlorine species and vapor residence time inside the reactor, and therefore also by the inert gas flow rate. In fact, very short or long contact times of vapours with the sorbent bed can limit the CaCl₂ formation in favour of gaseous HCl and chlorinated hydrocarbons generation, respectively [112,113].

On the other hand, Aluminium-based catalysts and catalyst/sorbent composites have been also widely investigated. Aluminium in form of Al₂O₃ or SA has been found to have just a slight HCl fixing power, acting mainly as catalyst [114]. Instead, when catalyst/sorbent composites were used, such as Red Mud [115] and Al-Zn Composite Catalyst (AZCC) [116], the chlorine concentration in pyrolysis oil dropped dramatically, as evidence of the ability of iron and zinc to fix chlorine in form of metallic chlorides.

2. PYROLYSIS OF PLASTIC MATERIALS

2.3.2 De-bromination treatments

The main bromine source in waste plastic lays in Brominated Flame Retardants (BFRs), widely used as additives in plastic products to increase the fire resistance. Among many commercially available BFRs, Polybrominated Diphenyl Ethers (PBDE), Brominated Epoxy Resins (BE), Tetrabromobisphenol A (TBBPA), Hexabromocyclododecane (HBCD), Polybromobiphenyls (PBB) represent the most used classes. When pyrolysis is performed, no early decomposition of BFRs is observed as it occurs in the same temperature range of the polymers chain reaction. Therefore, stepwise pyrolysis does not represent a suitable option for bromine removal [117]. The conventional way to address the debromination of pyrolysis products consists of adding sorbents able to physically adsorb or chemically react with organobromines, bromine radicals and hydrobromic acid, resulting from BFRs decomposition. It must be considered that the BFRs are usually used in combination with antimony trioxide as synergist, able to increase their activity by quenching the radicals formed during the combustion. Therefore, SbO_3 represents an additional pollutant, which makes the achievement of contaminants-free pyrolysis products even more challenging.

Due to their double nature of catalyst and sorbent, zeolites have been widely investigated in catalytic pyrolysis in presence of brominated compounds, under different operation conditions and feedstocks. Zeolite pores size plays a key role in the debromination efficiency: larger pores, such as in 13X and NaY, led to the complete cracking of big BFRs, while it was inhibited by partial pores inaccessibility of the molecular sieve 4A [118].

To enhance the debromination efficiency, iron-containing zeolites and composites (natural zeolites, Red Mud [119], Fe over HZSM-5 [120], iron particles and Ni-SA-supported [121,122] were also tested in catalytic pyrolysis of BFRs-containing polymer mixtures. It has been shown that iron oxide can react with HBr and bromine radicals to form brominated salts, simultaneously inhibiting the formation of volatile SbBr_3 , and thus avoiding its migration in the oil and enhancing the capture of both antimony and bromine in the sorbent's pores. Nevertheless, the interaction between Fe and organobromines proved to be more effective than that with hydrobromic acid. Therefore, both reaction parameters (such as temperature) and catalyst features need to be carefully tailored to avoid the complete cracking of BFRs in HBr. A further oil debromination was achieved (up to 95 %) by using mesoporous materials as iron supports, as the bigger channels allow access to larger organic

2. PYROLYSIS OF PLASTIC MATERIALS

bromides, improving the cracking by acidic terminal silanols [117,119,122,123]. In this way, also the interaction between iron oxide and antimony is enhanced, leading to a stronger Sb trapping in the sorbent, and the conversion of organobromines to coke is promoted, due to the carbon solubility of metal oxides.

Similarly to chlorine capture, Ca-based sorbents have been designed also in debromination processes. CaCO₃ and Ca-C composite were tested by Brebu et al., achieving a 40 % and 80 % reduction of Br in pyrolysis oil at 450 °C, respectively [122]. Jung et al. demonstrated that the bromine removal in oil rises in the order CaO, CaCO₃, Ca(OH)₂ (57.4, 65.5 and 75.4%), with a substantial increase of 83.4 % of antimony trapped in the solid residue when calcium hydroxide was used [124]. The mechanism of bromine trapping by calcium hydroxide was studied by Gao et al., which integrated experimental pyrolysis of BE-containing PCBs and absorption computational tests [125]. The authors demonstrated that, at temperature above 450 °C, Ca(OH)₂ decomposes in CaO, leading to an oxide/hydroxide blend with a higher specific area and larger diameter, which promote the interaction between calcium and hydrobromic acid, resulting in brominated salts formation. Furthermore, it has been showed that the metal can interact also with bromophenols, acting directly as debromination agent of organobromine compounds.

2.3.3 Ex situ de-halogenation treatments of pyrolysis oil

Despite the effort on dehalogenation processes described below, still limitations hold such as catalyst/sorbent deactivation and severe reaction conditions. Therefore, post-pyrolysis treatment still represents a valid alternative step to obtain a low-halogen content liquid fraction. The ex-situ oil upgrading mainly consists of a catalyst/sorbent-mediated process, which allows to customize the liquid fraction properties by simultaneous cracking and dehalogenation. It is usually performed downstream of thermal and/or catalytic pyrolysis, in inert atmosphere, and the reaction parameters are strictly related to the oil composition and the product target properties.

Several sorbents and catalysts have been tested in catalytic dehydrochlorination and dehalogenation by adsorption, such as heavy metals-based, metal oxides, FCC, and zeolites [125,129].

2. PYROLYSIS OF PLASTIC MATERIALS

Among the others, zeolites have been widely studied thanks to the possibility of customizing their adsorbent and catalytic properties by modifying structural and acidic properties. As mentioned above, their catalytic activity must be considered, since hydrocarbons cracking reactions can lead to the formation of halogenated gases instead of halogen retention. The loading of metals (Mg, Zn, Cu, Ag) over zeolites can help to overcome this problem, by reducing the catalyst acidity and increasing the dehalogenation efficiency by metal halides formation [126,127].

It must be considered that if the same catalyst/sorbent material is employed, other parameters as zeolite properties, holding time and adsorbent dosage affect the dehalogenation efficiency, depending on the availability and saturation of active sites.

As mentioned before, the dehalogenation ability of iron-based sorbents is well known. α -Fe₂O₃, γ -Fe₂O₃ and Fe-C composite were tested in the dechlorination of pyrolysis oil from PE, PP and PVC mixture, in a fixed bed reactor at 350 °C [128,129]. The results revealed that iron oxide initially reacts with HCl, being converted into FeCl₂. The formed salt is still able to convert organochlorines by reversible interactions, but its cracking activity rapidly decreases, leading to no substantial change in the carbon number distribution. Higher dechlorination efficiency and longer sorbent activity can be reached by continuously removing the developed hydrochloric acid, i.e., by properly modulating the carrier gas flow rate.

The combined effect of metals oxides as iron, silicon, and aluminium, was studied by Lopez-Urionabarrenechea et al., by testing waste Red Mud in the dehalogenation of two pyrolysis oils in a stirred autoclave at 325 °C [130]. When compared with thermal experiment, the chlorine retention in the heavy fraction increased by 43-84 % in presence of Red Mud, together with the gas yield rise, confirming that the zeolitic nature of silica and alumina promotes the cracking, whilst iron mainly acts as sorbent. Furthermore, it was demonstrated that the oil composition plays a key role, as the higher the unsaturated hydrocarbons content, the higher the cracking, and then conversion in chlorinated light oil and gases. On the contrary, a high aromatics content-oil undergoes polymerization rather than cracking in these reaction conditions, leading to higher heavy fraction yield and dechlorination efficiency (84 %).

The dechlorination mechanism of aromatic and aliphatic hydrocarbons in presence of metal oxides was recently studied [131]. Using 2-chlorobutane, 2-chloroethylbenzene, and

2. PYROLYSIS OF PLASTIC MATERIALS

chlorobenzene as model compounds, it has been demonstrated that when an aliphatic hydrogen is adjacent to chlorine, the interaction with metals easily leads to HCl release and olefin formation at relatively low temperature (180 °C). On the contrary, higher temperature is required for the dechlorination of aromatic hydrocarbons (300 °C), as it firstly involves the interaction with a carbocation, which increases the positive charge of the aromatic ring, allowing the negatively charged oxygen of metal oxide to break the carbon-chlorine bond (Figure 2.8).

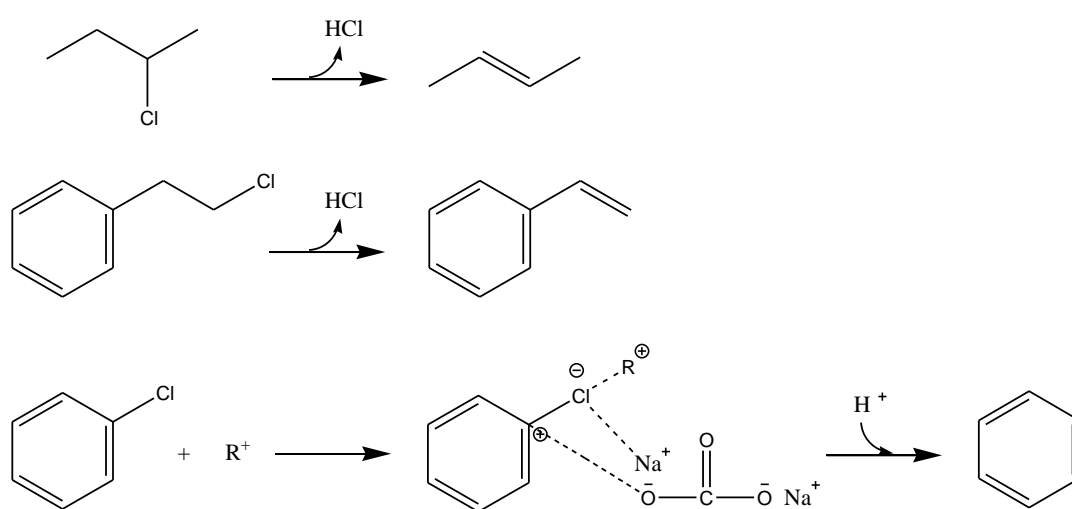


Figure 2.8 - Dechlorination mechanism of aliphatic and aromatic chloro-compounds in presence of metals (adapted from [131]).

3. MATERIALS AND METHODS

3.1 Catalysts preparation

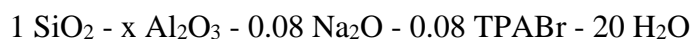
In this work, ZSM-5 type zeolites were selected as catalysts for the catalytic *ex-situ* upgrading of WEEE plastic's pyrolysis vapours. To evaluate the influence of the acidity, ZSM-5 zeolites with different silicon-to-aluminium ratios were synthesized and tested. Furthermore, hierarchical ZSM-5 was prepared, to investigate the role of the secondary mesoporosity.

3.1.1 Nanocrystalline ZSM-5 zeolite

Nanocrystalline ZSM-5 with Si/Al ratio of 42 was purchased by Clariant and used as reference to be compared with synthesized catalysts. The commercial n-ZSM-5 has been labelled as MFI_42 in the following sections.

3.1.2 Synthesis of ZSM-5 zeolites

The syntheses of ZSM-5 zeolites were carried out by using the following synthesis gel composition, as reported in literature [132]:



The reactions were performed by using precipitated silica gel (SiO₂ 100 %, Merck) as silica source, tetrapropylammonium bromide (TPABr 98 %, Fluka) as structure directing agent (SDA), aluminium hydroxide (Al(OH)₃ 98 %, Fluka), sodium hydroxide (NaOH 97 %, Carlo Erba Reagenti), and ultrapure water.

The stoichiometric coefficient of aluminium (x) was varied to obtain Si/Al ratios equal to 11, 25 and 100, i.e., x = 0.044, 0.020, and 0.005, respectively.

Figure 3.1 shows the procedure followed for the synthesis of ZSM-5 zeolites. For each catalyst, the reactant mixture was stirred for 2 h at room temperature, then transferred to a Teflon-coated stainless-steel autoclave and heated in a static oven at 170 °C. The

3. MATERIALS AND METHODS

crystallization time was dependent upon the x value (8 days for $x = 0.044$, 4 days for $x = 0.020$ and 3 days for $x = 0.005$).

After crystallization, the solid was recovered by filtration and calcined at $550\text{ }^{\circ}\text{C}$ for 8 h (heating rate of $5\text{ }^{\circ}\text{C}/\text{min}$) to remove the SDA. The resulting zeolite with Na^+ as counter-ion was ion-exchanged two consecutive times with an aqueous solution of NH_4Cl (1 M, pH 5.5) at $80\text{ }^{\circ}\text{C}$ for 2 h. The solid was then filtered and washed with ultrapure water up to neutral pH. Finally, NH_4^+ -form was thermally treated at $550\text{ }^{\circ}\text{C}$ for 8 h, in order to remove the ammonia and to obtain the H^+ -form catalyst.

In this work, the synthesized catalysts have been labelled MFI_11, MFI_25 and MFI_100 based on their theoretical silicon-to-aluminium ratios.

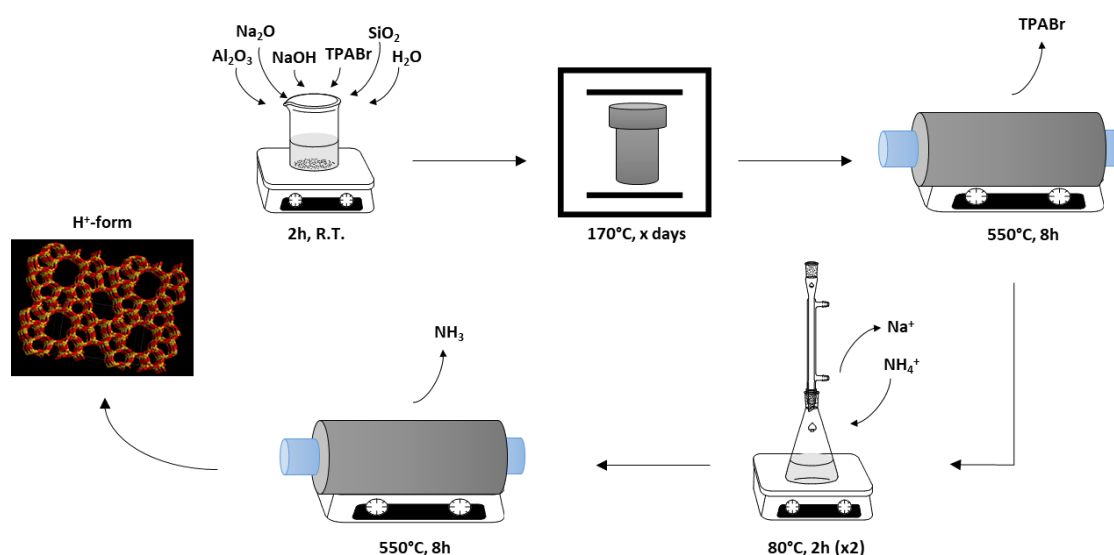


Figure 3.1 - Synthesis method of ZSM-5 zeolites.

3.1.3 Preparation of hierarchical ZSM-5 zeolite

To produce the hierarchical h-ZSM-5, the H^+ -form of MFI_25 was desilicated using a 0.1 M solution of NaOH . The reaction was carried out at $65\text{ }^{\circ}\text{C}$ for 60 minutes, under stirring, and with a solution-to-solid ratio equal to 20 ml/g. At the end of the reaction, the suspension was quenched in a water/ice bath, filtered, and the solid was dried at $80\text{ }^{\circ}\text{C}$ overnight.

The resulting zeolite with Na^+ as counterion was ion-exchanged two consecutive times with a 1 M solution of NH_4Cl , at $80\text{ }^{\circ}\text{C}$ for 2 h, and finally calcinated at $550\text{ }^{\circ}\text{C}$ for 8 h (heating rate = $5\text{ }^{\circ}\text{C}/\text{min}$) to decompose the ammonium ion and obtain the acidic hierarchical

3. MATERIALS AND METHODS

H⁺-ZSM-5. The overall procedure [133] followed to prepare the hierarchical catalyst is shown in Figure 3.2, and in this work, the sample has been labelled as h-MFI.

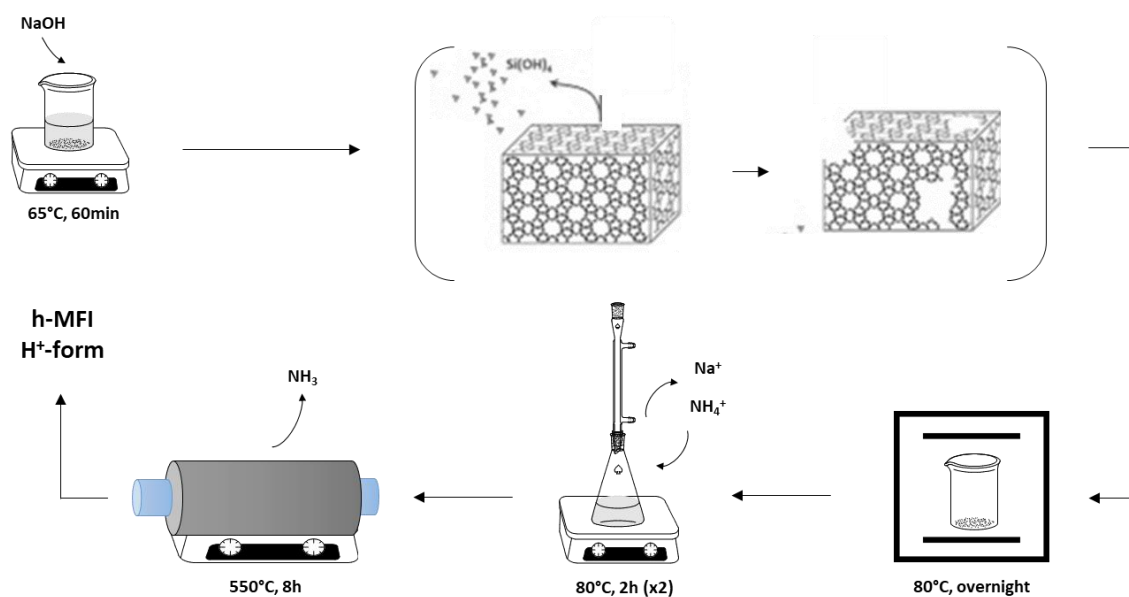


Figure 3.2 - Scheme of the ZSM-5 desilication procedure.

3. MATERIALS AND METHODS

3.2 Characterization techniques

To determine the morphological and physicochemical properties of the WEEE raw and dechlorinated plastic used as feedstocks, as well as the synthesized catalysts, different characterization techniques were employed.

The polymer mixtures composition and properties were evaluated by proximate and ultimate analyses, X-Ray powder Diffraction (XRD) and Fourier Transform Infrared spectroscopy (FT-IR). The chlorine content was estimated by combustion followed by Ion Chromatography (AOD-IC).

The synthesized catalysts were characterized by X-Ray powder Diffraction (XRD), Inductively Coupled Plasma Optical Emission Spectrometry (ICP-OES), Nitrogen physisorption at 77 K, Thermal Programmed Desorption of ammonia (NH₃-TPD), FT-IR with the adsorption of deuterated acetonitrile, ²⁷Al MAS ssNMR, and Scanning Electron Microscopy.

3.2.1 X-Ray Powder Diffraction (XRD)

X-ray Powder Diffraction technique provides information about crystalline phase of solid materials, on the basis of the Bragg's Law [134]. A XRD pattern consists of a set of peaks which correspond to the crystalline reflections planes of indices *h k l* and spacing *d*.

The crystallinity of the zeolite catalysts, as well as of the polymers in the WEEE mixtures, was evaluated by X-ray powder diffraction analysis using a Philips X'Pert PRO diffractometer, with Cu K α radiation ($\lambda = 1.5406 \text{ \AA}$), operating at 40 kV and 30 mA. All the spectra were recorded in the 2θ range of $5 - 70^\circ$.

3.2.2 Ultimate and proximate analyses

The ultimate analyses were performed on a Thermo Scientific FLASH 2000 CHNS/O micro-elemental analyser. The oxygen content was calculated by difference.

Proximate analysis was carried out by using a TA Instruments Q600 SDT thermobalance and the volatile matter was quantified from the weight loss of sample heated at $10 \text{ }^\circ\text{C}/\text{min}$ from room temperature to $900 \text{ }^\circ\text{C}$ in Ar atmosphere (flow rate of $100 \text{ ml}/\text{min}$).

3. MATERIALS AND METHODS

3.2.3 Fourier-Transform Infrared Spectroscopy (FT-IR) in Attenuated Total Reflectance (ATR) mode

The polymers mixture composition was qualitatively evaluated by FT-IR spectroscopy by using a Nicolett 6700 equipped with a diamond ATR crystal and a DTGS TEC detector. The spectra were collected in 550 – 4000 cm^{-1} range, with an optical resolution of 4 cm^{-1} , and acquiring 64 scans.

3.2.4 Oxidative combustion followed by Ion Chromatography (AOD/IC)

The chlorine content in the WEEE raw and dechlorinated plastic was determined by oxidative combustion in a calorimetric bomb (AOD 1 Decomposition System by IKA), followed by Ion Chromatography (IC) analysis, according to DIN/EN 14582 and DIN 51527 standards. Few mg of sample were placed in a quartz crucible inside the steel decomposition vessel and burnt under oxygen pressure (32 bar). The combustion vapours were condensed in 10 ml of trapping solution ($\text{Na}_2\text{CO}_3 = 0.99 \mu\text{mol}$, $\text{NaHCO}_3 = 0.38 \mu\text{mol}$, $\text{H}_2\text{O}_2 = 2.9 \mu\text{mol}$, $\text{NaOH} = 0.01 \mu\text{mol}$), which was then properly diluted to be analysed on a 930 Compact IC Flex (Metrohm). The chromatographic analyses were performed at 45 °C, by using a Polyvinyl alcohol with quaternary ammonium groups column (Metrosep A Supp 7 - 150/4.0) as stationary phase and a sodium carbonate solution as eluent, with a flow rate of 0.8 ml/min. The equipment was calibrated for chloride ion identification in the range 1.3 – 200 ppm.

3.2.5 Inductively Coupled Plasma Optical Emission Spectrometry (ICP-OES)

The quantification of aluminium in the zeolite catalysts and metals in the WEEE plastic ashes was carried out by Inductively Coupled Plasma Optical Emission Spectrometry (ICP-OES). Before the analysis, the WEEE plastic was burned in a static oven up to 900 °C in air flow, with a holding time of 30 min. For each analysis, a known amount of solid sample was firstly digested in an acidic solution of nitric and hydrofluoric acid (2:1 in volume), using an Anton Paar Multi-wave 3000 microwave. The liquid sample was then analysed employing a Perking Elmer Optima 7300AD instrument, feeding 1.5 mL/min of sample in 15 L/min of argon as carrier.

3. MATERIALS AND METHODS

3.2.6 Nitrogen physisorption at 77 K

The textural properties of the investigated catalysts were studied by the adsorption - desorption of Nitrogen at 77 K. The analyses were performed using an ASAP 2020 instrument, from Micromeritics.

Before the analysis, 100 mg of sample was subjected to the degassing procedure, which firstly includes the decreasing of the pressure down to 6.6 Pa at 30 °C, then the rise of the temperature up to 350 °C for 6 h, the further reduction of the pressure to 6.6 Pa at 30 °C and, finally, the backfilling of the measuring cell with He.

The specific surface area was estimated by applying the Brunauer, Emmett and Teller (BET) method [135]. The microporous volume and the external surface area were assessed by the t-plot method, using the Harkins and Jura equation [136]. The pore size distribution was determined by applying the Non-Local Density Functional Theory (NL-DFT) method on the adsorption branch of the isotherm, assuming cylindrical pores [137].

3.2.7 Ammonia Temperature Programmed Desorption (NH₃-TPD)

The concentration and the strength of the acid sites of zeolites were measured by Temperature Programmed Desorption of ammonia (NH₃-TPD), on a ThermoFisher TPDRO1100 instrument. For each analysis, 100 mg of sample were previously dried at 180 °C for 3 h, then placed in a quartz reactor and firstly heated up to 300 °C in helium flow to remove moisture. Subsequently, the catalyst was cooled down to 150 °C and saturated by flowing a gaseous mixture with 10 vol.% of ammonia in helium (flow rate = 20 ml/min, holding time = 2 h). Afterwards, the physically adsorbed ammonia was purged with a helium flow for 90 min and the sample was cooled down to 100 °C. Finally, the NH₃ desorption was carried out from 100 to 700 °C, at 10 °C/min, keeping the final temperature until the TCD signal stabilization. Curves deconvolution by using Gaussian functions was carried out for the quantification of weak and strong acid sites.

3. MATERIALS AND METHODS

3.2.8 Fourier-Transform Infrared Spectroscopy (FT-IR) with CD₃CN adsorption

To discriminate between the Brønsted and Lewis acid sites of the investigated catalysts, deuterated acetonitrile adsorption followed by FT-IR analysis was performed by using a Nicolet iS 10 - FTIR Spectrometer (ThermoScientific, USA), with 4 cm⁻¹ optical resolution and a DTGS detector. 25 mg of sample was pressed into a disk of 1.3 cm radius, and then heated up to 400 °C (heating rate = 10 °C/min, holding time = 2 h) and outgassed up to 10⁻⁵ torr. CD₃CN was subsequently adsorbed on the activated sample at 30 °C for 30 min, and the excess of basic probe was finally removed by vacuum evacuation at 10⁻⁵ torr for 10 h [138,139]. The spectra were recorded in the range 4000 – 400 cm⁻¹ (mid-IR) and analyzed by deconvolution through Peak Fit software, by using Gaussian curves. To calculate the concentration of Brønsted and Lewis acid sites, extinction factors of 2.05 and 3.60 cm/μmol were used for the peaks centred at 2325 and 2297 cm⁻¹, respectively [140].

3.2.9 Magic Angle Spinning solid state Nuclear Magnetic Resonance (²⁷Al MAS ssNMR)

Aluminium environment of zeolites was studied by ²⁷Al Magic Angle Spinning solid state Nuclear Magnetic Resonance (MAS ssNMR) on a Bruker Avance III spectrometer, supported with a 3.2 mm MAS probe, at 11.7 T. Spectra were recorded at room temperature, by using 15 kHz MAS. RF fields of 50 kHz and 40 kHz were used for the ²⁷Al π/12 pulse, followed by 26 ms acquisition. The number of scans accumulated was 10240, with a 1 s inter-scan delay. The ²⁷Al chemical shift was externally referred to an aqueous solution of aluminium nitrate. NMR spectra were analysed by deconvolution with Gaussian functions, and the curves areas were used to estimate the ratio between intra- and extra-framework aluminium species.

3.2.10 Scanning Electron Microscopy (SEM)

Scanning Electron Microscopy (SEM) was used in order to investigate the morphologies of the zeolites catalysts. SEM micrographs were acquired by means of a Hitachi TM-100 microscope, without pre-treating the samples.

3. MATERIALS AND METHODS

3.3 Reaction system

In this work, the thermochemical valorisation of real WEEE-derived plastic is investigated. In order to study products and chlorine distribution, de-chlorination thermal pretreatment, thermal and thermo-catalytic (by ex-situ vapour upgrading) fast-pyrolysis reactions were carried out. In this paragraph, the experimental setup, the operating conditions, and the methods used for the products characterization are described.

3.3.1 Experimental setup

De-chlorination pretreatment

De-chlorination thermal pretreatment was carried out by using the experimental setup shown in Figure 3.3. The sample is located at the centre of a downdraft stainless steel reactor, which is placed inside an electrical furnace. The system was firstly inertized with nitrogen for 5 minutes, and then the sample was heated up, at 10 °C/min, to the final temperature (300 or 350°C), which was kept for 30 minutes. Nitrogen (flow rate = 50 ml/min) was used as inertizing and carrier gas during the whole test. The outgoing vapours were passed through a 125 ml condenser, submerged in an ice-water bath (0-4 °C), to condense the organics, and then through a series of two flasks containing 100 ml of distilled water each one for the HCl trapping. The non-condensable gases were finally collected and quantified by means of a closed water-containing column: in this system, the water is replaced by the vapours and accumulated in a connected graduated cylinder.

3. MATERIALS AND METHODS

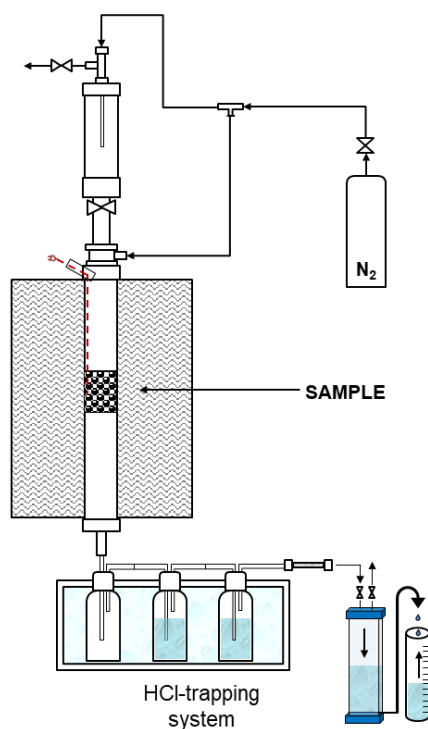


Figure 3.3 - Schematic diagram of the experimental setup used for the WEEE plastic dehydrochlorination thermal pretreatment.

Thermal and catalytic pyrolysis tests

The schematic diagram of the experimental setup used for thermal and thermo-catalytic experiments is shown in Figure 3.4. The reaction system consists of a downdraft fixed-bed stainless steel reactor, with internal diameter of 16 mm and length of 400 mm. Thermal and catalytic zones are independently heated by two electrical furnaces, and the internal temperatures are monitored by two K-type thermocouples, located in the char bed (thermal zone) and in the catalyst bed (catalytic zone). The two regions inside the reactor were physically separated by metallic tubes and plates, and quartz wool.

Once the reactor reached the set temperature, the sample was made to fall by opening the feeding valve. The reaction occurred through the formation of solid char, which was retained in the thermal zone, and primary pyrolysis vapours, that were upgraded by passing through the catalyst bed.

At the end of the reaction, solid products (i.e., the char and the coke deposited on the catalyst) were independently collected for further characterization. The upgraded vapours were

3. MATERIALS AND METHODS

conveyed to a series of two empty 125 ml condensers, for oil condensation, and other two filled with pure water (2 x 100 ml), for hydrochloric acid solubilization. The temperature of the condensation system was kept at 0-4 °C by means of an ice-water bath. Finally, the gaseous fraction was collected in the water-containing column described in the previous section.

All reactions were carried out at atmospheric pressure, by using a 100 ml/min nitrogen flow as carrier gas and inertizing agent.

In catalytic experiments, the catalysts were previously pelletised, grinded, and sieved to obtain a particle size range of 180 - 250 μm , in order to prevent pressure drops during the reaction. The waste WEEE plastic used as feedstock was subjected to size reduction and sieving, and the fraction 0.5 – 1 mm was used in all experiments.

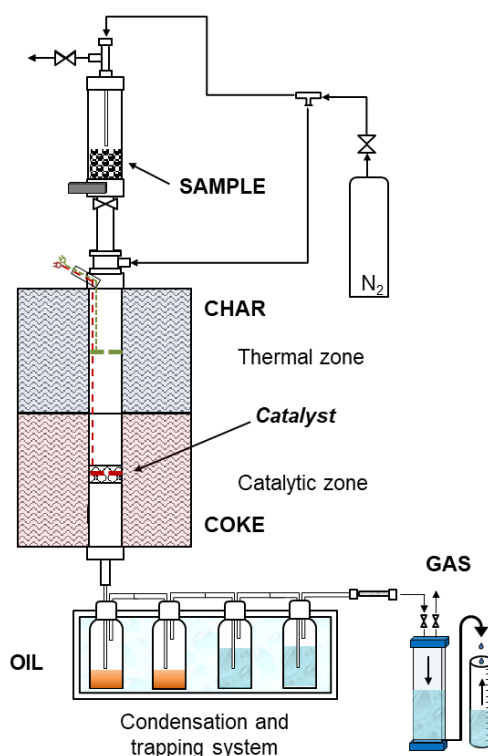


Figure 3.4 - Schematic diagram of the experimental setup used for the WEEE plastic thermo-catalytic experiments.

3. MATERIALS AND METHODS

3.3.2 Analytical methods for products characterization

As a result of the thermal and thermo-catalytic experiments, gaseous, liquid (oil) and solid (wax, char and the coke deposited on the catalyst) products were collected for further characterizations. As an example, a picture of the obtained pyrolysis products is reported in Figure 3.5.

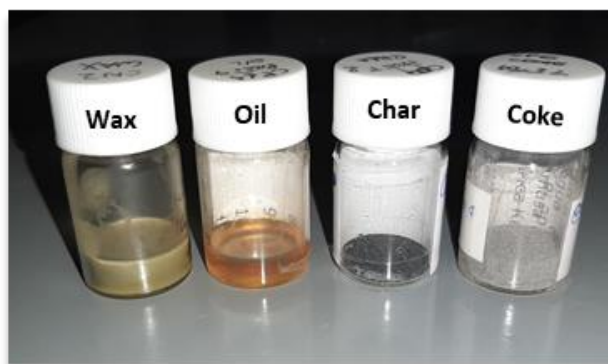


Figure 3.5 - Picture of wax, oil, char and coke fractions obtained from thermal and thermo-catalytic pyrolysis reactions of WEEE plastic.

The analytic techniques employed for the characterization of the WEEE plastic pyrolysis products are described below.

- The chlorine content in the solid and liquid pyrolysis products was determined by the oxidative combustion followed by Ion Chromatography (AOD/IC), as reported in section 3.2.4. The same chromatographic method and parameters were employed to directly quantify the chlorine solubilized in water. Before the injection, the samples were diluted 1:10 in Milli-Q water.
- The coke deposited on the spent catalysts was calculated from the weight change related to the combustion in 30 – 850 °C temperature range (air flow = 100 ml min⁻¹, heating rate = 10 °C min⁻¹), by using a TA Instruments Q600 SDT thermobalance.
- The composition of the oil fraction was evaluated by Paraffins, Iso-Paraffins, Olefins, Naphthenes, Aromatics (PIONA) analysis on a Gas Chromatograph Agilent 7890A, equipped with a CP-Sil PONA CB GC Column (100 m, 0.25 mm, 0.50 µm) and a Flame Ionization Detector (FID). The samples were previously diluted in carbon disulphide (1 wt.%) and the analyses were carried out using an injection volume of 0.5 µl, in 35 - 250 °C temperature range. For the compounds identification and quantification, the equipment was

3. MATERIALS AND METHODS

calibrated with a multi-standard containing 360 different molecules in the range C4 – C15.

- The wax composition was evaluated by GC analysis, by using the Gas Chromatograph Agilent 7890A, equipped with a Flame Ionization Detector (FID). The sample was firstly diluted to 3 wt.% in carbon disulphide and then analysed by means of a DB-5ht GC column (30 m x 320 μ m x 0.1 μ m) in 50 – 370 °C temperature range, under He flow. A calibration standard in C18 – C36 carbon number range was used for peaks identification and quantitative analysis.
- Pyrolysis gases were analysed by using a dual channel Agilent CP-4900 Micro Gas Chromatograph, fitted with a Thermal Conductivity Detector (TCD), and calibrated for different concentration of O₂, H₂, CO, CO₂, CH₄, C₂H₄, C₂H₆, C₃H₆, C₃H₈, C₄H₈, and C₄H₁₀. Chromatographic analysis was performed by using two separation columns: a molecular sieve (Molsieve 5 Å) and HayeSep A, under He flow.

From the calculated weight of gas, coke and water-trapped chlorine fractions and from the measured quantities of wax, oil and char, the total mass balances were closed on the amount of plastic fed, according to the equation:

$$\text{Mass yield}_x (\text{wt. \%}) = [\text{Mass}_x(\text{g}) / \text{Plastic Fed (g)}] * 100$$

Where x = wax, oil, gas, char, coke, and chlorine. For all the tests, the experimental error was lower than 5 %.

Finally, Higher Heating Value (HHV) was calculated by the following equation valid for solid, liquid, and gaseous fuels, according to literature [141]:

$$HHV_i (MJ/Kg_i) = 0.3491 C + 1.1783 H + 0.1005 S - 0.1034 O - 0.0151 N - 0.0211 A$$

Where C, H, S, O, N, and A represent carbon, hydrogen, sulphur, oxygen, nitrogen, and ash contents, respectively, expressed in wt.%.

4. RESULTS AND DISCUSSION

4.1 Physicochemical properties of WEEE plastic

In this section the main physicochemical properties of the waste plastic used as feedstock are described and discussed. As reported in section 1.1, the waste plastic was collected from pre- and post- consumer electrical wires, coming from the recycling chain of the company R.ED.EL. srl. Therefore, the sample appeared to be highly heterogeneous, made up of particles of different size and colours. To overcome this problem, a size reduction by milling was performed before each treatment and analysis and, in addition, all the reported results are arithmetical average of independent analyses.

4.1.1 Proximate and ultimate analysis

The proximate and ultimate analyses of the raw plastic are reported in Table 4. Average volatiles content was quantified by three independent thermogravimetric analyses in Argon, and the results revealed a double-step decomposition (Figure 4.1 A). The average differential thermogravimetric analysis (DTG) shows the presence of a low-temperature peak at 284.4 °C, with a corresponding weight loss of 3.36 ± 0.9 wt.%, which is an indication of the PVC presence, being associated to the hydrochloric acid release. This has been also confirmed by the DSC curve analysis (Figure 4.1 B), in which the endothermic peak related to degradation of the PVC and the HCl release can be observed in 275 – 325 °C temperature range.

Given that Cl represents the 57 wt.% of the PVC polymer, it is possible to estimate the PVC content in the raw plastic from the weight loss in the low-temperature range (3.36 ± 0.9 wt.%), which would stand at the average value of 5.8 ± 1.5 wt.%.

A second peak in the DTG curve, centred at 476.7°C, can be related to the thermal cracking of both PE chain and C-C bonds of the remaining PVC-derived solid, but it cannot be distinguished since they occur in the same temperature range, i.e., 380 – 520 °C [20,142]. The total weight loss stood at 97.2 ± 1.8 wt.%, and the relatively high standard deviations which have been observed can be attributed to the high heterogeneity of the sample, even after milling.

4. RESULTS AND DISCUSSION

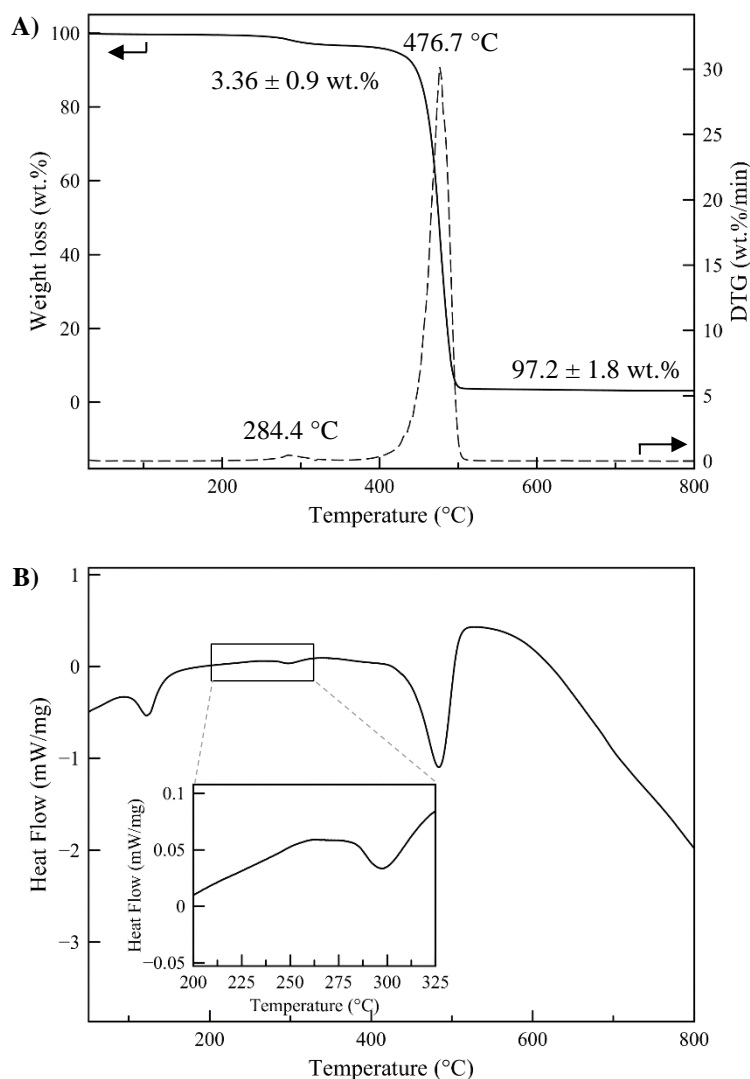


Figure 4.1 - Thermogravimetric analysis of raw plastic. **A)** TG curve in solid line and DTG curve in dashed line. **B)** DSC curve (parameters: Ar flow = 100 ml/min; from R. T. to 850 °C, at 10 °C/min).

On the other hand, the elemental composition of the raw plastic shows the presence of 1.95 ± 0.48 wt.% of chlorine (Table 4), which corresponds to 3.44 ± 0.85 wt.% of PVC. This value appears lower than that obtained from the TG analysis ($= 5.8 \pm 1.5$ wt.%), and this can be attributed to the simultaneous release of other compounds (benzene, 1,3-butadiene) from PVC occurring during the early stage decomposition, i.e. concurrently with HCl release, which leads to an overestimation of the PVC content [143].

Therefore, for the rest of the work, the PVC and chlorine contents estimated from the AOD-IC analyses have been considered as more accurate.

4. RESULTS AND DISCUSSION

Table 4 - Proximate and ultimate analysis of the raw waste plastic.

Proximate Analysis (wt.%)			Ultimate Analysis (wt.%)							
Volatiles ^a	Fixed C ^b	Ash ^c	C	H	N	S	Cl ^d	Trace metals ^e	O ^b	HHV (MJ/Kg)
97.2 (± 1.8)	0 – 1.8	3.0 (± 0.2)	78.0	13.3	0.0	< 0.1	1.95 (±0.48)	0.9	4.0	42.3

^a Quantified by TGA.

^b Calculated by difference.

^c Measured by combustion at 900°C.

^d Analysed by AOD/IC.

^e Measured by ICP-OES of ashes.

The analysis of the WEEE chemical composition shows average C and H contents equal to 78 and 13 wt.%, respectively, leading to the heating value (HHV) of 42.3 MJ/Kg (Table 4). Moreover, it can be observed also the presence of oxygen (4 wt.%), which can be related to the PVC photo-oxidation during its lifetime, according to the literature [144,145].

The ash composition was analysed by ICP-OES after the WEEE plastic combustion, and the obtained results are reported in Table 5. It can be observed the presence of different alkaline and heavy metals, collectively amounting to 0.92 wt.%. The major contribution is represented by Ca, Ti and Si, mainly deriving from additives, such as TiO₂, SiO₂ and CaO, used in polymers for improving their properties, as well as from impurities accumulated during the plastic products lifetime.

Table 5 - ICP-OES analysis of ash from raw plastic sample.

Trace Metal	Concentration (ppm)	Trace Metal	Concentration (ppm)
Al	372.8	Na	263.5
B	48.3	P	46.4
Ca	2020.5	Si	2041.0
Cu	571.5	Pb	34.5
Fe	49.9	Sn	82.7
K	58.6	Ti	3360.1
Mg	168.3	Zn	117.9
Total content = 0.92 wt.%			

4. RESULTS AND DISCUSSION

4.1.2 XRD and FT-IR analyses

In the view of obtaining information about the polymer composition of the WEEE plastic mixture, the raw plastic was analysed by XRD and FT-IR.

Figure 4.2 shows the XRD pattern of the WEEE plastic sample employed as feedstock in this work. The analysis revealed the presence of two sharp high-intensity peaks at $2\theta = 22^\circ$ and 24° , and another moderately strong peak at 36° , which correspond to the inter planner spacing of 4.132, 3.707, and 2.481 Å, related to (110), (200), and (020) lattice planes, respectively. These data indicate the presence of crystalline orthorhombic polyethylene polymer structure [146,147]. In addition, a broad band centred at $2\theta = 20.4^\circ$ can be attributed to the amorphous phase of PE [148].

According to literature, the PVC diffraction peaks are centred at $2\theta = 17^\circ$ and 24.5° . However, in presence of plasticizers as additives, the peak at 17° is shifted toward higher angle values [149]. Therefore, the XRD peaks of PVC in the WEEE plastic pattern (Figure 4.2) are hardly distinguished as they overlap with signals of the PE polymer, which is predominant in the WEEE plastic waste [150].

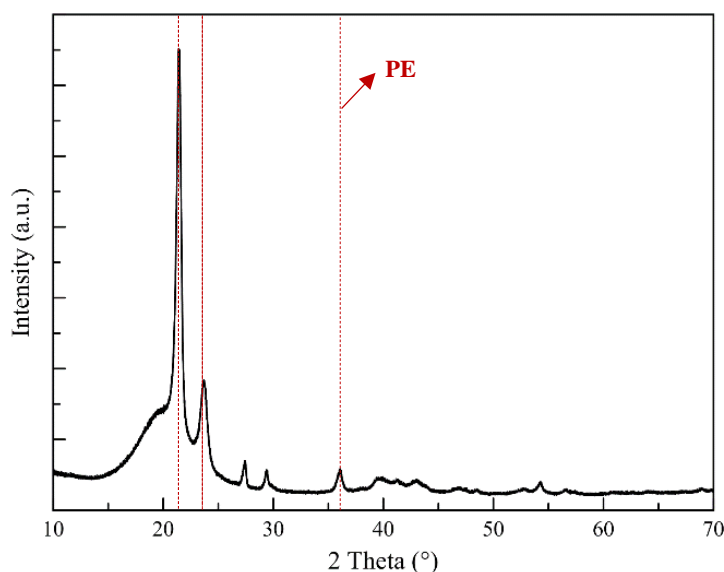


Figure 4.2 - XRD pattern of raw WEEE plastic.

The IR spectra confirmed the simultaneous presence of PE and PVC in the plastic mixture. From the FT-IR analysis of the mixed WEEE plastic (Figure 4.3 A), it is possible to identify the PE characteristic bands, corresponding to C-H stretching at 2849 and 2916 cm^{-1} , CH_2

4. RESULTS AND DISCUSSION

bending at $1472\text{-}1462\text{ cm}^{-1}$, CH_2 rocking at $730\text{-}717\text{ cm}^{-1}$, and a small band at 1379 cm^{-1} related to CH_3 bending [151].

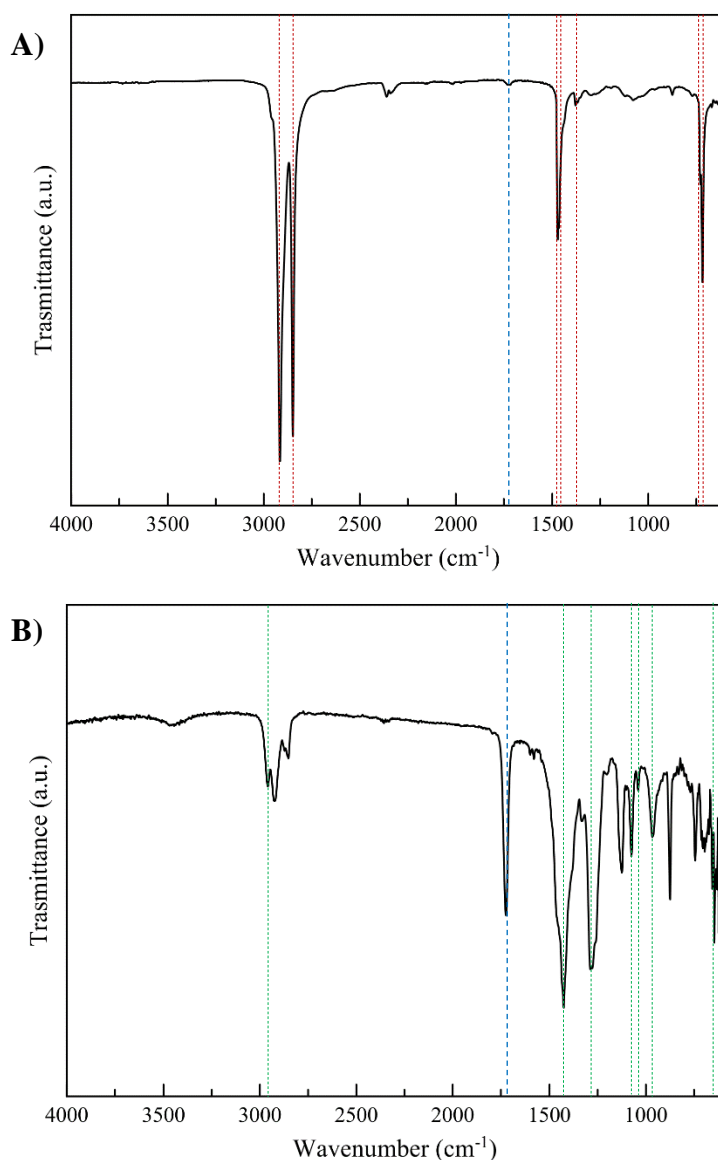


Figure 4.3 - FT-IR spectra of raw A) mixed WEEE plastic and B) isolated particles mainly composed by PVC. Dashed lines are guides for readers: red = PE, green = PVC, blue = HC=O.

However, the characteristic peaks of PVC are difficult to be identified due to the low amount of the polymer in the mixture ($\approx 3.4\text{ wt.}\%$). Therefore, particles identified in the raw WEEE waste as being mainly composed by this polymer were manually separated and analysed by FT-IR. In the obtained spectrum, shown in Figure 4.3 B, it is possible to observe the PVC

4. RESULTS AND DISCUSSION

bands at 610-637, 706, 1425, and 2970 cm^{-1} , related to C-Cl stretching, C-Cl bending, C-H₂ bending, and the α -stretching of C-H adjacent to C-Cl group, respectively, in agreement with literature data [150].

Moreover, a band centred at 1723 cm^{-1} appeared in the spectra, usually observed in commercial PVC resins [152,153], which is attributed to the hydrogen bonded C=O groups of different acrylic processing aids employed to modify the polymer properties [154,155].

4.1.3 Conclusions

The characterization of the raw WEEE plastic that has been used as feedstock in this work revealed a high heterogeneity of the sample, even after the size homogenization. This is consistent with the nature of the plastic mixture, which derives from real pre- and post-consumer electric cables, and therefore was contacted with several contaminants during the products lifetime. Moreover, different additives (such as plasticizers, stabilizers, flame retardants, etc.) are usually added to pure polymers aiming to tailor the physicochemical properties of the plastic products on the basis of the specific application field, which contribute to increase the pollutants amount in the waste plastic mixtures.

In terms of polymer composition, the investigated WEEE plastic mainly consists of PE, followed by PVC, which amounts to about 3.4 wt.% of the WEEE plastic mixture.

High C and H contents were detected by the chemical analysis, equal to 78 and 13 wt.%, respectively, which lead to a heating value of 42.3 MJ/Kg, whilst the contaminants account for less than 5 wt.% of the mixture, including inorganics and oxygen, resulting in about 3 wt.% of ashes. Finally, the relatively large standard deviations that have been observed can be thus assigned to the high heterogeneity of the WEEE plastic mixture, and therefore in the following sections of this work the average measured values have been taken into account for further calculations.

4. RESULTS AND DISCUSSION

4.2 Physicochemical properties of investigated catalysts

The physicochemical properties of the investigated catalysts are examined in this section. The structural features of the studied catalysts were evaluated by X-Ray Diffraction, N₂ physisorption and Scanning Electron Microscopy, while acidic properties, such as the type and strength of acid sites and the aluminium content and location, were assessed by NH₃-TPD, FT-IR with the adsorption of D₃-acetonitrile, ICP-OES and ²⁷Al ssNMR analyses.

4.2.1 Commercial nanocrystalline ZSM-5 zeolite

Structural and textural properties

A commercial nanocrystalline H-ZSM-5 zeolite supplied by Clariant (MFI_42) has been characterized to be employed as catalyst in the following pyrolysis of WEEE plastic tests. The XRD spectrum of MFI_42 zeolite is shown in Figure 4.4. The sample exhibited the characteristic pattern of MFI structure [64], with the most intense peaks located in the 2 θ ranges of 7.9 – 9.6 ° and 23.0 – 24.0 °, and no other phases were detected. Furthermore, no bottom reflection was observed, demonstrating the high crystallinity of the sample and the absence of amorphous material.

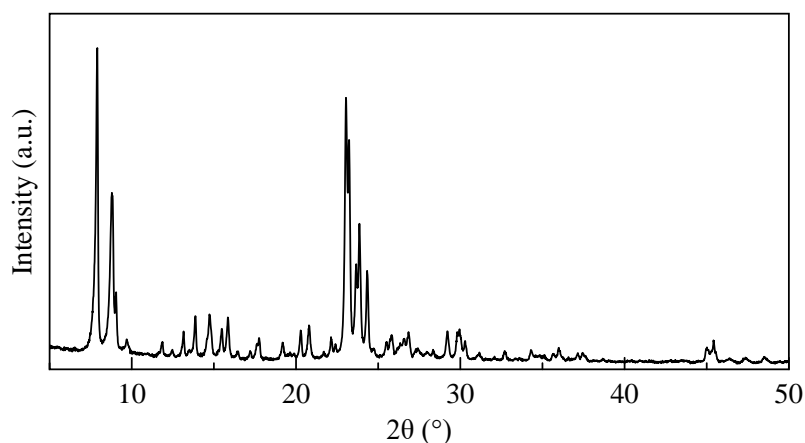


Figure 4.4 - XRD patterns of commercial nanocrystalline ZSM-5.

N₂ adsorption-desorption isotherms at 77 K, as well as the pore size distribution, obtained by applying the Non-Local Density Functional Theory (NL-DFT) model assuming cylindrical pore geometry, are shown in Figure 4.5. The BET surface area of MFI_42 is 418 m²/g, while its external surface area, calculated by the t-plot method, is 66 m²/g, accounting

4. RESULTS AND DISCUSSION

for 16 % of the total BET surface area (Table 6). The analysis revealed an adsorption isotherm of type I, typical of microporous materials, with a hysteresis loop at $p/p_0 \sim 0.95$, indicating the presence of interparticular mesoporosity. From the pore size distribution, obtained by applying NL-DFT model on the adsorption branch, it is possible to identify the main peak centred at 5.5 Å, typical of the micropores in MFI structure [64], together with weaker broad bands in the ranges 20 – 50 Å and 60 – 200 Å, mainly related to the voids existing within the crystals aggregates.

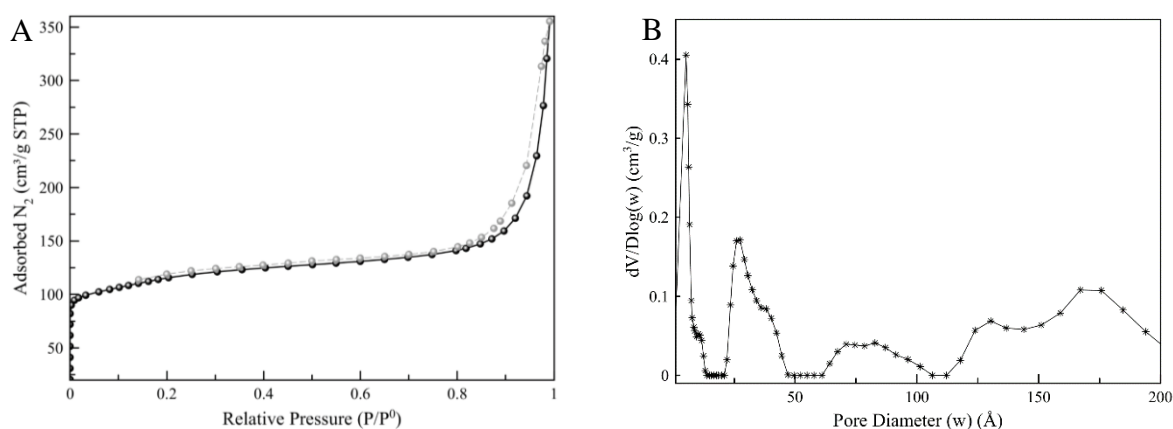


Figure 4.5 - A) N₂ adsorption (black lines) and desorption (grey lines) isotherms at 77 K, and B) Pore size distribution, obtained by applying NL-DFT model, of MFI₄₂ zeolite.

Table 6 - Textural properties of commercial nanocrystalline MFI₄₂ zeolite.

Sample	Si/Al ^a bulk (mol/mol)	S _{BET} ^b (m ² /g)	S _{mic} ^c (m ² /g)	S _{EXT} ^c (m ² /g)	V _{tot} ^d (cm ³ /g)	V _{mic} ^c (cm ³ /g)	V _{non-mic} ^e (cm ³ /g)
MFI ₄₂	42	418	352	66	0.432	0.154	0.278

^a Determined by ICP-OES.

^b BET specific surface area.

^c Calculated by *t*-plot method.

^d Estimated by applying the NL-DFT method.

^e Calculated by difference, V_{tot} - V_{mic}.

Acidity and Aluminium environment assessment

The environment of aluminium in the zeolite MFI₄₂ was studied by ²⁷Al ssNMR, which allows the quantification of the tetrahedrally coordinated aluminium species (Al^{IV}) at 54 ppm and the extra-framework penta-coordinated Al^V or octahedral Al^{VI} at 30 and 0 ppm, respectively.

4. RESULTS AND DISCUSSION

The recorded spectrum (Figure 4.6) proved the presence of just a small fraction of extra-framework octahedral Al^{VI} , accounting for the 1.8 % of the total calculated area, probably extracted during the calcination processes [62,72]. On the other hand, no penta-coordinated Al species were found. Finally, the Full Width at Half Maximum (FWHM) of the framework aluminium peak at 54 ppm was measured, which stood at 6.95, that is in agreement with the data reported elsewhere [156].

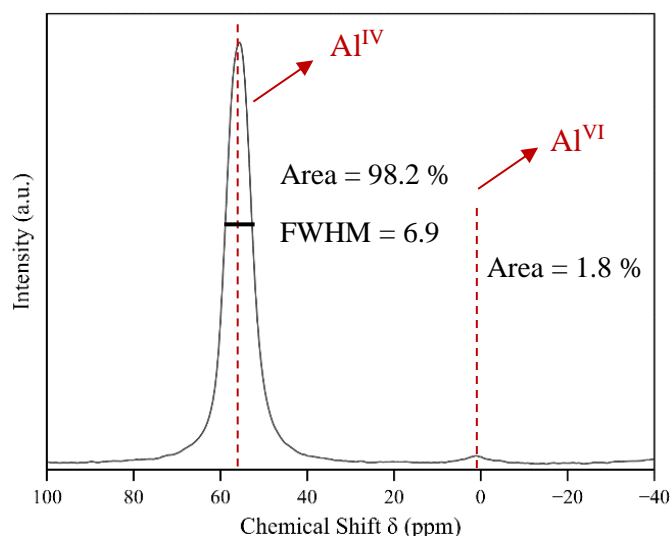


Figure 4.6 - ^{27}Al ssNMR spectrum of MFI_42 sample.

NH_3 -TPD measurement was performed to evaluate the concentration and the strength of the nanocrystalline zeolite acid sites. The analysis revealed the characteristic bimodal desorption curve, showing the desorption peaks centred at 235 °C and at 445 °C (Figure 4.7 A). The deconvolution of the desorption curve allowed to calculate the concentration of weak and strong acid sites, and the obtained results are summarized in Table 7.

The peak at temperature lower than 325 °C corresponds to the interaction between ammonia molecules and weak sites, including silanols, and leads to a concentration of 102 $\mu\text{mol}_{\text{NH}_3}/\text{g}_{\text{CAT}}$. The desorption peak located above 350 °C is attributed to ammonia adsorbed onto strong acid sites, and the calculated concentration stood at 278 $\mu\text{mol}_{\text{NH}_3}/\text{g}_{\text{CAT}}$. The total measured acidity amounted to 380 $\mu\text{mol}_{\text{NH}_3}/\text{g}_{\text{CAT}}$, in line with the measured Si/Al ratio.

4. RESULTS AND DISCUSSION

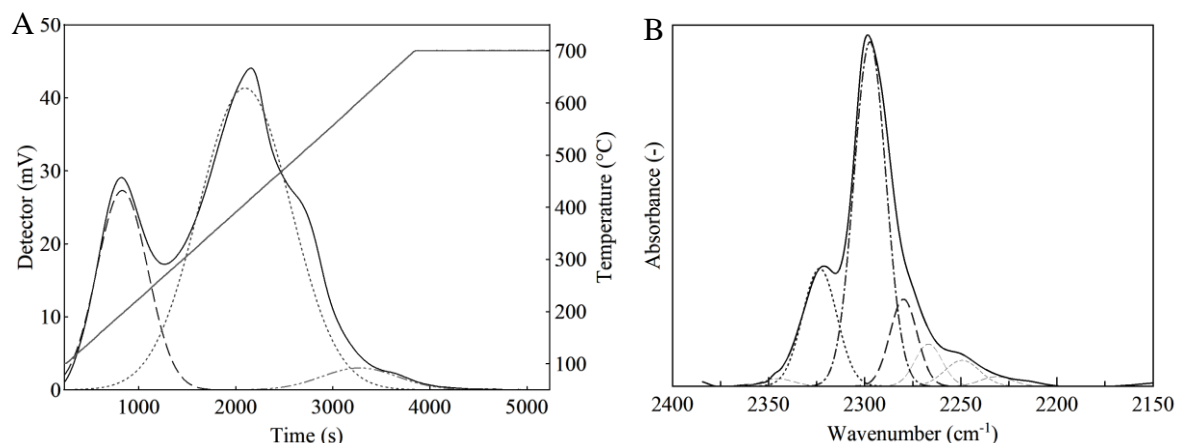


Figure 4.7 - A) NH_3 -TPD data and deconvolution curves, and B) FT-IR spectrum and deconvolution curves after the absorption of D_3 -acetonitrile of MFI_42.

FT-IR analysis after the adsorption of D_3 -acetonitrile, used as probe molecule, was carried out in order to assess the types of acid centres. Brønsted and Lewis acid sites were identified considering the ν -stretching vibration bands ($\text{C}\equiv\text{N}$) at 2297 and 2325 cm^{-1} , respectively (Figure 4.7 B) [138,139]. The number of both acid sites was calculated by the integrated area of the bands, by using the appropriate extinction factors ($\text{LAS} = 3.6\text{ cm}/\mu\text{mol}$, $\text{BAS} = 2.05\text{ cm}/\mu\text{mol}$), and the experimental results are shown in Table 7.

Table 7 - Acidic properties of MFI_42 zeolite.

Sample	Weak AS ^a ($\mu\text{mol}_{\text{NH}_3}/\text{g}_{\text{CAT}}$)	$T_{\text{weak}}^{\text{b}}$ ($^{\circ}\text{C}$)	Strong AS ^a ($\mu\text{mol}_{\text{NH}_3}/\text{g}_{\text{CAT}}$)	$T_{\text{strong}}^{\text{c}}$ ($^{\circ}\text{C}$)	Brønsted AS ^d ($\mu\text{mol}/\text{g}_{\text{CAT}}$)	Lewis AS ^d ($\mu\text{mol}/\text{g}_{\text{CAT}}$)	B/L ratio	Total AS ^e ($\mu\text{mol}/\text{g}_{\text{CAT}}$)
MFI_42	102	235	278	445	267	56	4.77	323 (380)

^a Calculated by NH_3 -TPD.

^b Temperature of desorption of weak acid sites calculated by NH_3 -TPD.

^c Temperature of desorption of strong acid sites calculated by NH_3 -TPD.

^d Determined by FT-IR after adsorption of D_3 -acetonitrile.

^e Into brackets the total acid sites calculated from NH_3 -TPD.

The total acidity measured by FT-IR revealed to be in good agreement with the NH_3 -TPD result, despite being slightly lower. Moreover, the B/L ratio amounted to 4.77, in line with the Al content, whilst the strong-to-weak (s/w) acid sites ratio stood at 2.73. These differences can be explained by considering both the nature of the analyses employed and of the type of zeolite acid sites. NH_3 -TPD analysis allows the quantification of strong and weak

4. RESULTS AND DISCUSSION

acid sites, which are attributed on the basis of the desorption temperature, but it does not provide any information about the nature of the site from which the probe molecule desorbs [157]. On the other side, FT-IR analysis allows to discriminate between Brønsted and Lewis acid sites, since the reversible protonation of the probe molecule by the acid sites results in changes of the absorption energy in the infrared region, which differ according to the nature of the acid sites themselves [158].

Furthermore, it must be taken into account that, despite being the proton in the Si-OH-Al bridge of zeolites usually identified as strong Brønsted acid site, different silanols (nest, vicinal, geminal or terminal) can be generated by hydroxyl groups differently bonded to silicon atoms, which induce the formation of weak acid centres with Brønsted character. This can explain the higher total acidity measured by NH₃-TPD, which does not discriminate between the type of acid sites, as well as the differences in B/L and s/w ratios, since the weak silanols adsorb in a different IR region and, therefore, they are counted in the ammonia-TPD low-temperature band, but not into the ν -stretching vibration band at 2297 cm⁻¹ [157,159,160].

4.2.2 Synthesized ZSM-5 zeolites

Structural and textural properties

The three synthesized ZSM-5 zeolites with different Si/Al ratio (MFI_11, MFI_25, and MFI_100) have been characterized in order to assess both textural and acidic properties.

X ray diffractograms of the investigated catalysts are shown in Figure 4.8. All the analysed samples exhibited the characteristic pattern of MFI zeolites, according to the published reference patterns [64]. The intensity of the peaks at $2\theta = 7.9$ and 8.9° decreases following the Si/Al ratio, which could be related to the different growth of the crystals, since no other phases were detected. However, all the samples showed both good crystallinity and high purity, without detectable proportions of amorphous phase.

The silicon to aluminium ratio of the synthesized catalysts was measured by ICP-OES analysis, and the results, shown in Table 8, revealed measured values very similar to the theoretical ones.

4. RESULTS AND DISCUSSION

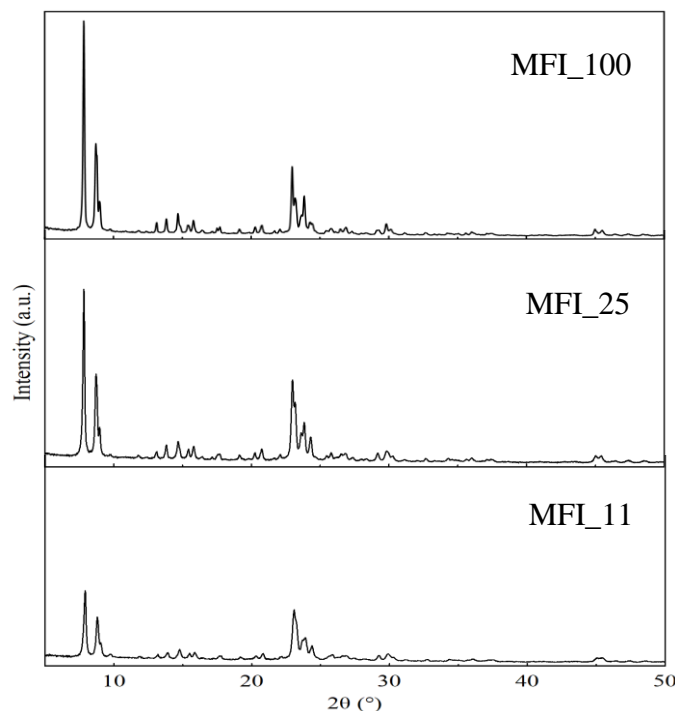


Figure 4.8 - XRD patterns of synthesized ZSM-5 zeolites with different Si/Al ratio.

The N₂ adsorption-desorption isotherms at 77 K of the investigated ZSM-5 zeolites are reported in Figure 4.9. The analysis of the samples with silicon to aluminium ratio of 11 and 25 revealed adsorption isotherms of type I, typical of microporous materials. Moreover, a lesser extent of adsorption can also be observed at p/p^0 higher than 0.4, indicating a small contribution of the external surface. This was also confirmed by the pore size distribution obtained by applying the Non-Local Density Functional Theory (NL-DFT) model to the nitrogen adsorption branch, assuming cylindrical pore geometry (Figure 4.10). Both samples exhibit a high intensity peak centred at 5.5 Å, which is characteristic of micropores of the ZSM-5 structure, and another contribution in the range 20-40 Å, attributable to the voids existing within the crystals aggregates. Finally, the desorption branch of the investigated samples shows a H4 hysteresis loop at p/p^0 at 0.5, which is typical of aggregated or hierarchical zeolites materials.

MFI_100 sample showed a I/IV type adsorption isotherm, which is typical of mesoporous materials. However, no specific procedures have been carried out to induce mesoporosity in this sample, and therefore the cause is to be searched in the crystals features. It has been showed that an increase in mesoporosity can be observed in presence of small and/or stacked crystals, and this results in wider pore size distribution, as well as in higher external-mesoporous area [161].

4. RESULTS AND DISCUSSION

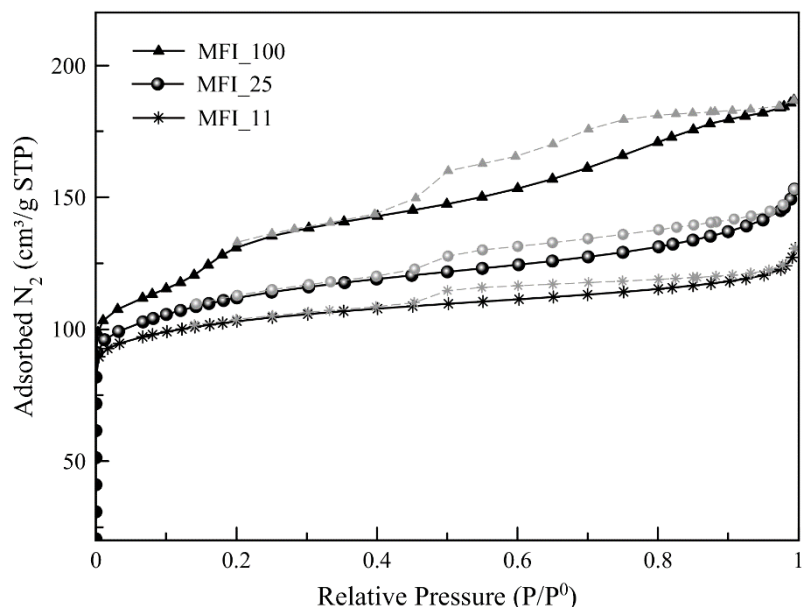


Figure 4.9 - N_2 adsorption (black lines) and desorption (grey lines) isotherms at 77 K of the investigated ZSM-5 zeolites.

As shown in Figure 4.10, in the case of MFI_100, the characteristic peak of ZSM-5 micropores (5.5 Å) lost intensity, while the broad peak in 20-40 Å range was shifted both to larger diameter (29 Å) and higher intensity, compared to the other investigated catalysts. Furthermore, other broad peaks can be observed in the range 45-250 Å, centred at 65, 101 and 176 Å, confirming the presence of different families of mesopores.

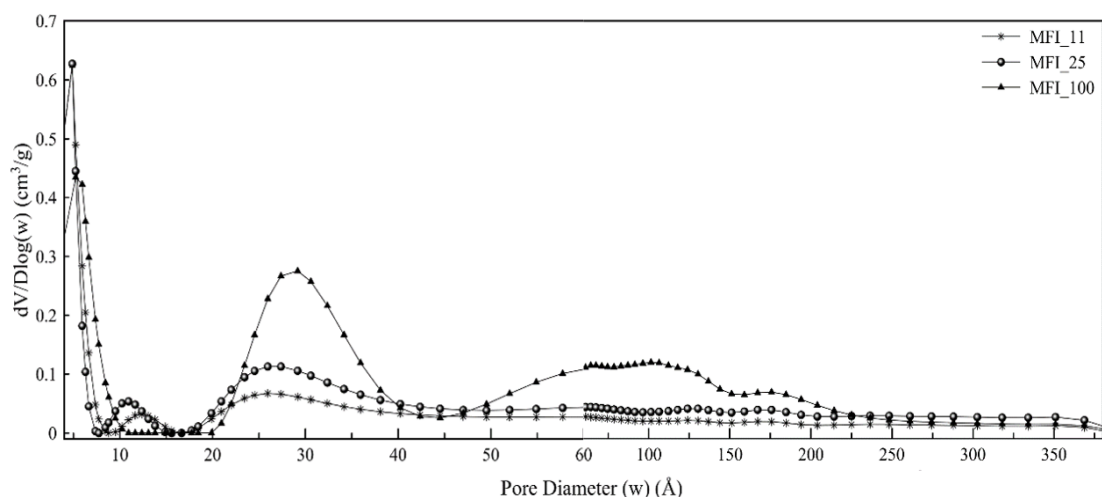


Figure 4.10 - Pore size distribution of the investigated ZSM-5 zeolites determined by applying NL-DFT model.

4. RESULTS AND DISCUSSION

Table 8 summarizes the textural properties of the synthesized ZSM-5 zeolites, in terms of specific surface area (S_{BET}), micropores area (S_{mic}), external/mesopores surface area ($S_{\text{Ext-Mes}}$), total pores volume (V_{tot}), micropores volume (V_{mic}), and non-microporous volume ($V_{\text{non-mic}}$).

As the Si/Al ratio increases, a rise of the proportion of external porosity can be observed, as also evidenced by the increase of the adsorption branch inclination at p/p_0 above 0.4 (Figure 4.9), and this is even more evident in MFI_100 sample, supporting the hypothesis of presence of stacked crystals.

Table 8 - Textural properties of the ZSM-5 synthesized samples.

Sample	Si/Al ^a bulk (mol/mol)	S_{BET} ^b (m ² /g)	S_{mic} ^c (m ² /g)	$S_{\text{Ext-Mes}}$ ^c (m ² /g)	V_{tot} ^d (cm ³ /g)	V_{mic} ^c (cm ³ /g)	$V_{\text{non-mic}}$ ^e (cm ³ /g)
MFI_11	10.9	399	312	87	0.201	0.121	0.080
MFI_25	23.6	418	283	135	0.233	0.114	0.119
MFI_100	109.5	455	141	314	0.298	0.063	0.235

^a Determined by ICP-OES.

^b BET specific surface area.

^c Calculated by t-plot method.

^d Estimated by applying the NL-DFT method.

^e Calculated by difference, $V_{\text{tot}} - V_{\text{mic}}$.

The crystals morphology of the investigated samples was explored by SEM analysis, and the obtained images are shown in Figure 4.11.

All samples showed spheroidal aggregates of interconnected crystals with the typical MFI coffin-shaped morphology [62,63]. However, differences can be observed both in terms of aggregates size and in crystals size and packing.

A comparable grains size was measured in MFI_11 and MFI_25 samples, in the order of 5 μm , whilst slightly smaller aggregates were detected in MFI_100 catalyst ($\sim 4 \mu\text{m}$). On the other side, the crystals size of this last proved to be similar to that of MFI_25, being in the 100 – 400 nm range, and, in both cases, smaller than that of MFI_11, this last standing in 800 – 1000 nm range.

Finally, by comparing the SEM images at both magnifications, it can be observed the MFI_100 crystals assume a more close-packed structure, compared with the other catalysts, in accordance with the textural properties discussed above.

4. RESULTS AND DISCUSSION

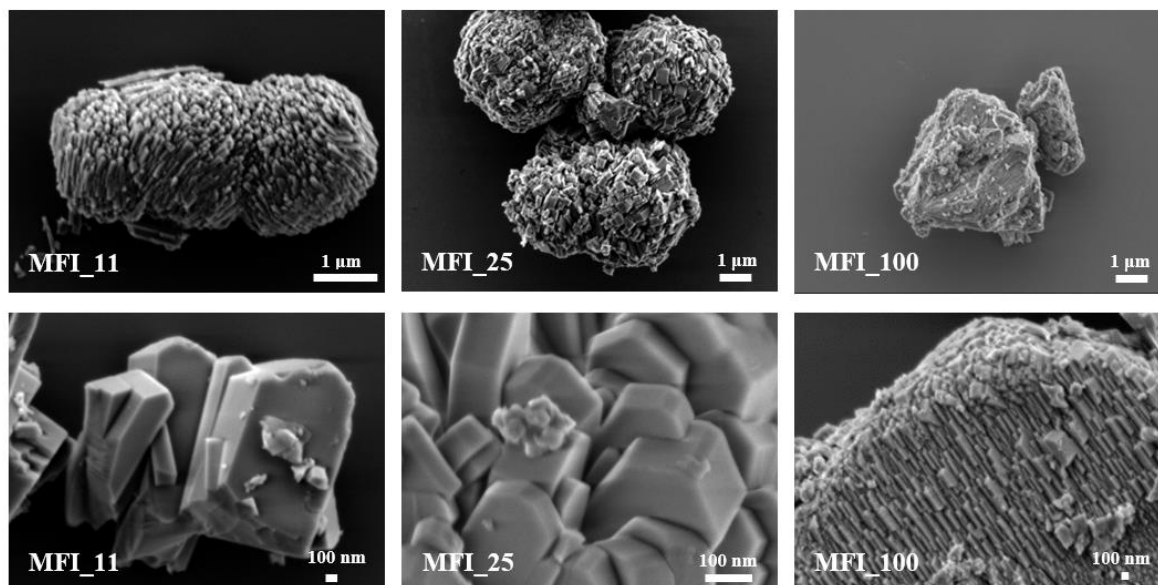


Figure 4.11 - SEM images at different magnifications of MFI_11, MFI_25, and MFI_100.

Acidity and Aluminium environment assessment

Aluminium speciation in the synthesized catalysts was studied by solid-state ^{27}Al NMR and the obtained spectra are shown in Figure 4.12. For all the investigated samples, it is possible to observe the most intense peak centred at 54 ppm, which is related to framework Al^{IV} tetrahedrally coordinated. A second smaller peak was identified at 0 ppm, associated to the Extra-Framework octahedral Al^{VI} species (EFAl), whilst no penta-coordinated extra-framework Al^{V} species were detected at 30 ppm [162].

The proportion of EFAl was estimated as percentage relative area of the NMR peaks, obtained by spectra deconvolution using Gaussian functions. The results revealed that the extra-framework aluminium concentration increases with the rise of the total Al content, in accordance with literature data [161], thus growing in the order MFI_100 (1.1 %), MFI_25 (8.0 %), and MFI_11 (16.9 %). The presence of extra-framework octahedral aluminium species even in low-Al content ZSM-5 zeolites, as in the synthesized MFI_100 sample, has been attributed to the partial framework dealumination which occurs during the post-synthesis treatments, such as the calcination processes, whose extent is higher when the total Al content is greater [163].

4. RESULTS AND DISCUSSION

The EFAl species are recognised as the main responsible of Lewis acid sites formation [73, 164], so that an increase in the proportion of this type of acidic centres with the decreasing of the Si/Al ratio is expected.

The Full Width at Half Maximum (FWHM) related to the peak of the Al incorporated in the framework (at 54 ppm) was calculated for each sample, which is index of the uniformity of the Al environment in the zeolitic structure. In fact, for the bridging OH, each T-atom can be Si or Al, and therefore there are four possible configurations, expressible as $\text{Al}_3\text{Si-OH-AlSi}_3$, $\text{Al}_2\text{SiSi-OH-AlSi}_3$, $\text{AlSi}_2\text{Si-OH-AlSi}_3$, and $\text{Si}_3\text{Si-OH-AlSi}_3$, characterized by different T-O-T angles (T being Si or Al). A large variety of aluminium environments in the structure is reflected in the widening of the NMR peak, and therefore in higher FWHM values [157]. The measured FWHM values (Figure 4.12) increases according to the total aluminium content, denoting a change in the T-O-T angles and thus confirming the larger variety of structural Al environments with the decrease of the Si/Al ratio.

It must be considered that the Al environment also affects the strength of the Brønsted acid site, since the higher the electronegativity of nearest atoms, the stronger the electron shift from H to O, resulting in a weakening of the O-H bond, and therefore in the rise of the acid strength. On this basis, as the total aluminium content increases, it is expected a decrease of the B/L ratio, due to the growth of L-AS concentration (EFAl), as well as a greater proportion of weak acid sites than the stronger, related to lower electronegativity of Al than Si [157].

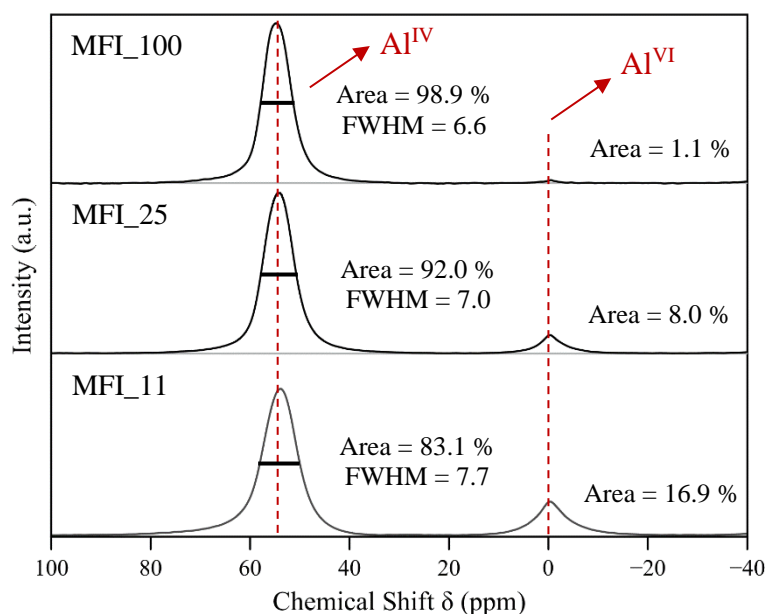


Figure 4.12 - ^{27}Al ssNMR spectra of synthesized MFI zeolites.

4. RESULTS AND DISCUSSION

The concentration and the strength of acid sites of the synthesized catalysts was evaluated by NH₃-TPD measurement. Experimental results (Figure 4.13) revealed bimodal desorption curves for all the investigated samples, which are typical of ZSM-5 zeolites. The first desorption peak in the range 150-325 °C is attributed to ammonia molecules adsorbed onto weak acid sites, whilst the peak observed above 350 °C is generated by the interaction between NH₃ and the strong acid sites. Curves deconvolution with Gaussian functions was used to calculate the acid sites concentrations.

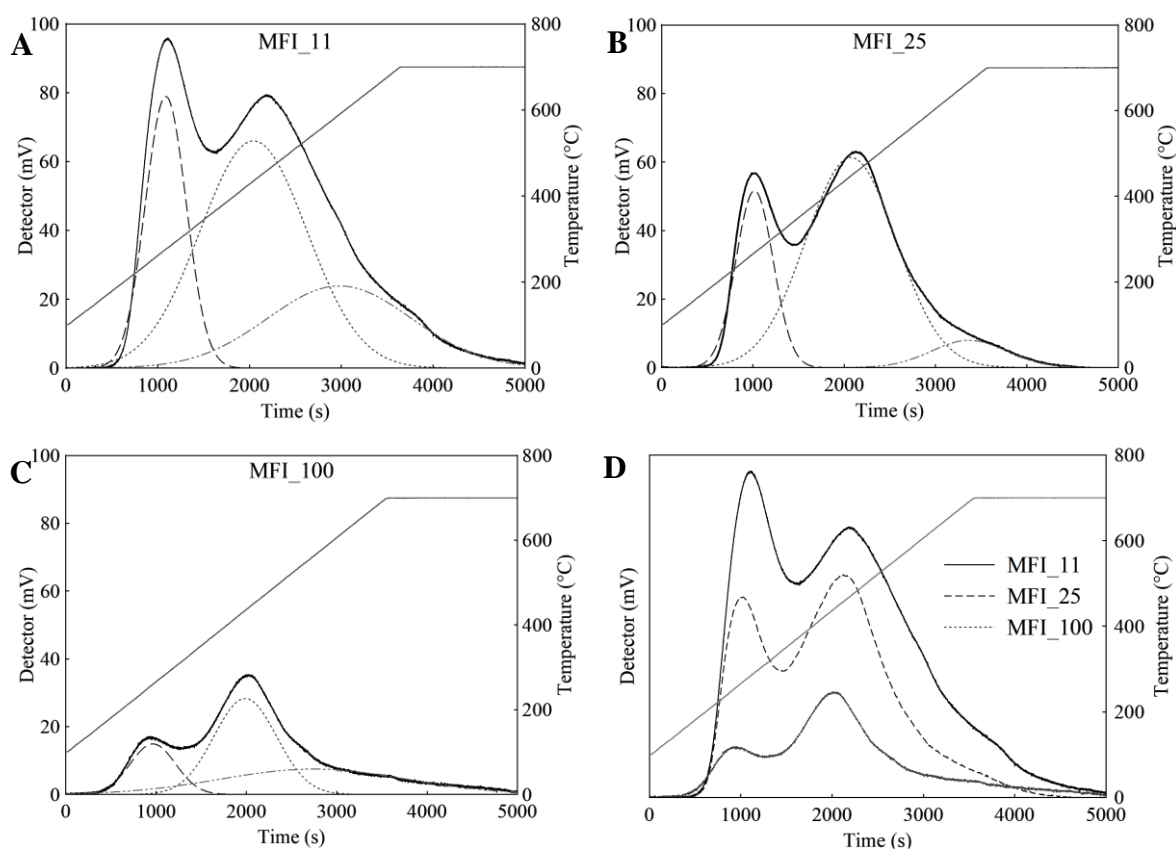


Figure 4.13 - NH₃-TPD data and deconvolution curves (A-C) and comparison of the three investigated catalysts (D).

Data from Table 9 show that the total acidity decreases as the ratio $S_{\text{ext-Mes}}/S_{\text{Mic}}$ is augmented, in accordance with literature data [165], going from 713, to 540, and 152 $\mu\text{mol}_{\text{NH}_3}/\text{g}_{\text{CAT}}$ for MFI_11, MFI_25, and MFI_100, respectively. This trend is ascribed to the total aluminium content, which contributes to the formation of both Lewis and Brønsted acid sites, as previously discussed.

4. RESULTS AND DISCUSSION

On the other side, the strong-to-weak (S/W) acid sites ratio does not follow a linear trend: the lowest value was detected for MFI_11 (2.2), whilst 2.8 and 2.6 have been calculated for MFI_25 and MFI_100, respectively. In the case of MFI_11, the observed S/W value is in line with the NMR results, since the high Al content leads to both the strengthening of the O-H bond in the T-OH-T bridges and L-AS formation, and thus to a higher concentration of weak acid centres. MFI_25 and MFI_100 samples exhibit similar S/W values: as already discussed, ammonia-TPD analysis does not discriminate between Brønsted and Lewis acid sites, therefore it can be assumed that in presence of a higher Al content (MFI_25) the greatest contribution to the weak acid sites formation is provided by EFAl species, whilst Brønsted terminal silanols, generally weaker than T-OH-T bridges, mainly affect the weak acid sites concentration at higher Si/Al ratios.

To discriminate between Brønsted and Lewis acid sites, the synthesised zeolites were studied by FT-IR analysis with the adsorption of deuterated acetonitrile as a probe molecule.

For all the investigated catalysts, a first band in the range 2321-2325 cm^{-1} , associated to the Lewis acid sites, and a second band, centred at 2297 cm^{-1} and related to the Brønsted acid sites, were identified (Figure 4.14). Smaller bands at lower wavenumbers, associated to physisorbed acetonitrile, also appeared.

The concentration of Brønsted and Lewis acid sites was calculated by the FT-IR curves deconvolution, by using the extinction factors of 2.05 and 3.60 $\text{cm}/\mu\text{mol}$, respectively. Table 9 summarizes the quantitative results referring to the investigated samples and the Brønsted-to-Lewis ratios (B/L) measured at room temperature.

The total acidity calculated by FT-IR proved to be in good agreement with the NH_3 -TPD results. However, the values measured by TPD are slightly higher than those estimated by IR for MFI_25 and MFI_100 samples, supporting the hypothesis that the contribution of weak silanols increases at lower Al contents.

As expected, with the Si/Al ratio rise, both Brønsted and Lewis acid sites concentrations decreased, while the B/L ratio proved to be augmented. However, this last ratio does not follow a linear trend, being more quickly increased from MFI_11 to MFI_25 than from MFI_25 to MFI_100. This finding can be explained by studying the trends of B-AS and L-AS as a function of the Si/Al ratio. With the increase of total Al content, the B-AS concentration almost linearly increased, being mainly related to the share of Si-OH-Al bridges in the structure, whilst the L-AS amount quickly augmented from MFI_11 to

4. RESULTS AND DISCUSSION

MFI_25 and in a lesser extent from MFI_25 to MFI_100, showing an almost linear correlation with the EFAl content measured by NMR (Figure 4.12).

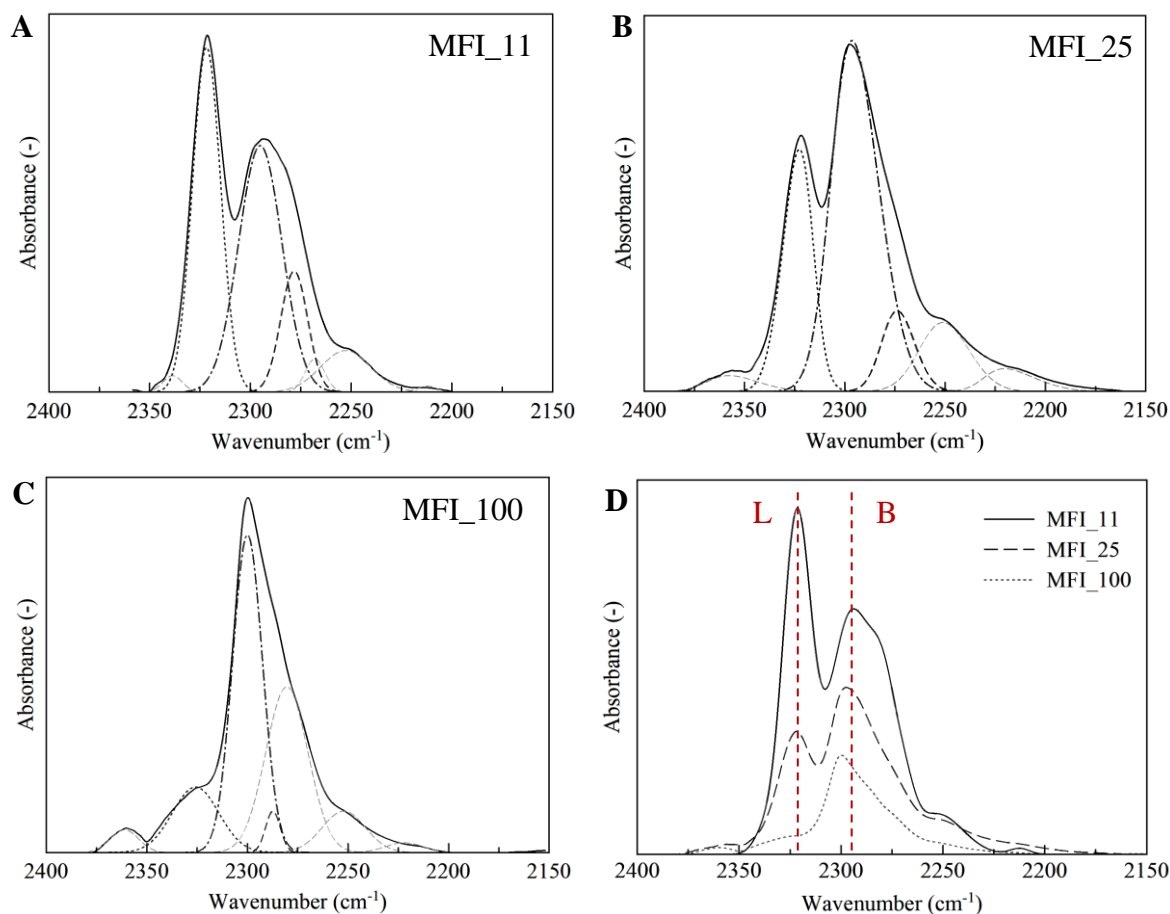


Figure 4.14 - FT-IR spectra after the adsorption of D₃-acetonitrile. Data and deconvolution curves (A-C) and comparison of the three studied samples (D).

Table 9 - Acidic properties of the synthesized MFI samples.

Sample	Weak AS ^a (μmol _{NH₃} /g _{CAT})	T _{weak} ^b (°C)	Strong AS ^a (μmol _{NH₃} /g _{CAT})	T _{strong} ^c (°C)	Brønsted AS ^d (μmol/g _{CAT})	Lewis AS ^d (μmol/g _{CAT})	B/L ratio	Total AS ^e (μmol/g _{CAT})
MFI_11	224	276	489	435	488	253	1.93	741 (713)
MFI_25	141	268	399	447	378	95	3.98	473 (540)
MFI_100	42	260	110	435	125	23	5.43	148 (152)

^a Calculated by NH₃-TPD.

^b Temperature of desorption of weak acid sites calculated by NH₃-TPD.

^c Temperature of desorption of strong acid sites calculated by NH₃-TPD.

^d Determined by FT-IR after adsorption of D₃-acetonitrile.

^e Into brackets the total acid sites calculated from NH₃-TPD.

4. RESULTS AND DISCUSSION

4.2.3 Hierarchical h-ZSM-5 zeolite

Structural and textural properties

The hierarchical ZSM-5 zeolite has been characterized and compared with the parent MFI_25 to evaluate the effects of the desilication process on its textural and acidic properties.

The XRD pattern of the h-MFI catalyst is shown in Figure 4.15. After the desilication procedure, the sample exhibits the characteristic pattern of ZSM-5 zeolites, with good purity and crystallinity, and no other phases or amorphous were observed, indicating that no rearrangements in the framework occurred.

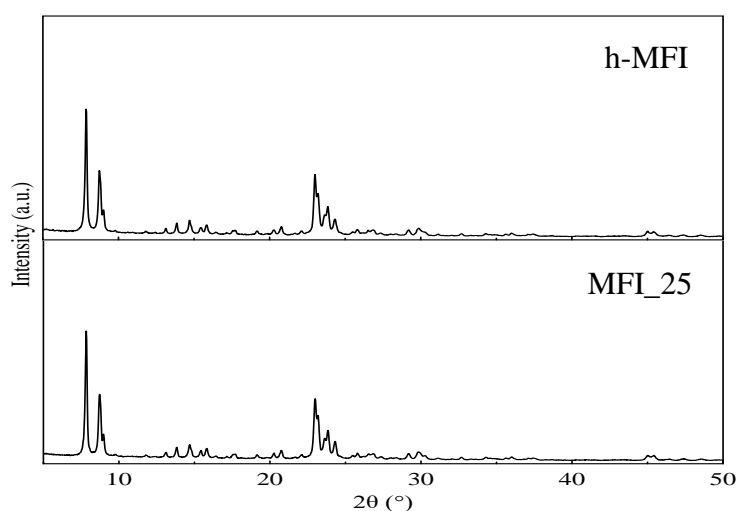


Figure 4.15 - XRD patterns of the parent MFI_25 and hierarchical h-MFI samples.

As expected, the measured Si/Al ratio of h-MFI proved to be lower than that of MFI_25 because of the selective alkaline-induced silicon removal from the zeolite framework, being reduced from 23.6 to 21.7 mol/mol (Table 10).

N₂ physisorption at 77 K was performed to evaluate the textural properties of the hierarchical catalyst and the results are reported in Figure 4.16.

4. RESULTS AND DISCUSSION

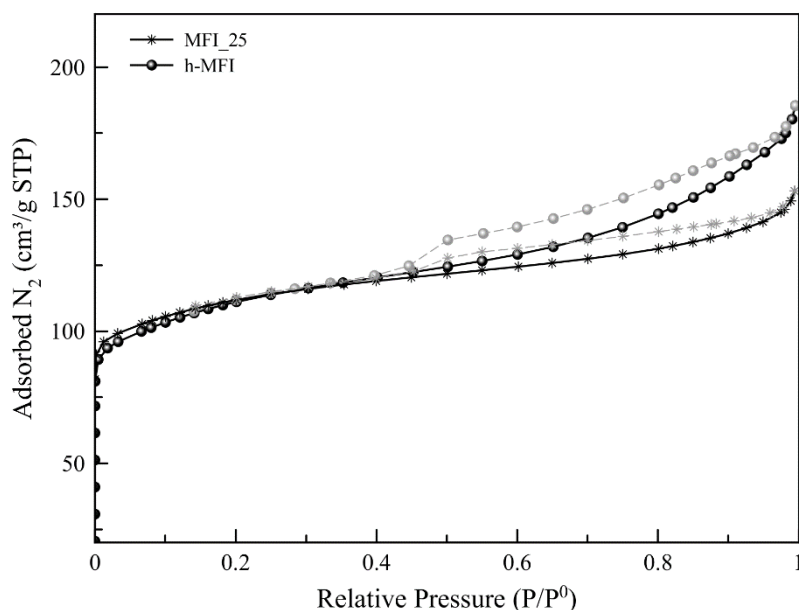


Figure 4.16 - N₂ adsorption (black lines) and desorption (grey lines) isotherms at 77 K of the parent MFI₂₅ and hierarchical h-MFI samples.

The adsorption-desorption isotherms of the h-MFI catalyst are characteristic of aggregated or hierarchical ZSM-5 zeolites, being of I/IV type. Compared to the parent MFI₂₅, the desilication treatment induced a significant change in the shape of the isotherms, since enhanced adsorption appears at intermediate-high relative pressures. Furthermore, a wide hysteresis loop of type H4, with almost parallel adsorption and desorption branches, can be observed, typically associated to open mesopores on the outer surface [166].

The rise of the secondary porosity was also confirmed by the rise of the external/mesopores area, being increased with respect to the parent sample from 135 to 166 m²/g (Table 10).

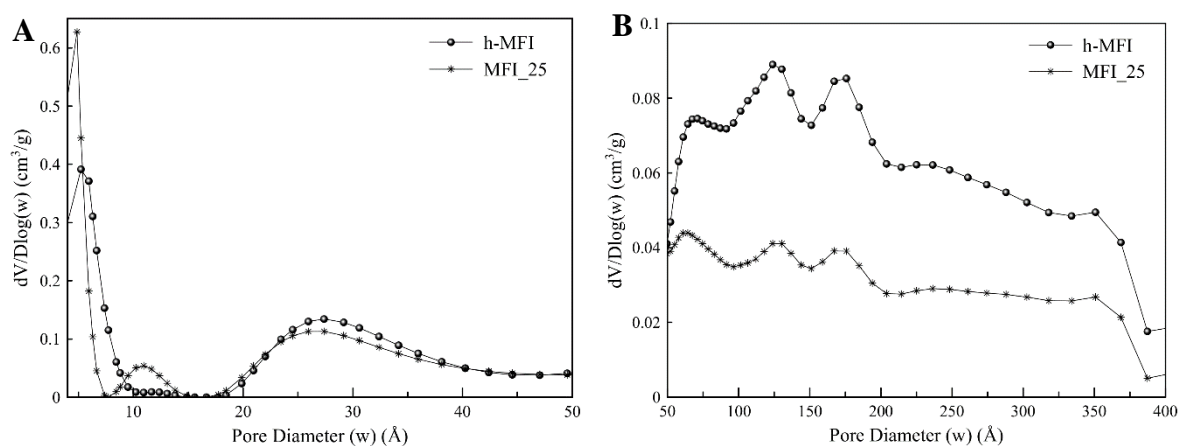


Figure 4.17 - Pore size distribution obtained by applying NL-DFT model.

4. RESULTS AND DISCUSSION

This finding was also confirmed by the pore size distribution, obtained by applying the NL-DFT model to the nitrogen adsorption branch (Figure 4.17). Compared to the parent MFI_25 catalyst, the concentration of micropores (5.5 Å) was decreased and shifted toward bigger diameters because of the desilication treatment, indicating a partial collapse of the micropores originally present. Furthermore, a rise can be observed in mesopores concentration ranged between 20 and 50 Å, together with a smaller growth of bigger mesopores in the 50 – 400 Å interval.

Table 10 - Textural properties of hierarchical h-MFI, compared with the parent sample MFI_25.

Sample	Si/Al ^a bulk (mol/mol)	S _{BET} ^b (m ² /g)	S _{mic} ^c (m ² /g)	S _{Ext-Mes} ^c (m ² /g)	V _{tot} ^d (cm ³ /g)	V _{mic} ^c (cm ³ /g)	V _{non-mic} ^e (cm ³ /g)
MFI_25	23.6	418	283	135	0.233	0.114	0.119
h-MFI	21.7	407	241	166	0.281	0.099	0.182

^a Determined by ICP-OES.

^b BET specific surface area.

^c Calculated by t-plot method.

^d Estimated by applying the NL-DFT method.

^e Calculated by difference, V_{tot} - V_{mic}.

The generation of the secondary porosity by means of alkaline-induced desilication treatment was also confirmed by the Scanning Electron Microscopy (Figure 4.18). Both the MFI-25 and h-MFI samples exhibited spheroidal aggregates, similar in size, of interconnected crystals with the typical MFI coffin-shaped morphology.

However, when compared with the parent MFI_25 at higher magnifications, the crystals of desilicated zeolite showed a rougher external surface, due to the partial dissolution of framework silicon species.

Moreover, abundant voids within the crystals aggregates can be detected, which contribute of some mesoporosity in all samples, as observed in the textural properties of Table 10, and whose dimensions fit well with the pore size distribution previously described.

4. RESULTS AND DISCUSSION

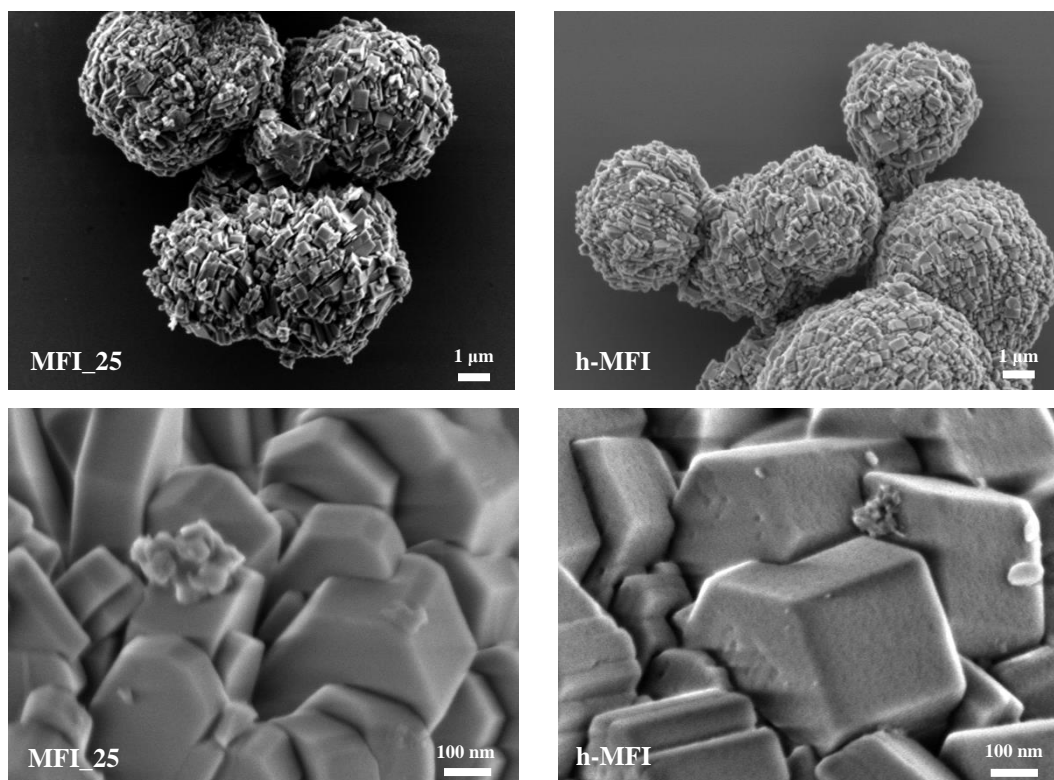


Figure 4.18 - SEM images at different magnifications of desilicated h-MFI and the parent zeolite MFI_25.

Acidity and Aluminium environment assessment

The change in the aluminium environment after the desilication process was studied by ^{27}Al ssNMR. The obtained spectra of the hierarchical h-MFI and the parent MFI_25 are shown in Figure 4.19.

On the total integrated area, the extra-framework aluminium increased from 8 % to 11 % as a result of the desilication, due to the ejection of a fraction of aluminium atoms from the framework concurrently with the silicon species during the alkaline treatment.

Furthermore, the desilication also induced structural changes in MFI_25, since the value of Full Width at Half Maximum (FWHM), measured for the peak at 54 ppm, has been increased from 7.0 to 7.9. The distortion of the tetrahedral aluminium environment can be ascribed to partial reinsertion of previously extracted Al into zeolite framework positions close to the vacancies generated during desilication [165].

4. RESULTS AND DISCUSSION

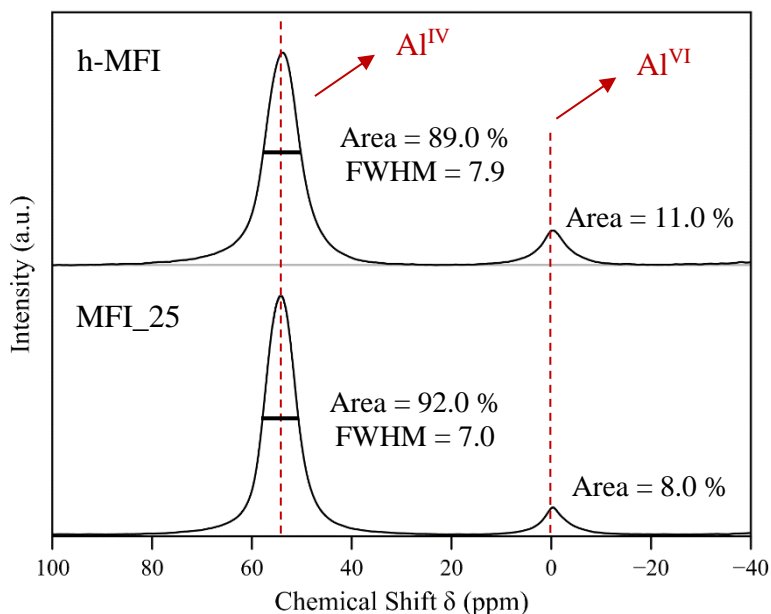


Figure 4.19 - ^{27}Al ssNMR spectra of parent MFI_25 and hierarchical h-MFI samples.

To assess the impact of the desilication treatment on the concentration and the strength of the acid sites, NH_3 -TPD of the desilicated catalyst h-MFI was carried out and compared with the parent sample MFI_25. The acid sites concentrations were calculated by performing the curve deconvolution, using Gaussian curves, and the experimental results are shown in Figure 4.20.

When compared with MFI_25, the weak acid sites concentration (at $T < 350$ °C) of h-MFI was incremented by 10 % as a consequence of the selective removal of the framework silicon.

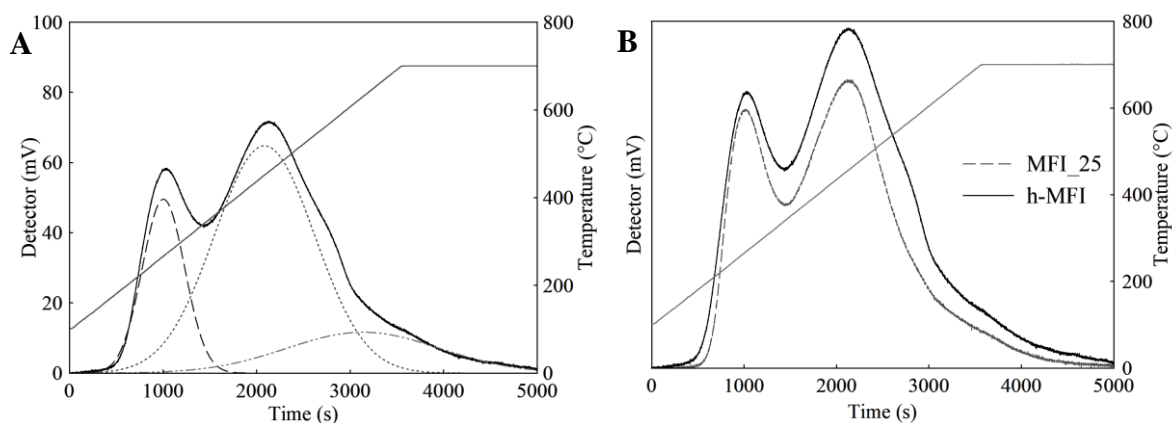


Figure 4.20 - NH_3 -TPD data and deconvolution curves (A) and comparison between hierarchical h-MFI and parent MFI_25 samples (B).

4. RESULTS AND DISCUSSION

The strong acid sites concentration (at $T > 350\text{ }^{\circ}\text{C}$) proved also to be augmented in h-MFI, whilst the S/W ratio increased from 2.8 to 3.1 as a result of the desilication process. These findings can be explained by considering the partial reinsertion of the extracted Al in the zeolite framework, which generates Brønsted acidity. However, the new formed B-AS are supposed to be weaker, since the proportion between Si and Al in the framework was partially shifted toward aluminium, as proved by the reduction of Si/Al ratio, causing an increase in the strength of the bridging OH bonds due to the lower Al electronegativity.

Finally, the total acidity resulted therefore to be enhanced from 540 to 635 $\mu\text{mol/gCAT}$ (Table 11) as a consequence of the selective removal of the framework silicon, which can be ascribed not only to the already mentioned presence of EFAl species and reinsertion of Al atoms, but also to the improved accessibility of the acid sites, as suggested by the measured textural properties (Table 10).

To discriminate Brønsted and Lewis acid sites, the desilicated sample was studied by FT-IR analysis with the adsorption of $\text{d}_3\text{-CH}_3\text{CN}$ (Figure 4.21). The integrated areas were used for the acid sites quantification and the results are reported in Table 11.

From the comparison with the parent MFI_25, it clearly appears that the desilication treatment led to an increase of the intensities of both bands centred at 2297 cm^{-1} and 2322 cm^{-1} , related to the Brønsted and Lewis acid sites, respectively.

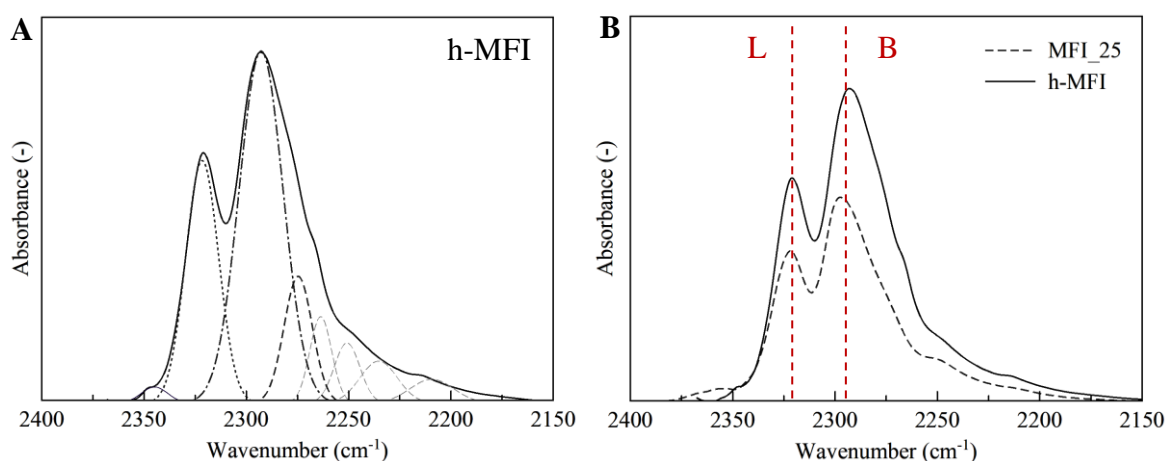


Figure 4.21 - FT-IR spectra after the adsorption of $\text{D}_3\text{-acetonitrile}$. Data and deconvolution curves of h-MFI (A) and comparison with the parent catalyst MFI_25 (B).

4. RESULTS AND DISCUSSION

However, the B/L ratio proved to be reduced from 4.0 to 3.4, indicating a larger contribution provided by L-AS than B-AS to the total acidity, which is consistent with the higher concentration of EFAl species detected in the sample with lower Si/Al ratio.

The total acidity measured by IR appears in good agreement to that calculated from NH₃-TPD, recalling that the small differences detected are mainly related to the intrinsic differences between the characterization techniques.

Table 11 - Acidic properties of h-MFI catalyst, compared with the parent MFI_25 sample.

Sample	Weak AS ^a ($\mu\text{mol}_{\text{NH}_3}/\text{g}_{\text{CAT}}$)	T ^{weak} ^b (°C)	Strong AS ^a ($\mu\text{mol}_{\text{NH}_3}/\text{g}_{\text{CAT}}$)	T ^{strong} ^c (°C)	Brønsted AS ^d ($\mu\text{mol}/\text{g}_{\text{CAT}}$)	Lewis AS ^d ($\mu\text{mol}/\text{g}_{\text{CAT}}$)	B/L ratio	Total AS ^e ($\mu\text{mol}/\text{g}_{\text{CAT}}$)
MFI_25	141	268	399	447	378	95	3.98	473 (540)
h-MFI	155	267	480	452	523	154	3.40	678 (635)

^a Calculated by NH₃-TPD.

^b Temperature of desorption of weak acid sites calculated by NH₃-TPD.

^c Temperature of desorption of strong acid sites calculated by NH₃-TPD.

^d Determined by FT-IR after adsorption of D₃-acetonitrile.

^e Into brackets the total acid sites calculated from NH₃-TPD.

4.2.4 Conclusions

The characterization of ZSM-5 zeolites has evidenced significant differences in terms of both structural and acidic properties. A summary of the main measured properties of all the investigated samples is reported in Table 12.

The study of the textural properties has shown a rise of the proportion of external porosity with the Si/Al ratio increase. However, the highest values of external-mesopores areas were detected in the samples MFI_42, MFI_100, and h-MFI, despite they have been attributed to different reasons. In the case of MFI_42 and MFI_100, the secondary mesoporosity has proved to be mainly related to the voids within the crystals aggregates, and this is attributable to the presence of nanocrystals and a close-packed structure, respectively. On the other hand, in h-MFI zeolite, the increase of S_{ext-Mes}, compared to the parent MFI_25, is due to the new open mesopores on the outer surface generated by the alkaline-induced desilication treatment, as demonstrated by both N₂ adsorption-desorption isotherms shape and SEM images.

4. RESULTS AND DISCUSSION

The acidic properties of the investigated ZSM-5 zeolites proved to be strictly affected by both Al content and environment. This was confirmed by the calculated B/L ratios, which increase with the Si/Al ratio, but more quickly at higher Al content, denoting that a greater contribution is provided from the Lewis acid sites to the total acidity as the total aluminium content increases. Moreover, it has been observed that the Lewis acid sites concentration in all samples is almost linearly correlated to the EFAl species quantity, since they proportionally increase. The only slight deviation was found in the sample MFI_42, which is a commercial zeolite and may have been subjected to different and less intrusive calcination processes.

Accordingly, also the Brønsted acid sites concentration resulted to be influenced by both Al environment and content. It can be noted that the amount of B-AS almost exponentially decreases according with the total aluminium content, since less T-OH-T (T being Si or Al) bridges can form in the zeolite structure, which are the main responsible of the strong Brønsted acidity. However, the desilicated h-MFI sample showed a B-AS concentration even greater than MFI_11, despite the lower total Al content. This has been attributed to a combination of two effects induced by the desilication treatment, i.e., i) the formation of new defects by etching, and therefore new terminal OH groups into MFI crystals, and ii) the partial reinsertion of the previously extracted aluminium atoms, resulting in a more heterogeneous Al environment, as also showed by the FWHM measured in the NMR peaks related to the intra-framework aluminium.

Table 12 - Summary of the main textural and acidic properties of the investigated catalysts.

Sample	Si/Al bulk (mol/mol)	S _{BET} (m ² /g)	S _{Ext-Mes} (m ² /g)	EFAl (area %)	FWHM ^a	Total AS ^b (μmol/g _{CAT})	B/L ratio
MFI_11	10.9	399	87	16.9	7.7	741	1.93
h-MFI	21.4	407	166	11.0	7.9	678	3.40
MFI_25	23.6	418	135	8.0	7.0	473	3.98
MFI_42	42.0	418	66	1.8	6.9	303	4.77
MFI_100	109.5	455	314	1.1	6.6	148	5.43

^a Calculated on the NMR peak at 54 ppm.

^b Determined by FT-IR after adsorption of D₃-acetonitrile.

4. RESULTS AND DISCUSSION

4.3 Dehydrochlorination of WEEE Plastic

In this section, the effect of the temperature on the dehydrochlorination efficiency of the real WEEE plastic is reported. As described in section 3.3, the pure PVC can be efficiently dechlorinated at 300 °C. However, the presence of other polymers and additives in the waste plastic mixture can shift the hydrochloric acid release toward higher temperature.

The TG Analysis (Figure 4.1) of the raw WEEE plastic (here labelled as P_Raw) revealed that the peak related to the HCl elimination extends in 200 – 350 °C temperature range, so that the dechlorination treatment was carried out by selecting two temperatures, i.e., 300 and 350 °C, in nitrogen flow, by heating the samples at 10 °C/min, with a holding time of 30 minutes.

On the basis of the reaction's temperature, the samples have been labelled as P_300 and P_350 in the following sections.

4.3.1 Reaction yields

The reactions yields obtained from the thermal dechlorination treatment at the two investigated temperatures are reported in Table 13.

By treating the sample at 300 °C, the 2 wt.% of oil was collected, while just the 0.04 wt.% accounted for the gaseous fraction. At higher temperature (350 °C), the fraction of organics lost increased by 61% in total, giving rise mainly to light molecules.

The hydrochloric acid trapped in water accounted for about 1 wt.% of the raw plastic waste at 300 °C, whilst at higher temperature, its concentration resulted to be increased by 43 %, amounting to 1.7 wt.%.

The loss of organics during the thermal treatment can be explained by considering that in the first stage of PVC decomposition, the HCl release from side-groups-elimination leads to the formation of polyolefin chains, which simultaneously undergo partial cracking reactions [142].

Moreover, it must be considered that the hydrochloric acid released, as well as chlorine radicals, can assume an auto-catalytic role, promoting both the dehydrochlorination and the unsaturated chains decomposition [18,167,168,169].

Therefore, the temperature rise caused the enhancement of both these effects, leading to both higher HCl elimination and thermal degradation degree.

4. RESULTS AND DISCUSSION

Table 13 - Product yields in the thermal dechlorination tests at 300 °C and 350°C.

Sample	Products yield (wt.%)			
	Dechlorinated Plastic	Water-Condensed gases*	Oil	Gas
P_300	97.00	0.96	2.00	0.04
P_350	94.91	1.70	3.10	0.29

*Calculated by difference

4.3.2 Products characterization

De-chlorinated plastics analysis

To estimate the dechlorination efficiency of the thermal treatment at the two investigated temperatures, the chlorine content of the dechlorinated plastic samples was measured by burning them in the calorimetric bomb and by analysing the resulting solutions by Ion Chromatography (AOD/IC). Furthermore, to evaluate any structural changes, the obtained samples were characterized by TG analysis and FT-IR spectroscopy.

Data from Table 14 show the residual chlorine content in the WEEE plastics after the thermal dechlorination treatments. It can be observed that more than 6000 ppm are still present in the P_300 sample, representing the 31.7 % of the initial chlorine, while a dechlorination efficiency of 86.4 % has been achieved by using 350 °C as reaction temperature.

The obtained results are in good agreement with literature data. In fact, previous works reported that small amounts of chlorine can be still present after mild thermal treatment of PVC-containing materials [104-107], since the released HCl could react again with the polyenes formed after its elimination, giving rise to chlorinated hydrocarbons [170].

Moreover, as mentioned in section 4.1, PVC can suffer photo-oxidation during the goods lifetime, leading to the formation of α -chlorinated conjugated polyenes, such as β -chlorocarboxylic acid, α,α -dichloro ketone and β -chloro anhydride, which could be also responsible for the remaining halogen in the pretreated plastics [144-145].

The TG analyses of raw and dechlorinated samples are reported in Figure 4.22. The sample R_300 shows a peak in the DTG curve in the range 200 – 350 °C, corresponding to a weight loss of 0.9 wt.%, denoting that further hydrochloric acid release occurred even after the thermal treatment.

4. RESULTS AND DISCUSSION

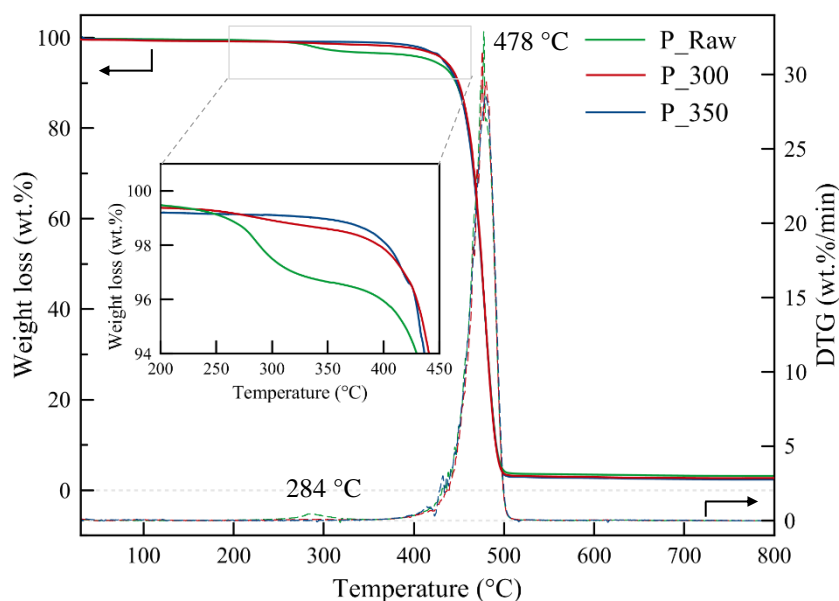


Figure 4.22 - Thermogravimetric analysis of raw plastic (P_Raw, green) and dechlorinated samples at 300 °C (P_300, red) and 350 °C (P_350, blue). TG in solid line and DTG in dashed line.

Increasing the reaction temperature up to 350 °C, no weight loss can be appreciated in the HCl-elimination temperature range, as evidence of the better chlorine removal effectiveness (Table 14).

Table 14 - Chlorine content and TGA results of dechlorinated samples.

Sample	Cl content in plastic ^a (ppm)	LT Weight Loss ^b (%)	HT Weight Loss ^c (%)	Total Weight Loss (%)
P_Raw	19518	3.4	93.8	97.2
P_300	6124	0.9	96.5	97.4
P_350	2652	0.0	97.6	97.6

^a Measured by AOD/IC.

^b Weight loss by TGA calculated in the range 200 °C – 350 °C.

^c Weight loss by TGA calculated in the range 350 °C – 800 °C.

The dechlorinated samples were characterized by FT-IR and the collected spectra in 500 – 4000 cm⁻¹ range are shown in Figure 4.23.

It can be observed that there are not significant differences among the spectra, since they are almost a copy of the fingerprint of PE (see section 4.1.2), accounting this last for about 95 wt.% of the raw WEEE plastic sample.

4. RESULTS AND DISCUSSION

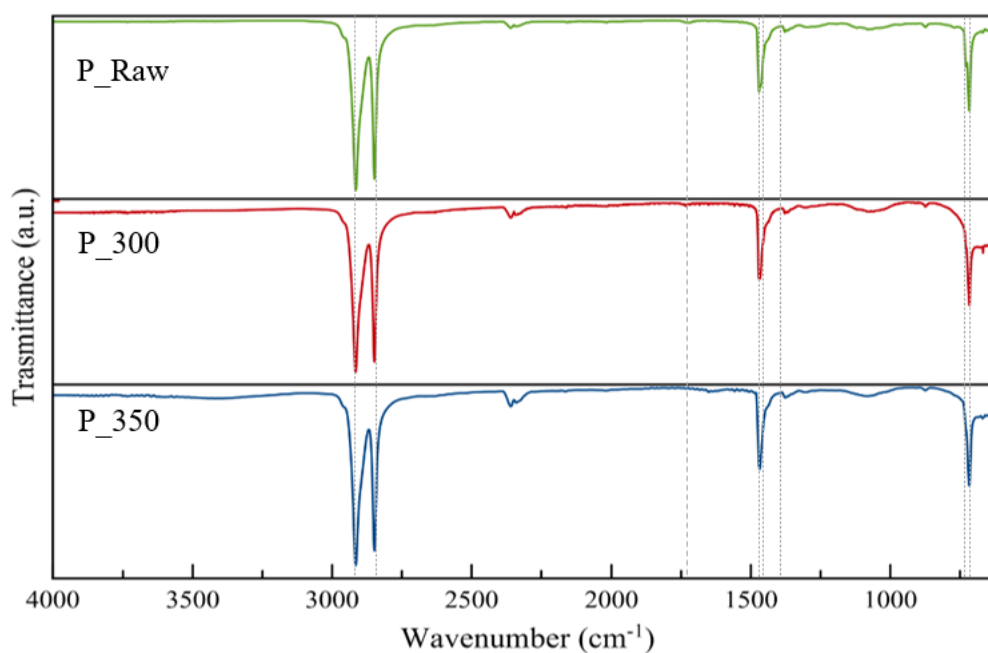


Figure 4.23 - ATR-FTIR spectra of raw WEEE plastic (P_Raw) and dechlorinated samples thermally treated at 300 °C (P_300) and 350 °C (P_350). Dashed lines are guides for readers.

In the view of reaching a deeper understanding of the changes induced in the WEEE plastic by the thermal treatment, the sample that showed the highest dechlorination efficiency, i.e. R_350, has been further analysed.

The chemical composition of P_350 was determined by proximate and elemental analysis and compared with the raw sample. Table 15 displays the experimental results.

Proximate analyses proved to be similar, since both samples loss about 97 – 98 wt.% of volatiles, with an ash content lower than 3 wt.%, related to the presence of inorganic additives in the polymers.

The elemental analysis shows that a decline of the oxygen content occurred simultaneously with the dechlorination, being reduced by about 32 wt.%, as well as an increase of the HHV value, due to the concurrent elimination of contaminants (O and Cl).

4. RESULTS AND DISCUSSION

Table 15 - Proximate and ultimate analyses of raw and dechlorinated sample at 350 °C.

	Proximate Analysis (wt.%)		Ultimate Analysis (wt.%)							
	Volatile ^a	Ash ^b	C	H	N	S	Cl ^c	Trace metals ^d	O ^e	HHV (MJ/Kg)
P_Raw	97.2	2.8 ^c	78.0	13.3	0.0	< 0.1	1.95 (±0.48)	0.9	4.0	42.3
P_350	97.6	2.4 ^b	82.0	14.1	0.0	0.0	0.26 (±0.04)	0.9	2.7	45.1

^a Quantified by TGA.

^b Measured by combustion at 900°C.

^c Analysed by AOD/IC.

^d Measured by ICP-OES of ashes.

^e Calculated by difference.

The DSC analysis of P_Raw and P_350 was also performed and the results are reported in Figure 4.24. The profiles appear to be pretty similar, but a significant difference between the samples can be observed in the PVC decomposition temperature range (Figure 4.24, inset). In fact, the endothermal degradation of PVC and the release of HCl can be clearly observed in the raw sample in the temperature range of 275 – 325 °C. However, this signal is absent in R_350, demonstrating that no PVC fragments are still present after the treatment at 350 °C and supporting the hypothesis that the residual Cl in the solid exists in form of chlorinated hydrocarbons.

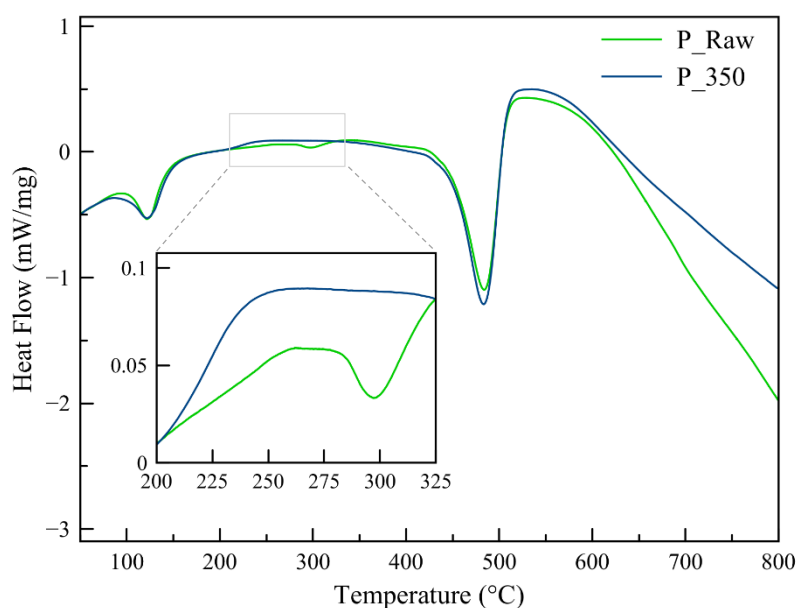


Figure 4.24 - DSC curves of raw WEEE plastic (P_Raw) and dechlorinated sample P_350.

4. RESULTS AND DISCUSSION

In order to investigate more deeply the changes induced in the polymers structure by the dechlorination treatment at 350 °C, particles identified in the raw WEEE waste as mainly composed by PVC were manually separated, thermally treated and analysed by FT-IR (Figure 4.25).

As described in section 4.1.2, the spectrum of the raw plastic particle fits well with that of pure PVC [150]. After the thermal treatment, it can be observed the disappearance of different bands associated to the presence of chlorine, such as 2970 cm^{-1} and 1255 cm^{-1} , which correspond to C-H stretching of CHCl and C-H deformation of CHCl , respectively. Moreover, other PVC bands disappear, such as 1100-1070 cm^{-1} (C-C stretching) and 966 cm^{-1} (CH_2 rocking), whilst a new band at 1625 cm^{-1} arises, associated to C=C bond stretching, due to the formation of vinyl groups during the PVC dechlorination [105].

On the other side, the band centred at 1723 cm^{-1} , which is attributed to the hydrogen bonded C=O groups of PVC additives [151-154], is completely absent in P_350 spectrum, confirming that the deoxygenation occurred simultaneously with the dechlorination, as evidenced by the elemental analysis.

Finally, a broad band can be observed at $\approx 3500 \text{ cm}^{-1}$, which is more pronounced after the thermal dechlorination treatment, due to the ambient hydration of the sample [152].

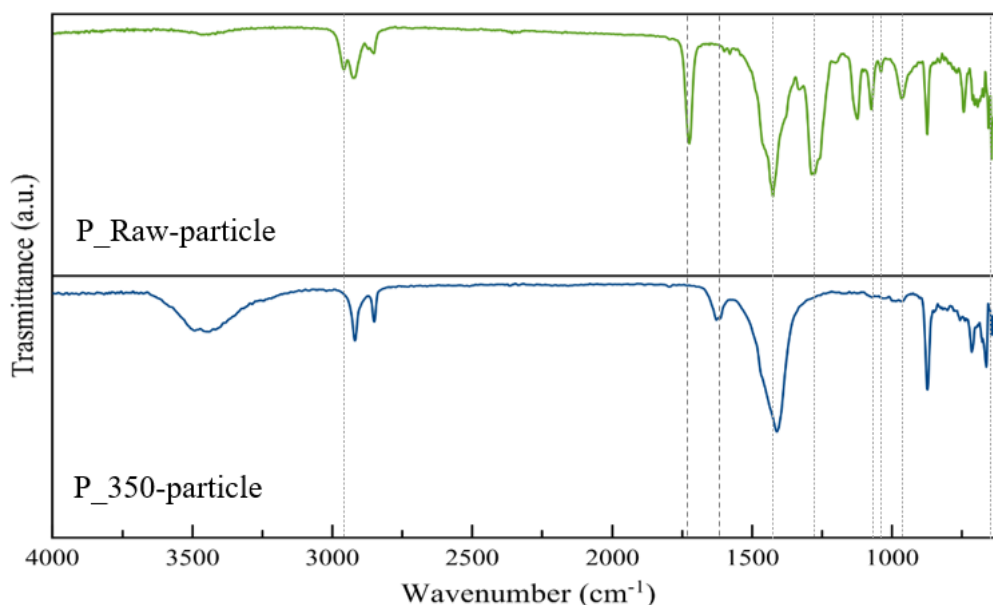


Figure 4.25 - FT-IR spectra of raw (P_Raw-particle) and dechlorinated (P_350-particle) isolated particles mainly composed by PVC. Dashed lines are guides for readers.

4. RESULTS AND DISCUSSION

Gas and oil analysis

The non-condensable gases collected at the end of the dechlorination treatments were analysed by μ -GC. The results, reported in Figure 4.26, revealed that the emitted light hydrocarbons account for just a small fraction. However, a slight increase of both gaseous (C2 -C4) paraffins (GP) and especially olefins (GO) concentrations with the temperature rise was detected, denoting that a partial cracking of the polymers chains occur by treating the plastic at 350 °C. This finding agrees well with previous literature works, that also identified the release of short hydrocarbons, especially C4 olefins, during the first stage of PVC decomposition [142].

On the other hand, oxygenated compounds, i.e., CO and CO₂, were also detected in the gaseous stream, whose concentration also increased with the temperature rise. However, recalling that the gas yield amount to 0.04 wt.% for P_300 and 0.29 wt.% for P_350, it clearly appears that just a small fraction of oxygen was released in the gaseous phase, accounting for about 1 and 6 % of the initial content at 300 and 350 °C, respectively.

Finally, at both dechlorination temperatures, the oil yields were too low to be properly collected and analysed. However, a qualitative GC-MS analysis of both oils was performed, and the results have revealed the presence of oxygenated long-chain hydrocarbons, mainly carboxylic acids, which may be related to the presence of photo-oxidative-derived compounds in the raw WEEE plastic [142-144].

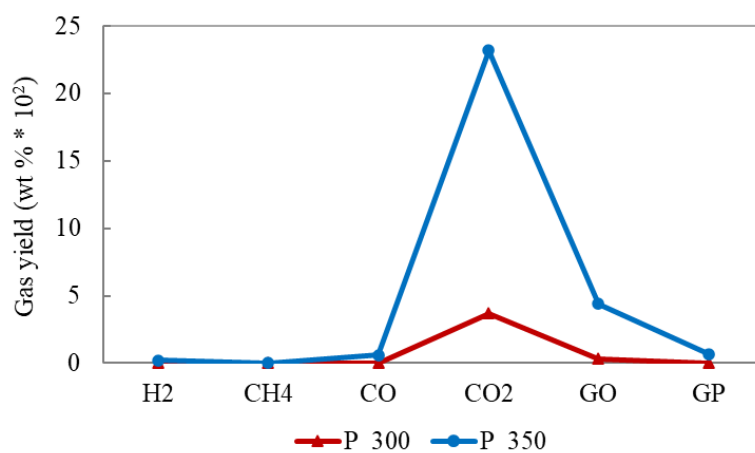


Figure 4.26 - Gas yields distribution in dechlorination treatments at 300 °C and 350 °C.

4. RESULTS AND DISCUSSION

4.3.3 Conclusions

The results obtained from the dechlorination treatment at 300 and 350 °C revealed that a small amount of organics is lost at both tested temperatures, mainly related to both the temperature-mediated and the HCl-catalysed cracking reactions [18,167-169].

However, on the total mass balances, the organics lost can be considered as negligible compared to the good dechlorination degrees achieved. More specifically, the progressive growth of temperature led to the increasing of the dechlorination efficiency, resulting in a halogen removal of about 68 and 86 % of the initial content, at 300 and 350 °C, respectively. In addition, the thermal pretreatment allowed the concurrent partial removal of oxygenated compounds from the raw plastic, as evidenced by FT-IR and elemental analyses, whose extent was augmented according with the temperature.

Accordingly, 350 °C revealed to be the most efficient temperature for the dehydrochlorination treatment of the WEEE plastic, leading to the greatest dechlorination and deoxygenation efficiencies, negligibly affecting the polymers chains cracking. Therefore, it has been selected for the WEEE plastic pretreatment in the following of this work.

4. RESULTS AND DISCUSSION

4.4 Thermal pyrolysis of raw WEEE plastic

In this section, the results of thermal fast-pyrolysis experiments are reported and discussed. The reactions were carried out at different thermal zone temperatures by using the raw WEEE plastic as feedstock, in order to evaluate the influence of this parameter on the products and chlorine distributions.

Considering the TG analysis (section 4.1, Figure 4.1), by heating the raw WEEE plastic at 10 °C/min, the polymers chains decomposition stood in the range 380 – 550 °C, with the maximum evolution rate centred at 478 °C. However, in these conditions, the stepwise heating allows a homogeneous heat distribution among the sample particles, offsetting the low thermal conductivity of the plastic [171,172].

As previously described, in this work the fast-pyrolysis process has been applied, in which the heating rate of the feedstock is in the order of 10 – 20 °C/s [59]. On this basis, higher operating temperatures were selected for thermal fast-pyrolysis tests, i.e., 550, 600 and 650 °C, with the aim to promote the polymers cracking, compensating the heat transfer limitations.

Based on the thermal zone temperature applied, the pyrolysis tests have been labelled as T_550, T_600, and T_650 in the following.

4.4.1 Reaction yields

The products distribution of the thermal pyrolysis tests carried out at the three selected temperatures is shown in Table 16.

Table 16 - Products yields distribution (wt.%) in thermal fast-pyrolysis of WEEE plastic as a function of thermal zone temperature.

Sample	Products yield (wt.%)				
	Wax	Oil	Gas	Char	Water-trapped Cl*
T_550	76.3	9.5	4.4	8.6	1.3
T_600	70.2	10.9	9.5	7.8	1.6
T_650	57.3	7.5	24.1	9.8	1.2

*Referred to the weight of the raw plastic waste, measured by IC.

4. RESULTS AND DISCUSSION

All tests led to the formation of solid wax as major product, and its yield decreased almost linearly with the increasing of the temperature. On the other side, different results were found in terms of oil and gas distribution (Figure 4.24). Increasing the temperature from 550 °C to 600 °C, both the gas and oil yields increased by 118 % and 17 %, respectively. On the contrary, the further rise in the operating temperature from 600 to 650 °C led to a 32 % reduction of oil, together with a stronger increment of gaseous fraction (+ 151 %).

These results can be explained by considering the cracking mechanism of polyolefins. As mentioned above (section 2.1.2), the thermal degradation firstly involves a radical mechanism, which induces the random cleavage of C-C bonds (initiation step), followed by intramolecular or intermolecular reactions among the intermediate radicals (propagation step), and then the recombination of unstable radicals to form stable molecules (termination). The pyrolysis temperature drives the cracking reactions by providing the energy required for the polymers bonds breaking. Therefore, the higher the pyrolysis temperature, the greater the extent of cracking, resulting in lighter hydrocarbons formation [59,173].

The products yields obtained from the thermal pyrolysis of the raw WEEE plastic denote that at low temperature (550 °C) just a partial cracking occurred, mainly leading to the formation of long-chain hydrocarbons (wax fraction). With the temperature rise (600 °C) the heavy chains underwent further cracking reactions, resulting in the increment of both oil (C5 – C14) and gas (C1 – C4) yields. By further increasing the pyrolysis temperature up to 650 °C, the cleavage of C-C bonds became more effective, leading to a strong increase of the gaseous fraction, at the expenses of both wax and oil yields.

Previous works showed that when pure HDPE is pyrolyzed in semi-batch conditions in 500 – 600 °C temperature range, the char yield increases as a function of the temperature [172]. In presence of PVC, high char yields are supposed to be promoted by the stronger cracking through an intermolecular mechanism, which involves the key precursors formation by crosslinking between adjacent fragments of polymer backbones after the partial intermolecular breaking of C-H and C-Cl [174].

However, taking into account the heterogeneity of the waste WEEE plastic employed as feedstock in this work (see section 4.1), the char yields at the three tested temperature can be considered within the standard deviation range.

Furthermore, it can be observed that the gaseous chlorine solubilized in water is maximized at the intermediate temperature, i.e., 600 °C, and that its total yield is lower than that

4. RESULTS AND DISCUSSION

collected during the pretreatment at 350 °C (= 1.7 wt.%, see section 4.3) at all tested temperatures. This can be explained by considering that cracking and dehydrochlorination reactions occurs simultaneously in fast-pyrolysis conditions. Therefore, it can be assumed that the two reactions pathways become competitive, involving the interaction between H and Cl released from PVC and several radicals derived from carbon chains cracking, leading to the formation of chlorinated hydrocarbons rather than HCl [169].

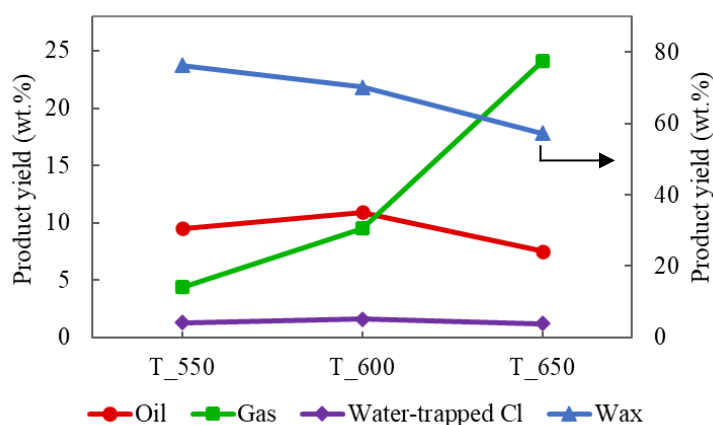


Figure 4.27 - Products yields distribution in thermal fast-pyrolysis reactions at 550 (T_550), 600 (T_600) and 650 °C (T_650). The wax yield is on secondary axis.

4.4.2 Products characterization

Gas analysis

The gaseous fraction was studied by μ -GC analysis and Figure 4.28 provides the yield of the different components that have been detected. As noted above, the total gas yield increased as a function of the temperature, reaching the maximum value of 24.1 wt.% at 650 °C.

With the temperature rise, a sharp increase of all gaseous hydrocarbon was detected, which is more pronounced in the case of methane and gaseous olefins (GO). Hydrogen was produced in very low amount at all tested temperatures, however increasing with the temperature rise, while minor contents of CO and CO₂ are also present in the gaseous streams, which is consistent with the presence of oxygen in the raw WEEE plastic (section 4.1).

The gaseous olefins-to-gaseous paraffins (GO/GP) ratio increases almost linearly with the temperature. This finding fits well with literature data, that indicate a linear correlation

4. RESULTS AND DISCUSSION

between GO/GP and temperature, since the higher the energy provided, the stronger end-chain cracking, β -scissions and dehydrogenation reactions, resulting in increasing concentrations of unsaturated light hydrocarbons, as well as H_2 and CH_4 [21,175].

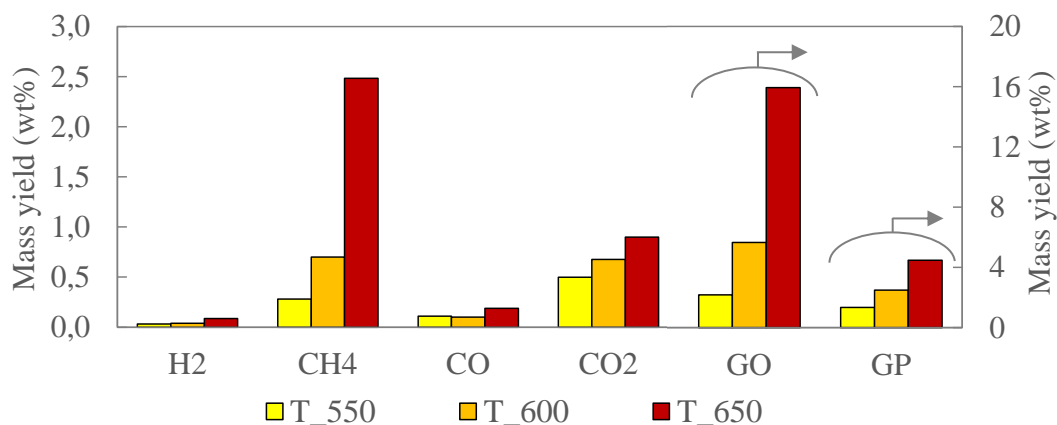


Figure 4.28 - Gas yields distribution in thermal pyrolysis tests at 550, 600 and 650 °C. Gaseous olefins (GO) and paraffins (GP) are on secondary axis.

Wax analysis

The waxes composition in terms of paraffins, iso-paraffins, and olefins families was evaluated by GC analysis. On the total measured area, the wax fraction in C15 and C40 carbon number range linearly decreased with the increasing temperature (Table 16), in favour of the formation of lighter compounds (< C15).

Analysing the normalized yield of each family in the wax range C15 – C40 (Figure 4.26), it can be observed that paraffins represent the main component at all tested temperature, showing comparable yields. On the other hand, branched paraffins and olefins showed almost symmetrical trends, as the higher the temperature, the lower the iso-paraffins and the higher the alkenes concentrations. These results are in good agreement with the gas analysis, since also in wax fraction the olefins/ paraffins ratio proved to be almost linearly augmented with the temperature rise.

4. RESULTS AND DISCUSSION

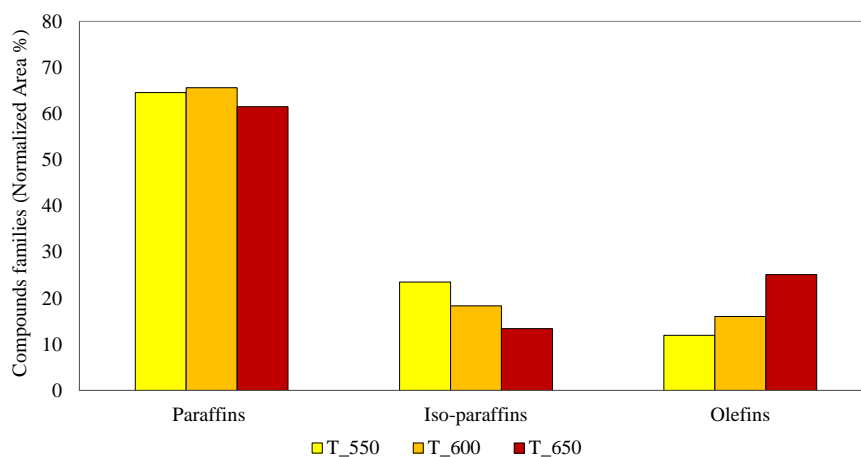


Figure 4.29 - Compounds families distribution of wax fraction in thermal pyrolysis tests at 550, 600 and 650 °C.

By analysing the carbon number distribution for each compounds family (Figure 4.27), it is possible to observe that in the low molecular weight range, i.e., C15 – C20, both olefins and paraffins increase with the temperature, whilst iso-paraffins follow the opposite trend.

The same trends were detected in C21 – C30 carbon number range for olefins and iso-paraffins, being the former augmented and the last reduced with the temperature rise. On the other side, similar concentrations of paraffins are present in this carbon number range at all tested temperatures.

Finally, almost only heavy paraffins were found in the high molecular weight range (C31 – C40), with the greatest concentration produced at 550 °C.

Again, these findings are attributed to the changes of the reaction pathway as a consequence of the temperature rise [21,172]. At 550 °C just a partial random cracking of the polymer chains followed by recombination (termination) occurred, which led to the formation of high molecular weight paraffins ($C > 30$), as well as of great concentrations of iso-paraffins in C15 – C32 range. Recalling that the branching formation during the thermal pyrolysis is precluded [21], the presence of iso-paraffins in the wax fractions can be only related to the presence of branching in the polymers chains, which, at the lowest temperature, have been undergone random cracking and termination reactions.

At the intermediate temperature (600 °C), higher concentrations of short-paraffins and olefins, and lower amounts of iso-paraffins and high molecular weight alkanes can be observed, compared to T_550, indicating that the cracking degree was augmented, and

4. RESULTS AND DISCUSSION

especially in correspondence of tertiary chains carbons (able to form more stable tertiary radicals), as well as the dehydrogenation reactions.

Finally, the highest tested temperature, i.e., 650 °C, promotes further cracking, β -scission and dehydrogenation reactions, as also evidenced by the gas analysis, resulting in higher concentration of both short alkanes and alkenes.

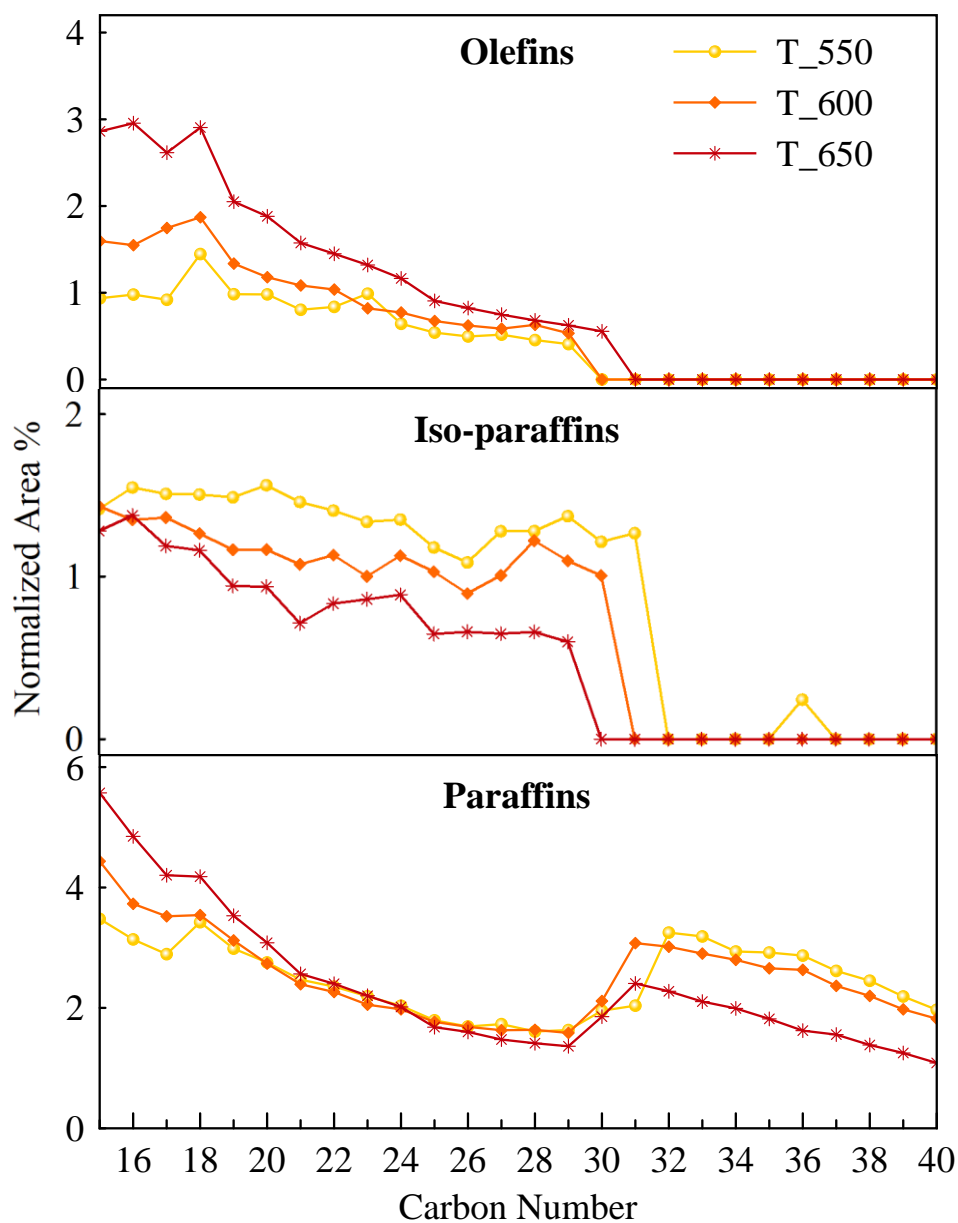


Figure 4.30 - Compounds families by carbon atom number distribution of wax fraction in thermal pyrolysis tests at 550, 600 and 650 °C.

4. RESULTS AND DISCUSSION

Chlorine distribution

The Ion Chromatography analysis allowed to quantify the chlorine content trapped in water, as well as in wax and char fractions after their combustion in the AOD system. The obtained results in terms of chlorine distribution percentage related to the average chlorine measured in the raw plastic (19518 ppm, see section 4.3) are shown in Table 17. The pyrolysis oils were not analysed due to the recovery problems related to the low yields in all studied reactions, so that the fraction labelled as “other” in the Table includes both Cl in the oil and the eventual chlorinated gases in the non-condensable stream, which could not be measured, as well as the dispersion of the measurements related to the high heterogeneity of the WEEE plastic used as feedstock.

Table 17 - Chlorine distribution among products in thermal pyrolysis reactions.

Sample	Chlorine distribution (%)			
	Wax	Char	Water-trapped	Others*
T_550	3.6	13.3	63.2	19.8
T_600	3.1	12.6	76.8	7.5
T_650	4.9	21.1	61.2	12.7

*Calculated by difference.

The chlorine distribution analysis revealed that most of the halogen was stored in form of water-soluble hydrochloric acid, reaching the maximum concentration at 600 °C. As mentioned above (section 4.4.1), the total HCl concentration trapped in water in all thermal pyrolysis tests is lower than that removed by the thermal treatment at 350 °C, which may be due to the formation of chlorinated hydrocarbons by reaction between H and Cl radicals with the carbon chains promoted by the higher temperature.

This last hypothesis has been confirmed by the AOD/IC analysis of wax and char, that revealed the presence of chlorine in both fractions in variable percentages.

Entering into details, wax fractions have accumulated between 3 and 5 % of the initial halogen, being its concentration within the standard deviation range at 550 and 600 °C and maximized at 650 °C, in contrast to the mass yields. A higher proportion of chlorine was retained by char, which may be related to the presence of some inorganic components, like

4. RESULTS AND DISCUSSION

Ca-containing compounds, that are known to be able of forming the corresponding chlorides. Char fractions show comparable values of Cl ($\approx 13\%$) at low and intermediate temperatures, being instead maximized at $650\text{ }^{\circ}\text{C}$, despite the comparable mass yields detected among the samples.

These trends (Figure 4.31) suggest that the changes in the reactions pathways would also affect the chlorinated compounds formation at high pyrolysis temperature ($650\text{ }^{\circ}\text{C}$), since the enhanced cracking reactions could promote the shortening of chlorinated bulky molecules, rather than the HCl release from side-groups-elimination, resulting in chlorinated shorter hydrocarbons. Moreover, if the proportion of short Cl-olefins, compared to those not halogenated, should be greater, also the high chlorine concentration in char at $650\text{ }^{\circ}\text{C}$ would be justified, being the unsaturated hydrocarbons char precursors [171].

However, the explanation of these trends can just be hypothesized, due to the high heterogeneity of the raw WEEE plastic used as feedstock, as well as to the inability to measure the chlorine content in oils and non-condensable gases.

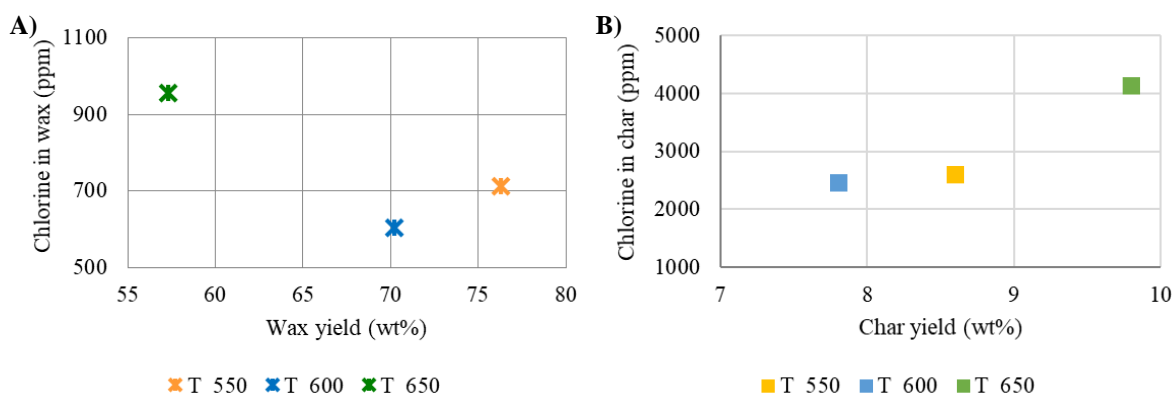


Figure 4.31 - Chlorine content versus wax (A) and char (B) yields in thermal pyrolysis reactions carried out at 550, 600 and $650\text{ }^{\circ}\text{C}$.

4.4.3 Conclusions

The obtained results revealed that solid wax represents the main product at all the tested temperatures. At $550\text{ }^{\circ}\text{C}$, just the 13.9% accounted for light organics, i.e., gas and oil fractions. At the intermediate temperature ($600\text{ }^{\circ}\text{C}$), oil and gas amounts increased, as well as the water-trapped chlorine, at the expenses of wax yield. The further increasing of the reaction temperature up to $650\text{ }^{\circ}\text{C}$ led to the decreasing of both wax and oil yields in favour

4. RESULTS AND DISCUSSION

of gases formation. As expected, the cracking reactions became stronger with the temperature rise, leading to higher yields of low-molecular weight products.

Furthermore, the composition of both gaseous and wax fractions suggested that an enhancement in end-chain cracking, β -scission and dehydrogenation reactions takes place, resulting in increasing olefins/paraffins ratios, as well as H₂ and CH₄ formation.

Finally, the chlorine analysis revealed that the higher the temperature, the greater the probability of chlorinated hydrocarbons formation, confirming that the cracking degree plays a key role also in the chlorine distribution among the pyrolysis products.

The intermediate temperature, i.e., 600 °C, thus proved to be the best compromise in terms of cracking degree, since it led to the highest oil yield, and chlorine distribution, as the gaseous HCl release prevailed over the chlorinated hydrocarbons formation. Therefore, 600 °C was selected as temperature for the thermal zone in all thermo-catalytic pyrolysis tests which will be discussed in the following of this work.

4. RESULTS AND DISCUSSION

4.5 Catalytic pyrolysis of raw WEEE plastic at different catalytic temperatures

In this section, products distribution and properties from catalytic pyrolysis experiments of raw WEEE plastic as a function of the catalytic temperature are described and discussed.

As mentioned in section 3.3, in this work thermo-catalytic fast-pyrolysis experiments were carried out, in which the feedstock was firstly thermally degraded, and then the primary pyrolysis vapours were passed through the catalyst fixed-bed to be upgraded. The two zones of the reactor (thermal and catalytic) were separately heated by independent electrical furnaces. Starting from the previously examined results (section 4.4), the temperature of the thermal zone was set at 600 °C in all tests.

The catalytic reactions were carried out in presence of commercial nanocrystalline ZSM-5, using a catalyst-to-feedstock (C/F) ratio of 0.2. The complete characterization of the employed catalyst is reported in section 4.2.1. However, its main features in terms of acidity and textural properties are summarized below (see Table 18).

Table 18 - Textural and acidic properties of commercial nanocrystalline MFI_42 zeolite.

Sample	Si/Al ^a bulk (mol/mol)	S _{BET} ^b (m ² /g)	S _{Ext-Mes} ^c (m ² /g)	V _{tot} ^d (cm ³ /g)	Brønsted AS ^e (μmol/g _{CAT})	Lewis AS ^e (μmol/g _{CAT})	B/L ratio	Total AS ^f (μmol/g _{CAT})
MFI_42	42	418	66	0.432	267	56	4.8	380

^a Determined by ICP-OES.

^b BET specific surface area.

^c Calculated by *t*-plot method.

^d Estimated by applying the NL-DFT method.

^e Determined by FT-IR after adsorption of D₃-acetonitrile.

^f Calculated from NH₃-TPD.

On the basis of literature data, the catalyst bed temperature affects the products distribution in the catalytic pyrolysis of plastics. Bagri *et al.* carried out thermo-catalytic pyrolysis of pure LDPE, in batch mode, using a downdraft fixed bed reactor, with thermal and catalytic zones independently heated. The feedstock was thus heated up to 500 °C (at 10 °C/min) in the thermal zone of the reactor and the vapours were then passed through the catalyst bed (ZSM-5, Si/Al = 50), the temperature of which was varied between 400 and 600 °C. The authors showed that both oil yield and composition were enhanced in 400 – 500 °C temperature range, while higher temperatures led to a sharp increase of the gas yield [54]. More recently, Onwundili *et al.* reported similar results by pyrolyzing a mixture of HDPE, LDPE, PP, PS, and PET in similar conditions (two stage fixed bed reactor, batch mode,

4. RESULTS AND DISCUSSION

thermal zone heated at 10 °C/min up to 500 °C, ZSM-5 zeolite as catalyst). The authors showed that by increasing the catalyst bed temperature from 500 to 600 °C, the products distribution was strongly shifted toward gas formation [176].

Accordingly, to evaluate the influence of the catalyst bed temperature on the distribution and composition of pyrolysis products in the view of optimizing the oil yield and properties, three temperatures have been selected in this work for the vapours upgrading in the thermo-catalytic pyrolysis tests of the raw WEEE plastic, i.e., 400, 450, and 500 °C, on the basis of which the samples have been labelled as MFI_42(400), MFI_42(450), and MFI_42(500) in the following.

4.5.1 Reaction yields

Table 19 shows the products yields resulting from the catalytic pyrolysis experiments at the tested catalytic temperatures, compared with the thermal pyrolysis, i.e., in absence of catalyst (T_600). The catalytic vapours upgrading using ZSM-5 zeolite drastically changed the products distribution, leading to the increase of light hydrocarbons amount, i.e., oil and gas fractions, at the expenses of wax, which was not detected at all tested catalytic temperatures.

Table 19 - Products yields distribution (wt.%) in catalytic pyrolysis of WEEE plastic as a function of catalytic temperature.

Sample	Products yield (wt.%)					
	Wax	Oil	Gas	Char	Coke	Water-trapped Cl*
T_600	70.2	10.9	9.5	7.8	--	1.6
MFI_42(400)	0.0	64.9	25.6	8.3	0.8	0.4
MFI_42(450)	0.0	62.3	28.1	8.3	0.7	0.6
MFI_42(500)	0.0	56.7	33.5	8.2	1.2	0.4

* Referred to the weight of the raw plastic waste, measured by IC.

It can be observed that the increase of the catalytic temperature led to a progressive increment in the gas production, and this change is even more pronounced at higher temperatures. In fact, an increment of 10 % in gas and a 4 % reduction in oil amounts were

4. RESULTS AND DISCUSSION

found with the first temperature rise (from 400 to 450 °C), whilst the gaseous fraction proved to be augmented by 19 % with the further temperature rise (from 450 to 500 °C), at the expense of oil, being reduced by 10 %.

In terms of chlorine trapped in water, no substantial differences have been detected among the samples, since the measured concentration at all tested catalytic temperatures stands within the standard deviation range. However, it can be noted that the average Cl amount in this fraction is much lower than that solubilized in water in absence of catalyst (T_600). It may be due to the enhancement of cracking reactions catalysed by the ZSM-5 zeolite, leading to lighter chlorinated hydrocarbons formation rather than HCl release, as well as to the reaction between the evolved HCl and the primary pyrolysis products.

The coke deposited on the spent catalysts showed comparable yields at 400 and 450 °C, whilst it proved to be increased by about 60 % with the further temperature rise up to 500 °C.

Finally, the solid carbonaceous residue formation (char) occurs before the contact between the primary pyrolysis vapours and the catalyst, and it is directly related to thermal zone temperature and vapours residence time in the reactor [177], which were set up for being equal in all thermal and catalytic pyrolysis experiments. Accordingly, the char yields values were found to be comparable, standing in the range 7.8 – 8.3 wt.%, with a percentage standard deviation of 3 %, mainly related to the heterogeneity of the raw WEEE plastic.

4.5.2 Products characterization

Gas analysis

The gaseous fractions coming from the thermal and thermo-catalytic pyrolysis tests carried out at different catalytic temperatures were analysed by μ -GC, and the results are shown in Figure 4.32.

By comparing the gaseous streams obtained in absence (T_600) and in presence of the catalyst (MFI_42(400)), differences can be observed both in terms of total gas yield and composition. The catalyst has strongly favoured the formation of light olefins and paraffins, whilst a higher CH₄ content was observed in T_600, compared to MFI_42(400). This can be explained by considering the changes in the cracking mechanisms occurring when an acid catalyst is employed, which promotes a carbocationic pathways, in contrast with the thermal

4. RESULTS AND DISCUSSION

cracking, involving radical mechanisms (see section 2.2.1). As a consequence, the carbon chains breaking is enhanced by β -scission and end-chain cracking reactions of the formed carbocations, promoted by the zeolite acid sites, resulting in the increase of lighter hydrocarbons concentrations [59,79,80].

The comparison among the gas fractions obtained at different catalytic temperatures reveals increasing concentration of both light olefins and paraffins with the temperature rise, and especially of C_2H_4 and C_3H_6 , at the expense of the heavier fraction (C4). The gaseous olefins/paraffins ratio proved also to be almost linearly increased according to the temperature (amounting to 1.8, 2.0, and 2.3 at 400, 450, and 500 °C, respectively), denoting the enhancement of C-C β -scission reactions, which promote the unsaturated hydrocarbon formation.

Small amount of CO and CO_2 have been also detected in the gaseous streams, which is consistent with the presence of oxygen in the raw WEEE plastic, whose concentration was comparable at all tested temperatures.

Finally, H_2 and CH_4 formation was augmented by increasing the catalytic temperature, suggesting the enhancement of both end-chain cracking and dehydrogenation-secondary reactions [54,176].

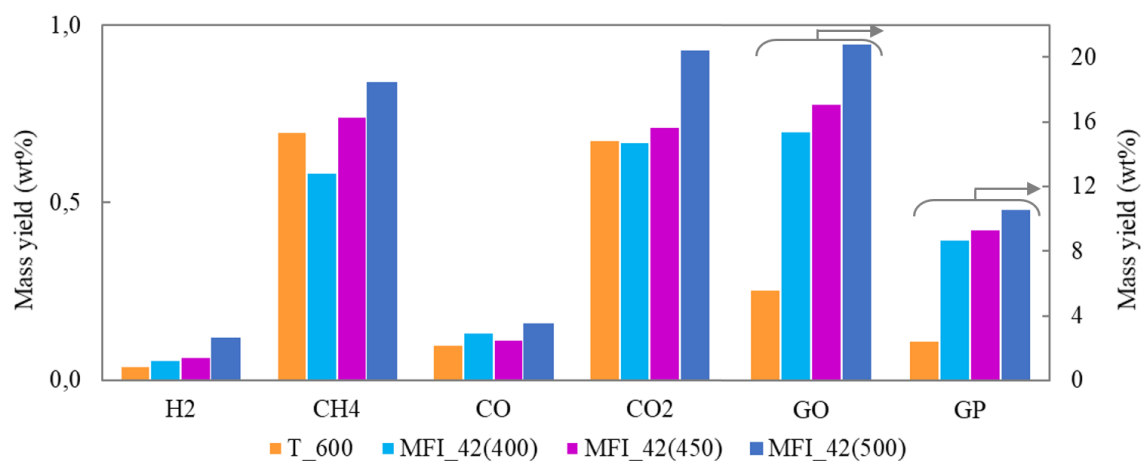


Figure 4.32 - Gas yields distribution in thermal and catalytic pyrolysis reactions performed at thermal zone temperature of 600 °C and catalytic temperatures of 400, 450 and 500 °C (cat./feed. = 0.2). Gaseous olefins (GO) and paraffins (GP) are on secondary axis.

4. RESULTS AND DISCUSSION

Oil analysis

The chemical composition in terms of hydrocarbons families of the oil fractions was evaluated by means of PIONA analysis. The oil components are classified into five groups of compounds, i.e., paraffins, branched-paraffins (I-paraffins), aromatics, naphthenes, and olefins, in the carbon number range of C3 – C15.

However, the pyrolysis oil derived from the pyrolysis test in absence of catalyst (T_600) could not be analysed due to the recovery problems related to the low yield, as discussed in the previous section.

Figure 4.33 provides information about the composition of the oils generated in the catalytic fast-pyrolysis of raw WEEE plastic in presence of nanocrystalline ZSM-5 (Si/Al = 42), at 400, 450, and 500 °C as catalytic temperatures.

It can be observed that the temperature strongly affects the oils composition. The increase from 400 to 450 °C led to a 67 % drop in olefins concentration, as well as a growth in the range 27 – 29 % of both branched-paraffins and naphthenes. The largest increase was observed in the aromatics compounds concentration, being improved by nearly 50 %.

These results suggest that the catalytic activity of the ZSM-5 zeolite was improved by the higher temperature, affecting the propagation and termination reactions in the carbocation chain pathway. Therefore, the mono-aromatics (BTX) formation was enhanced by means of catalyst-mediated cyclization and dehydrogenation reactions, as confirmed also by the higher naphthenes concentration [59].

Moreover, it has been demonstrated that the presence of acidic catalyst at temperature close to 450 °C promotes also the C4 and C5 fractions oligomerization followed by cyclization, resulting in a further increment of aromatics formation [178].

On the other side, the concentrations of paraffins proved to be comparable at all tested temperature, standing in the standard deviation range.

With the further temperature rise from 450 to 500 °C, a dramatic increase in unsaturated hydrocarbons was found at the expenses of the other fractions, and especially of aromatics, being reduced by more than 80 %. This effect could be related to the combination of different factors. On one hand, at higher temperatures a competition between carbocation pathways and thermal degradation reactions can take place, which shifts the products distribution towards olefins, rather than promoting aromatization reactions [59]. On the other side, it has been showed that with the temperature rise, partial dealumination of ZSM-5 zeolites can

4. RESULTS AND DISCUSSION

occur, resulting in a decrease of Brønsted acid sites concentration, and therefore in the efficiency of aromatization reactions, of which this type of acid sites is the main responsible [179].

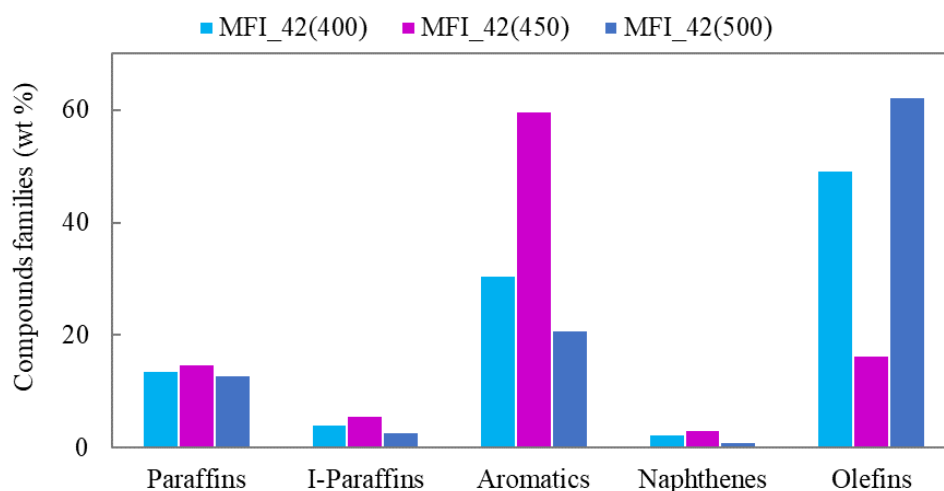


Figure 4.33 - Compounds families in the oil obtained by catalytic pyrolysis at 400, 450 and 500 °C (thermal zone temperature = 600 °C, cat./feed. = 0.2).

It is to be noted that not only the total yield of aromatics drastically changed with the temperature rise, but also its composition. Figure 4.34 shows the selectivity towards mono- and poly-aromatic compounds families at the three tested temperatures. It can be observed that a slight increment in benzenes (mainly toluene, xylene, bi-, tri-, and tetra-substituted benzenes) took place switching the catalytic temperature from 400 to 450 °C.

In contrast, a dramatic modification occurred at 500 °C, leading mainly to the formation of naphthalenes, indanes, and indenes. The ratio between mono- and poly-aromatics resulted to be 4.5, 5.8, and 0.8 at 400, 450, and 500 °C, respectively.

This finding fits well with previous literature works that also identified an increase in the PAHs formation with the temperature rise in presence of ZSM-5 zeolites, which results in an increase of the polyaromatic character of both oil and coke [180].

4. RESULTS AND DISCUSSION

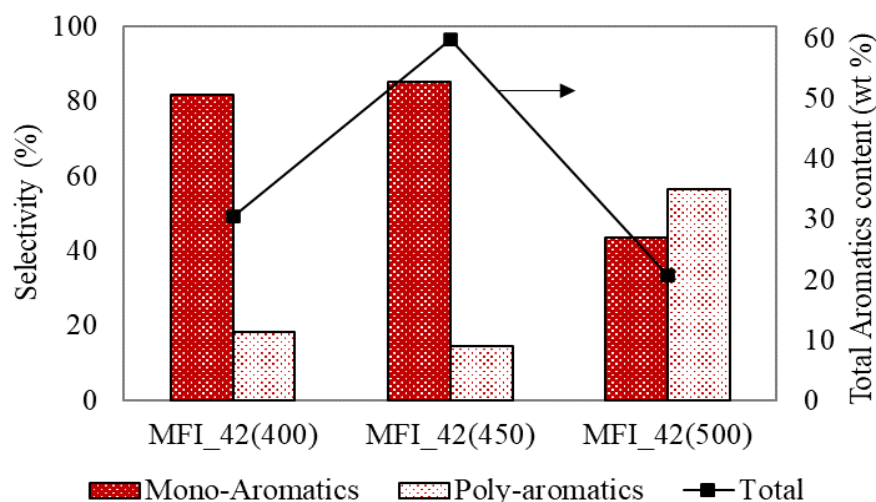


Figure 4.34 - Mono- and poly-aromatics selectivity in oil (Catalytic temperatures = 400, 450 and 500 °C, thermal zone temperature = 600 °C, cat./feed. = 0.2). The total aromatics content is on secondary axis.

Chlorine distribution

As reported in section 2.3, the chlorine content in pyrolysis products plays a crucial role in determining the quality and then the possibility of re-use them as second raw materials. Moreover, the presence of halogens can also affect the catalyst deactivation, reducing both its activity and life-time.

Accordingly, the chlorine content and distribution among the products derived from fast-pyrolysis tests performed at the catalytic temperatures of 400, 450, and 500 °C were evaluated. Oil, char and coke fractions were firstly combusted in a calorimetric bomb, and the resulting solutions were analysed by Ion Chromatography, together with the gaseous chlorine solubilized in water.

On the total measured chlorine, the largest portion was released in form of gaseous hydrochloric acid, amounting to more than 50 % at all tested temperatures, followed by the chlorinated solid carbonaceous residue formation (char), which represents the 27 – 36 % of the total. Just the residual 12 – 19 % of halogen was distributed between oil and coke fractions (Figure 4.35). Entering into detail, with the progressive temperature rise, the water-trapped chlorine shows an increment of 17 %, and then a 16 % reduction. However, these values could be due to the heterogeneity of the raw WEEE plastic, and therefore considered as comparable. The halogen concentration in oils resulted to be linearly reduced with the temperature rise, whilst the chlorine content in the deposited coke was found to be slightly

4. RESULTS AND DISCUSSION

increased changing the temperature from 400 to 450 °C, and strongly augmented with the further temperature rise up to 500 °C. These findings suggest that the bulky Cl-containing species tend to be accumulated in the heavier fractions, such as char and heavy coke.

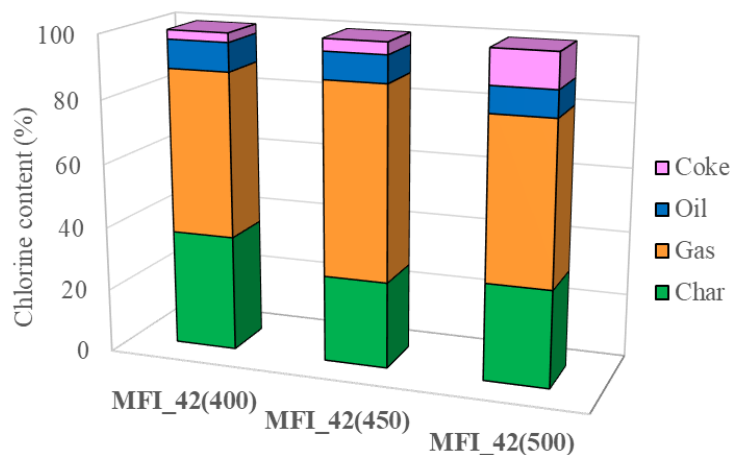


Figure 4.35 - Chlorine distribution in catalytic fast-pyrolysis products (catalytic temperature = 400, 450 and 500 °C, thermal zone temperature = 600 °C, cat./feed. = 0.2).

4.5.3 Conclusions

The study of the influence of catalyst bed temperature in catalytic fast-pyrolysis of raw WEEE plastic confirmed that the products composition and distribution are directly affected, as considerable differences were found among the reactions performed.

If compared with the thermal experiment, the presence of ZSM-5 zeolite as catalyst drastically changed the overall mass distribution, promoting the polymers chains cracking reactions and leading to more than 90 wt.% of light liquid and gaseous hydrocarbons. This effect was found to be even more pronounced with the progressive increase in the catalytic temperature, as a further rise in the gaseous fraction at the expenses of oil yield was detected, indicating an improvement of the catalyst activity according to the temperature.

The analysis of the gas composition revealed increasing concentrations of light hydrocarbons with the catalytic temperature rise, confirming not only the enhancement of end-chain and β -scission cracking reactions mediated by the ZSM-5 zeolite acid sites, but also the improvement of secondary reactions, such as dehydrogenation, as confirmed by the increasing H_2 and light olefins amounts. Cyclization and aromatization reactions were also promoted when the temperature was increased from 400 to 450 °C, as shown from the oils

4. RESULTS AND DISCUSSION

analyses, whilst with the further temperature rise (500 °C), a probable competition between radical and cationic reactions pathways occurs, resulting in a reduction of the aromatics content in favours of olefins. Moreover, the highest temperature tested led to the formation of a larger proportion of poly-aromatics in oil, which act as coke precursors, and indeed the highest yield of coke deposited on the catalyst has been measured at this catalytic temperature [33].

Finally, the chlorine distribution among pyrolysis products proved also to be affected by the change in the catalytic temperature. The halogen content in oils linearly decreased with increasing the catalyst bed temperature, whilst the coke fractions follow the opposite trend. Therefore, it is reasonable to assume that the higher the temperature, the greater the probability that the released HCl reacts again with the intermediate species, giving rise to chlorinated molecules, which tend to be accumulated in the heavier fractions, such as coke [167].

In conclusion, at the intermediate temperature tested, i.e., 450 °C, the best compromise between catalyst-mediated cracking and secondary reactions was observed, resulting in a good oil yield with high mono-aromatics content, which represent valuable compounds usable as raw chemicals and/or for the formulation of gasoline-range fuels, and a relatively low-chlorine concentration, that allows its further processing.

Therefore, since aim of this work is the optimization of the oil fraction, in terms of both yield and composition, 450 °C has been selected as catalytic temperature for the fast-catalytic pyrolysis tests which will follow.

4. RESULTS AND DISCUSSION

4.6 Catalytic pyrolysis of raw WEEE plastic with different catalyst to feedstock ratios

This section describes thermo-catalytic fast-pyrolysis of raw WEEE plastic in presence of different catalyst-to-feedstock (C/F) ratios, in the view of assessing the effects of this parameter on the products and chlorine distribution.

As reported in literature [181], the amount of catalyst affects the products selectivity, so that depending on the target products, the proper equilibrium between primary and secondary reactions needs to be achieved.

In this work, two catalyst-to-feedstock ratios were studied, i.e., 0.2 and 0.4. According to the previously discussed results, the temperatures of thermal and catalytic zones were set at 600 °C and 450 °C, respectively. The reactions were performed by using the commercial nanocrystalline ZSM-5 (Si/Al = 42) as catalyst.

On these bases, the samples have been labelled as MFI_42(450_0,2) and MFI_42(450_0,4) in the following.

4.6.1 Reaction yields

The products distribution experimentally obtained when the raw WEEE plastic pyrolysis vapours were upgraded by passing them through the ZSM-5 zeolite catalyst bed in different proportions is reported in Table 20.

The changes in the catalyst to feedstock ratio led to strong modifications in the overall products balance, as the gas fraction yield was strongly augmented by 68 % with the increasing amount of catalyst, simultaneously with a dramatic 30 % reduction in the oil formation.

Opposite trends in HCl trapping and coke deposition were observed, as the lower the catalyst amount, the larger the halogen concentration in water and the lower the carbonaceous compounds quantity deposited on the catalyst, and vice versa.

Finally, since the char formation is mainly generated before the pyrolysis vapours reach the catalyst bed, it does not depend on the presence and amount of catalyst. Accordingly, all the char yields resulting from thermal and catalytic experiments revealed to be comparable in the range 7.8 – 8.3 wt.% [177].

4. RESULTS AND DISCUSSION

Table 20 - Products yields distribution in catalytic pyrolysis of WEEE plastic as a function of the catalyst-to-feedstock ratio.

Sample	Products yield (wt.%)					
	Wax	Oil	Gas	Char	Coke	Water-trapped Cl*
T_600	70.2	10.9	9.5	7.8	--	1.6
MFI_42(450_0,2)	0.0	62.3	28.1	8.3	0.7	0.6
MFI_42(450_0,4)	0.0	43.3	47.2	8.1	0.9	0.4

* Referred to the weight of the raw plastic waste, measured by IC.

4.6.2 Products characterization

Gas analysis

The light fractions obtained by thermo-catalytic pyrolysis tests performed by using different catalyst to feedstock ratios were analysed by μ -GC, and the products distribution is shown in Figure 4.36.

In absolute terms, despite the big differences in the total gas yields, methane and carbon monoxide concentrations were comparable in all thermal and thermo-catalytic pyrolysis experiments, ranging between 0.7 – 0.9 wt.% and 0.1 – 0.2 wt.%, respectively.

The carbon dioxide concentration apparently increased with the catalyst amount rise, but actually it represents the 2.5 % of the total analysed gases in both MFI_42(450_0,2) and MFI_42(450_0,4) reactions. The existence of CO and CO₂ in the gaseous streams is consistent with the presence of oxygen in the raw WEEE plastic, this last amounting to 4 wt.% (section 4.1). However, the total oxygenated compounds concentrations account for 0.8 and 1.4 wt.% in MFI_42(450_0,2) and MFI_42(450_0,4), respectively, whilst the remaining 65 – 80 % of O may be accumulated in the char fraction in form of metallic oxides (TiO₂, SiO₂, and CaO, see section 4.1).

On the other hand, switching the catalyst/feedstock proportion from 0.2 to 0.4, the hydrogen concentration resulted to be doubled. Moreover, a gaseous paraffins growth of 9 % was observed, especially propane, at the expenses of light olefins, being reduced by about 4 %, resulting in an increment of the light paraffins/olefins ratio with the catalyst amount.

The obtained results evidenced that the impact of the cracking reactions was enhanced by doubling the amount of catalyst, moving the products distribution towards gases production.

4. RESULTS AND DISCUSSION

Moreover, an improvement of secondary reactions simultaneously occurred involving the primary cracking products (olefins), resulting therefore in the increment of H₂ concentrations, as well as of the proportion of light paraffins, in accordance with literature data [95].

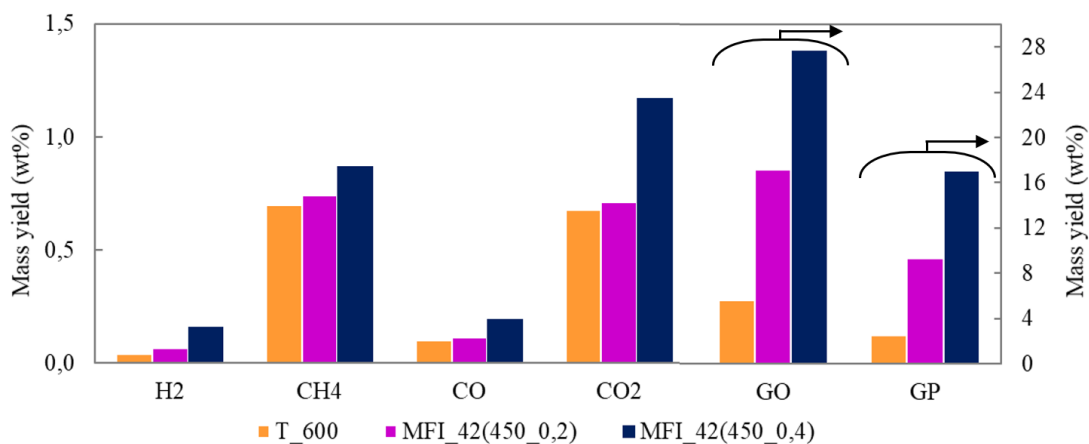


Figure 4.36 - Gas yields distribution in thermal and catalytic pyrolysis reactions (Temperature 600/450 °C, catalyst/feedstock = 0,2 and 0,4). Gaseous olefins (GO) and paraffins (GP) are on secondary axis.

Oil analysis

PIONA GC-analysis was performed in order to evaluate the composition and properties of the oil fractions obtained from the catalytic pyrolysis of WEEE plastic, carried out by using two different catalyst-to-feedstock ratios. The obtained results in terms of compounds families distribution are reported in Figure 4.37.

The proportion among the compounds families in oil considerably changed depending on the catalyst amount. The concentrations of linear paraffins decreased upon increasing the C/F, being reduced by 51 %. On the other side, no significant differences were observed in the branched-paraffins concentration.

The olefins content was 94 % higher when a lower catalyst quantity was used, to the extent that its concentration can be considered as negligible in MFI_42(450_0,4) oil.

In contrast, strong increments of both aromatics and especially naphthenes according to the C/F rise were detected, being the cycloalkanes concentration more than quadrupled.

4. RESULTS AND DISCUSSION

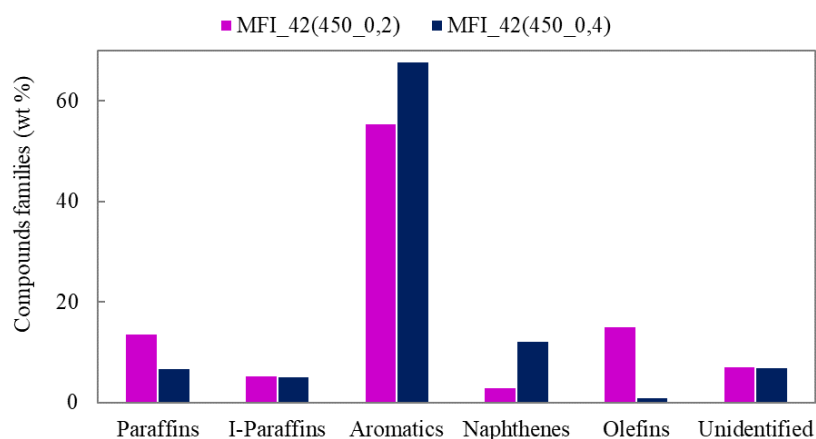


Figure 4.37 - Compounds families in the oil obtained by catalytic pyrolysis at 400, 450 and 500 °C (thermal zone temperature = 600 °C, cat./feed. = 0.2).

These findings are clear evidence of the improved catalytic contribution when doubling the catalyst amount. In fact, by increasing the available catalyst acid sites ($C/F = 0.4$), a strong enhancement of secondary reactions took place, such as cyclization, aromatization, and dehydrogenation, at the expense of the primary cracking products, i.e. olefins, whose concentration proved to be almost negligible in MFI_42(450_0,4) oil. As a consequence, aromatics and naphthenes resulted to be drastically augmented, as well as H_2 in the gaseous stream.

Additional information about the effect of doubling the catalyst amount can be obtained by analysing the selectivity by carbon number in the gas C1 – C4 and gasoline C5 – C15 ranges (Figure 4.38).

Higher concentrations of light C2 – C4 compounds were produced increasing the catalyst/feedstock ratio, in accordance with the gas analysis reported in Figure 4.36. On the other side, heavier C7 – C15 hydrocarbons were mainly formed when a smaller quantity of ZSM-5 was used, i.e., in MFI_42(450_0,2), confirming that an improvement of the cracking activity occurs when a higher proportion of the catalyst acid sites is available.

Finally, the change in the catalyst amount not only led to different selectivity towards carbon number in oil and gas fractions, but also caused modifications in both total concentration and type of aromatic compounds.

4. RESULTS AND DISCUSSION

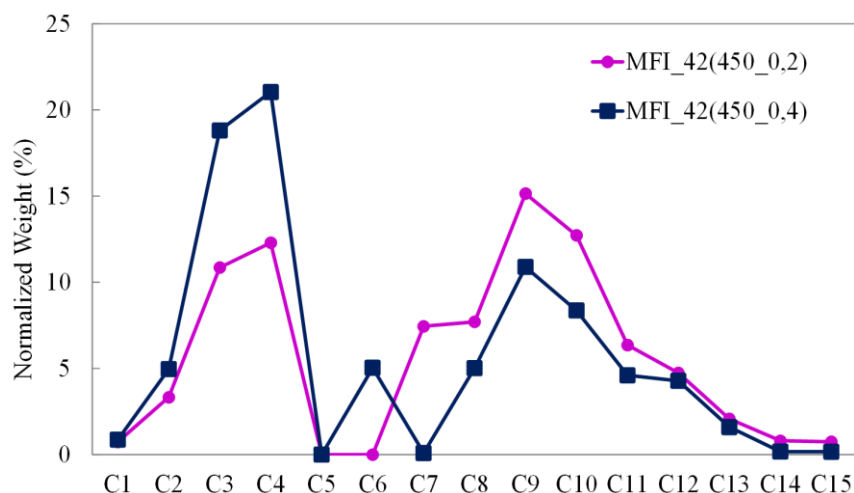


Figure 4.38 - Selectivity by carbon atom number in oil and gas fractions generated by the catalytic pyrolysis experiments carried out with catalyst/feedstock = 0.2 and 0.4.

As shown in Figure 4.39, the poly-aromatics concentration in oil was increased by 40 % using a greater amount of catalyst, accounting for 21 % of the total aromatics compared to the 15 % detected in the oil produced in MFI_42(450_0,2) pyrolysis test. And again, this demonstrates the crucial role of the catalyst in promoting cyclization, aromatization, and oligomerization reactions.

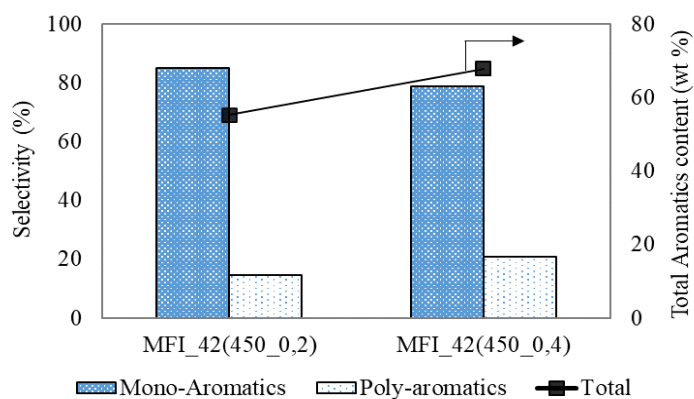


Figure 4.39 - Aromatics compounds selectivity in oils obtained by using different catalyst/feedstock ratios. The total aromatics content is on secondary axis.

It is to be noted that the combined effect between the preferential formation of heavy PAHs in MFI_42(450_0,4) pyrolysis products and the higher concentration of Brønsted acid sites also justify the greater amount of coke deposited on the catalyst, since they act as coke precursors [84] and catalyse its formation [81-83].

4. RESULTS AND DISCUSSION

Chlorine distribution

The solid fractions generated from the catalytic pyrolysis of WEEE plastic by using two different C/F ratios were combusted and then analysed by IC, together with the water trapping solution, in order to evaluate the chlorine content and distribution among products. On the total measured chlorine, the halogen was mostly released in form of hydrochloric acid, accounting for the 61 and 41 % in MFI_42(450_0,2) and MFI_42(450_0,4) samples, respectively.

However, the improvement on the catalytic contribution due to the increase in the catalyst amount led to the formation of several halogenated hydrocarbons, resulting in an oil which contains a significant amount of Cl (about 1700 ppm), definitely far from the limits allowed for being processed in refinery units [28,101].

Finally, with the C/F ratio rise, the chlorine concentration in coke fraction was almost doubled, against a 32 % reduction of the gaseous HCl emitted, suggesting that the external/mesopore surface area of ZSM-5 catalyst may favour the trapping of the heavy Cl-containing compounds.

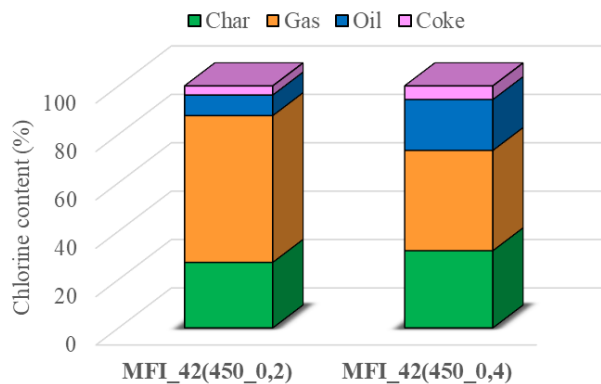


Figure 4.40 - Chlorine distribution in pyrolysis products obtained by using different catalyst/feedstock ratios.

4.6.3 Conclusions

The results achieved denote that in presence of n-ZSM-5 zeolite, the catalyst-to-feedstock ratio plays a key role in both products distribution and composition.

The small crystals size of the nanocrystalline ZSM-5 zeolite used as catalyst ensures a high external surface (see section 4.2.1), which makes the acid sites available for the interaction

4. RESULTS AND DISCUSSION

with the bulky molecules [95]. Therefore, by doubling the catalyst amount, a significant enhancement of the catalytic effects is expected.

This has been confirmed by both the mass yields and the gases composition, since when a C/F ratio of 0.4 was employed, the products distribution was shifted toward saturated gas formation, denoting the improvement of the end-chain scissions through the influence of the catalyst strong acid sites [79,80]. The carbon number distribution among gas and liquid fractions has also supported this evidence, as longer hydrocarbons were formed by using a smaller amount of catalyst, i.e., when C/F ratio was set at 0.2.

In addition, the composition of the oil fractions in terms of compound families confirmed that secondary reactions are strongly dependent on the concentration of the acid sites, and thus on the catalyst amount [49]. In fact, in MFI_42(450_0,4), the primary cracking olefins have been almost totally consumed by cyclization and dehydrogenation, giving rise to high concentrations of cycloalkanes and aromatics in oil and H₂ in the gaseous fraction. On the other side, aromatization and oligomerization catalysed by the increased number of strong acid sites (C/F = 0.4) also led to a greater proportion of PAHs in oil, as well as to a larger amount of coke deposited on the catalyst [84].

Finally, the high-chlorine content in oil and coke fractions observed at higher C/F ratio can also be justified by considering the improvement of the catalytic effect, since the enhanced cracking, aromatization, and oligomerization reactions may have favoured the formation of light Cl-hydrocarbons in C₅–C₁₅ carbon number range and chlorinated coke precursors.

Therefore, the catalyst-to-feedstock ratio of 0.2 represents the best compromise between primary and secondary catalyst-mediated reactions, as, in these reaction conditions, a good oil mass yield is supported by a high monoaromatics and cycloalkanes content and a lower chlorine concentration.

For these reasons, 0.2 has been selected as catalyst-to-feedstock ratio to be used in the thermo-catalytic fast-pyrolysis experiments in the following of this work.

4. RESULTS AND DISCUSSION

4.7 Catalytic pyrolysis of raw and dechlorinated WEEE plastic

In this paragraph, the products distribution and composition obtained from the thermo-catalytic pyrolysis of raw and dechlorinated WEEE plastics are described and discussed.

As reported in section 4.3, an efficient dechlorination degree has been achieved by thermally treating the raw WEEE plastic in inert atmosphere, at 350 °C per 30 minutes. In these reaction conditions, up to 87 % of the initial chlorine was removed in form of HCl, which was captured by solubilisation in water. However, the dechlorinated plastic still contains a relatively high concentration of Cl (\approx 2600 ppm) which can limit the following pyrolysis products applications.

It must be recalled that proximate and elemental analysis (Table 15, reported below to allow an easier access) of both, raw WEEE and pre-treated, samples were pretty similar, as both materials lose about 97 – 98 wt.% of volatiles, with a remaining ash content below 3 wt.%. Moreover, no significant changes were observed in the polymers mixture from the FT-IR and TG/DSC analyses, except the appearance of new C=C bonds related to the formation of vinyl groups during the PVC dechlorination [105].

On the other side, a portion of oxygen, related to the presence of additives, production processes residues and/or to the oxidation of the plastics during the lifetime [144,145], was also released during the thermal pretreatment in form of CO and CO₂, accounting for \approx 32 % reduction.

Table 15 - Products yields distribution in catalytic fast-pyrolysis of raw and dechlorinated WEEE

	Proximate Analysis (wt.%)		Ultimate Analysis (wt.%)							
	Volatile ^a	Ash ^b	C	H	N	S	Cl ^c	Trace metals ^d	O ^e	HHV (MJ/Kg)
P_Raw	97.2	2.8 ^c	78.0	13.3	0.0	< 0.1	1.95 (\pm 0.48)	0.9	4.0	42.3
P_350	97.6	2.4 ^b	82.0	14.1	0.0	0.0	0.26 (\pm 0.04)	0.9	2.7	45.1

^a Quantified by TGA.

^b Measured by combustion at 900°C.

^c Analysed by AOD/IC.

^d Measured by ICP-OES of ashes.

^e Calculated by difference.

Therefore, the catalytic fast-pyrolysis of dechlorinated WEEE plastic was carried out and compared with the raw WEEE plastic pyrolysis results, in order to investigate if the changes

4. RESULTS AND DISCUSSION

in the feedstock related to the dehydrochlorination treatment may have any impact on the pyrolysis products.

The pyrolysis tests were carried out by using commercial n-ZSM-5 zeolite (Si/Al = 42) as catalyst, at 600 and 450 °C for the thermal and catalytic zones, respectively, and with a catalyst/feedstock ratio of 0.2.

The reaction MFI_42(450_0,2) described in the previous section is here used as reference and its name has been simplified as MFI_42 below, while the test performed by using the dechlorinated plastic as feedstock has been labelled as MFI_42(P_350) in the following.

4.7.1 Reaction yields

The experimental products yields of the catalytic pyrolysis of raw and dechlorinated plastics are shown in Table 21.

The dechlorination pretreatment of WEEE plastic had just a slight impact on the mass balances, since no significant differences have been detected in oil and gases yields, standing within the variability of the samples.

The main effects can be appreciated in the coke amount deposited on the catalyst, as well as in the water-trapped Cl, as the former was drastically reduced by more than 71 %, whilst almost no halogen was detected in the gaseous phase, mostly as a consequence of the lower initial chlorine concentration in the feedstock (≈ 19500 in P_raw and ≈ 2600 in P_350).

Table 21 - Products yields distribution in catalytic fast-pyrolysis of raw and dechlorinated WEEE plastics.

Sample	Products yield (wt.%)					
	Wax	Oil	Gas	Char	Coke	Water-trapped Cl*
MFI_42	0.0	62.3	28.1	8.3	0.7	0.6
MFI_42(P_350)	0.0	60.8	30.9	8.1	0.2	< 0.1

* Referred to the weight of the plastic waste, measured by IC.

4. RESULTS AND DISCUSSION

4.7.2 Products characterization

Gas analysis

The μ -GC analysis results of the gaseous fractions obtained from the catalytic pyrolysis of raw and pretreated plastics are reported in Figure 4.41.

It can be observed that the gas distribution is just slightly affected by the changes in the feedstock. Gaseous olefins and paraffins concentrations are pretty similar, and the small differences can be considered within the variability of the plastics samples.

The total amounts of oxygenated compounds (carbon monoxide and dioxide) are apparently lower in the gaseous stream of the pretreated plastic, since represent the 0.8 wt.% and 0.3 wt.% in MFI_42 and MFI_42(P_350), respectively. However, it must be recalled that a partial deoxygenation already occurred during the dechlorination treatment, which led to a 1.3 wt.% oxygen reduction, and therefore the double-step process (dechlorination + catalytic pyrolysis) results in a global greater O removal.

On the other side, significant changes can be appreciated in H₂ and CH₄ concentrations, being reduced by 33 and 54 %, respectively, as a consequence of the dechlorination treatment. These results suggest that a smaller extent of end-chain cracking and dehydrogenation reactions would have been occurred in presence of the dechlorinated plastic, and this has been attributed to partial degradation and rearrangement of polymers structures which could take place during the dechlorination step, leading to different pyrolysis pathways and thus pyrolysis products [182].

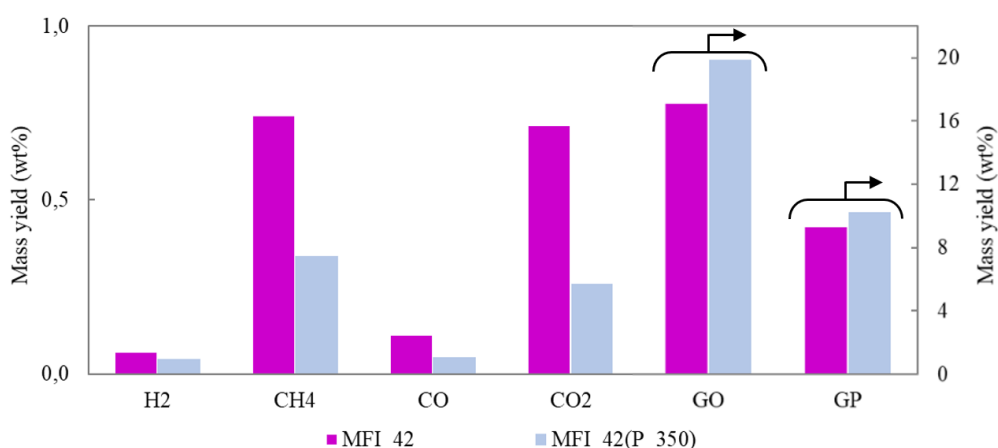


Figure 4.41 - Gas yields distribution in catalytic pyrolysis of raw and dechlorinated plastics.

(Thermal/catalytic zones temperature = 600/450 °C, catalyst/feedstock = 0.2). Gaseous olefins (GO) and paraffins (GP) on secondary axis.

4. RESULTS AND DISCUSSION

Oil analysis

The GC-PIONA analysis was performed in order to get information about the composition of the oil fractions obtained from the pyrolysis tests of raw and dechlorinated plastics. The distribution by compounds families revealed remarkable differences depending on the feedstock employed. As it can be observed in Figure 4.42, dechlorinated plastic led to an increment of olefins yield, from 15 to 31 wt.%, at the expenses of aromatics content, which was reduced by 55 % in MFI_42(P_350) derived oil.

Significant changes were observed also in alkanes families, but with different trends. Linear paraffins concentration were reduced by 19 %, whilst strong increments were detected in both branched and cyclo-alkanes, being almost doubled and increased sixfold, respectively.

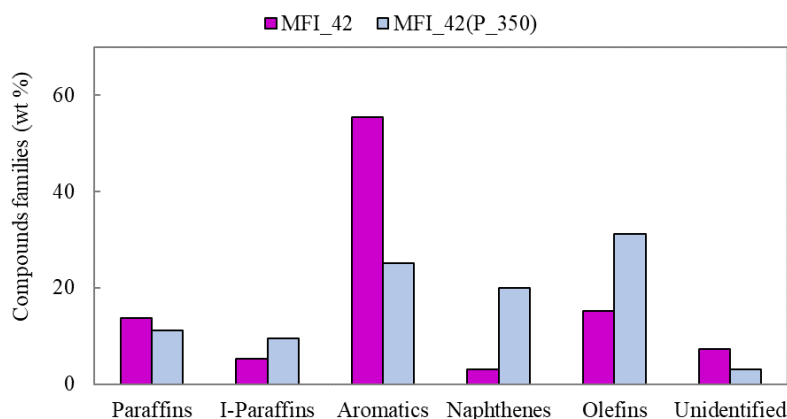


Figure 4.42 - Products distribution by compounds families in oil fractions obtained by catalytic pyrolysis of raw and dechlorinated plastics (thermal/catalytic zones temperature = 600/450 °C, cat./feed. = 0.2).

Looking at aromatics family, it clearly appears that also the type of formed compounds was different as a function of the feedstock employed (Figure 4.43). On the total amounts, pyrolysis of dechlorinated plastic determined mainly the formation of monoaromatics, such as toluene, xylene, and substituted-benzenes, while the total concentration of polyaromatics resulted 30 % higher in MFI_42 derived oil. This last effect is also reflected in coke formation, as it resulted much lower when a smaller quantity of PAHs was formed, being these last coke precursors [180].

4. RESULTS AND DISCUSSION

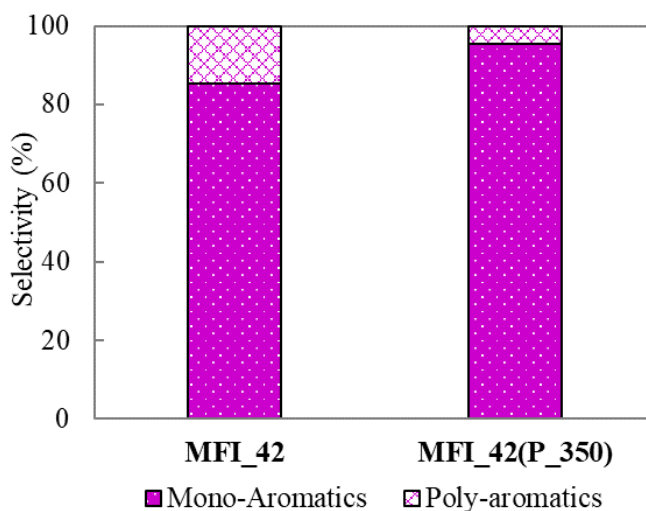


Figure 4.43 - Aromatics families selectivity in oil fractions obtained by catalytic pyrolysis of raw and dechlorinated plastics.

Further information about the products properties can be obtained by analysing the selectivity by carbon number in C1 – C15 range (Figure 4.44). No significant differences were detected at low molecular weight, i.e., C1 – C3, which fits well with the gas analysis (Figure 4.41), whilst greater concentrations in C4 – C8 range can be observed in the dechlorinated plastic derived oil, at the expenses of the heavier fraction (C9 – C15).

Similar results have been reported by Lopez-Urionabarrenechea et al. [182], which carried out a comparison between the conventional catalytic pyrolysis and a double step process (thermal dehydrochlorination + catalytic pyrolysis) of a PVC-containing plastic mixture, in semi-batch conditions, by using a ZSM-5 zeolite as catalyst. The detected differences in the products composition have been attributed to the partial deactivation of the catalyst by coke deposition and Cl-poisoning which occur in the catalytic pyrolysis of raw plastic, resulting in reduced extent of catalyst-mediated secondary reactions. This finding would explain well the lower cracking degree observed in the C5 – C15 carbon number range of MFI_42 derived oil, which led to the formation of longer hydrocarbons, since a higher initial chlorine content was present and a greater coke deposition has been detected, compared to MFI_42(P_350).

4. RESULTS AND DISCUSSION

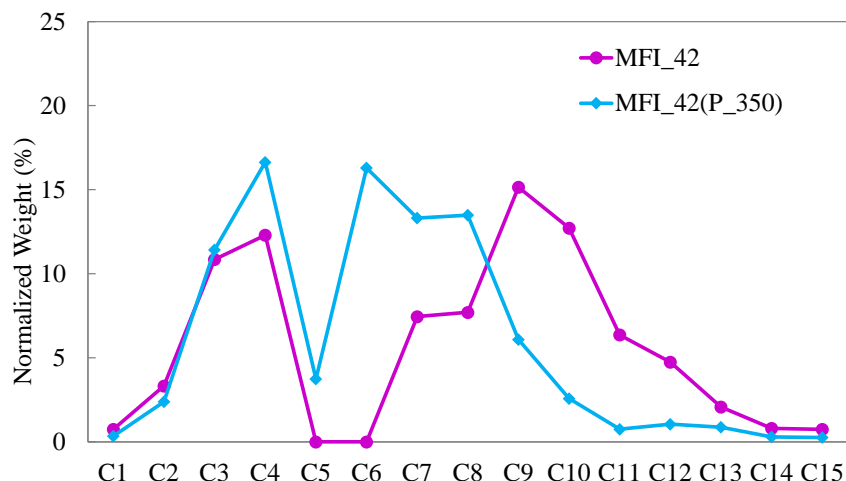


Figure 4.44 - Selectivity by carbon atom number in C1 –C 15 range of the oil fractions generated by the catalytic of raw and dechlorinated WEEE plastic.

Chlorine distribution

As described in section 4.3, the dechlorination treatment at 350 °C has allowed to remove up to 86 % of the initial chlorine in form of hydrochloric acid, which was easily captured by solubilization in a cooled pure-water trap.

Therefore, the initial chlorine content in the dechlorinated plastic used as feedstock in the catalytic pyrolysis tests was much lower than that of the raw WEEE plastic, being on average equal to about 2600 and 19500 ppm, respectively.

The chlorine distribution among the pyrolysis products, calculated on the total measured halogen in each reaction, is shown in Figure 4.45 A, taking into account also the portion of HCl removed during the dechlorination treatment (labelled as P_350).

By pyrolyzing the raw WEEE plastic about 60 % of chlorine was released in form of gaseous HCl, while more than 12 % was distributed between oil and coke fractions.

On the other side, when the dechlorinated plastic was used as feedstock in the catalytic fast-pyrolysis test, very low concentrations of chlorine were detected in all reaction products, except in char.

Additional information about the halogen distribution in MFI_42(P_350) reaction can be obtained by analysing the Cl balance calculated on the residual chlorine in the pre-treated plastic, i.e., 2652 ppm. As reported in Figure 4.45 B, downstream the pyrolysis reaction, up to 95.5 % of chlorine was retained in the solid residue (char), while just the 0.2 % was

4. RESULTS AND DISCUSSION

released as hydrochloric acid (gas). The chlorine contents in oil and coke fractions accounted for 2.8 and 1.5 %, respectively.

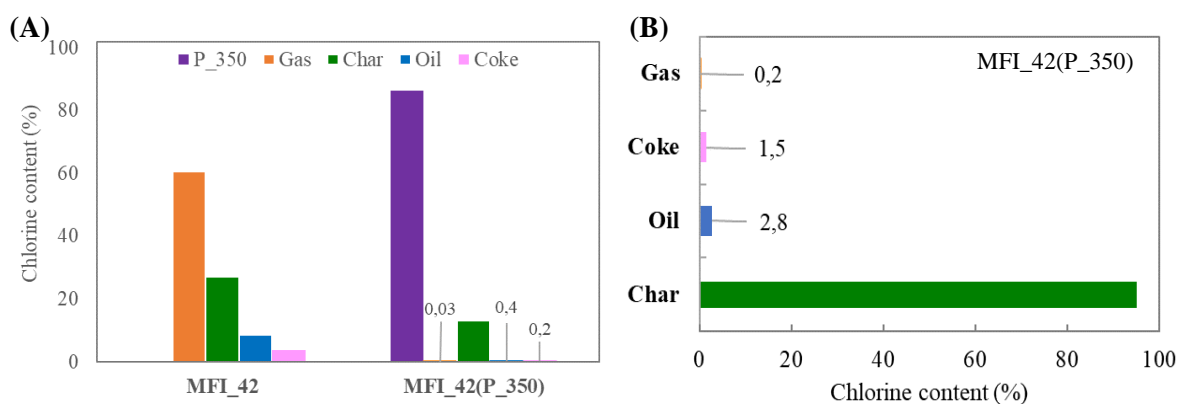


Figure 4.45 - (A) Chlorine distribution in pyrolysis products obtained by using raw and dechlorinated plastics as feedstock, and **(B)** chlorine balance of MFI_42(P_350) calculated on residual chlorine content in dechlorinated plastic.

Accordingly, the combined effect of the thermal dechlorination treatment and the catalytic fast-pyrolysis led to a drastic drop of chlorine in oil, compared to the conventional one-step catalytic pyrolysis. Despite the comparable mass yields (Table 21), the dechlorinated plastic-derived liquid fraction accumulated 121 mg of Cl per kg of oil, compared to 1295 ppm detected by pyrolyzing the raw plastic, resulting in an overall 91 % reduction (Figure 4.46).

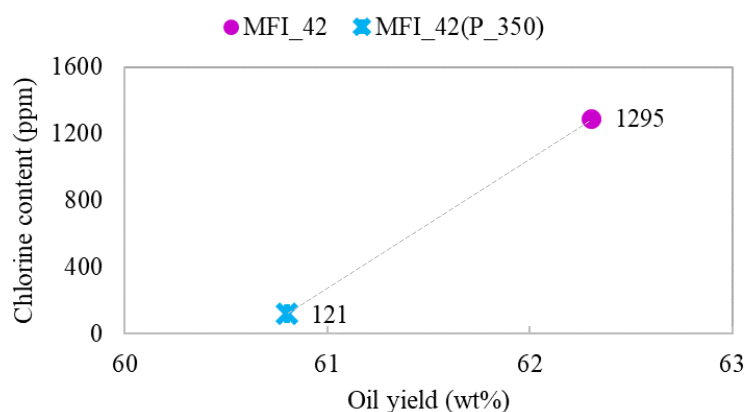


Figure 4.46 - Chlorine content in oils obtained from catalytic fast-pyrolysis of raw and dechlorinated plastics.

4. RESULTS AND DISCUSSION

4.7.3 Conclusions

The obtained results show few differences among the pyrolysis products distribution and composition related to the type of feedstock employed.

Entering into details, similar oil and gas yields have been detected regardless of the type of feedstock used. However, the catalytic pyrolysis of dechlorinated plastic led to the formation of lower hydrogen and methane concentrations in the gaseous stream, as well as to shorter hydrocarbons in the liquid fraction.

Based on previous works, detected differences could be ascribed to the partial deactivation of the catalyst by coke deposition and Cl-poisoning which takes place when the raw plastic is pyrolyzed, due to the much greater chlorine content in the feedstock [112,182,183].

In contrast, downstream the dechlorination treatment, the oil composition, in terms of compound families, proved to be rich in olefins, which are the primary cracking products, and naphthenes, denoting that a smaller share of aromatization reactions took place, as also confirmed by the lower proportion of PAHs. According to literature data, this may be due some partial thermal cracking and rearrangement of polymers structures that may have taken place during the dechlorination step, which may lead to changes in the pyrolysis pathways [108,182].

As reported in section 4.3, thermally treating the plastic sample at 350 °C a partial deoxygenation occurred simultaneously with the dehydrochlorination. Moreover, about 3 wt.% of organics were released in gaseous and liquid phases. Therefore, cracking reactions, HCl elimination and decarboxylation could have induced partial polymers chains rearrangement, resulting in the detected changes of the pyrolysis products composition.

Nevertheless, it must be considered that, beside the of halogen already removed during the dechlorination treatment, throughout the catalytic pyrolysis further chlorine has been retained by the heavy fractions, i.e., char and coke, resulting in a 91 % decline of Cl in oil, compared to that obtained by pyrolyzing the raw plastic. The catalytic fast-pyrolysis of the dechlorinated plastic over n-ZSM-5 thus led to the formation of an oil with a low chlorine content (121 ppm), close to the limits set out for its processing in refinery facilities [28,101]. Therefore, in the view of optimizing the oil properties and further lowering its chlorine content, in the following of this work the dechlorinated plastic has been used as feedstock in the thermo-catalytic fast-pyrolysis reactions over different synthesized ZSM-5 zeolites.

4. RESULTS AND DISCUSSION

4.8 Catalytic pyrolysis of dechlorinated WEEE plastic in presence of synthesized ZSM-5 zeolites

In order to evaluate the role of acidity and textural properties on products and chlorine distributions, three ZSM-5 zeolites with different Si/Al ratio (11, 25, and 100 in the synthesis gel) were synthesized and tested in the catalytic pyrolysis of dechlorinated WEEE plastic. The whole catalysts characterization is reported in section 4.2.2. However, the main properties are summarized in the Table 22 reported below.

Table 22 - Main acidic and textural properties of the synthesized ZSM-5 catalysts.

Sample	Si/Al ^a bulk (mol/mol)	S _{BET} ^b (m ² /g)	S _{Ext-Mes} ^c (m ² /g)	Weak AS ^d (μmol _{NH3} /g _{CAT})	Strong AS ^d (μmol _{NH3} /g _{CAT})	Brønsted AS ^e (μmol/g _{CAT})	Lewis AS ^e (μmol/g _{CAT})	B/L	EF-Al ^f (Area%)
MFI_11	10.9	399	87	224	489	488	253	1.9	16.9
MFI_25	23.6	418	135	141	399	378	95	4.0	8.0
MFI_100	109.5	455	314	42	110	125	23	5.4	1.1

^a Determined by ICP-OES. ^b BET specific surface area. ^c Calculated by *t*-plot method.

^d Calculated by NH₃-TPD. ^e Determined by FT-IR after adsorption of D₃-acetonitrile.

^f Calculated from ²⁷Al MAS NMR.

The catalysts activity was evaluated in the thermo-catalytic fast-pyrolysis reactions by using as feedstock the dechlorinated WEEE plastic after its pretreatment at 350 °C (see section 4.3), and the results have been compared with those obtained from the thermal test (without catalyst). On the basis of the results discussed in the previous chapters, all experiments were carried out by using thermal and catalytic zones temperatures of 600 and 450 °C, respectively, including the thermal test, in which the catalyst bed was replaced by inert glass wool and metallic grids. Finally, when a catalyst was employed, the catalyst-to-feedstock ratio was fixed at 0.2.

The activity of the investigated catalysts in terms of products and chlorine distribution is reported and discussed in this section, and the results have been compared to those obtained in the thermal pyrolysis tests (named as “Thermal” below).

On the basis of the theoretical Si/Al ratio of the catalysts, the pyrolysis tests have been labelled as MFI_11, MFI_25, and MFI_100 in the following.

4. RESULTS AND DISCUSSION

4.8.1 Reaction yields

The products distribution obtained from the thermal and catalytic pyrolysis reactions of pretreated WEEE plastic over the investigated catalysts is shown in Table 23. As previously discussed, the presence of a ZSM-5 zeolite catalyst dramatic changes the products yields. In fact, in presence of MFI_11 a 58 % reduction of solid wax was detected, compared to the thermal test, and even its zeroing by using MFI_25 and MFI_100.

Table 23 - Product yields after thermal and catalytic pyrolysis of dechlorinated WEEE plastic.

Sample	Products yield (wt.%)					
	Wax	Oil	Gas	Char	Coke	Water-trapped Cl*
Thermal	74.1	8.4	9.2	8.4	--	0.00051
MFI_11	31.1	31.4	27.8	8.7	1.0	0.00034
MFI_25	0.0	50.6	39.9	8.7	0.8	0.00025
MFI_100	0.0	69.0	21.6	8.9	0.4	0.00078

* Referred to the weight of the dechlorinated plastic waste, measured by IC.

To evaluate the role of the catalyst acidity on the products distribution, the mass yield of each component has been plotted versus the total acidity measured by NH₃-TPD (Figure 4.47). From the graph, it can be observed that the greater the total acidity, the smaller the liquid fraction formation. However, the reduction in the oil yield proved to be complemented by the gases concentration rise (+ 43 %), switching from MFI_100 to MFI_25. On the other side, when MFI_11 was employed both lighter fractions concentrations (oil and gas) were reduced in favour of wax formation.

These findings suggest that MFI_25 is more active in promoting cracking reactions, compared to both MFI_100 and MFI_11. However, the different results obtained for these two last catalysts in terms of gas and wax yields can be explained by considering the different types of acid sites assessed by FT-IR analysis. The measured B/L ratios increase non-linearly with the Si/Al ratio (Figure 4.48), indicating that the Lewis acid sites rise in larger extent with the total Al content. Therefore, despite the much higher total acidity, MFI_11 showed the greatest proportion of Lewis acid sites, according to the EF-Al species concentrations detected by ²⁷Al-NMR, which led to a lower cracking activity, that is mainly promoted by

4. RESULTS AND DISCUSSION

the Brønsted acid sites [60,83], and thus to the formation of heavier hydrocarbons (wax fraction).

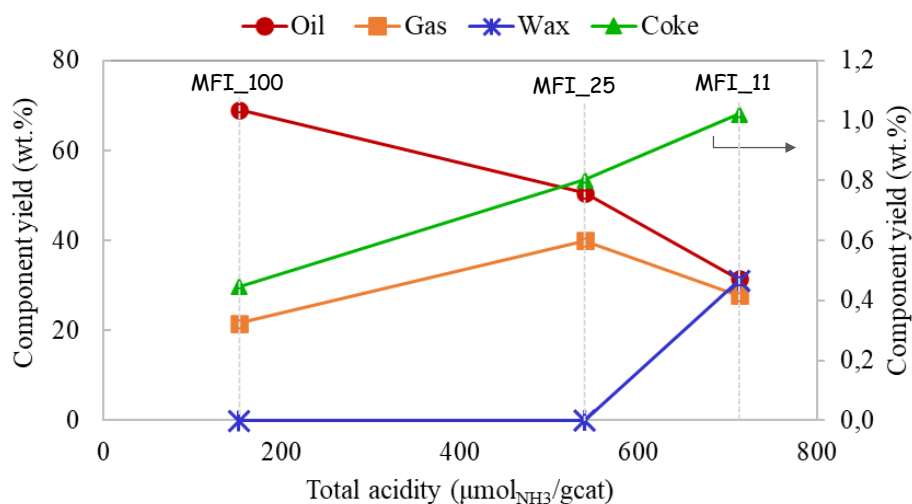


Figure 4.47 - Yield of catalytic pyrolysis products as a function of the total acidity of the investigated catalysts (Coke yield is on secondary axis).

On the contrary, MFI_100 showed a higher proportion of Brønsted acid sites, but the overall acidity is significantly smaller than that of MFI_25, resulting therefore in a lower formation of lighter components (gas fraction). Finally, Figure 4.48 displays very similar trends for the oil yields and B/L ratios as a function of the Si/Al ratios, demonstrating the strong dependence of the liquid fraction production on both type and proportion of acid sites.

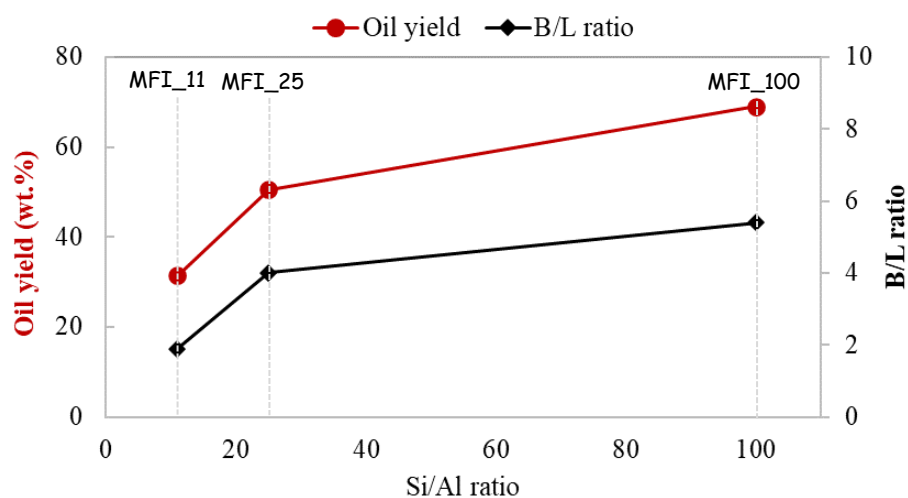


Figure 4.48 - Oil yields and B/L ratios as a function of the Si/Al ratios of the studied catalysts.

4. RESULTS AND DISCUSSION

It must be noted that also the textural properties play a key role in the pyrolysis products distribution. The lower activity of MFI_11 can be also ascribed to the lower proportion of external/mesopore surface area, which accounts for the 22 % of the total surface area (Table 22). In MFI_25 and MFI_100 instead the $S_{\text{Ext-Mes}}$ represent the 32 and 69 % of the S_{BET} , respectively, resulting in a higher accessibility of the bulky molecules to the catalysts active sites and therefore to greater cracking degrees.

From the products yields (Figure 4.47), it can be also observed that the amount of the coke deposited on the catalyst increased almost linearly with the total acidity, which fits well with literature data [81-83,184].

Moreover, the char yields were found to be comparable in all the thermal and catalytic tests (8.4 – 8.9 wt.%), that is consistent with the occurrence of the char formation before the contact between the primary pyrolysis vapours and the catalyst bed.

Finally, the amount of gaseous chlorine trapped in water resulted to be negligible in all the pyrolysis tests, being in the range 0.00025 – 0.00078 wt.%, as a consequence of the halogen removal during the dehydrochlorination pre-treatment (≈ 87 %, see section 4.3).

4.8.2 Products characterization

Gas analysis

The mass yields of the gaseous products obtained from the catalytic pyrolysis of the pretreated plastic in presence of the investigated zeolites are reported in Figure 4.49 and compared to those obtained from the reaction performed without catalyst (Thermal).

In absence of catalyst, the 7.6 % of the total gas yield was represented by methane, accompanied by a very small quantity of hydrogen. The main fractions consisted of olefins followed by paraffins, accounting for the 67 and 22 % of the total gaseous stream, respectively.

When the low-acidity zeolite MFI_100 was employed, a dramatic increment in the total gaseous products was observed, as a result of the catalyst cracking activity. The compounds distribution was also changed, compared to the thermal test, being the concentration of methane drastically reduced in favour of gaseous olefins and paraffins. Moreover, the GO/GP ratio was also reduced (from 3.0 in thermal test to 2.1 in presence of MFI_100), as

4. RESULTS AND DISCUSSION

evidence of the occurrence of catalyst-mediated secondary reactions at the expenses of the primary pyrolysis products (olefins).

With the increasing in the total acidity, the GO/GP ratio was almost linearly reduced, indicating the rising extent of secondary reactions, as confirmed also by the progressive increasing of hydrogen concentration. However, compared to MFI_25, the more acidic MFI_11 led to lower amount of light hydrocarbons (GO and GP) in the gaseous stream, as well as to a high methane concentration, evidencing its lower cracking activity, as also confirmed by the presence of wax among the reaction products.

Finally, minor amounts of CO₂ and CO are present in all gaseous streams, which is consistent with some still remaining oxygen in the pre-treated plastic waste employed as feedstock.

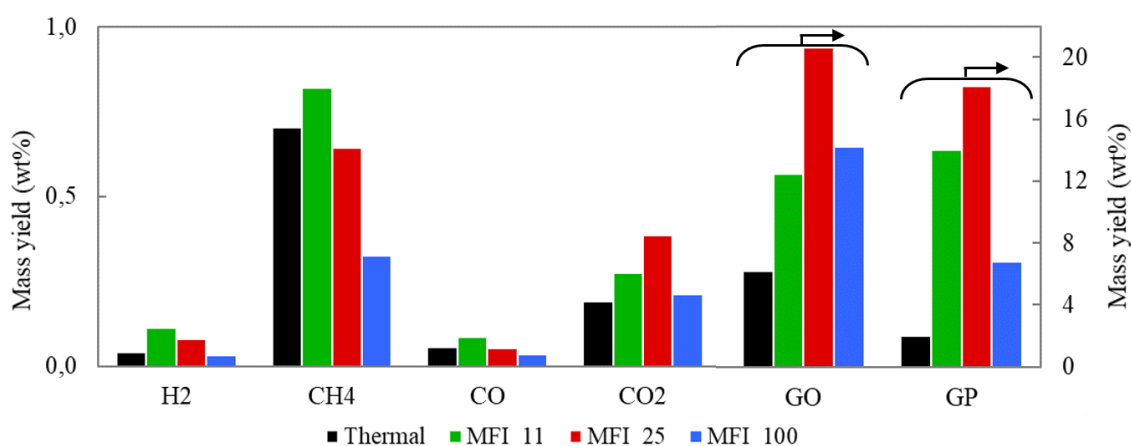


Figure 4.49 - Gas yields distribution in thermal and catalytic pyrolysis reactions. Gaseous olefins (GO) and paraffins (GP) are on secondary axis.

Oil and wax analyses

As seen above, both MFI_11-catalyzed and thermal pyrolysis experiments led to the formation of low oil yields, in the range 8 – 31 wt.%, which were not such that to be physically recovered and analysed. On the other hand, the composition of the liquid fractions deriving from the pyrolysis tests in presence of MFI_25 and MFI_100 was investigated by PIONA analysis, and the results are reported in Figure 4.50.

By comparing the selectivity by compounds families, it clearly appears that MFI_25 reaction mainly led to the formation of aromatics, which account for more than 60 wt.% of the total

4. RESULTS AND DISCUSSION

liquid fraction, whilst MFI_100 reaction resulted in higher concentrations of aliphatics compounds, especially olefins and naphthenes.

Additional information can be obtained by analysing the total products distribution in terms of selectivity by carbon number for the two considered catalysts (Figure 4.51). Bimodal distributions were found in both cases, with a first peak placed at C3 – C4, that is predominant in MFI_25, and a second peak centred in C6 – C8 range, which is instead greater in MFI_100.

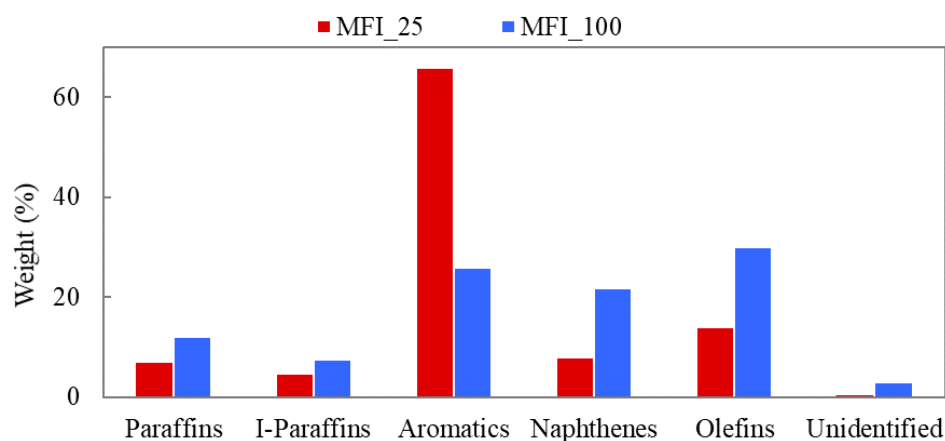


Figure 4.50 - Products distribution by compounds families in oil fractions obtained by catalytic pyrolysis in presence of the investigated catalysts.

Based on previous works [60,83], C3-C4 compounds are related to the end-chain cracking reactions promoted by the strong Brønsted acid sites of the ZSM-5 zeolites. The C6 – C8 components can be instead associated to the occurrence of secondary reactions of light hydrocarbons, mainly olefins, present in the primary thermal pyrolysis vapours, which involve oligomerization, cyclization, and aromatization.

Therefore, the obtained results confirm the higher activity of MFI_25 in promoting the cracking reactions, compared to MFI_100, which is consistent with the greater Brønsted acid sites content measured by IR analysis, equal to 378 and 125 $\mu\text{mol/g}_{\text{CAT}}$, respectively (see Table 22). Moreover, MFI_25 proved also to be more active in enhancing the secondary reactions, and especially aromatization and dehydrogenation, as evidenced by the greater aromatics and hydrogen contents in oil and gases, respectively.

On the other side, the absence of wax among the pyrolysis products, as well as the high concentration of cycloalkanes in oil, suggest that MFI_100 also promoted both cracking and

4. RESULTS AND DISCUSSION

secondary reactions, despite its much lower total acidity (about three times smaller than MFI_25, Table 22). This can be ascribed to the high proportion of external/mesopore surface area, which results in catalyst active sites more accessible to bulky molecules.

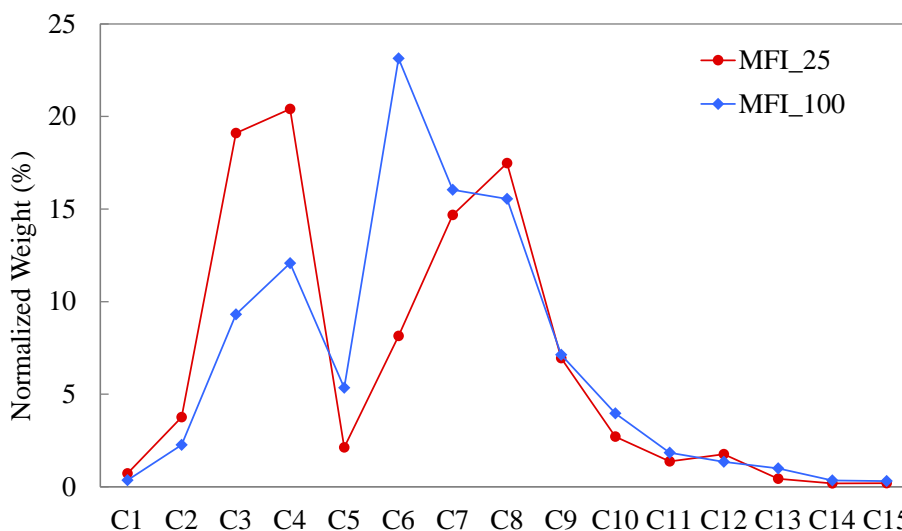


Figure 4.51 - Distribution of hydrocarbons of the gas and oil fractions obtained from the catalytic pyrolysis of dechlorinated WEEE plastic in presence of MFI_25 and MFI_100.

As mentioned above, even though its highest total acidity, a considerable amount of wax was detected among the pyrolysis products by using MFI_11 zeolite as catalyst.

Then the wax fraction was

analysed by GC-paraffins analysis in C15 – C40 carbon number range and compared to that obtained from the thermal test, i.e., in absence of catalyst.

Figure 4.52 displays that in presence of the ZSM-5 catalyst, higher proportions of branched alkanes and olefins were formed, being augmented by 26 and 55 %, respectively, compared to the thermal pyrolysis-derived wax, at the expenses of linear paraffins, which were instead reduced by 18 %. These findings suggest that MFI_11 partially promoted secondary reactions, such as isomerization, that is instead precluded in thermal pyrolysis reactions pathways [21,89,90], and dehydrogenation, as confirmed by both the high olefins and hydrogen contents in wax and gas fractions, respectively.

4. RESULTS AND DISCUSSION

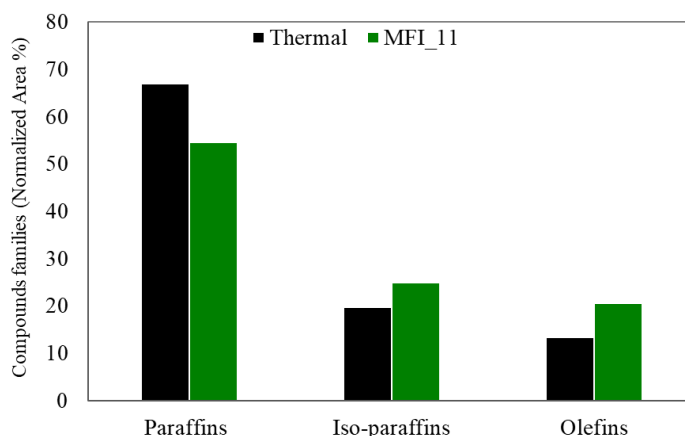


Figure 4.52 - Compounds families distribution of wax fractions produced in pyrolysis tests carried out in absence (thermal) or in presence of MFI_11 as catalyst.

Chlorine distribution

The chlorine content in the thermal and catalytic pyrolysis products was measured by AOD/IC and the distribution among the fractions is reported in Table 24. Recalling that the 86 % of the initial chlorine content in the raw plastic was already removed during the pretreatment at 350 °C (section 4.3), the halogen balances have been calculated on the basis of the average Cl concentration in the pretreated feedstock, i.e., 2652 ppm. The overall Cl mass balance is closed in the range 98.8 – 117.7 %, which can be considered an accurate result taking into account the heterogeneity of the raw plastic waste, formed by a mixture of PE and PVC, which leads to a dispersion in the determination of its Cl content.

In all tests, the most of chlorine was accumulated in the char fraction (91.3 – 94.0 wt.%), which may be related to the presence of inorganic components, like Ca-containing compounds, that can act as Cl traps by forming the corresponding chlorides [111,112].

The gaseous HCl was found to be practically negligible in all tests, accounting for 0.1 – 0.2 wt.% of the total chlorine, as a consequence of the thermal pretreatment in which a great part of the Cl originally contained in the raw plastic waste was already removed as HCl.

Compared to the thermal test, MFI_11-derived wax accumulated almost three times more of chlorine, despite its much lower mass yield (\approx 31 wt.% in MFI_11 versus \approx 74 wt.% in the thermal test). The Cl concentration in the coke deposited on the catalyst was found to be very similar in presence of MFI_11 and MFI_25, whilst a dramatic decrease of halogen content, of about 75 %, was measured when MFI_100 was employed as catalyst. Finally, the

4. RESULTS AND DISCUSSION

lowest chlorine content in oil was observed in presence of MFI_25, which accumulated the 4.5 wt.% of the halogen originally present in the pretreated WEEE plastic.

Table 24 - Cl distribution in the pyrolysis fractions referred to the average Cl content of the pretreated WEEE plastic waste.

Sample	Cl Balance (wt.%)					
	Wax	Oil	Gas ^b	Char	Coke	Total
Thermal	5.2	0.0 ^a	0.2	93.9	--	99.3
MFI_11	14.4	8.7	0.1	91.6	2.8	117.7
MFI_25	--	4.5	0.1	91.3	2.9	98.8
MFI_100	--	5.7	0.1	94.0	0.7	100.5

^a No oil was recovered.

^b Chlorine in the gases, collected in water traps.

Further information can be obtained by analysing the relative concentration of chlorine in the different components, i.e., by calculating the Cl content per kilogram of each fraction. The results, presented in Figure 4.53, revealed that the chlorine concentration in char is above 20000 ppm in all pyrolysis tests, with a significant variation among the experiments, that can be assigned to the great heterogeneity of the raw plastic waste. The following fraction in terms of halogen content is the coke deposited on the catalyst. MFI_11 and MFI_25 showed similar Cl concentrations, being the values within the variability due to the feedstock heterogeneity, whilst the lowest Cl content was observed for MFI_100-derived coke, in accordance with the mass yields. The rest of the chlorine is distributed between wax and oil fractions. In the last case, compared to MFI_11, lower and similar Cl contents were found in MFI_25 and MFI_100 liquid fractions. These findings suggest that the external/mesopore surface area of the catalyst may affect the dechlorination degree of the pyrolysis oils by favouring the trapping of the bulky Cl-containing species, since the lower proportion of $S_{\text{Ext-Mes}}$ of MFI_11, compared to the other investigated catalysts, led to the highest concentration of chlorinated hydrocarbons (wax and oil fractions).

4. RESULTS AND DISCUSSION

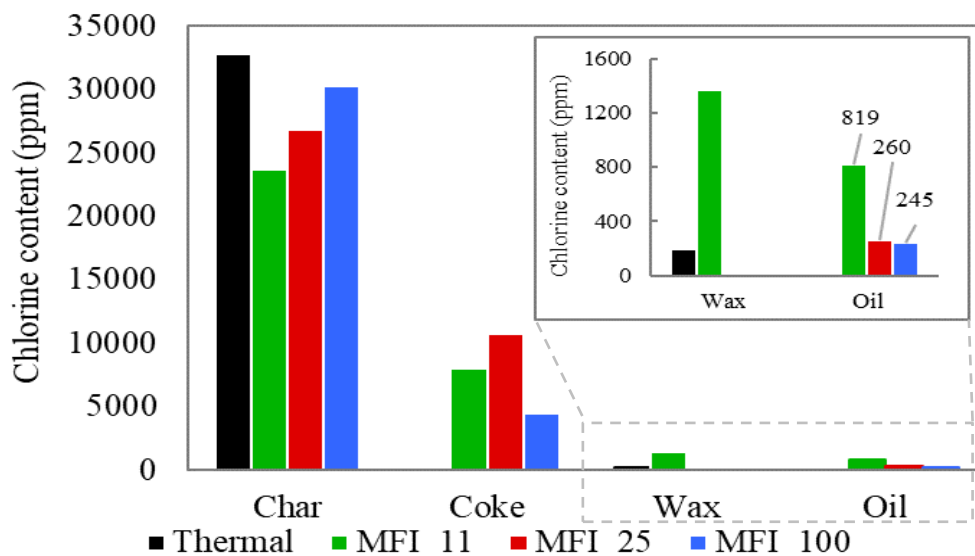


Figure 4.53 - Thermal and catalytic pyrolysis of pre-treated WEEE plastic: Cl concentration in the different fractions.

4.8.3 Conclusions

The results attained by pyrolyzing the dechlorinated WEEE plastic in presence of ZSM-5 zeolites with different Si/Al ratios confirmed that the products distribution strongly depends on the acidic and textural properties of the catalyst employed.

When the reaction was performed in absence of catalyst, the plastic decomposition followed the random radical scission pathway [59,173], mainly leading to the formation of heavy aliphatics hydrocarbons (wax), whilst just ≈ 18 wt.% accounted for light fractions, i.e., oil and gas.

As expected, the primary pyrolysis vapours were drastically upgraded by introducing the zeolite catalysts, due to both the enhanced cracking activity and the changes in the reactions pathways.

Entering into details, despite the highest total acidity, MFI_11 showed the lowest catalytic activity, which led to the formation of 31 wt.% of solid wax among products.

However, if compared with the thermal results, it clearly appears that not only the presence of catalyst improved the cracking reactions, reducing the wax yield by ≈ 60 % in favour of lighter hydrocarbons, but also the secondary reactions were implemented. In fact, the gas composition moved toward paraffins formation, at the expenses of the primary pyrolysis vapours (olefins), while oligomerization and dehydrogenation reactions also occurred,

4. RESULTS AND DISCUSSION

resulting in unsaturated heavy hydrocarbons in wax fraction, as well as in a high hydrogen concentration in the gaseous stream.

When MFI_25 was employed, the products distribution was strongly shifted toward the formation of lighter fractions (oil and gases) and no wax was produced, indicating a higher cracking activity, compared to MFI_11, due to the greater proportion of Brønsted acid sites. Moreover, the oil analysis showed that catalyst-mediated secondary reactions, such as oligomerization, cyclization, and aromatization, also took place in a greater extent, giving rise to a high aromatics content in the liquid fraction.

Finally, with the further increase of Si/Al ratio (MFI_100), the overall catalytic activity was again reduced due to the much lower total acidity, with regard to MFI_25, as evidenced by the lower gas yield, as well as the smaller aromatics concentration in oil. Nevertheless, MFI_100 led to the highest oil yield, which can be ascribed to the great proportion of accessible Brønsted acid sites due to the high share of external/mesopore surface area.

The chlorine distribution among the catalytic pyrolysis products revealed that the most of halogen was accumulated in char fraction, which is formed in the thermal zone of the reactor. It must be recalled that alkaline, alkaline earth, and heavy metals were detected in the raw plastic as contaminants, which account for the 0.9 wt.% (section 4.1). Therefore, the high-Cl content in char fractions has been attributed to the ability of metals of trapping chlorine by forming the corresponding metallic chlorides [111,112].

Moreover, negligible chlorine contents were detected in the gaseous phases, independently of the catalyst employed, suggesting that if any HCl is formed during the pyrolysis process, it is fast captured by the mineral matter contained in the char.

Finally, MFI_25 and MFI_100 showed the highest oil dechlorination degrees, and as a consequence, the oils produced over these catalysts present a Cl content (≈ 250 ppm) that is close to the limit imposed by refineries, and therefore the further upgrading and processing can be facilitated.

4. RESULTS AND DISCUSSION

4.9 Catalytic pyrolysis over hierarchical ZSM-5 zeolite

In this section, the effects of the secondary porosity of hierarchical ZSM-5 zeolite on pyrolysis products and chlorine distribution are described and discussed.

Starting from the H⁺-form of the parent MFI_25, the secondary mesoporosity was generated by NaOH-induced desilication. The desilication procedure and the characterization of h-MFI zeolite are reported in section 4.2.3. However, the main textural and acidic properties of the catalyst investigated in this section are shown below and compared to the parent sample (Table 25).

Table 25 - Main textural and acidic properties of h-MFI, compared to the parent MFI_25.

Sample	Si/Al ^a bulk (mol/mol)	S _{BET} ^b (m ² /g)	S _{EXT-Mes} ^c (m ² /g)	Weak AS ^d (μmol _{NH3} /g _{CAT})	Strong AS ^d (μmol _{NH3} /g _{CAT})	Brønsted AS ^e (μmol/g _{CAT})	Lewis AS ^e (μmol/g _{CAT})	B/L	EF-Al ^f (Area%)
MFI_25	23.6	418	135	141	399	378	95	4.0	8.0
h_MFI	21.7	407	166	155	480	523	154	3.4	11.0

^a Determined by ICP-OES. ^b BET specific surface area. ^c Calculated by *t*-plot method.

^d Calculated by NH₃-TPD. ^e Determined by FT-IR after adsorption of D₃-acetonitrile.

^f Calculated from ²⁷Al MAS NMR.

The hierarchical ZSM-5 zeolite was tested in the catalytic fast-pyrolysis of dechlorinated WEEE plastic, i.e., after the dehydrochlorination pretreatment at 350 °C, by employing 600 and 450 °C as temperatures of the thermal and catalytic zones, respectively, and 0.2 as catalyst-to-feedstock ratio.

The obtained results have been compared to both thermal pyrolysis test (without catalyst) and the thermo-catalytic experiment in presence of the parent zeolite (MFI_25).

The pyrolysis reactions have been labelled on the basis of the catalyst employed, i.e., as MFI_25, h-MFI, and Thermal (in absence of catalyst) in the following.

4.9.1 Reaction yields

The products distribution per fraction obtained from the thermal and catalytic pyrolysis tests in presence of h-MFI and MFI_25 zeolites is presented in Table 26.

As discussed in the previous sections, the reaction carried out in absence of catalyst (Thermal) produced wax as major product, whilst less than 18 wt.% accounted for lighter

4. RESULTS AND DISCUSSION

fractions, i.e., liquid oil and permanent gases, as a consequence of the random radical cracking reaction mechanism [59].

When a zeolite was employed for the pyrolysis vapours upgrading, a drastic change in the overall products distribution took place due to the improvement of cracking and the occurrence of secondary reactions mediated by the catalyst. As widely discussed in the previous sections, the catalyst active sites, mainly the strong Brønsted acid centres, promote the change of the reaction mechanism from radical to ionic, resulting in a strong increment of C-C bonds breaking, and thus in shorter hydrocarbons formation [59,79.80].

As a result, no wax was produced in presence of MFI_25 and h-MFI, being instead the total yield of liquid and gaseous fractions higher than 90 wt.% in both cases.

By comparing MFI_25 and h-MFI reactions, it can be observed that with the increase of the secondary porosity, the oil yield was augmented by 15 %, at the expenses of the gas fraction, being reduced by 17 %. This finding suggests a slight lower cracking activity of h-MFI, that is consistent with the acidic properties of the investigated catalysts. In fact, downstream the desilication treatment the B/L acid sites ratio decreased, compared to the parent zeolite, in accordance with the rise of EF-Al species concentration.

Nevertheless, h-MFI has likewise shown a high overall activity. This can be explained by considering that the Brønsted acid sites concentration was found to be augmented as a consequence of the desilication treatment (see section 4.2.3), which has been attributed to a partial reinsertion of previously extracted Al into zeolite framework positions close to the vacancies generated during desilication, therefore having a higher accessibility [166].

Table 26 - Product yields of pyrolysis of dechlorinated WEEE plastic in absence (Thermal) and in presence of MFI_25 and h-MFI zeolites as catalysts.

Sample	Products yield (wt.%)					
	Wax	Oil	Gas	Char	Coke	Water-trapped Cl*
Thermal	74.1	8.4	9.2	8.4	--	0.00051
MFI_25	0.0	50.6	39.9	8.7	0.8	0.00025
h-MFI	0.0	58.2	33.2	8.1	0.5	0.00054

* Referred to the weight of the dechlorinated plastic waste, measured by IC.

4. RESULTS AND DISCUSSION

Furthermore, the coke deposited on the catalysts proved to be lower in presence of h-MFI, whilst all char yields stood in the range 8.1 – 8.7 wt.%, since its formation occurs before the contact of the primary pyrolysis vapours with the catalyst.

Finally, the chlorine content in the gaseous streams proved to be negligible in all pyrolysis experiments, as a consequence of the dechlorination pretreatment, in which the 87 % of the initial chlorine in the raw WEEE plastic was already removed in form of HCl.

4.9.2 Products characterization

Gas analysis

Figure 4.54 provides information about the yield of the different components detected in the gaseous streams.

Small amounts of CO and CO₂ have formed because of the presence of residual oxygen in the waste dechlorinated plastic used as feedstock.

Methane concentration proved to be similar in all pyrolysis tests, while hydrogen was mainly produced in the catalytic experiments, although similar contents have been detected in presence of both the investigated catalysts.

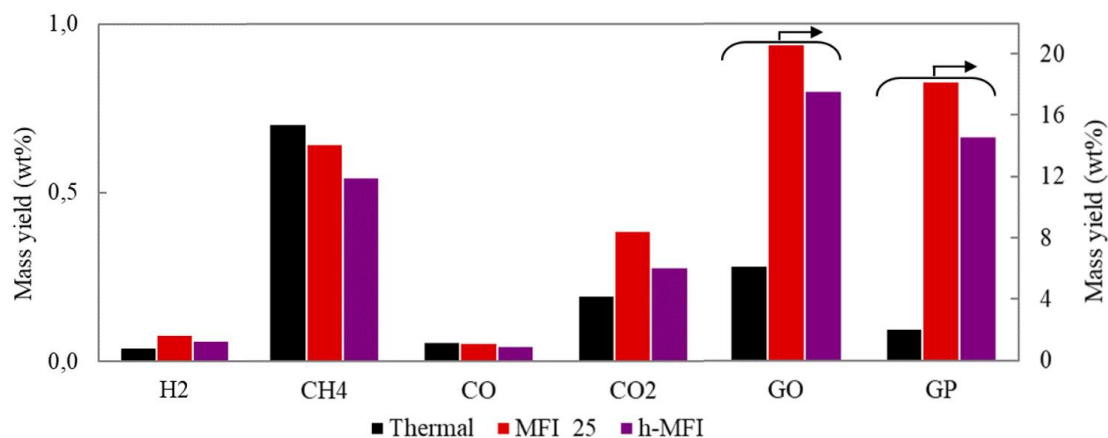


Figure 4.54 - Gas yields distribution after thermal and catalytic pyrolysis in presence of h-MFI and MFI_25. Gaseous olefins (GO) and paraffins (GP) are shown on secondary axis.

The highest impact derived from the presence of the catalysts has been observed in the formation of light hydrocarbons, since a sharp increase in the yield of both gaseous olefins and paraffin yields was detected, due to the extension of end-chain cracking reactions.

4. RESULTS AND DISCUSSION

However, the gaseous hydrocarbons formation proved to be somewhat lower in presence of h-MFI, compared to MFI_25, confirming the slight decrease of the cracking activity related to the larger proportion of Lewis acid sites, as discussed in the previous section.

Oil analysis

Recalling that no oil was collected in the thermal pyrolysis tests, the composition of the oil fractions obtained from the catalytic pyrolysis experiments in presence of the investigated catalysts was evaluated by GC PIONA analysis, and the results are reported in Figure 4.55. Both oils mainly consist of aromatics hydrocarbons, which account for the 66 and 56 wt.% in presence of MFI_25 and h-MFI, respectively. Paraffins concentration was also slightly reduced with the increasing of mesopores concentration, in favour of branched alkanes formation.

On the other side, greater concentrations of naphthenes and olefins have been detected in the h-MFI zeolite-derived oil, being increased by 69 % and 21 %, respectively, with regard to MFI_25.

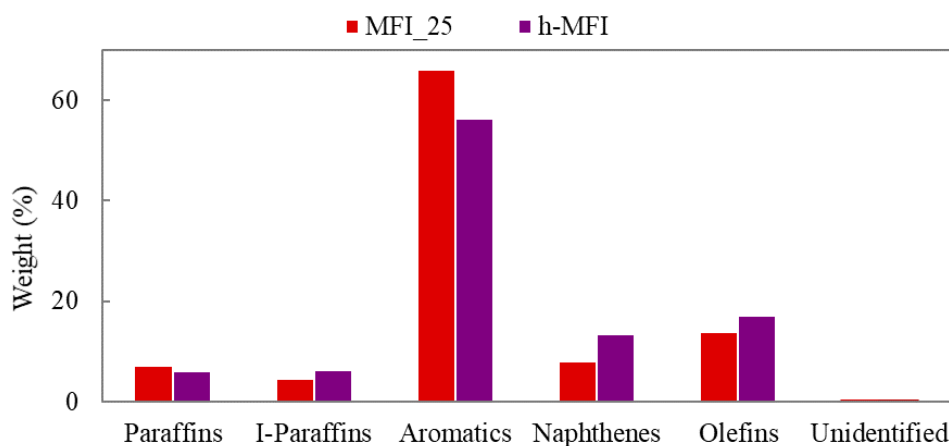


Figure 4.55 - Products distribution by compounds families in pyrolysis oils after catalytic pyrolysis tests with MFI_25 and h-MFI.

It must be pointed out that mono-aromatic compounds (mainly BTX) represent the major component among the total aromatics, amounting to more than 90 % with both tested catalysts (Figure 4.56). However, h-MFI reaction led to a greater mono-aromatic hydrocarbons proportion, despite the 10 wt.% lower total aromatics content in the oil. This

4. RESULTS AND DISCUSSION

can explain also the lower coke deposited on h-MFI catalyst, since the polyaromatics compounds can act as coke precursors [84].

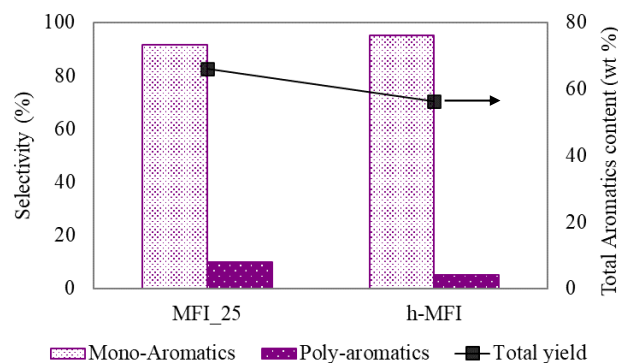


Figure 4.56 - Aromatic families selectivity in pyrolysis oils obtained from catalytic pyrolysis with MFI₂₅ and h-MFI. Total aromatics content is on secondary axis.

Additional information about the hydrocarbons distribution can be obtained by investigating the selectivity by carbon number (Figure 4.57). Similar profiles were found for both investigated catalysts, which show a bimodal distribution with the peaks placed in C3 – C4 and C6 – C9 ranges. The higher share of C3 – C4 hydrocarbons has been observed in presence of MFI₂₅ catalyst, and it is related to end-chain cracking reactions. On the contrary, h-MFI mainly led to the formation of compounds in C6 – C8 carbon number range, that can be associated to the occurrence of catalyst-mediated secondary reactions [60,83].

The obtained results suggest that some changes in the reactions pathways took place on the basis of the catalyst employed. MFI-25 mainly promoted end-chain cracking reactions, resulting in a higher gas yield, as well as dehydrogenation, isomerization, and aromatization among the secondary reactions, as demonstrated by the oil composition and higher hydrogen concentration in the gaseous fraction.

On the other side, the hierarchical zeolite h-MFI proved to be less active in end-chain scission, but it favoured β -scission, oligomerization, cyclization and aromatization reactions, mostly leading to longer hydrocarbons, and especially mono-aromatics, cycloalkanes, and olefins in the liquid fraction.

These findings are supported by the textural and acidic properties of the studied catalysts. In fact, MFI₂₅ presents a higher proportion of strong Brønsted acid sites, that are known to be the main responsible for end-chain cracking reactions [59]. In contrast, h-MFI shows a

4. RESULTS AND DISCUSSION

higher total acidity, due to the rise of Al proportion in the zeolite framework accordingly to the desilication treatment, but a greater percentage of Lewis acid sites, as well as of weaker Brønsted acidity, resulting in a lower cracking activity.

Nevertheless, the higher absolute concentration of Brønsted acid sites and their improved accessibility, associated to the augmented proportion of external/mesopore surface area downstream the selective Si removal, allowed h-MFI catalyst to promote secondary reactions, leading not only to an oil rich in valuable hydrocarbons, such as mono-aromatics, but also to the highest liquid fraction yield.

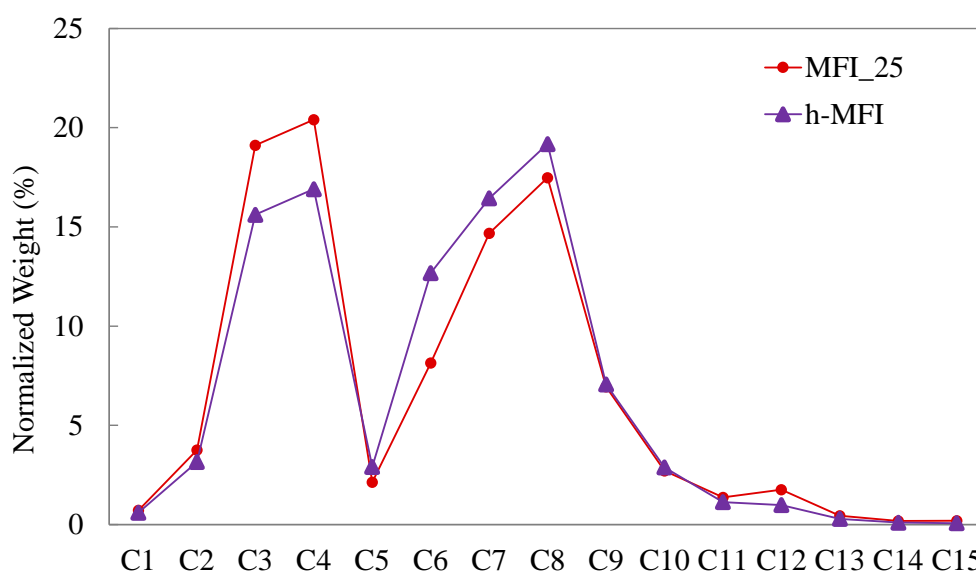


Figure 4.57 - Distribution per carbon atom number of the hydrocarbons obtained in pyrolysis tests with MFI_25 and h-MFI zeolites as catalysts.

Chlorine distribution

The chlorine distribution among pyrolysis products obtained in presence of h-MFI and MFI_25 is shown in Figure 4.58. The plastic feedstock employed in these set of reactions was thermally dechlorinated at 350 °C, thus the halogen balances have been calculated by using the Cl concentration measured in the dechlorinated plastic as basis (average value = 2652 ppm).

The analysis revealed that, in both reactions, the most of chlorine was retained in the char fraction ($\approx 93\%$), while the portion of Cl in gases was found to be negligible.

Opposite trends can be observed in oil and coke fractions. With the external/mesopore surface area rise, i.e., in presence of h-MFI, the chlorine content in the coke deposited on the

4. RESULTS AND DISCUSSION

catalyst increased, despite the drop detected in the mass yield, while the lowest Cl concentration was measured in the oil fraction.

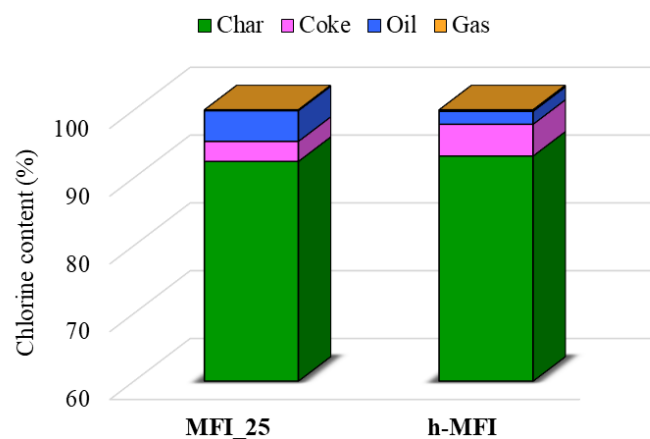


Figure 4.58 - Chlorine distribution among pyrolysis products obtained in presence of desilicated and parent zeolites catalysts.

By analysing the relative concentration of chlorine per kilogram of each fraction (Figure 4.59), it clearly appears that the coke deposited on h-MFI catalyst shows the highest chlorine concentration, suggesting that the presence of mesoporosity in this material favours the trapping of bulky Cl-containing species, which in contrast is more difficult to occur on the parent MFI_25 zeolite. Therefore, the good catalyst performance of trapping chlorinated species within the carbonaceous matter results in the lowest Cl-content oil, amounting to 88 ppm, that is below the limit of 100 ppm usually imposed to be processed in refinery facilities [28,101].

4. RESULTS AND DISCUSSION

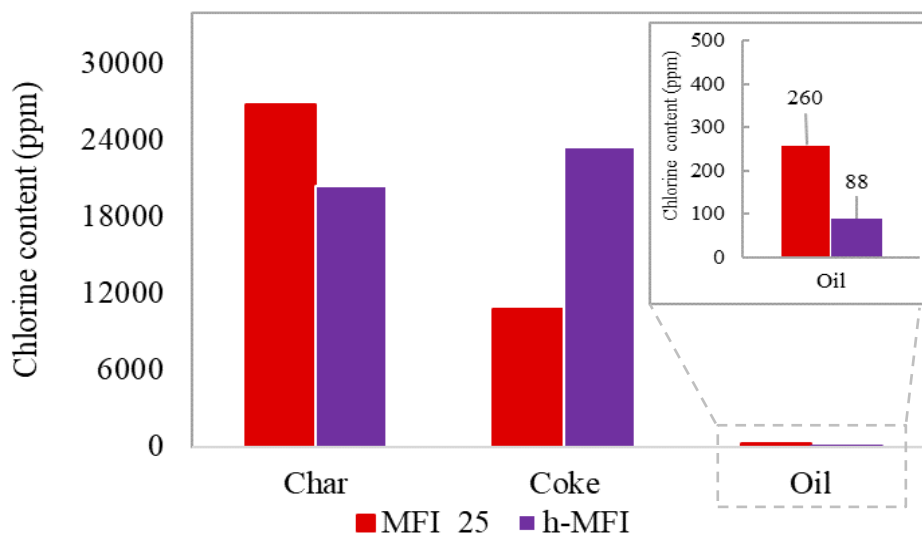


Figure 4.59 - Cl concentration in the different fractions derived from catalytic pyrolysis of pretreated WEEE plastic in presence of h-MFI and MFI_25 catalysts.

4.9.3 Conclusions

The results achieved by the catalytic pyrolysis tests of dechlorinated WEEE plastic in presence of hierarchical and parent ZSM-5 catalysts evidenced a correlation between the nature of zeolite pores and both products and chlorine distributions.

Entering into details, the products distribution was slightly shifted towards oil formation at the expense of the gaseous components in presence of h-MFI, denoting a reduction of the overall cracking activity compared to MFI_25, which is consistent with the lower B/L acid sites ratio measured downstream the desilication treatment.

This has been also confirmed by the analysis of the gaseous streams composition, that showed lower amounts of both gaseous paraffins and olefins, just slightly in favour of saturated hydrocarbons, when h-MFI was employed as catalyst.

The oils composition revealed that the secondary reactions, such as oligomerization, cyclization, and aromatization, are promoted by both catalysts, even if in different way and extent, resulting in liquid fractions rich in mono-aromatics, that are valuable raw chemicals. Moreover, h-MFI zeolite proved to be less prone to promote PAHs formation, due to the improved accessibility of the acid sites, resulting in a higher proportion of mono-aromatics in oil, as well as in a lower coke deposition on the catalyst.

4. RESULTS AND DISCUSSION

From the chlorine distribution analysis, it is possible to assume that the halogen still present in the dechlorinated WEEE plastic is mainly released in form of bulky chlorinated compounds during the pyrolysis process, that thus tend to be accumulated in the heavier fractions, such as coke and char. Furthermore, since almost no chlorine has been detected in the gaseous streams, the HCl that could be formed during the pyrolysis process should be captured by the inorganic species contained in the char.

Finally, it seems that the external/mesopore surface area plays a key role in the oil dechlorination degree, as the accessibility and the trapping of bulky chlorine-containing compounds can be favoured, resulting in low-Cl content oils.

In conclusion, h-MFI zeolite showed the best catalytic performances among all tested catalysts, since the combined effect of the acidic properties and the enhanced pores accessibility resulted in a high oil yield (≈ 60 wt.%) with the lowest chlorine content, being within the limits for its further processing in refineries units.

5. CONCLUSIONS AND FUTURE TRENDS

Aim of this work was to investigate the valorisation of a real waste plastic mixture by thermo-catalytic pyrolysis processes in presence of ZSM-5 zeolites as catalysts. In this section, a summary of the previous chapters and the main achieved results is reported.

In **Chapter 1**, the background of this work is depicted and discussed, in terms of both specific needs of the company R.ED.EL. srl., that is partner of this project, and global issues concerning the WEEE plastic management. In the view of reaching the “zero-waste circular economy” model, R.ED.EL. srl has started a recycling process which allows to separate and recover the metallic components of the waste electric cables, so that the plastic fraction represents the only remaining waste, that is currently landfilled. Therefore, the valorisation of the WEEE plastic would help the company to close its virtuous cycle, by also contributing to increasing the proportion of the globally recycled materials. In fact, it has been estimated that wastes from electric and electronic equipment (WEEE) account for the 2 % of the total solid streams and just the 20 % is properly recycled to date, mainly due to the high complexity of the matrixes to be treated. The plastic fraction represents a significant portion of the WEEE, being on average greater than the 30 %, and it presents a very complex composition, that includes different polymers, additives, halogens, and hazardous substances, which makes safe and efficient recycling processes still challenging. Among the current waste plastic recycling methods, chemical recycling by pyrolysis represents the most promising technology, since valuable raw chemicals and fuels can be obtained by tailoring the process parameters, as well as by using appropriate catalysts and/or sorbents for the contaminants management. This doctoral thesis therefore fits into this context, aiming to reduce the existing research gap by investigating the thermo-catalytic fast-pyrolysis of the real PVC-containing WEEE plastic provided by R.ED.EL. srl, with a special focus on the chlorine quantification and distribution among the pyrolysis products.

In **Chapter 2**, thermal and catalytic pyrolysis processes are outlined and discussed, focusing on the parameters governing the reactions, as well as on zeolites as catalysts. Moreover, the issue concerning the presence of halogens in pyrolysis products and the current technologies for their reduction are also addressed in the same section.

5. CONCLUSIONS AND FUTURE TRENDS

The thermal decomposition involves the bonds breaking of the polymers chains in absence of oxygen, producing primary radicals that then undergo further decomposition and recombination. Downstream the reaction, hydrocarbons in a wide range of molecular weights can be produced, resulting in the formation of different fractions, i.e. char, wax, oil and gases. It clearly appears that temperature represents the most important reaction parameter, followed by both the type of reactor and the residence time of the vapours. Several benefits can be associated to the use of catalysts in the process, that include the reduction of the overall energy costs, by increasing the conversion rate at lower temperature and time, and the selectivity improvement, by enhancing cracking and secondary reactions. Among the most used in heterogeneous catalysis, zeolites represent reliable and widely investigated catalysts for plastics pyrolysis products upgrading, due to their high versatility in terms of both acidic (typology, quantity, strength) and textural (shape-selectivity related to the pore architecture) properties. The presence of Brønsted and Lewis acid sites in the zeolite framework modify the reactions pathways from radical to carbocationic, thus promoting cracking and secondary oligomerization-cyclization- aromatization reactions and giving rise to narrower and targeted hydrocarbons distributions, that can be used as source of raw chemicals and/or fuels, once properly treated. Therefore, a careful evaluation of acidity and pore architecture can allow to optimize the catalytic system to upgrade the primary plastic pyrolysis products with high selectivity and resistance to deactivation by coke deposition. In this context, ZSM-5 zeolites have shown promising performances, also in terms of halogens trapping, that represents one of the main issues in real waste plastic management due to the release of corrosive hydro halides acids and organohalides, which can be partially oxidized to toxic halogenated compounds in the following processing steps.

In **Chapter 3**, the procedures employed for the preparation of the investigated catalysts, as well as the techniques and methods used for catalysts, WEEE plastic mixtures, and pyrolysis products characterization are described. Furthermore, the description of the experimental setups and parameters used for dehydrochlorination thermal treatment and thermo-catalytic pyrolysis experiments are also reported in this section.

In this work, ZSM-5 zeolites with different Si/Al ratios have been synthesized to evaluate the influence of the acidic and textural properties on the products and chlorine distributions in thermo-catalytic fast-pyrolysis of the investigated waste plastic mixture. Moreover, to evaluate the effects of the secondary mesoporosity, hierarchical ZSM-5 zeolite has been

5. CONCLUSIONS AND FUTURE TRENDS

prepared by NaOH-induced desilication treatment. In addition, a commercial nanocrystalline ZSM-5 zeolite has been employed to optimize the process parameters, such as catalytic temperature and catalyst-to-feedstock ratio. All investigated catalysts have been completely characterized by XRD, SEM, ICP-OES, N₂ physisorption, NH₃-TPD, FT-IR with the adsorption of CD₃CN, and ²⁷Al MAS NMR.

On the other side, both raw and dechlorinated WEEE plastic mixtures have been characterized in terms of polymers and chemical compositions, presence and quantification of halogens and other contaminants, and thermal behaviour, by XRD, FT-IR, TG, DSC, AOD/IC, and ICP-OES analyses.

The raw WEEE plastic has been subjected to thermal dechlorination treatment at different temperatures, in a downdraft stainless steel reactor, under nitrogen flow, aiming to reduce the halogen content in the waste plastic mixture to be pyrolyzed.

Thermo-catalytic fast-pyrolysis experiments has been carried out in a downdraft fixed bed reactor, with thermal and catalytic zones independently heated. In this system, the feedstock thermal decomposition occurs in the thermal zone and the primary pyrolysis vapours are guided by a nitrogen flow to pass through the catalyst bed (if any) to be upgraded in an *ex-situ* configuration. The output products have been separately collected for further characterization. The chlorine content in liquid and solid fractions was measured by AOD/IC, while the quantification of coke deposited on the catalysts was performed by TG analysis in air. Oil and wax compositions were investigated by GC-PIONA and GC-paraffins analyses, respectively, whilst the non-condensable gases composition was evaluated by μ -GC analysis.

In **Chapter 4**, all experimental results achieved in this doctoral work are described and discussed, involving the physicochemical characterization of raw WEEE plastic and the prepared catalysts, the thermal WEEE plastic dehydrochlorination treatments, and the thermo-catalytic fast-pyrolysis tests.

The characterization of the raw WEEE plastic revealed a high heterogeneity of the sample, which consists of a mixture of PE, PVC, metals and oxygen as a consequence of photooxidation and contamination of products during their lifetime, as well as of the presence of additives. The chlorine content stood at 1.95 ± 0.48 wt.%, which corresponds to 3.44 ± 0.85 wt.% of PVC in the mixture. The relatively large standard deviations in the

5. CONCLUSIONS AND FUTURE TRENDS

determination of the Cl content can be thus assigned to the high heterogeneity of the WEEE plastic waste, even after the size homogenization by milling.

The physicochemical characterization of the investigated ZSM-5 zeolites showed that all catalysts present high crystallinity and purity. However, significant differences have been detected among the samples, in terms of both textural and acidic properties. As expected, the acidic properties proved to be affected by the total aluminium content, as well as by the Al environment. In fact, the measured B/L acid sites ratios increase with the Si/Al ratio, but Lewis acid sites rise in a greater extent at higher total Al contents, which is consistent with the increase of EFAl species concentration. Just a slight deviation in this trend can be observed for the commercial nanocrystalline ZSM-5 zeolite, that has been ascribed to different calcination processes to which it may have been subjected, resulting in lower EFAl species formation. Accordingly, also the Brønsted acid sites concentration decreases with the total aluminium content, except for the desilicated h-MFI zeolite, that shows the highest absolute B-AS content, due to the partial reinsertion into zeolite framework of the previously extracted aluminium atoms and the generation of additional structure defects during the desilication treatment. In addition, the study of the textural properties shows that the BET surface area increases according with the Si/Al ratio. Moreover, a higher value of external-mesopores surface area can be observed in MFI_100 zeolite, revealing a contribution of the voids existing within the crystals aggregates, as well as in the desilicated ZSM-5 sample, compared to the parent MFI_25, due to the new open mesopores on the outer surface generated downstream the desilication treatment.

The thermal dehydrochlorination treatment carried out at 300 and 350 °C revealed that the reaction temperature rise leads to a higher dechlorination efficiency, amounting to 68 and 86 % of the initial chlorine, respectively. Moreover, a partial deoxygenation occurs concurrently, also in a greater extent at higher temperature, allowing to simultaneously reduce the oxygen content, that also represents a limiting factor for the further processing of pyrolysis oils. On the other side, small amounts of organics are also released during the thermal treatment at both temperatures, indicating a partial decomposition of the polymers chains, which can however be considered as negligible compared to the high dechlorination efficiency achieved. Accordingly, 350 °C proves to be most efficient temperature for the dehydrochlorination treatment of the raw WEEE plastic, and therefore it has been selected for the WEEE plastic pretreatments in this work.

5. CONCLUSIONS AND FUTURE TRENDS

The thermal pyrolysis experiments of raw WEEE plastic revealed that solid wax represents the main product at all tested temperatures. However, the products distribution is shifted towards lighter hydrocarbons formation with the temperature rise, denoting a temperature-induced improvement of cracking reactions. In fact, the oil yield is maximised at 600 °C, accounting for about 11 wt.%, whilst the further temperature rise mainly promotes the non-condensable gases formation (C1 – C4), at the expenses of both oil and wax fractions. The chlorine distribution analysis showed that most of the halogen is released in form of gaseous hydrochloric acid, reaching the maximum concentration at 600 °C. However chlorinated hydrocarbons formation preferentially occurs rather than HCl release with increasing temperature, suggesting that the shortening of chlorinated bulky molecules was favoured over the HCl elimination. Accordingly, 600 °C as pyrolysis temperature led to highest oil and gaseous HCl yields, and therefore it has been selected and employed as thermal decomposition temperature in the thermo-catalytic pyrolysis tests.

The commercial nanocrystalline ZSM-5 zeolite with Si/Al ratio of 42 has been employed to investigate the effects of catalytic temperature and catalyst-to-feedstock ratio on products and chlorine distributions in the thermo-catalytic fast-pyrolysis of raw WEEE plastic. The catalytic vapours upgrading by means of ZSM-5 zeolite drastically changed the products distribution, compared to the thermal reactions, leading to high yields of oil and gas, at the expenses of wax, which was not detected in all catalytic experiments. The improvement of cracking and secondary reactions is observed increasing the catalyst bed temperature from 400 to 450 °C, resulting in greater proportion of mono-aromatics in oil, as well as of hydrogen in the gaseous stream. However, the competition between radical and cationic reactions pathways may occur at an even higher temperature, resulting in high olefins and low aromatics content in oil. Furthermore, the catalyst bed temperature also affects the chlorine distribution among the pyrolysis products, since the halogen content in oils almost linearly decreases with the temperature rise, whilst the coke fractions follow the opposite trend. These findings suggest that the released HCl reacts again with the intermediate species at high temperatures, giving rise to chlorinated compounds, which accumulate in the heavier coke fraction. On these bases, 450 °C has been selected as catalyst bed temperature, at which the influence of the catalyst-to-feedstock ratio on products and chlorine distributions has been assessed. As expected, the increasing catalyst proportion affects both cracking and secondary reactions, since a significant greater number of acid sites, as well as a higher

5. CONCLUSIONS AND FUTURE TRENDS

external surface, are available to interact with the bulky molecules present in the primary pyrolysis vapours. In fact, by doubling the catalyst amount, shorter hydrocarbons are produced, thus increasing the non-condensable gases yield, and oligomerization, cyclization, and aromatization reactions occur in a greater extent, resulting in a high aromatics content oil. On the other side, a greater proportion of PAHs (that act as coke precursors) is produced at higher C/F ratio, resulting in a larger amount of coke deposited on the catalyst. Finally, most of chlorine was released in form of HCl at both C/F ratios, whose concentration however decreases by increasing the catalyst amount, contrary to what happens to oil and coke fractions. These results suggest that the improvement on the catalytic contribution due to the increasing catalyst amount leads to the formation of halogenated hydrocarbons, rather than HCl release, resulting in an oil which contains a significant amount of Cl definitely far from the limits imposed for its further processing.

In the view of minimizing the chlorine content in pyrolysis oil, the dechlorinated WEEE plastic has been used as feedstock in the following thermo-catalytic pyrolysis tests, by using the previously optimized reaction parameters (600 and 450 °C as temperatures for the thermal and catalytic zones, respectively, and a catalyst/feedstock ratio of 0.2). First of all, the catalytic pyrolysis results obtained by using raw and dechlorinated plastics as feedstocks have been compared, in order to investigate if the differences detected downstream the dehydrochlorination treatment could have any impact on the pyrolysis products. The reactions have been carried out in presence of commercial n-ZSM-5 zeolite (Si/Al = 42) as catalyst. The obtained results show just small differences in the products yields, being within the variability of waste plastics samples. However, the dechlorinated plastic results in lighter hydrocarbons formation and lower coke deposition on the one hand, and in lower aromatics content in oil on the other, denoting that some changes occur in the reactions pathways. Based on literature data, these findings can be ascribed to both partial deactivation of the catalyst for Cl-poisoning and coke deposition when the more contaminated raw plastic is employed as feedstock, as well as to some partial rearrangement among polymers which may take place during the dehydrochlorination thermal pretreatment. Nevertheless, the most important result involves the chlorine content in the oil fraction, since the combined effect of the thermal dechlorination treatment and the catalytic fast-pyrolysis leads to a drastic 91 % drop of chlorine in oil, compared to the conventional one-step catalytic pyrolysis, resulting

5. CONCLUSIONS AND FUTURE TRENDS

in an oil which contains 121 ppm of chlorine, that is very close to the limit imposed for its further processing (100 ppm).

In the view of further reducing the halogen content by simultaneously improving the oil properties, synthesized ZSM-5 zeolites with different acid and textural properties have been tested as catalysts in the thermo-catalytic fast-pyrolysis of dechlorinated WEEE plastic. The results confirm the strong dependence of the cracking degree and the occurrence of secondary reactions on the Brønsted acid sites concentration, since the activity of the investigated catalysts does not increase with the total acidity, but according with the B/L acid sites ratio. This last is in turn strictly related to the extra-framework aluminium species concentration, that increases with total aluminium content. As a result, the highest acidic zeolite (MFI_11) leads to the lower cracking degree, due to the greater EFAl content and thus to the greater proportion of less active Lewis acid sites, such that about 31 wt.% of wax is produced among the pyrolysis products. On the other side, the least acidic MFI_100 zeolite presents the lowest absolute content of Brønsted acid sites, but with the highest B/L ratio, which results in the maximization of the liquid fraction yield. Finally, the MFI_25 zeolite shows intermediates content of EFAl species and proportion of Brønsted acid sites, but a high absolute concentration, leading to a greater cracking degree, and therefore to the growth of the gas yield at the expense of oil fraction. The accessibility of the catalysts active sites also plays a key role on the extent to which both cracking and secondary reactions occur. The external/mesopore surface area of the investigated catalysts increases with the Si/Al ratio, thus providing increasing proportions of accessible Brønsted acid sites to the bulky molecules present in the primary pyrolysis vapours, which result in a greater catalyst activity. This last fact is also reflected in the selectivity, since greater proportions of C3-C4 compounds, related to the end-chain cracking reactions, and aromatics in oil are observed when the more active MFI_25 zeolite is employed as catalyst. In terms of chlorine distribution, the most of halogen is retained by the char fractions, due to the presence of metals that may act as Cl-trapping, whilst the gaseous HCl is negligible in all tests, as a consequence of the drastic Cl reduction during the thermal pretreatment. Finally, a good oil dechlorination degree is achieved in presence of the more active catalysts, i.e. MFI_25 and MFI_100, that results in oils with about 250 ppm of chlorine.

The effects of the alkaline-induced mesoporosity in the zeolite on the products and chlorine distributions have been investigated by pyrolyzing the dechlorinated plastic in the same

5. CONCLUSIONS AND FUTURE TRENDS

reaction conditions (600 and 450 °C as temperatures for the thermal and catalytic zones, respectively, and a catalyst/feedstock ratio of 0.2). The attained results showed a slightly lower activity of the hierarchical zeolite, compared to the parent sample, that is consistent with the increase of the EFAl species and Lewis acid sites proportion which occurs during the desilication process. However, the absolute concentration of Brønsted acid sites increase downstream the alkaline treatment, resulting in a high overall activity of the desilicated catalyst. Accordingly, the secondary reactions, such as oligomerization, cyclization, and aromatization, are promoted by both catalysts, even if in a different extent, resulting in liquid fractions rich in mono-aromatics, that are valuable raw chemicals. Therefore, the lower cracking activity of the hierarchical zeolite maximizes the oil yield at the expense of the gaseous fraction, compared to the parent MFI_25, while its improved accessibility inhibits PAHs formation and coke deposition. Finally, the chlorine distribution analysis revealed that also in this case the most of chlorine is collected in the char fractions, while the portion of Cl in gases is negligible.

A significant result is represented by the Cl content in the desilicated zeolite-derived oil, that amounts to 88 ppm which is below the legal limits to be processed in refineries facilities. This is complemented by a higher content of chlorine in the coke deposited on the catalyst, with regard to the parent sample, suggesting that the presence of mesoporosity favours the trapping of bulky Cl-containing species, which in contrast is more difficult to occur on the microporous parent MFI_25 zeolite.

The catalytic behaviour of the hierarchical ZSM-5 zeolite in the thermo-catalytic conversion of the dechlorinated WEEE plastic is quite interesting. More specifically, the combination between the improved accessibility and Brønsted acidity has led to a high catalytic activity, in terms of both cracking degree and mono-aromatics selectivity, as well as to a high oil dechlorination degree.

On the basis of the results obtained in this doctoral work, the following further studies should be carried out.

Regeneration of the spent catalyst should be investigated, in order to evaluate whether the halogens present in the coke can be removed without irreversibly affecting the catalyst properties. The stability of the acid sites after the coke burning can be studied by FT-IR. Moreover, the catalytic activity could be assessed as a function of catalyst regeneration

5. CONCLUSIONS AND FUTURE TRENDS

cycles, as well as in a continuous system that would allow to determine the deactivation rate, thus obtaining information for industrial applications.

On the other side, different post-synthesis methodologies could be used to create hierarchical porous systems, such as selective dealumination and desilication in different reactions conditions, aiming to further improve both the active sites accessibility to the bulky molecules and the chlorinated compounds trapping.

Finally, to the same purpose, mesoporous materials, such as MCM-41 and SBA-15, could be tested in the thermo-catalytic fast-pyrolysis of the raw and dechlorinated waste plastic mixture.

LIST OF FIGURES

- Figure 1.1** - Schematic representation of electric medium voltage cable.
- Figure 1.2** - Pictures of the recycle chain set up by R.ED.EL. srl.
- Figure 2.1** - Size of rings in the zeolitic frameworks (adapted from []).
- Figure 2.2** - Zeolite framework types and number of T-atoms in the unit (adapted from [60]).
- Figure 2.3** - Two-dimensional representation of the zeolite framework (adapted from [60]).
- Figure 2.4** - Representation of strong B-AS and weak L-AS in the zeolite framework (adapted from []).
- Figure 2.5** - Products and reaction pathways of catalytic cracking of polyolefins over acid solid catalysts [181].
- Figure 2.6** - Conversions in thermal and catalytic cracking of the polyolefin mixture (feedstock/catalyst = 50, temperature = 400 °C, holding time = 30 min) [95].
- Figure 2.7** - Scheme of plastic waste dehalogenation processes.
- Figure 2.8** - Dechlorination mechanism of aliphatic and aromatic chloro-compounds in presence of metals (adapted from [131]).
- Figure 3.1** - Synthesis method of ZSM-5 zeolites.
- Figure 3.2** - Scheme of the ZSM-5 desilication procedure.
- Figure 3.3** - Schematic diagram of the experimental setup used for the WEEE plastic dehydrochlorination thermal pretreatment.
- Figure 3.4** - Schematic diagram of the experimental setup used for the WEEE plastic thermo-catalytic experiments.
- Figure 3.5** - Picture of wax, oil, char and coke fractions obtained from thermal and thermo-catalytic pyrolysis reactions of WEEE plastic.
- Figure 4.1** - Thermogravimetric analysis of raw plastic. **A)** TG curve in solid line and DTG curve in dashed line. **B)** DSC curve (parameters: Ar flow = 100 ml/min; from R. T. to 850 °C, at 10 °C/min).
- Figure 4.2** - XRD pattern of raw WEEE plastic.

LIST OF FIGURES

- Figure 4.3** - FT-IR spectra of raw A) mixed WEEE plastic and B) isolated particles mainly composed by PVC. Dashed lines are guides for readers: red = PE, green = PVC, blue = HC=O.
- Figure 4.4** - XRD patterns of commercial nanocrystalline ZSM-5.
- Figure 4.5** - A) N₂ adsorption (black lines) and desorption (grey lines) isotherms at 77 K, and B) Pore size distribution, obtained by applying NL-DFT model, of MFI_42 zeolite.
- Figure 4.6** - ²⁷Al ssNMR spectrum of MFI_42 sample.
- Figure 4.7** - A) NH₃-TPD data and deconvolution curves, and B) FT-IR spectrum and deconvolution curves after the absorption of D₃-acetonitrile of MFI_42.
- Figure 4.8** - XRD patterns of synthesized ZSM-5 zeolites with different Si/Al ratio.
- Figure 4.9** - N₂ adsorption (black lines) and desorption (grey lines) isotherms at 77 K of the investigated ZSM-5 zeolites.
- Figure 4.10** - Pore size distribution of the investigated ZSM-5 zeolites determined by applying NL-DFT model.
- Figure 4.11** - SEM images at different magnifications of MFI_11, MFI_25, and MFI_100.
- Figure 4.12** - ²⁷Al ssNMR spectra of synthesized MFI zeolites.
- Figure 4.13** - NH₃-TPD data and deconvolution curves (A-C) and comparison of the three investigated catalysts (D).
- Figure 4.14** - FT-IR spectra after the adsorption of D₃-acetonitrile. Data and deconvolution curves (A-C) and comparison of the three studied samples (D).
- Figure 4.15** - XRD patterns of the parent MFI_25 and hierarchical h-MFI samples.
- Figure 4.16** - N₂ adsorption (black lines) and desorption (grey lines) isotherms at 77 K of the parent MFI_25 and hierarchical h-MFI samples.
- Figure 4.17** - Pore size distribution obtained by applying NL-DFT model.
- Figure 4.18** - SEM images at different magnifications of desilicated h-MFI and the parent zeolite MFI_25.
- Figure 4.19** - ²⁷Al ssNMR spectra of parent MFI_25 and hierarchical h-MFI samples.
- Figure 4.20** - NH₃-TPD data and deconvolution curves (A) and comparison between hierarchical h-MFI and parent MFI_25 samples (B).
- Figure 4.21** - FT-IR spectra after the adsorption of D₃-acetonitrile. Data and deconvolution curves of h-MFI (A) and comparison with the parent catalyst MFI_25 (B).

LIST OF FIGURES

- Figure 4.22** - Thermogravimetric analysis of raw plastic (P_Raw, green) and dechlorinated samples at 300 °C (P_300, red) and 350 °C (P_350, blue). TG in solid line and DTG in dashed line.
- Figure 4.23** - ATR-FTIR spectra of raw WEEE plastic (P_Raw) and dechlorinated samples thermally treated at 300 °C (P_300) and 350 °C (P_350). Dashed lines are guides for readers.
- Figure 4.24** - DSC curves of raw WEEE plastic (P_Raw) and dechlorinated sample P_350.
- Figure 4.25** - FT-IR spectra of raw (P_Raw-particle) and dechlorinated (P_350-particle) isolated particles mainly composed by PVC. Dashed lines are guides for readers.
- Figure 4.26** - Gas yields distribution in dechlorination treatments at 300 °C and 350 °C.
- Figure 4.27** - Products yields distribution in thermal fast-pyrolysis reactions at 550 (T_550), 600 (T_600) and 650 °C (T_650). The wax yield is on secondary axis.
- Figure 4.28** - Gas yields distribution in thermal pyrolysis tests at 550, 600 and 650 °C. Gaseous olefins (GO) and paraffins (GP) are on secondary axis.
- Figure 4.29** - Compounds families distribution of wax fraction in thermal pyrolysis tests at 550, 600 and 650 °C.
- Figure 4.30** - Compounds families by carbon atom number distribution of wax fraction in thermal pyrolysis tests at 550, 600 and 650 °C.
- Figure 4.31** - Chlorine content versus wax (A) and char (B) yields in thermal pyrolysis reactions carried out at 550, 600 and 650 °C.
- Figure 4.32** - Gas yields distribution in thermal and catalytic pyrolysis reactions performed at thermal zone temperature of 600 °C and catalytic temperatures of 400, 450 and 500 °C (cat./feed. = 0.2). Gaseous olefins (GO) and paraffins (GP) are on secondary axis.
- Figure 4.33** - Compounds families in the oil obtained by catalytic pyrolysis at 400, 450 and 500 °C (thermal zone temperature = 600 °C, cat./feed. = 0.2).
- Figure 4.34** - Mono- and poly-aromatics selectivity in oil (Catalytic temperatures = 400, 450 and 500 °C, thermal zone temperature = 600 °C, cat./feed. = 0.2). The total aromatics content is on secondary axis.

LIST OF FIGURES

- Figure 4.35** - Chlorine distribution in catalytic fast-pyrolysis products (catalytic temperature = 400, 450 and 500 °C, thermal zone temperature = 600 °C, cat./feed. = 0.2).
- Figure 4.36** - Gas yields distribution in thermal and catalytic pyrolysis reactions (Temperature 600/450 °C, catalyst/feedstock = 0,2 and 0,4). Gaseous olefins (GO) and paraffins (GP) are on secondary axis.
- Figure 4.37** - Compounds families in the oil obtained by catalytic pyrolysis at 400, 450 and 500 °C (thermal zone temperature = 600 °C, cat./feed. = 0.2).
- Figure 4.38** - Selectivity by carbon atom number in oil and gas fractions generated by the catalytic pyrolysis experiments carried out with catalyst/feedstock = 0.2 and 0.4.
- Figure 4.39** - Aromatics compounds selectivity in oils obtained by using different catalyst/feedstock ratios. The total aromatics content is on secondary axis.
- Figure 4.40** - Chlorine distribution in pyrolysis products obtained by using different catalyst/feedstock ratios.
- Figure 4.41** - Gas yields distribution in catalytic pyrolysis of raw and dechlorinated plastics. (Thermal/catalytic zones temperature = 600/450 °C, catalyst/feedstock = 0.2). Gaseous olefins (GO) and paraffins (GP) on secondary axis.
- Figure 4.42** - Products distribution by compounds families in oil fractions obtained by catalytic pyrolysis of raw and dechlorinated plastics (thermal/catalytic zones temperature = 600/450 °C, cat./feed. = 0.2).
- Figure 4.43** - Aromatics families selectivity in oil fractions obtained by catalytic pyrolysis of raw and dechlorinated plastics.
- Figure 4.44** - Selectivity by carbon atom number in C1 –C 15 range of the oil fractions generated by the catalytic of raw and dechlorinated WEEE plastic.
- Figure 4.45** - (A) Chlorine distribution in pyrolysis products obtained by using raw and dechlorinated plastics as feedstock, and (B) chlorine balance of MFI_42(P_350) calculated on residual chlorine content in dechlorinated plastic.
- Figure 4.46** - Chlorine content in oils obtained from catalytic fast-pyrolysis of raw and dechlorinated plastics.

LIST OF FIGURES

- Figure 4.47** - Yield of catalytic pyrolysis products as a function of the total acidity of the investigated catalysts (Coke yield is on secondary axis).
- Figure 4.48** - Oil yields and B/L ratios as a function of the Si/Al ratios of the studied catalysts.
- Figure 4.49** - Gas yields distribution in thermal and catalytic pyrolysis reactions. Gaseous olefins (GO) and paraffins (GP) are on secondary axis.
- Figure 4.50** - Products distribution by compounds families in oil fractions obtained by catalytic pyrolysis in presence of the investigated catalysts.
- Figure 4.51** - Distribution of hydrocarbons of the gas and oil fractions obtained from the catalytic pyrolysis of dechlorinated WEEE plastic in presence of MFI_25 and MFI_100.
- Figure 4.52** - Compounds families distribution of wax fractions produced in pyrolysis tests carried out in absence (thermal) or in presence of MFI_11 as catalyst.
- Figure 4.53** - Thermal and catalytic pyrolysis of pre-treated WEEE plastic: Cl concentration in the different fractions.
- Figure 4.54** - Gas yields distribution after thermal and catalytic pyrolysis in presence of h-MFI and MFI_25. Gaseous olefins (GO) and paraffins (GP) are shown on secondary axis.
- Figure 4.55** - Products distribution by compounds families in pyrolysis oils after catalytic pyrolysis tests with MFI_25 and h-MFI.
- Figure 4.56** - Aromatic families selectivity in pyrolysis oils obtained from catalytic pyrolysis with MFI_25 and h-MFI. Total aromatics content is on secondary axis.
- Figure 4.57** - Distribution per carbon atom number of the hydrocarbons obtained in pyrolysis tests with MFI_25 and h-MFI zeolites as catalysts.
- Figure 4.58** - Chlorine distribution among pyrolysis products obtained in presence of desilicated and parent zeolites catalysts.
- Figure 4.59** - Cl concentration in the different fractions derived from catalytic pyrolysis of pretreated WEEE plastic in presence of h-MFI and MFI_25 catalysts.

LIST OF TABLES

- Table 1** - Type of pyrolysis processes and target products.
- Table 2** - Classification of zeolites on Si/Al ratio basis [64].
- Table 3** - Typical contaminants in raw MPW and in pyrolysis products at 500 °C [100].
- Table 4** - Proximate and ultimate analysis of the raw waste plastic.
- Table 5** - ICP-OES analysis of ash from raw plastic sample.
- Table 6** - Textural properties of commercial nanocrystalline MFI_42 zeolite.
- Table 7** - Acidic properties of MFI_42 zeolite.
- Table 8** - Textural properties of the ZSM-5 synthesized samples.
- Table 9** - Acidic properties of the synthesized MFI samples.
- Table 10** - Textural properties of hierarchical h-MFI, compared with the parent sample MFI_25.
- Table 11** - Acidic properties of h-MFI catalyst, compared with the parent MFI_25 sample.
- Table 12** - Summary of the main textural and acidic properties of the investigated catalysts.
- Table 13** - Product yields in the thermal dechlorination tests at 300 °C and 350°C.
- Table 14** - Chlorine content and TGA results of dechlorinated samples.
- Table 15** - Proximate and ultimate analyses of raw and dechlorinated sample at 350 °C.
- Table 16** - Products yields distribution (wt.%) in thermal fast-pyrolysis of WEEE plastic as a function of thermal zone temperature.
- Table 17** - Chlorine distribution among products in thermal pyrolysis reactions.
- Table 18** - Textural and acidic properties of commercial nanocrystalline MFI_42 zeolite.
- Table 19** - Products yields distribution (wt.%) in catalytic pyrolysis of WEEE plastic as a function of catalytic temperature.
- Table 20** - Products yields distribution in catalytic pyrolysis of WEEE plastic as a function of the catalyst-to-feedstock ratio.
- Table 21** - Products yields distribution in catalytic fast-pyrolysis of raw and dechlorinated WEEE plastics.
- Table 22** - Main acidic and textural properties of the synthesized ZSM-5 catalysts.
- Table 23** - Product yields after thermal and catalytic pyrolysis of dechlorinated WEEE plastic.

LIST OF TABLES

Table 24 - Cl distribution in the pyrolysis fractions referred to the average Cl content of the pre-treated WEEE plastic waste.

Table 25 - Main textural and acidic properties of h-MFI, compared to the parent MFI_25.

Table 26 - Product yields of pyrolysis of dechlorinated WEEE plastic in absence (Thermal) and in presence of MFI_25 and h-MFI zeolites as catalysts.

REFERENCES

- [1] Directive 2012/19/EU of the European Parliament and of the Council of 4 July 2012 on waste electrical and electronic equipment (WEEE). Current version: 2018.
- [2] V. Forti, C. P. Baldé, R. Kuehr, G. Bel, “The Global E-waste Monitor 2020: Quantities, flows and the circular economy potential.”, United Nations University (UNU)/United Nations Institute for Training and Research (UNITAR) – co-hosted SCYCLE Programme, International Telecommunication Union (ITU) & International Solid Waste Association (ISWA), Bonn/Geneva/Rotterdam.
- [3] “A New Circular Vision for Electronics” report of World Economic Forum (2019).
- [4] Baldé, C. P., Forti, V., Gray, V., Kuehr, R., Stegmann, P., The Global E-waste Monitor 2017, UNU, ITU, ISWA, 2017.
- [5] A. Buekens, J. Yang, “Recycling of WEEE plastics: a review.”, *Journal of Material Cycles and Waste Management*, 16 (2014) 415–434.
- [6] J. Cui, E. Forssberg, “Mechanical recycling of waste electric and electronic equipment: a review.”, *Journal of Hazardous Materials*, 99 (2003) 243-263.
- [7] C. Wang, H. Wang, J. Fu, Y. Liu, “Flotation separation of waste plastics for recycling - A review.”, *Waste Management*, 41 (2015) 28-38.
- [8] X. Yang, L. Sun, J. Xiang, S. Hu, S. Su, “Pyrolysis and dehalogenation of plastics from waste electrical and electronic equipment (WEEE): A review.”, *Waste Management*, 33 (2013) 462–473.
- [9] EERA - European Electronic Recyclers Association, 2020. Figures on the state of play on collection of plastics from WEEE in EU May 2020.
- [10] A. R. Rahimi, J. M. García, “Chemical recycling of waste plastics for new materials production.”, *Nature Reviews Chemistry*, 1 (2017).
- [11] J. Morris, “Recycling versus incineration: an energy conservation analysis.”, *Journal of Hazardous Materials*, 47 (1996) 277-293.

REFERENCES

- [12] G. F. Cardamone, F. Ardolino, U. Arena, "About the environmental sustainability of the European management of WEEE plastics.", *Waste Management*, 126 (2021) 119–132.
- [13] M. Arabiourrutia, G. Elordi, G. Lopez, E. Borsella, J. Bilbao, M. Olazar, "Characterization of the waxes obtained by the pyrolysis of polyolefin plastics in a conical spouted bed reactor.", *Journal of Analytical and Applied Pyrolysis*, 94 (2012) 230–7.
- [14] P. T. Williams, E. A. Williams, "Fluidised Bed Pyrolysis of Low Density Polyethylene to Produce Petrochemical Feedstock.", *Journal of Analytical and Applied Pyrolysis*, 51 (1999) 107–126.
- [15] T. Tsuji, K. Hasegawa, T. Masuda, "Thermal Cracking of Oils from Waste Plastics.", *Journal of Material Cycles and Waste Management*, 5 (2003) 102–106.
- [16] D. A. Wijesekara, P. Sargent, C. J. Ennis, D. Hughes, "Prospects of using chars derived from mixed post waste plastic pyrolysis in civil engineering applications.", *Journal of Cleaner Production*, 317 (2021) 128212 – 128232.
- [17] A) N. Dimitrov, L. K. Krehula, A. P. Sirocic and Z. Hrnjak-Murgic, "Analysis of recycled PET bottles products by pyrolysis-gas chromatography.", *Polymer Degradation and Stability*, 98 (2013) 972-979. B) M. E. Bednas, M. DAY, K. Ho, R. Sander and D. M. Wiles, "Combustion and Pyrolysis of Poly(ethyleneTerephthalate). I. The Role of Flame Retardants on Products of Pyrolysis," *Journal of Applied Polymer Science*, 26 (1981) 277-289.
- [18] J. Yu, L. Sun, C. Ma, Y. Qiao, H. Yao. "Thermal degradation of PVC: A review.", *Waste Management*, 48 (2016) 300-314.
- [19] B. Gui, Y. Qiao, D. Wan, S. Liu, Z. Han, H. Yao, M. Xu, "Nascent tar formation during polyvinylchloride (PVC) pyrolysis.", *Proceedings of the Combustion Institute*, 34 (2013) 2321-2329.
- [20] A. Marongiu, T. Faravelli, G. Bozzano, M. Dente, E. Ranzi, "Thermal degradation of poly(vinyl chloride).", *Journal of Analytical and Applied Pyrolysis*, 70 (2003) 519-553.
- [21] T. P. Wampler, "Thermometric behavior of polyolefins.", *Journal of Analytical and Applied Pyrolysis*, 15 (1989) 187–195.

REFERENCES

- [22] S. M. Al-Salem, A. Antelava, A. Constantinou, G. Manos, A. Dutta, "A review on thermal and catalytic pyrolysis of plastic solid waste (PSW).", *Journal of Environmental Management*, 197 (2017) 177-198.
- [23] P. T. Williams, E. Stanley, "Analysis of products from the pyrolysis and liquefaction of single plastics and waste plastic mixtures.", *Resources, Conservation and Recycling*, 51 (2007) 754-769.
- [24] D. S. Scott, S. R. Czernik, J. Piskorz, D. S. A. G. Radlein, "Fast pyrolysis of plastic wastes.", *Energy Fuel*, 4 (1990) 407-411.
- [25] S. M. Fakhrhoseini, M. Dastanian, "Predicting pyrolysis products of PE, PP, and PET using NRTL activity coefficient model.", *Journal of Chemistry*, (2013) 1-5.
- [26] W. Kaminsky, B. Schlesselmann, C. M. Simon, "Thermal degradation of mixed plastic waste to aromatics and gas.", *Polymer Degradation and Stability*, 53 (1996) 189-197.
- [27] P. J. Donaj, W. Kaminsky, F. Buzeto, W. Yang, "Pyrolysis of polyolefins for increasing the yield of monomers' recovery.", *Waste Management*, 32 (2012) 840-846.
- [28] S. Uçar, S. Karagöz, T. Karayildirim, J. Yanik, "Conversion of polymers to fuels in a refinery stream.", *Polymer Degradation and Stability*, 75 (2002) 161-171.
- [29] N. Miskolczi, L. Bartha, A. Angyal, "Pyrolysis of Polyvinyl Chloride (PVC)-Containing Mixed Plastic Wastes for Recovery of Hydrocarbons.", *Energy & Fuels*, 23 (2009) 2743-2749.
- [30] D. Li, S. Lei, P. Wang, L. Zhong, W. Ma, G. Chen, "Study on the pyrolysis behaviors of mixed waste plastics.", *Renewable Energy*, 173 (2021) 662-674.
- [31] S. D. A. Sharuddin, F. Abnisa, W. M. A. Wan Daud, M. K. Aroua, "A review on pyrolysis of plastic wastes.", *Energy Conversion and Management*, 115 (2016) 308-326.
- [32] J. A. Onwudili, N. Insura, P. T. Williams, "Composition of products from the pyrolysis of polyethylene and polystyrene in a closed batch reactor: effects of temperature and residence time.", *Journal of Analytical and Applied Pyrolysis*, 86 (2009) 293-303.
- [33] A. Demirbas, "Pyrolysis of municipal plastic wastes for recovery of gasoline range hydrocarbons.", *Journal of Analytical and Applied Pyrolysis*, 72 (2004) 97-102.

REFERENCES

- [34] A. Marcilla, J. C. García-Quesada, S. Sánchez, R. Ruiz, “Study of the catalytic pyrolysis behaviour of polyethylene–polypropylene mixtures.”, *Journal of Analytical and Applied Pyrolysis*, 74 (2005) 387–92.
- [35] S. H. Jung, M. H. Cho, B. S. Kang, J. S. Kim, “Pyrolysis of a fraction of waste polypropylene and polyethylene for the recovery of BTX aromatics using a fluidized bed reactor.”, *Fuel Processing Technology*, 91 (2010) 277–284.
- [36] B. L. F. Chin, S. Yusup, A. Al Shoaibi, P. Kannan, C. Srinivasakannan, S. A. Sulaiman, “Kinetic studies of co-pyrolysis of rubber seed shell with high density polyethylene.”, *Energy Conversion and Management*, 87 (2014) 746–53.
- [37] A. Marcilla, M. I. Beltrán, R. Navarro, “Evolution of products during the degradation of polyethylene in a batch reactor.”, *Journal of Analytical and Applied Pyrolysis*, 86 (2009) 14–21.
- [38] A. Marcilla, M. I. Beltrán, R. Navarro, “Thermal and catalytic pyrolysis of polyethylene over HZSM5 and HUSY zeolites in a batch reactor under dynamic conditions.”, *Applied Catalysis B: Environmental*, 86 (2009) 78–86.
- [39] O. Çepelioğullar, A. Pütün. “Utilization of Two Different Types of Plastic Wastes from Daily and Industrial Life.”, *Journal of Selcuk University Natural and Applied Science* (2013) 694-706.
- [40] D. Czajczyńska, L. Anguilano, H. Ghazal, R. Krzyżyńska, A. J. Reynolds, N. Spencer, H. Jouhara, “Potential of pyrolysis processes in the waste management sector.”, *Thermal Science and Engineering Progress*, 3 (2017) 171–197.
- [41] M. L. Mastellone, U. Arena, “Fluidized-bed pyrolysis of polyolefins wastes: Predictive defluidization model.”, *AIChE Journal*, 48 (2002) 1439–1447.
- [42] Y. Sakata, M. A. Uddin, A. Muto, “Degradation of polyethylene and polypropylene into fuel oil by using solid acid and non-solid acid catalysts.”, *Journal of Analytical and Applied Pyrolysis*, 51 (1999) 135–55.
- [43] Y-H. Seo, K-H. Lee, Shin D-H. “Investigation of catalytic degradation of high density polyethylene by hydrocarbon group type analysis.”, *Journal of Analytical and Applied Pyrolysis*, 70 (2003) 383–98.

REFERENCES

- [44] M. del Remedio-Hernández, Á. N. García, A. Marcilla, “Catalytic flash pyrolysis of HDPE in a fluidized bed reactor for recovery of fuel-like hydrocarbons, *Journal of Analytical and Applied Pyrolysis*, 78 (2007) 272–281.
- [45] S. M. Al-Salem, “Thermal pyrolysis of high density polyethylene (HDPE) in a novel fixed bed reactor system for the production of high value gasoline range hydrocarbons (HC)”, *Process Safety and Environmental Protection*, 127 (2019) 171–179.
- [46] F. J. Mastral, E. Esperanza, P. Garcia, M. Juste, “Pyrolysis of high-density polyethylene in a fluidized bed reactor. Influence of the temperature and residence time.”, *Journal of Analytical and Applied Pyrolysis*, 63 (2002) 1–15.
- [47] M. del Remedio-Hernández, A. N. García, A. Gómez, J. Agulló, A. Marcilla, “Effect of residence time on volatile products obtained in the HDPE pyrolysis in the presence and absence of HZSM-5.”, *Industrial and Engineering Chemistry Research*, 45, (2006) 8770-8778.
- [48] F. J. Mastral, E. Esperanza, C. Berruero, M. Juste, J. Ceamanos, “Fluidized bed thermal degradation products of HDPE in an inert atmosphere and in air–nitrogen mixtures. *Journal of Analytical and Applied Pyrolysis*, 70 (2003) 1–17.
- [49] R. Miandad, M. A. Barakat, A. S. Aburiazaiza, M. Rehan, A. S. Nizami, “Catalytic pyrolysis of plastic waste: A review.”, *Process Safety and Environmental Protection*, 102 (2016) 822-838.
- [50] S. R. Ivanova, E. F. Gumerova, K. S. Minsker, G. E. Zalkov, A. A. Berlin, “Selective catalytic degradation of polyolefins.”, *Progress in Polymer Science*, 15 (1990) 193-215.
- [51] A. A. Garforth, Y. H. Lin, P. N. Sharratt, J. Dwyer, “Production of hydrocarbons by catalytic degradation of high density polyethylene in a laboratory fluidised-bed reactor.”, *Applied Catalysis A: General*, 169 (1998) 331–342.
- [52] J. Aguado, D. P. Serrano, M. D. Romero, J. M. Escola, “Catalytic conversion of polyethylene into fuels over mesoporous MCM-41.”, *Chemical Communications* (1996) 725–726.
- [53] M. Artetxe, G. Lopez, M. Amutio, G. Elordi, J. Bilbao, M. Olazar, “Light olefins from HDPE cracking in a two-step thermal and catalytic process.”, *Chemical Engineering Journal*, 207–208 (2012) 27–34.

REFERENCES

- [54] R. Bagri, P. T. Williams, "Catalytic pyrolysis of polyethylene.", *Journal of Analytical and Applied Pyrolysis*, 63 (2002) 29-41.
- [55] J. Aguado, D. P. Serrano, G. San Miguel, M. C. Castro, S. Madrid, "Feedstock recycling of polyethylene in a two-step thermo-catalytic reaction system.", *Journal of Analytical and Applied Pyrolysis*, 79 (2007) 415–423.
- [56] A. Lopez, I. D. Marco, B. M. Caballero, M. F. Laresgoiti, A. Adrados, A. Aranzabal, "Catalytic pyrolysis of plastic wastes with two different types of catalytic: ZSM-5 zeolite and Red Mud.", *Applied Catalysis B: Environmental*, 104 (2011) 211–219.
- [57] D. Chen, L. Yin, H. Wang, P. He, "Pyrolysis technologies for municipal solid waste: a review.", *Waste Management*, 34 (2014) 2466-2486.
- [58] M. Syamsiro, H. Saptoadi, T. Norsujianto, Noviasri, S. Cheng, Z. Alimuddin, K. Yoshikawa, "Fuel oil production from Municipal plastic wastes in sequential pyrolysis and catalytic reforming reactors.", *Energy Procedia*, 47 (2014) 180-188.
- [59] J. Scheirs, W. Kaminsky Ed., "Feedstock Recycling and Pyrolysis of Waste Plastics: Converting Waste Plastics into Diesel and Other Fuels." (2006).
- [60] D. P. Serrano, J. Aguado, J. M. Escola, "Developing advanced catalysts for the conversion of polyolefinic waste plastics into fuels and chemicals.", *ACS Catalysis*, 2 (2012) 1924–1941.
- [61] C. Santella, L. Cafiero, D. De Angelis, F. La Marca, R. Tuffi, S. Vecchio Cipriotti, "Thermal and catalytic pyrolysis of a mixture of plastics from small waste electrical and electronic equipment (WEEE).", *Waste Management*, 54 (2016) 143–152.
- [62] J. B. Nagy, P. Bodart, I. Hannus, I. Kiricsi, *Synthesis, characterization and use of zeolitic microporous material*, DecaGEN ed., 1998, ISBN 9630497506.
- [63] M. Moshoeshoe, M. S. Nadiye-Tabbiruka, V. Obuseng, "A Review of the Chemistry, Structure, Properties and Applications of Zeolites.", *American Journal of Materials Science*, 7 (2017) 196-221.
- [64] International Zeolite Association. <http://www.iza-online.org>
- [65] B. Jha, D. N. Singh, *Fly Ash Zeolites*, *Advanced Structured Materials* 78. Springer, 2016.
- [66] E. M. Flanigen, "Molecular sieve zeolite technology - the first twenty-five years.", *Pure and Applied Chemistry*, 52 (1980) 2191 – 2211.

REFERENCES

- [67] B. Jha, D. N. Singh, "A review on synthesis, characterization and industrial application of fly ash zeolites.", *Journal of Materials Education*, 33 (2011) 65 - 132.
- [68] R. Ch. Deka, R. K. Roy, K. Hirao, "Basicity of the framework oxygen atom of alkali and alkaline earth-exchanged zeolites: a hard–soft acid–base approach." *Chemical Physics Letters*, 332 (2000) 576 – 582.
- [69] G. Busca, "Acidity and basicity of zeolites: A fundamental approach.", *Microporous and Mesoporous Materials*, 254 (2017) 3-16.
- [70] T. W. Cynthia, Ch. D. Chang, Cl. D. Chang, "Isomorphous substitution in zeolite frameworks. 1. Acidity of surface hydroxyls in [B]-, [Fe]-, [Ga]-, and [Al]-ZSM-5", *The Journal of Physical Chemistry*, 89 (1985) 1569–1571.
- [71] A. Corma, H. Garcia, "Lewis Acids as Catalysts in Oxidation Reactions: From Homogeneous to Heterogeneous Systems.", *Chemical Reviews*, 102 (2002), p. 3837-3892.
- [72] T. Chen, A. Men, P. Sun, J. Zhou, Z. Yuan, A. Guo, J. Wang, D. Ding, H. Li, "Lewis acid sites on dehydroxylated zeolite HZSM-5 studied by NMR and EPR.", *Catalysis Today*, 30 (1996) 189-192.
- [73] M. Elanany, M. Koyama, M. Kubo, E. Broclawik, A. Miyamoto, "Periodic density functional investigation of Lewis acid sites in zeolites: relative strength order as revealed from NH₃ adsorption.", *Applied Surface Science*, 246 (2005) 96-101.
- [74] G. L. Woolery, G. H. Kuehl, H. C. Timken, A. W. Chester, J. C. Vartuli, "On the nature of framework Brønsted and Lewis acid sites in ZSM-5.", *Zeolites*, 19 (1997) 288-296.
- [75] J. Xiao, J. Wei, "Diffusion mechanism of hydrocarbons in zeolites.", *Chemical Engineering Science*, 47 (1992) 1123-1141.
- [76] F. Di Renzo, "Zeolites as tailor-made catalysts: Control of the crystal size.", *Catalysis Today*, 41 (1998) 37-40.
- [77] M. Hartmann, "Hierarchical Zeolites: A Proven Strategy to Combine Shape Selectivity with Efficient Mass Transport.", *Angewandte Chemie International Edition*, 43 (2004) 5880-5882.
- [78] J. Pérez-Ramírez, C. H. Christensen, K. Egablad, C. H. Christensen, J. C. Groen, "Hierarchical zeolites: enhanced utilisation of microporous crystals in catalysis by advances in materials design.", *Chemical Society Reviews*, 37 (2008) 2530 – 2542.

REFERENCES

- [79] B. W. Wojciechowski, "Dichotomies in Catalytic Cracking.", *Industrial & Engineering Chemistry Research*, 36 (1997) 3323-3335.
- [80] A. Corma, "Inorganic Solid Acids and Their Use in Acid-Catalyzed Hydrocarbon Reactions.", *Chemical Reviews*, 95 (1995) 559-614.
- [81] G. Elordi, M. Olazar, G. Lopez, P. Castaño, J. Bilbao, "Role of pore structure in the deactivation of zeolites (HZSM-5, H β and HY) by coke in the pyrolysis of polyethylene in a conical spouted bed reactor.", *Applied Catalysis B: Environmental*, 102 (2011) 224–231.
- [82] M. Ibáñez, M. Artetxe, G. Lopez, G. Elordi, J. Bilbao, M. Olazar, P. Castaño, "Identification of the coke deposited on an HZSM-5 zeolite catalyst during the sequenced pyrolysis-cracking of HDPE.", *Applied Catalysis B: Environmental*, 148–149 (2014) 436–445.
- [83] D. P. Serrano, J. Aguado, J.M. Rodríguez, A. Peral, "Catalytic cracking of polyethylene over nanocrystalline HZSM-5: Catalyst deactivation and regeneration study.", *Journal of Analytical and Applied Pyrolysis*, 79 (2007) 456–464.
- [84] P. Castaño, G. Elordi, M. Ibáñez, M. Olazar, J. Bilbao, "Pathways of coke formation on an MFI catalyst during the cracking of waste polyolefins.", *Catalysis Science and Technology*, 2 (2012) 504–508.
- [85] G. Elordi, M. Olazar, P. Castaño, M. Artetxe, J. Bilbao, "Polyethylene cracking on a spent FCC catalyst in a conical spouted bed.", *Industrial & Engineering Chemistry Research*, 51 (2012) 14008–14017.
- [86] G. Manos, A. Garforth, J. Dwyer, "Catalytic degradation of high-density polyethylene over different zeolitic structures.", *Industrial & Engineering Chemistry Research*, 39 (2000) 1198–1202.
- [87] J. Aguado, J. L. Sotelo, D. P. Serrano, J. A. Calles, and J. M. Escola, "Catalytic conversion of polyolefins into liquid fuels over MCM-41: comparison with ZSM-5 and amorphous SiO₂–Al₂O₃.", *Energy Fuels*, 11 (1997) 1225.
- [88] M. Artetxe, G. Lopez, M. Amutio, G. Elordi, J. Bilbao, M. Olazar, "Cracking of high density polyethylene pyrolysis waxes on HZSM-5 catalysts of different acidity.", *Industrial and Engineering Chemistry Research*, 52 (2013) 10637–10645.

REFERENCES

- [89] A. K. Panda, R. K. Singh, D. K. Mishra, "Thermolysis of waste plastics to liquid fuel: A suitable method for plastic waste management and manufacture of value added products - A world prospective.", *Renewable and Sustainable Energy Reviews*, 14 (2010) 233–248.
- [90] R. van Grieken, D. P. Serrano, J. Aguado, R. García, C. Rojo, "Thermal and catalytic cracking of polyethylene under mild conditions.", *Journal of Analytical and Applied Pyrolysis*, 58–59 (2001) 127-142.
- [91] J. F. Mastral, C. Berrueco, M. Gea, J. Ceamanos, "Catalytic degradation of high density polyethylene over nanocrystalline HZSM-5 zeolite.", *Polymer Degradation and Stability*, 91 (2006) 3330-3338.
- [92] M. del Remedio-Hernández, A. Gómez, Á. N. García, J. Agulló, A. Marcilla, "Effect of the temperature in the nature and extension of the primary and secondary reactions in the thermal and HZSM-5 catalytic pyrolysis of HDPE.", *Applied Catalysis A: General*, 317 (2007) 183-194.
- [93] A. A. Garfoth, Y. H. Lin, P. N. Sharratt, J. Dwyer, "Production of hydrocarbons by catalytic degradation of high density polyethylene in a laboratory fluidized bed reactor.", *Applied Catalysis A: General*, 169 (1998) 331–42.
- [94] Y. H. Lin, H. Y. Yen, "Fluidised bed pyrolysis of polypropylene over cracking catalysts for producing hydrocarbons.", *Polymer Degradation and Stability*, 89 (2005) 101–8.
- [95] D. P. Serrano, J. Aguado, and J. M. Escola, "Catalytic cracking of a polyolefin mixture over different acid solid catalysts.", *Industrial & Engineering Chemistry Research*, 39 (2000) 1177-1184.
- [96] D. P. Serrano, J. Aguado, J. M. Escola, and J. M. Rodríguez, "Nanocrystalline ZSM-5: a highly active catalyst for polyolefin feedstock recycling.", *Studies in Surface Science and Catalysis*, 142 (2002) 77-84.
- [97] Y. H. Lin, M. H. Yang, "Catalytic reactions of post-consumer polymer waste over fluidised cracking catalysts for producing hydrocarbons.", *Journal of Molecular Catalysis A: Chemical*, 231 (2005) 113-122.
- [98] A. Angyal, N. Miskolczi, L. Bartha, I. Valkai, "Catalytic cracking of polyethylene waste in horizontal tube reactor.", *Polymer Degradation and Stability*, 94 (2009) 1678-1683.

REFERENCES

- [99] N. Miskolczi, A. Angyal, L. Bartha, I. Valkai, “Fuels by pyrolysis of waste plastics from agricultural and packaging sectors in a pilot scale reactor.”, *Fuel Processing Technology*, 90 (2009) 1032-1040.
- [100] N. Miskolczi, F. Ateş, N. Borsodi, “Comparison of real waste (MSW and MPW) pyrolysis in batch reactor over different catalysts. Part II: Contaminants, char and pyrolysis oil properties.”, *Bioresource Technology*, 144 (2013) 370-379.
- [101] Conference of the Parties to the Stockholm. Convention on Persistent Organic Pollutants. Item 5 (b), (2015).
- [102] Y. Shen, R. Zhao, J. Wang, X. Chen, X. Ge, M. Chen, “Waste-to-energy: Dehalogenation of plastic-containing wastes.”, *Waste Management*, 49 (2016) 287–303.
- [103] J. Aguado, D. P. Serrano, J. M. Escola, “Fuels from waste plastics by thermal and catalytic processes: A review.”, *Industrial & Engineering Chemistry Research*. 47 (2008) 7982–7992.
- [104] A. Castro, C. Vilarinho, D. Soares, F. Castro, “Kinetic study of thermal de-chlorination of PVC-containing waste.”, *Materials Science Forum*, 730–732 (2013) 611–616.
- [105] H. Bockhorn, J. Hentschel, A. Hornung, U. Hornung, “Environmental engineering: Stepwise pyrolysis of plastic waste.”, *Chemical Engineering Science*, 54 (1999) 3043–3051.
- [106] H. Bockhorn, A. Hornung, U. Hornung, P. Jakobströer, M. Kraus, “Dehydrochlorination of plastic mixtures.”, *Journal of Analytical and Applied Pyrolysis*, 49 (1999) 97–106.
- [107] S. Ma, J. Lu, J. Gao, “Study of the low temperature pyrolysis of PVC.”, *Energy and Fuels*, 16 (2002) 338–342.
- [108] A. López, I. De Marco, B. M. Caballero, M. F. Laresgoiti, A. Adrados, “Dechlorination of fuels in pyrolysis of PVC containing plastic wastes.”, *Fuel Processing Technology*, 92 (2011) 253–260.
- [109] G. Yuan, D. Chen, L. Yin, Z. Wang, L. Zhao, J. Y. Wang, “High efficiency chlorine removal from polyvinyl chloride (PVC) pyrolysis with a gas-liquid fluidized bed reactor.”, *Waste Management*, 34 (2014) 1045–1050.
- [110] J. Lei, G. Yuan, P. Weerachanchai, S. W. Lee, K. Li, J. Y. Wang, Y. Yang, “Investigation on thermal dechlorination and catalytic pyrolysis in a continuous process

REFERENCES

- for liquid fuel recovery from mixed plastic wastes.”, *Journal of Material Cycles and Waste Management*, 20 (2018) 137–146.
- [111] D. Perondi, D. Restelatto, C. Manera, M. Godinho, A. J. Zattera, A. C. Faria Vilela, “The role of CaO and its influence on chlorine during the thermochemical conversion of shredder residue.”, *Process Safety and Environmental Protection*, 122 (2019) 58–67.
- [112] B. Fekhar, L. Gombor, N. Miskolczi, “Pyrolysis of chlorine contaminated municipal plastic waste: In-situ upgrading of pyrolysis oils by Ni/ZSM-5, Ni/SAPO-11, red mud and Ca(OH)₂ containing catalysts.”, *Journal of the Energy Institute*, 92 (2019) 1270–1283.
- [113] B. Fekhar, V. Zsinka, N. Miskolczi, “Value added hydrocarbons obtained by pyrolysis of contaminated waste plastics in horizontal tubular reactor: In situ upgrading of the products by chlorine capture.”, *Journal of Cleaner Production*, 241 (2019) 118166–118176.
- [114] D. Torres, Y. Jiang, D. A. Sanchez-Monsalve, G. A. Leeke, “Hydrochloric acid removal from the thermogravimetric pyrolysis of PVC.”, *Journal of Analytical and Applied Pyrolysis*, 149 (2020) 104831–104841.
- [115] J. Yanik, M.A. Uddin, K. Ikeuchi, Y. Sakata, “The catalytic effect of Red Mud on the degradation of poly (vinyl chloride) containing polymer mixture into fuel oil.”, *Polymer Degradation and Stability*, 73 (2001) 335–346.
- [116] C. Tang, Y. Z. Wang, Q. Zhou, L. Zheng, “Catalytic effect of Al-Zn composite catalyst on the degradation of PVC-containing polymer mixtures into pyrolysis oil.”, *Polymer Degradation and Stability*, 81 (2003) 89–94.
- [117] C. Ma, J. Yu, B. Wang, Z. Song, J. Xiang, S. Hu, S. Su, L. Sun, “Chemical recycling of brominated flame retarded plastics from e-waste for clean fuels production: A review.”, *Renewable & Sustainable Energy Reviews*, 61 (2016) 433–450.
- [118] M. Blazsó, Z. Czégény, “Catalytic destruction of brominated aromatic compounds studied in a catalyst microbed coupled to gas chromatography/mass spectrometry.”, *Journal of Chromatography A*, 1130 (2006) 91–96.
- [119] H. Wu, Y. Shen, N. Harada, Q. An, K. Yoshikawa, “Production of pyrolysis oil with low bromine and antimony contents from plastic material containing brominated flame

REFERENCES

- retardants and antimony trioxide.”, *Energy and Environment Research*, 4 (2014), 105-118.
- [120] C. Ma, J. Yu, Q. Yan, Z. Song, K. Wang, B. Wang, L. Sun, “Pyrolysis-catalytic upgrading of brominated high impact polystyrene over Fe and Ni modified catalysts: Influence of HZSM-5 and MCM-41 catalysts.”, *Polymer Degradation and Stability*, 146 (2017) 1-12.
- [121] C. Ma, T. Kamo, “Two-stage catalytic pyrolysis and debromination of printed circuit boards: Effect of zero-valent Fe and Ni metals.”, *Journal of Analytical and Applied Pyrolysis*, 134 (2018) 614–620.
- [122] M. Brebu, T. Bhaskar, K. Murai, A. Muto, Y. Sakata., Md. A. Uddin, Removal of nitrogen, bromine, and chlorine from PP/PE/PS/PVC/ABS-Br pyrolysis liquid products using Fe- and Ca-based catalysts, *Polymer Degradation and Stability*, 87 (2005) 225-230.
- [123] T. Chen, J. Yu, C. Ma, K. Bikane, L. Sun, “Catalytic performance and debromination of Fe-Ni bimetallic MCM-41 catalyst for the two-stage pyrolysis of waste computer casing plastic.”, *Chemosphere*, 248 (2020) 125964-125975.
- [124] S. H. Jung, S. J. Kim, J. S. Kim, “Fast pyrolysis of a waste fraction of high impact polystyrene (HIPS) containing brominated flame retardants in a fluidized bed reactor: The effects of various Ca-based additives (CaO, Ca(OH)₂ and oyster shells) on the removal of bromine.”, *Fuel*, 95 (2012) 514–520.
- [125] R. Gao, B. Liu, L. Zhan, J. Guo, J. Zhang, Z. Xu, “In-situ debromination mechanism based on self-activation and catalysis of Ca(OH)₂ during pyrolysis of waste printed circuit boards.”, *Journal of Hazardous Materials*, 392 (2020).
- [126] N. Miskolczi, F. Buyong, A. Angyal, P.T. Williams, L. Bartha, “Two stages catalytic pyrolysis of refuse derived fuel: Production of biofuel via syncrude.”, *Bioresource Technology*, 101 (2010) 8881–8890.
- [127] N. Zhang, R. Li, G. Zhang, L. Dong, D. Zhang, G. Wang, T. Li, “Zn-Modified H β zeolites used in the adsorptive removal of organic chloride from model naphtha.”, *ACS Omega* 5 (2020) 11987–11997.

REFERENCES

- [128] N. Lingaiah, Md. A. Uddin, A. Muto, T. Imai, Y. Sakata, "Removal of organic chlorine compounds by catalytic dehydrochlorination for the refinement of municipal waste plastic derived oil.", *Fuel*, 80 (2001) 1901-1905.
- [129] N. Lingaiah, Md. A. Uddin, A. Muto, Y. Sakata, T. Imai, K. Murata, "Catalytic dechlorination of chloroorganic compounds from PVC-containing mixed plastic-derived oil.", *Applied Catalysis A: General*, 207 (2001) 79–84.
- [130] A. Lopez-Urionabarrenechea, I. deMarco, B. M. Caballero, M. F. Laresgoiti, A. Adrados, "Upgrading of chlorinated oils coming from pyrolysis of plastic waste.", *Fuel Processing Technology*, 137 (2015) 229–239.
- [131] G. Jiang, D. A. Sanchez Monsalve, P. Clough, Y. Jiang, G. A. Leeke, "Understanding the dechlorination of chlorinated hydrocarbons in the pyrolysis of mixed plastics.", *ACS Sustainable Chemistry & Engineering*, 9 (2021) 1576–1589.
- [132] M. Migliori, A. Aloise, G. Giordano, "Methanol to dimethylether on H-MFI catalyst: The influence of the Si/Al ratio on kinetic parameters.", *Catalysis Today*, 227 (2014) 138–143.
- [133] A. Aloise, A. Marino, F. Dalena, G. Giorgianni, M. Migliori, L. Frusteri, C. Cannilla, G. Bonura, F. Frusteri, G. Giordano, "Desilicated ZSM-5 zeolite: Catalytic performances assessment in methanol to DME dehydration.", *Microporous and Mesoporous Materials* 302 (2020) 110198-110205.
- [134] C. G. Pope, "X-Ray Diffraction and the Bragg Equation.", *Journal of Chemical Education*, 74 (1997) 129 – 131.
- [135] J. Rouquerol, P. Llewellyn, F. Rouquerol, "Is the BET equation applicable to microporous adsorbents?", *Studies in Surface Science and Catalysis*, 160 (2007) 49–56,
- [136] M. Thommes, K. Kaneko, A.V. Neimark, J.P. Olivier, F. Rodriguez-Reinoso, J. Rouquerol, K.S.W. Sing, "Physisorption of gases, with special reference to the evaluation of surface area and pore size distribution" (IUPAC Technical Report), *Pure and Applied Chemistry*, 87 (2015).
- [137] M. Jaroniec, M. Kruk, J.P. Olivier, S. Koch, "A new method for the accurate pore size analysis of MCM-41 and other silica based mesoporous materials", *Studies in Surface Science and Catalysis*, 128 (2000) 71–80.

REFERENCES

- [138] M. Trombetta, A. Gutiérrez Alejandro, J. Ramirez Solis, G. Busca, “An FT-IR study of the reactivity of hydrocarbons on the acid sites of HZSM5 zeolite.”, *Appl. Catal. Gen.* 198 (2000) 81–93.
- [139] T. Montanari, M. Bevilacqua, G. Busca, “Use of nitriles as probe molecules for the accessibility of the active sites and the detection of complex interactions in zeolites through IR spectroscopy.”, *Appl. Catal. Gen.* 307 (2006) 21–29.
- [140] M. Hunger, “Catalytically Active Sites: Generation and Characterization”, 2010.
- [141] S. A. Channiwala, P. P. Parikh, “A unified correlation for estimating HHV of solid, liquid and gaseous fuels.”, *Fuel*, 81 (2002) 1051-1063.
- [142] J. Yang, R. Miranda, C. Roy, “Using the DTG curve fitting method to determine the apparent kinetic parameters of thermal decomposition of polymers.”, *Polymer Degradation and Stability*, 73 (2001) 455–461.
- [143] J. Pan, H. Jiang, T. Qing, J. Zhang, K. Tian, “Transformation and kinetics of chlorine-containing products during pyrolysis of plastic wastes.”, *Chemosphere*, 284 (2021) 131348.
- [144] A. Torikai, H. Hasegawa, “Accelerated photodegradation of poly(vinyl chloride).”, *Polymer Degradation and Stability*, 63 (1999) 441–445.
- [145] J. L. Gardette, S. Gaumet, J. Lemaire, “Photooxidation of Poly (vinyl chloride). 1. A Reexamination of the Mechanism.”, *Macromolecules*, 22 (1989) 2576–2581.
- [146] A. A. Alsaygh, J. Al-hamidi, F. D. Alsewailem, I. M. Al-Najjar, V. L. Kuznetsov, “Characterization of polyethylene synthesized by zirconium single site catalysts.”, *Applied Petrochemical Research*, 4 (2014) 79–84.
- [147] F. Z. Benabid, N. Kharchi, F. Zouai, A. H. I. Mourad, D. Benachour, “Impact of co-mixing technique and surface modification of ZnO nanoparticles using stearic acid on their dispersion into HDPE to produce HDPE/ZnO nanocomposites.”, *Polymers and Polymer Composites*, 27 (2019) 389–399.
- [148] B. Papajani, E. Vataj, A. V. Hasımı, A. Sinanaj, “The study of the influence of additives in the crystallinity of recycled LDPE by IR and XRD analysis.”, *RAD Conference Proceedings* 3 (2019) 236–240.
- [149] A) S. T. Bee, W. R. Mok, T. S. Lee, T. T. Tee, G. Issabayeva, A. R. Rahmat. “Evaluation performance of multiple plasticizer systems on the physicomechanical,

REFERENCES

- crystallinity and thermogravimetry of polyvinyl chloride.”, *Journal of Polymer Engineering*, 34 (2014) 521–529. B) S. Rajendran, T. Uma, “Experimental investigations on PVC–LiAsF₆–DBP polymer electrolyte systems.”, *Journal of Power Sources*, 87 (2000) 218–222.
- [150] B. Yu, X. Xu, “Conductive properties and mechanism of polyvinyl chloride doped by a multi-walled carbon nanotube-polypyrrole nano-complex dopant”, *RSC Advances*, 4 (2014) 3966–3973.
- [151] S. S. Suresh, S. Mohanty, S. K. Nayak, “Composition analysis and characterization of waste polyvinyl chloride (PVC) recovered from data cables.”, *Waste Management*, 60 (2017) 100–111.
- [152] M. Beltran, A. Marcilla, “Fourier Transform Infrared Spectroscopy Applied to the Study of Unicellular Models.”, *European Polymer Journal*, 33 (1997) 1135–1142.
- [153] A. Ul-Hamid, K. Y. Soufi, L. M. Al-Hadhrami, A. M. Shemsi, “Failure investigation of an underground low voltage XLPE insulated cable.”, *Anti-Corrosion Methods and Materials*, 62 (2015) 281–287.
- [154] Y. Zhang, Y. Xu, Y. Song, Q. Zheng, “Study of poly(vinyl chloride)/acrylonitrile-styrene-acrylate blends for compatibility, toughness, thermal stability and UV irradiation resistance.”, *Journal of Applied Polymer Science*, 130 (2013) 2143–2151.
- [155] K. Aouachria, N. Belhaneche-Bensemra, “Miscibility of PVC/PMMA blends by vicat softening temperature, viscometry, DSC and FTIR analysis.”, *Polymer Testing*, 25 (2006) 1101–1108.
- [156] S. Gutiérrez-Rubio, M. Shamzhy, J. Čejka, D. P. Serrano, I. Moreno, J. M. Coronado, “Vapor phase acylation of guaiacol with acetic acid over micro, nano and hierarchical MFI and BEA zeolites.”, *Applied Catalysis B: Environmental*, 285 (2021) 119826.
- [157] R. Ch. Deka, “Acidity in zeolites and their characterization by different spectroscopic methods.”, *Indian Journal of Chemical Technology*, 5 (1998) 109–123.
- [158] A. Vimont, F. Thibault-Starzyk, M. Daturi, “Analysing and understanding the active site by IR spectroscopy.”, *Chemical Society Reviews*, 39 (2010) 4928–4950.
- [159] G. Busca, “The surface acidity of solid oxides and its characterization by IR spectroscopic methods. An attempt at systematization.”, *Physical Chemistry Chemical Physics*, 1 (1999) 723–736.

REFERENCES

- [160] P. Lanzafame, G. Papanikolaou, S. Perathoner, G. Centi, G. Giordano, M. Migliori, “Weakly acidic zeolites: A review on uses and relationship between nature of the active sites and catalytic behaviour.”, *Microporous and Mesoporous Materials* 300 (2020) 110157.
- [161] A. Petushkov, "Synthesis and characterization of nanocrystalline and mesoporous zeolites.", PhD (Doctor of Philosophy) thesis, University of Iowa, 2011.
- [162] L. Rodríguez-González, F. Hermes, M. Bertmer, E. Rodríguez-Castellón, A. Jiménez-López, U. Simon. “The acid properties of H-ZSM-5 as studied by NH₃-TPD and 27Al-MAS-NMR spectroscopy.”, *Applied Catalysis A*, 328 (2007) 174-182.
- [163] K. S. Triantafyllidis, L. Nalbandian, P. N. Trikalitis, A. K. Ladavos, T. Mavromoustakos, C. P. Nicolaides. “Structural, compositional and acidic characteristics of nanosized amorphous or partially crystalline ZSM-5 zeolite-based materials.”, *Microporous and Mesoporous Materials*, 75 (2004) 89-100.
- [164] S. Li, A. Zheng, Y. Su, H. Zhang, L. Chen, J. Yang, C. Ye, F. Deng, “Brønsted/Lewis Acid Synergy in Dealuminated HY Zeolite: A Combined Solid-State NMR and Theoretical Calculation Study.”, *Journal of the American Chemical Society*., 129 (2007) 11161 – 11171.
- [165] D. P. Serrano, R. A. García, G. Vicente, M. Linares, D. Procházková, J. Čejka. “Acidic and catalytic properties of hierarchical zeolites and hybrid ordered mesoporous materials assembled from MFI protozeolitic units.”, *Journal of Catalysis*, 279 (2011) 366-380.
- [166] J. C. Groen, L. A. A. Peffer, J. A. Moulijn, J. Pérez-Ramírez, “Mechanism of hierarchical porosity development in MFI zeolites by desilication: The role of aluminium as a pore-directing agent.”, *Chemistry – A European Journal*, 11 (2005) 4983–4994.
- [167] C. H. Wu, C. Y. Chang, J. L. Hor, S. M. Shih, L. W. Chen, F. W. Chang. “Two-Stage pyrolysis model of PVC.”, *Canadian Journal of Chemical Engineering*, 72 (1994) 644–650.
- [168] R. Bacaloglu, M. Fisch. “Degradation and stabilization of poly(vinyl chloride). V. Reaction mechanism of poly(vinyl chloride) degradation.”, *Polymer Degradation and Stability*, 47 (1995) 33–57.

REFERENCES

- [169] R. Knumann, H. Bockhorn. "Investigation of the Kinetics of Pyrolysis of PVC by TG-MS-Analysis.", *Combustion Science and Technology*, 101 (1994) 285-299.
- [170] I. C. McNeill, L. Memetea, W. J. Cole, "A study of the products of PVC thermal degradation.", *Polymer Degradation and Stability*, 49 (1995) 181–191.
- [171] P. Das, P. Tiwari, "The effect of slow pyrolysis on the conversion of packaging waste plastics (PE and PP) into fuel.", *Waste Management* 79 (2018) 615-624.
- [172] R. K. Singh, B. Ruj, A. K. Sadhukhan, P. Gupta, "Impact of fast and slow pyrolysis on the degradation of mixed plastic waste: Product yield analysis and their characterization.", *Journal of the Energy Institute*, 92 (2019) 1647-1657.
- [173] S. M. Al-Salem, P. Lettieri, "Kinetic study of high density polyethylene (HDPE) pyrolysis.", *Chemical Engineering Research and Design*, 88 (2010) 1599-1606.
- [174] L. Ye, T. Li, L. Hong, "Understanding enhanced char formation in the thermal decomposition of PVC resin: Role of intermolecular chlorine loss.", *Materials Today Communications*, 26 (2021) 102186.
- [175] X. Zhou, L. J. Broadbelt, R. Vinu, "Mechanistic Understanding of Thermochemical Conversion of Polymers and Lignocellulosic Biomass.", *Advances in Chemical Engineering*, 49 (2016) 95–198.
- [176] J. A. Onwudili, C. Muhammad, P. T. Williams, "Influence of catalyst bed temperature and properties of zeolite catalysts on pyrolysis-catalysis of a simulated mixed plastics sample for the production of upgraded fuels and chemicals.", *Journal of the Energy Institute*, 92 (2019) 1337-1347.
- [177] Z. Chen, X. Zhang, L. Che, H. Peng, S. Zhu, F. Yang, X. Zhang, "Effect of volatile reactions on oil production and composition in thermal and catalytic pyrolysis of polyethylene.", *Fuel*, 271 (2020) 117308.
- [178] K. Takuma, Y. Uemichi, A. Ayame, "Product distribution from catalytic degradation of polyethylene over H-gallosilicate.", *Applied Catalysis A*, 192 (2000) 273-280.
- [179] T. C. Hoff, R. Thilakaratne, D. W. Gardner, R. C. Brown, J-P. Tessonnier, "Thermal Stability of Aluminum-Rich ZSM-5 Zeolites and Consequences on Aromatization Reactions.", *The Journal of Physical Chemistry C*, 120 (2016) 20103–20113.
- [180] A. Marcilla, A. Gómez-Siurana, F. J. Valdés, "Influence of the temperature on the composition of the coke obtained in the catalytic cracking of low density polyethylene

REFERENCES

- in the presence of USY and HZSM-5 zeolites.”, *Microporous and Mesoporous Materials*, 109 (2008) 420-428.
- [181] J. Aguado, D. P. Serrano, J. L. Sotelo, R. Van Grieken, J. M. Escola, “Influence of the operating variables on the catalytic conversion of a polyolefin mixture over HMCM-41 and nanosized HZSM-5.”, *Industrial & Engineering Chemistry Research*, 40 (2001) 5696.
- [182] A. Lopez-Uriónabarrenechea, I. de Marco, B. M. Caballero, M. F. Laresgoiti, A. Adrados, “Catalytic stepwise pyrolysis of packaging plastic waste.”, *Journal of Analytical and Applied Pyrolysis*, 96 (2012) 54–62.
- [183] V. Daligaux, R. Richard, M.-H. Manero, “Deactivation and Regeneration of Zeolite Catalysts Used in Pyrolysis of Plastic Wastes—A Process and Analytical Review.”, *Catalysts*, 11 (2021) 770.
- [184] A. Coelho, L. Costa, M. M. Marques, I. M. Fonseca, M.A.N.D.A. Lemos, F. Lemos, “The effect of ZSM-5 zeolite acidity on the catalytic degradation of high-density polyethylene using simultaneous DSC/TG analysis.”, *Applied Catalysis A: General*, 413–414 (2012) 183-191.

La borsa di dottorato è stata cofinanziata con risorse del
Programma Operativo Nazionale Ricerca e Innovazione 2014-2020 (CCI 2014IT16M2OP005),
Fondo Sociale Europeo, Azione I.1 "Dottorati Innovativi con caratterizzazione Industriale"



UNIONE EUROPEA
Fondo Sociale Europeo



*Ministero dell'Istruzione,
dell'Università e della Ricerca*



PON
RICERCA
E INNOVAZIONE
2014 - 2020